2010

POLYURETHANE-BASED POLYMER SURFACE MODIFIERS WITH ALKYL AMMONIUM CO-POLYOXETANE SOFT BLOCKS: REACTION ENGINEERING, SURFACE MORPHOLOGY AND ANTIMICROBIAL BEHAVIOR

Kennard Brunson
Virginia Commonwealth University

POLYURETHANE-BASED POLYMER SURFACE MODIFIERS WITH ALKYL AMMONIUM CO-POLYOXETANE SOFT BLOCKS: REACTION ENGINEERING, SURFACE MORPHOLOGY AND ANTIMICROBIAL BEHAVIOR

A dissertation submitted in partial fulfillment of the requirement for the degree of Doctor of Philosophy at Virginia Commonwealth University

By

KENNARD MARCELLUS BRUNSON, JR.

B.S (2002), M.S (2006), Virginia Commonwealth University

Director: Kenneth J. Wynne, PhD

Professor, Department of Chemical and Life Science Engineering

Virginia Commonwealth University

Richmond, VA

August 2010

ACKNOWLEDGEMENTS

The author wishes to thank the many people who have given assistance and support in making this degree possible. First I'd like to thank my advisor, Prof. Kenneth J. Wynne, for his guidance, encouragement, and leadership. You have been a true mentor and I hope one day to be able to do the same for someone. I also want to thank my wife Natasha, my mother Sharon, my step-father Ronnell, my sisters Melani and Krystle, my grandmother (Ethel) as well as my aunts, uncles, cousins and other family and friends who have given me their love and moral support through my years at VCU. I would also like to thank the members of the Wynne Group past and present who have helped me make this project not only possible but enjoyable. I would also like to acknowledge the National Science Foundation (NSF) and Virginia Commonwealth University for providing financial support for this project. Finally, I would like to dedicate this dissertation to my grandmama (Helen) and great-grandmother (Granny). I know both of you will always be watching over me. I love and miss you.

TABLE OF CONTENTS

LIST OF FIGURES AND SCHEMES

LIST OF TABLES

ABSTRACT

POLYURETHANE-BASED POLYMER SURFACE MODIFIERS WITH ALKYL AMMONIUM CO-POLYOXETANE SOFT BLOCKS: REACTION ENGINEERING, SURFACE MORPHOLOGY AND ANTIMICROBIAL BEHAVIOR

By Kennard Marcellus Brunson, Jr.

A dissertation submitted in partial fulfillment of the requirement for the degree of Doctor of Philosophy at Virginia Commonwealth University, 2010

Major Director: Kenneth J. Wynne, PhD

Professor, Chemical and Life Science Engineering Department

Concentrating quaternary (positive) charge at polymer surfaces is important for applications including layer-by-layer polyelectrolyte deposition and antimicrobial coatings. Prior techniques to introduce quaternary charge to the surface involve grafting of quaternary ammonium moieties to a substrate or using polyurethanes with modified hard segments however there are impracticalities involved with these techniques.

In the case of the materials discussed, the quaternary charge is introduced via polyurethane based polymer surface modifiers (PSMs) with quaternized soft segments. The particular advantage to this method is that it utilizes the intrinsic phase separation between the hard and soft segments of polyurethanes. This phase separation results in the surface concentration of the soft segments. Another advantage is that unlike grafting, where modification

has to take place after device fabrication, these PSMs can be incorporated with the matrix material during device fabrication.

The soft segments of these quaternized polyurethanes are produced via ring opening co-polymerization of oxetane monomers which possess either a trifluoroethoxy (3FOx) side chains or a quaternary ammonium side chain (C12). These soft segments are subsequently reacted with 4,4'-(methylene bis (*p*-cyclohexyl isocyanate)), HMDI and butanediol (BD) to form the PSM.

It was initially intended to increase the concentration of quaternary ammonium charge by increasing PSM soft segment molecular weight. Unexpectedly, produced blends with surface microscale phase separation. This observation prompted further investigation of the effect of PSM soft segment molecular weight on phase separation in PSM-base polyurethane blends and the subsequent effects of this phase separation on the biocidal activity.

Analysis of the surface morphology via tapping mode atomic force microscopy (TM-AFM) and scanning electron microscopy (SEM) revealed varying complexities in surface morphology as a function of the PSM soft segment molecular weight and initial annealing temperature. Many of these features include what are described as nanodots (100-300 nm), micropits (0.5-2 μm) and micropeaks (1-10 μm). It was also observed that surface morphology continued to coarsen with time and that the larger features were typically observed in blends containing PSMs with low molecular weight soft segments. This appearance of surface morphological feature correlates with decreased biocidal activity of the PSM blends, that is, the PSM blends exhibit little to no activity upon development of phase separated features. A model has been developed for phase separation and concomitant reduction of surface quaternary charge. This model points the way to future work that will stabilize surface charge and provide durability of surface modification.

Chapter 1

Linear and crosslinked polyurethanes with methylene bis (p-cyclohexyl isocyanate) hard segments: compositions with new process-controlled nanomorphologies

Introduction

The overall objective of the research described in this dissertation is directed at understanding the chemistry, physics, and engineering involved in modifying a bulk polymer with a functional polymer surface modifier. With emphasis on surface science, a conventional, solution processable bulk polymer is chosen so that solution processing of base and modifier polymer can be used to create coatings where the bulk polymer is the majority component and the modifier is the minority component that determines surface properties. The surface science of these coatings is studied to elucidate modifier surface concentration and retention of modifier function.

Conventional linear polyurethanes have been chosen as the base polymer. Polyurethanes are easily prepared and have served well in prior research as tough matrixes.[1, 2] This Chapter describes the chemistry, processing, surface and bulk properties of conventional polyurethanes, one of which was chosen for modification as described in subsequent chapters.

Linear polyurethanes are segmented block copolymers in the class of thermoplastic elastomers that are composed of alternating hard and soft segments (Figure 1.1). The soft segment is typically a low glass transition temperature (T_g) polyester, polyether or polyalkyldiol with molecular weights ranging from 400-5000 Da while the hard segment is derived from diisocyanates linked to a low molecular weight chain extender such as 1,4-butanediol (BD).[3]

Scheme 1 shows the sequence of reaction for the "soft block first" preparation of the polyurethanes employed in this work. The first step is the reaction of the polyol with the diisocyanate which produces a diisocyanate capped soft segment (Eq. 1). Second, is the reaction of the diisocyanate terminated soft block with hydroxyl groups from the chain extender that forms the linear hard segment of the polyurethane (Eq. 2). As seen in Figure 1.2, the urethane groups within these hard segments can form hydrogen bonds with other hard segment urethane groups creating nanocrystalline domains surrounded by an amorphous soft segment region.

The nanoscale ordered hard domains have a high T_g and give the polyurethane mechanical strength while the low T_g amorphous soft segment allows polyurethanes to be flexible. By adjusting the ratio of hard and soft segments during synthesis the properties of polyurethanes can vary between brittle and hard to soft and tacky.[4-9] If the diisocyanate or the diol chain extender is replaced with a polyisocyanate or polyol with functionalities greater than 2, crosslinked polyurethanes (thermoset elastomers) can be made.

Phase separation in block copolymers was first described by Cooper and Tobolsky in 1966 during their study of styrene-butadiene-styrene triblock copolymers.[10] In their investigation they postulated that the properties of this block copolymer were due to clustering or microphase separation. Thomas and coworkers subsequently used electron microscopy to show microphase separation in polyurethanes,[11] while in the work of Runt,[12] tapping mode atomic force microscopy (TM-AFM) (Figure 1.3) was used to investigate the nanoscale phase separation in polyurethane-ureas. As seen from Figure 1.3, the featureless images taken at the higher setpoint ratio (soft tapping) is indicative of the amorphous soft segment being dominant at the surface. At the lower setpoint ratio (harder tapping) the near surface hard segment can be seen in the form of ordered

domains previously described. This surface segregation of the soft segment is typical for polyurethanes due to the soft segment having a lower surface energy that the hard segment.

Polyurethane phase separation has also been investigated by differential scanning calorimetry (DSC) where separate T_gs for the hard and soft segments were detected.[9, 13-17] Miller *et al*. demonstrated this in the study of 4,4'-methylene bis(pheny1 isocyanate)-butanediol-poly (tetramethylene oxide) (MDI-BD-PTMO) polyurethanes made via single and multistep polymerization.[15] As seen in Figure 1.4, thermal transitions for the hard and soft segment are clearly discerned in thermograms of annealed compositions with high hard block content as inflections at -50 ^{o}C (soft segment) and 150 ^{o}C (hard segment). These transitions are similar to those pure soft segment (PTMO) and pure hard segment (MDI-BD) and therefore signify that the polyurethane morphology consists of two distinct phases or domains.

The specific objective of the work discussed in this chapter is to assess the bulk, surface and mechanical properties of a number of methylene bis (p-cyclohexyl isocyanate) (HMDI) based polyurethanes to determine which composition would be suitable as a convenient matrix or "base" polyurethane when blended with HMDI based biocidal polymer surface modifiers (PSMs).[18]

Prior work utilized DSC as well as TM-AFM and dynamic contact angle analysis (DCA) to characterize a series of linear base polyurethanes for bulk and surface properties.[19] Base polyurethane with a PTMO 1000 soft segment and 50 wt% HMDI-BD was found suitable as a matrix polyurethane due to good bulk and surface characteristics. However, several considerations have led to broadening investigations of surface and bulk properties of HMDI-BD-PTMO polyurethanes.

Because the main intent in these systems is surface modification, a thorough knowledge of base PU surface morphologies as a function of composition and processing is necessary as background for understanding modified surfaces. Secondly, temporal and thermal instability of modified surfaces (Chapter 3) has led to a preliminary investigation of a crosslinked HMDI polyurethane. This research will provide experience on which to base future studies of the influence of a crosslinked matrix on modified surface stability.

Chemical crosslinks may hinder segmental motion of the polymer surface modifier which in turn may stabilize the surface morphology. In contrast to linear polyurethanes, however, crosslinked analogs cannot be melt processed. Therefore, surface modifiers must be added at an intermediate stage where reactants are miscible. While future work will determine modifier processing feasibility,[20] the present research focuses on establishing basic surface morphology of a "base" HMDI network coating.

Like the bulk and surface characterization of linear HMDI-BD-PTMO polyurethanes, a study of similar PUs crosslinked with glycerol was performed. An interesting result from AFM analysis on the thermoset polyurethane was the observation of what appear to be gel domains. Importantly, the length of scale of gelation (micro to nano) can be controlled by the order of addition of reactants.

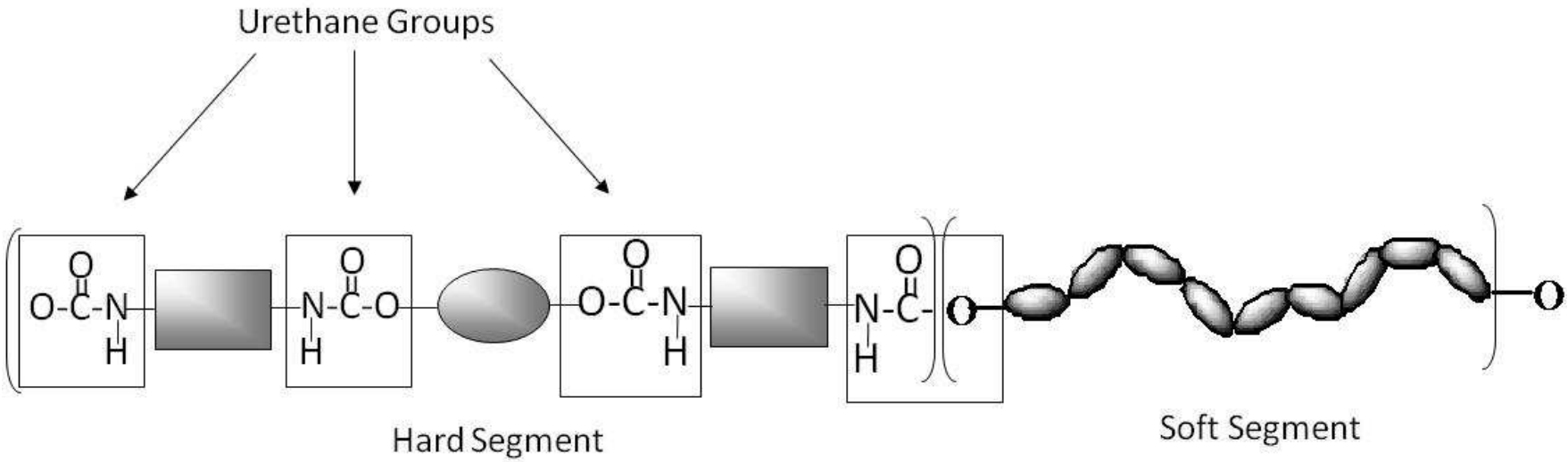

Figure 1.1**.** Representative Block Polyurethane Structure.

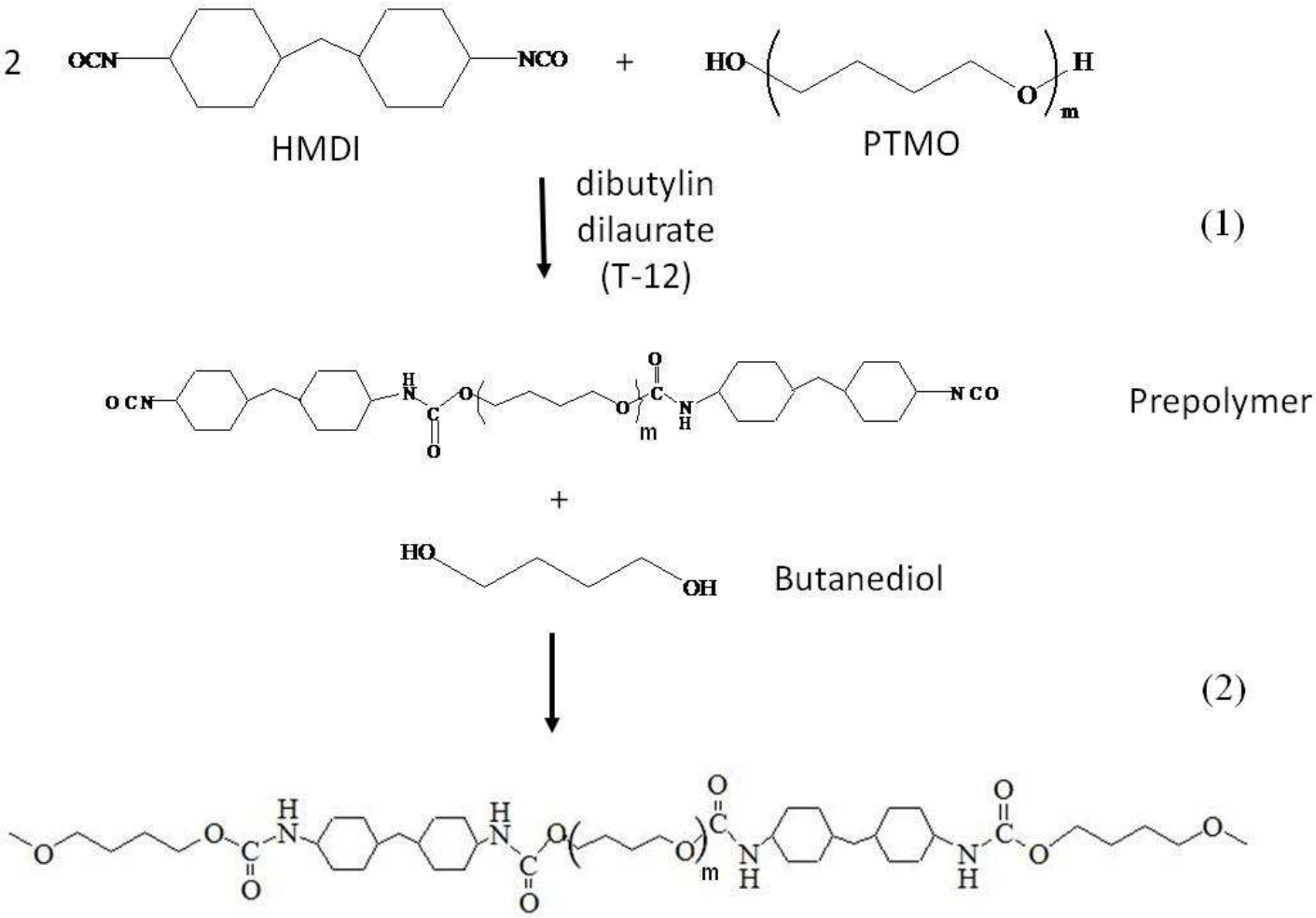

Scheme 1.1. Polyurethane reaction scheme,. Eq. 1, Prepolymer Synthesis, Eq. 2, Chain extension, to produce the HMDI-BD (30) PTMO (2000) product.

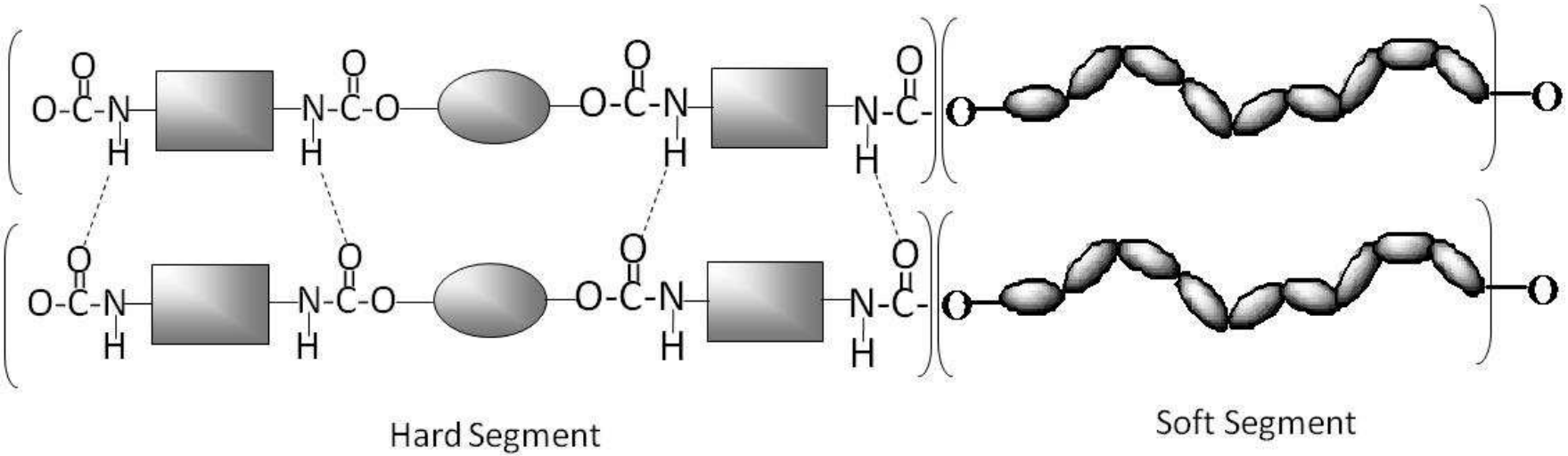

Figure 1.2. Hydrogen bonding between polyurethane hard segments.

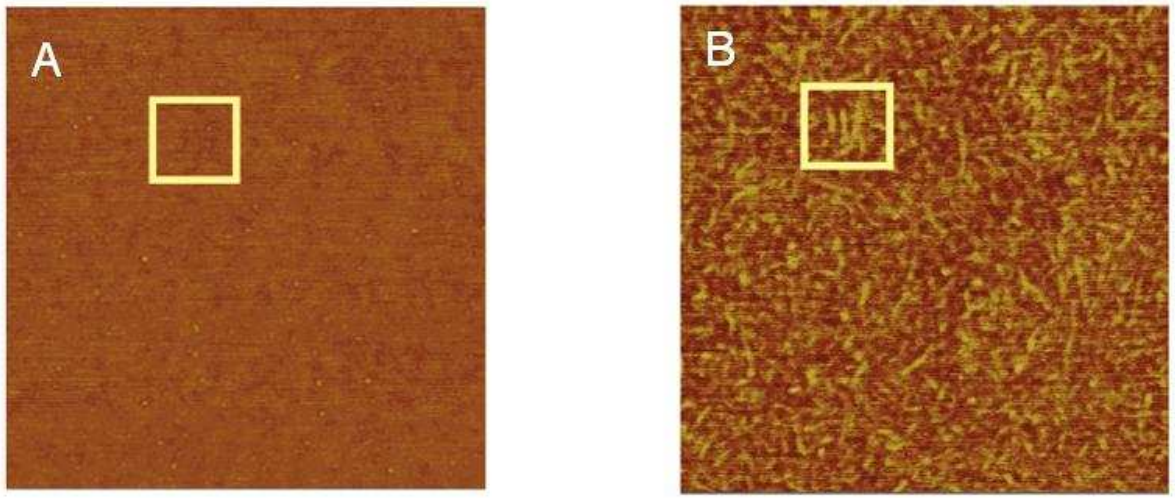

Figure 1.3. TM-AFM phase images of polyurethane-urea. Scan size = 500 x 500 nm phase angle 25^{o}. A) Amplitude set point ratio (A_{sp}/A_{o}) = 0.9, B) Amplitude set point ratio (A_{sp}/A_{o}) =0.8[12]

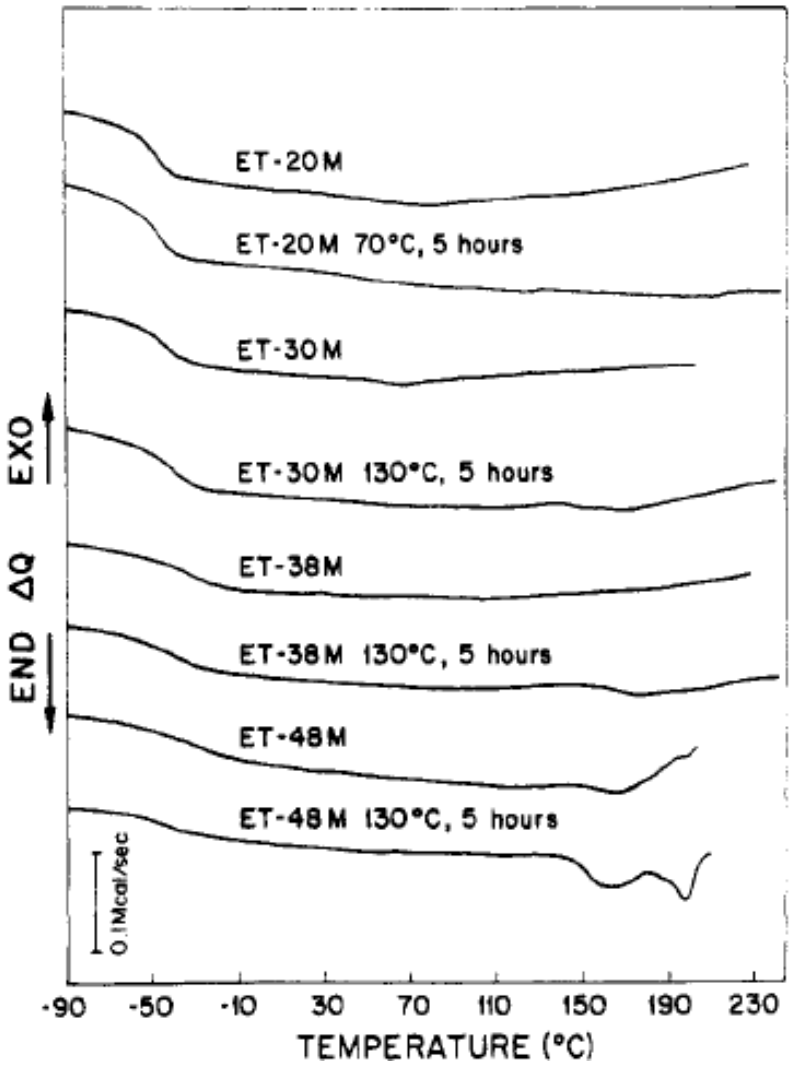

Figure 1.4. DSC curves of multistep polyurethanes; annealing temperatures indicated. [15]

Experimental Section

Terminology. When referring to the linear polyurethane the designation HMDI-BD (30wt%)-PTMO (2000) is used where 30 wt% represents the HMDI-BD hard segment weight percentage. For the cross-linked series, the representation HMDI-(GL/BD-f) (30 wt%)-PTMO is used with f represents the functionality, which is calculated from the ratio of diol and triol. For example, a crosslinked base polyurethane having a functionality of 2.1 would be designated HMDI-(GL/BD-2.1) (30 wt%) PTMO (2000). An example calculation for functionality f is provided in the Synthesis section below.

Materials. Poly(tetramethylene oxide) MW 2000 g/mol (PTMO-2000), reagent grade tetrahydrofuran (THF), bis(p-cyclohexyl isocyanate) HMDI, glycerol, and dibutyltin dilaurate catalyst were purchased from Aldrich and used as received. 1,4-butanediol (BD) and dimethylformamide (DMF) were purchased from Acros chemicals and used as received. Deuterated chloroform, 99.8 atom %D with 0.05 %v/v TMS was purchased Aldrich and used as received.

Linear polyurethane synthesis. Linear polyurethane (PUs) was prepared by a two-step polymerization technique. (Scheme 1.1, Eqs 1and 2) [3, 21-24] In the first stage, isocyanate-terminated prepolymer was synthesized. HMDI and PTMO (2000 MW) (Table 1) were charged into a three-neck round bottom flask equipped with a mechanical stirrer, nitrogen inlet, and condenser. The reaction was started in DMF with an initial reactant concentration of 80 wt%. After addition of dibutyltin dilaurate catalyst (5-7 drops, 10 vol% T-12 in THF), the reaction mixture was kept at 70-75 ºC. The formation of diisocyanate-terminated prepolymer was confirmed by FT-IR spectroscopy (urethane carbonyl, 1724 cm^{-1}, and N-H, 3346 cm^{-1} Figure 1.5).

In the second stage, BD was added dropwise with continued heating at 70-75 ºC until isocyanate was consumed. This polymer chain extension step was monitored via FT-IR by following the disappearance of the isocyanate peak at 2267 cm^{-1}. As the viscosity of the reaction mixture increased, DMF was periodically added to the point where the final polymer solution concentration was ca. 25 wt%. The reaction mixture was then added dropwise to a 1:4 vol/vol methanol/ DI water mixture and the white polymer precipitate and solvent mixture was magnetically stirred overnight.

After precipitation, the samples were filtered with vacuum and dried in an oven for 4 hrs at 100 ºC. The dried polymer was dissolved in THF and upon total dissolution the sample was poured into 10 in. Teflon® coated pans and allowed to dry in a hood for 2 days. After solvent evaporation, the polyurethane plaques were further dried in a vacuum oven at 65 ºC for 24 hrs and then weighed.

Crosslinked polyurethanes synthesis. The same soft block polyols and diisocyanate were used except crosslinking was accomplished with a combination of triol (glycerol) and diol (BD). The ratio of the diol to triol determines the functionality (f), which in turn determines the degree of crosslinking. The functionality is the average number of available functional groups (hydroxyls) per molecule (Eq. 1). Since butanediol has a functionality of 2 while glycerol has a functionality of 3, the functionality of a mixture of these two substances can range between 2 (100% butanediol chain extender) and 3 (100% glycerol chain extender). The selected values of f were 2.1, 2.3, and 2.5. As an example, a 5 g sample with 30% hard block and functionality of 2.1 was comprised of 3.5 g (1.8 mmol) PTMO-2000 (3.6 mmol OH), 0.18 g (2 mmol) BD (4 mmol OH), 0.02 g (0.2 mmol) glycerol (0.6 mmol OH), 1.3 g (5.0 mmol) HMDI (10 mmol NCO) with

dibutyltin dilaurate as catalyst . For this example, the functionality is calculated as follows:

$$f_{XPU} = n_{bd} f_{bd} + n_{gly} f_{gly} \quad (1)$$

$$2.1 = (.9)2 + (.1)3$$

Where f_{XPU} = functionality of crosslinked PU, n_{BD} = mole fraction of BD, f_{BD} = functionality of BD, n_{gly} = mole fraction of glycerol, f_{gly} = functionality of glycerol.

Initially, the above components were added simultaneously to 30 mL of THF or butyl acetate, pre-reacted for 2 hr and then drip coated onto a glass slide. Some of the solution was poured in PTFE dished for film casting. This method resulted in cloudy films. Optically transparent films and coatings were obtained by adding PTMO and HMDI first with pre-reaction overnight. BD was added followed by stirring for 5 hr. Glycerol was added followed by additional stirring for 1.5 hr. Finally, the solution was then drip coat onto glass slides.

Solvent was removed by drying in air for 24 hr at ambient conditions followed by vacuum oven drying at room temperature for 24 hr. The films and the coatings are usually firm at this stage, however to complete cure and ensure that all remaining solvent is removed, the films and coatings were heated at 60 °C for 24 hr for complete cure.[25]

Characterization. FT-IR and ATR-IR spectra of the linear polyurethane and crosslinked polyurethane were obtained using a Nicolet 400 FT-IR spectrometer. Differential Scanning Calorimetry was carried out on the TA –Q 1000 Series™ instrument (TA Instruments). Measurements were performed using a modulated DSC (MDSC) method where the polymer sample was ramped at a heating rate of 10 ºC/min

from -80 ºC to 180 ºC, cooled back to -80 ºC and held isothermally for 5 min. The temperature was then set to a modulation of ± 0.50 ºC and a ramped at a rate of 5 ºC/min to 180 ºC. ^{1}H-NMR Spectra were obtained using a Varian Inova 400 MHz Spectrometer. Linear polyurethane samples were dissolved in deuterated chloroform for ^{1}H NMR analysis.

Uniaxial Tensile Testing. Analysis of mechanical properties of linear and cross-linked polyurethanes was performed on an MTS uniaxial tensile tester. Samples (dog bones) were stamped out of cast plaques and measured for thickness, width and gauge (mm). After obtaining sample dimensions, the samples were clamped in the MTS grips. The sample elongation rate was set at 10 mm/min and the applied force and elongation data were recorded at 10 Hz. The stress, elastic modulus, and strain are calculated based on the sample dimensions, elongation and applied force.

Dynamic Mechanical Analysis (DMA). Samples for DMA were cut from 200-500 μm plaques. A TA instruments RSA 3 dynamic mechanical analyzer was employed using a dynamic temperature ramp test method. During analysis sample temperature was ramped from -100 to 100 ºC at 5 ºC/min while tension cycles were set at 1 Hz with maximum strain set to 0.05%. Maximum autotension was set to 2 mm with maximum autotension rate of 0.01 mm/s.

Tapping Mode Atomic Force Microscopy (TM-AFM). Samples were analyzed on a Digital Instruments Dimension 3100 TM-AFM with a Nanoscope V controller**.** Slides coated with linear polyurethane were prepared by drip coating one side of glass cover slip with a 10 wt% solution of PU samples. Samples were then dried at ambient temperature for 24 hrs and vacuum dried at ambient temperature for an additional 24 hrs

to remove residual solvent. As mentioned in the synthesis section, slides with crosslinked coatings were prepared by casting pre-reacted solutions.

After casting, samples were analyzed at setpoint ratios ($r_{sp} = A_{sp}/A_o$) between 0.95 and 0.8, where A_{sp} is the experimental amplitude and A_o is the free oscillating amplitude. As explained by Maganov,[26] and illustrated in Figure 1.3, the impact of varying r_{sp} is primarily on the phase image. At higher setpoint ratios, r_{sp} close to 1, or "soft tapping" the tip interaction with the surface is minimized and differences in phase image reflect the outermost surface of the sample. Regions of higher modulus cause a more elastic tip-sample response, while soft areas respond in an opposite way. Thus, by monitoring phase of the tip response in a visual (color) format, the surface morphology (hard/soft regions) may be identified. By decreasing $r_{sp,}$ tip-sample force interactions increase. Thus the tip interaction with the surface integrates mechanical response over increased depth. In favorable cases, by analyzing phase images at soft tapping, one can distinguish surface (soft tapping) and near surface (hard tapping) morphological features. This sensitivity of phase imaging is a very important feature in analyzing near surface morphology of polyurethanes and modified polyurethanes by TM-AFM.

AFM 2D and 3D topological images are also be valuable. While a noteworthy feature of base polyurethanes is remarkably smooth "leveling" on film / coating formation, it will be seen in Chapter 4 that surprisingly complex topologies are observed for modified surfaces. Because AFM provides quantitative evaluation of feature height, 3D height imaging is particularly important for evaluation of surface morphology for modified polyurethane.

Dynamic Contact Angle (DCA) analysis. In contrast to sessile drop measurements of wetting behavior, DCA integrates wetting behavior over the perimeter / area of a coated slide (Figure 1.5). In DCA, a sensitive electrobalance (Figure 1.5A) monitors the mass of a coated coverslip. As shown, when the coated slide impinges on the interrogating fluid, here water, an apparent increase in mass is registered if the surface is hydrophilic (Figure 1.5 D). The opposite response occurs for a hydrophobic surface (Figure 1.5 C). Advancing (θ_{adv}) and receding (θ_{rec}) contact angles are defined by the Equation shown in Figure 1.5. By extrapolating the force distance curve to the ordinate, the buoyancy term is eliminated. Advancing and receding contact angles are calculated from advancing (fdc_{adv}) and receding (fdc_{rec}) force distance curves.

For linear polyurethane samples, coated slides for DCA measurements were made by dip coating glass microscope cover slides (No. 1 ½ 22 x 40 mm glass cover slips) into 10 wt% PU solutions. The same drying procedure as described for drip-coated slides was followed. Dip coated slides for the crosslinked samples were made by dip coating glass microscope cover slips into the reaction components after glycerol addition. The curing process is the same as that discussed in previous sections.

Wetting behavior in nanopure water was analyzed using the Wilhelmy plate method via a Cahn Dynamic Contact Angle (DCA) instrument. PU coated slides were submerged to a depth of 15 mm at a rate of 100 μm/s and then withdrawn without a dwell time. Five immersion/emersion cycles were carried out. To examine whether there was contamination from the polymer samples, the wetting medium was tested with a flamed glass slide before and after the testing of the PU samples under the same conditions.[27]

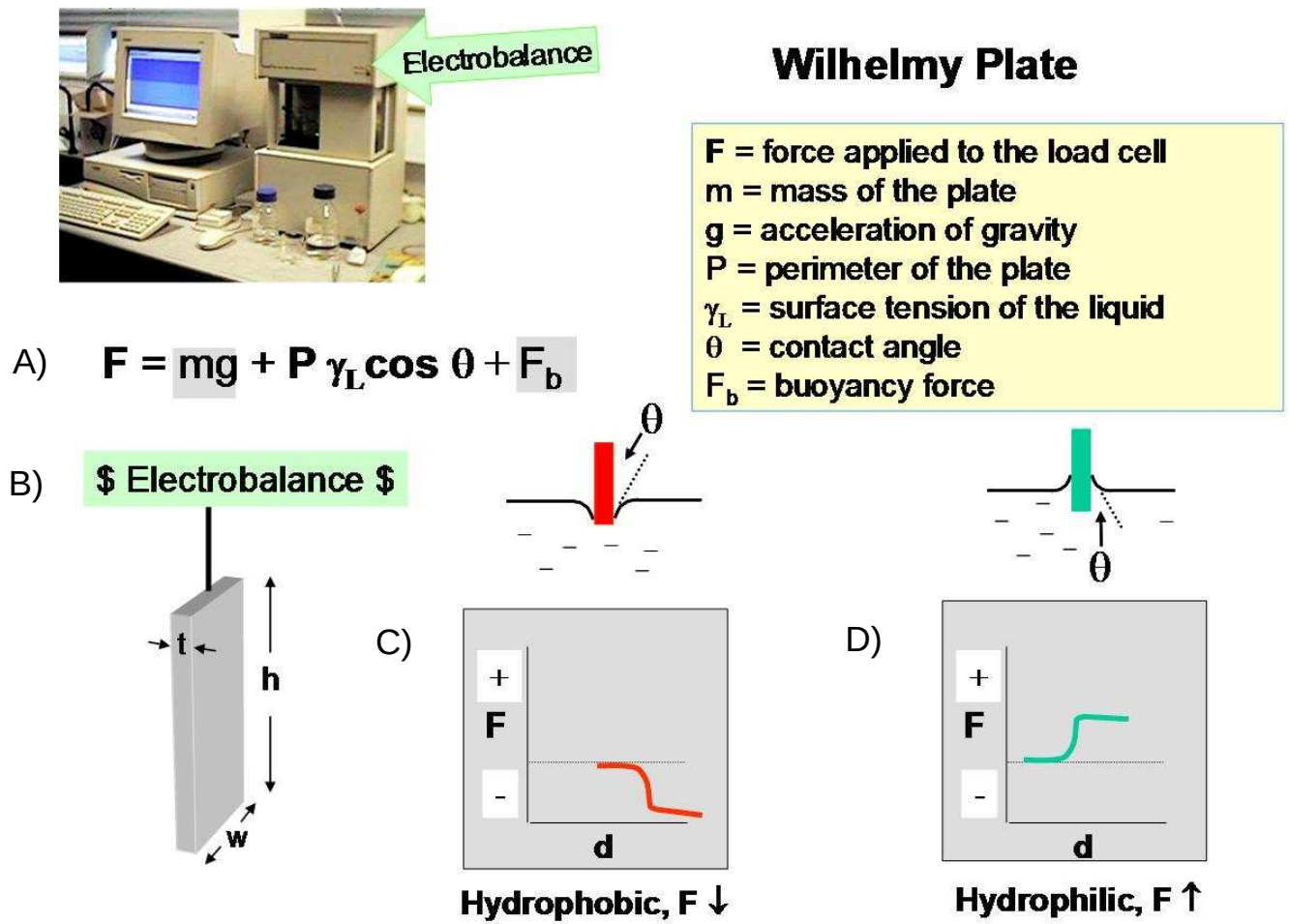

Figure 1.5 Model of Dynamic Contact Angle Analysis. A) Equation relating apparent force to contact angle. B) Model of DCA samples, C) Model of force-distance curve for hydrophobic surface, D) Model of force-distance curve for hydrophilic surface.

Results and Discussion

Synthesis. Progress of the reaction used to make linear polyurethanes was monitored at the start of the prepolymer stage, during prepolymer formation (Scheme 1.1, Eq. 1), and during chain extension (Scheme 1.1, Eq. 2). Before the addition of T-12 catalyst, the FT-IR spectra showed an O-H stretch peak of the PTMO at approximately 3500 cm^{-1} and an isocyanate peak at approximately 2300 cm^{-1} (Figure 1.6A). Upon the reaction of PTMO with HMDI, peaks at 3300 cm^{-1} and 1724 cm^{-1} denote formation of urethane amide (N-H) and carbonyl (C=O) groups respectively (Figure 1.6B). Since the feed had excess isocyanate, the 2300 cm^{-1} peak remained. During chain extension, the intensity of the isocyanate peak gradually diminished due to the reaction of the prepolymer isocyanate end groups with the butanediol (Figure 1.6C).

For the crosslinked polyurethanes HMDI-(GL/BD-f) (30wt%)-PTMO the order of addition of reagents was found to be important in determining the extent of gel formation (vida infra). The optimum process consisted of the same soft block first procedure used for the linear PU, followed by the addition of BD and GL sequentially. Comparisons of ATR-IR spectra for linear and crosslinked polyurethanes showed that all three crosslinked polyurethane compositions had no residual isocyanate. This indicates complete reaction.

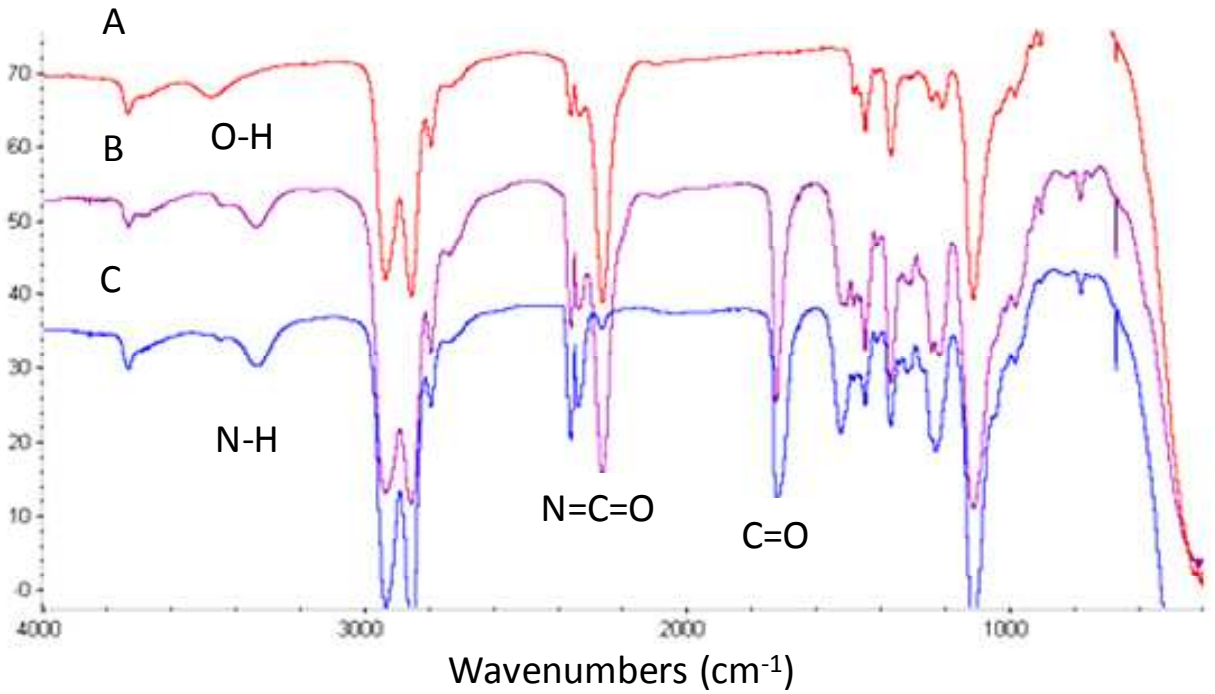

Figure 1.6. FT-IR Spectra PU-1 ((30wt%HMDI-BD) PTMO (2000)): A) start of prepolymer reaction, B) 1.5hr prepolymer reaction, C) 30min chain extension.

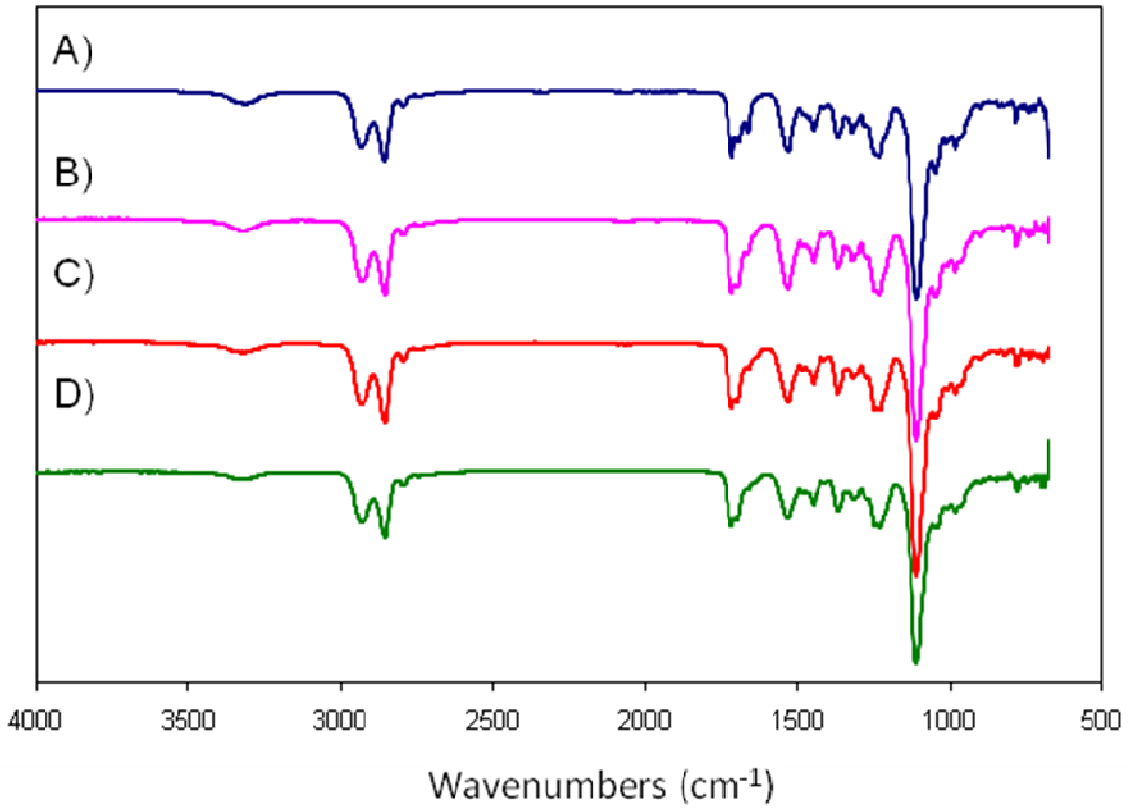

Figure 1.7. ATR-IR Spectra of base polyurethane: A) linear, B) HMDI-(BD/GL-2.1) (30) PTMO (2000), C) HMDI-(BD/GL-2.3) PTMO (2000), D) HMDI-(BD/GL-2.5) (30) PTMO (2000).

As seen in Figure 1.7, an isocyanate peak is not detected in any spectra for the crosslinked polyurethanes. The crosslinked polyurethane spectra are very similar to that for the linear polyurethane. Characteristic carbonyl and amide peaks are seen at 1723 cm^{-1} and 3300 cm^{-1} respectively.

NMR Spectroscopy. Figure 1.8 shows a representative ^{1}H-NMR spectrum for linear HMDI/BD (30 wt%) PTMO (2000). The large peak which appears at 1.2 ppm (Figure 1.8-A peak a) is assigned to central methylene protons which include methylene protons in the HMDI structure, the two methylenes in the center of the BD chain extender and the methylenes of the PTMO soft block. The peak at 1.6 ppm (Figure 1.8-A peak e) is due to the cyclic methylene protons of HMDI. The other large peak at 3.4 ppm (Figure 1.8-B peak b) is assigned to ether group protons, includes methylene groups in PTMO and BD. A smaller peak at 4.1ppm (Figure 1.8-C peak c) is assigned to protons near the carboxyl and amide end of the urethane linkage respectively. The apparent doublet between 4.6-4.8 ppm (Figure 1.8-C-d) is due to the amide proton of the urethane linkage since amides typically show peaks in the range of 4.5-8.5 ppm.[28]

Calculation of the hard block percentage for the linear polyurethanes was performed using the area of peaks A-a and C-d in Figure 1.8 (areas in Table 1.1). As observed in the structure of the hard block, for every amide proton there are 10 protons methylene group. Therefore the area due to protons adjacent to methylene groups in HMDI should be 10 times the area of the peaks due to the amide proton. In order to differentiate PTMO methylene from BD methylene groups we make the assumption that all isocyanates react with BD or PTMO. In the case of BD there are four methylene protons for every amide proton, therefore the area due to methylene protons in BD should be four times the area of the peaks due to the amide proton. The calculated areas for

HMDI and BD were then subtracted from the total area due to methylene protons to give the area due to PTMO methylene protons thus giving the minimum PTMO present in the polymer. From the areas of HMDI, BD and PTMO the mass present in each polymer were calculated and used to calculate the hard block percentages. An example calculation is as follows:

Area of amide H (peak C-d) = 0.46
Area of CH_2-CH_2 (peak A-a) = 29.4
Area of HMDI = 10 × Area of amide H = 4.6
Area of tetramethylene oxide (TMO) units = (Area of CH_2-CH_2) - (Area of HMDI) =24.8
Area of BD = 4 × (Area of amide H) = 1.84
Area of PTMO = (Area of TMO) – (Area of BD) = 22.9
Mass of PTMO = (Area of PTMO/ # H in PTMO (212)) × MW_{PTMO} (2000) = 216 mg
Mass of BD = (Area of BD/ # H in BD (4)) × MW_{BD} (90.12) = 41 mg
Mass of HMDI = (Area of HMDI/ # H in HMDI (22)) × MW_{HMDI} (262.35) = 54 mg
HMDI-BD wt% = (Mass of BD + HMDI)/ (Mass of HMDI + BD + PTMO) = 30.5%

As seen in Table 1.1, the hard block percentages calculated from the 1H-NMR spectra are very close (± 1 wt%) to the feed values.

Table 1.1. Reactant feed for HMDI-BD (30)-PTMO (2000), ^{1}H-NMR peak areas and hard block weight percentage.

HMDI-BD (30)-PTMO (2000) Reactant Feed	
PTMO feed (g)	21.6
BD feed (g)	4.1
HMDI feed (g)	5.5
HMDI-BD (30)-PTMO (2000) H-NMR peak areas	
Urethane H (peak d)	0.46
Total Methylenes (peak a)	29.4
HMDI methylenes	4.6
BD methylenes	1.84
PTMO methylenes	22.9
experimental wt%	30
HB wt%	30.8

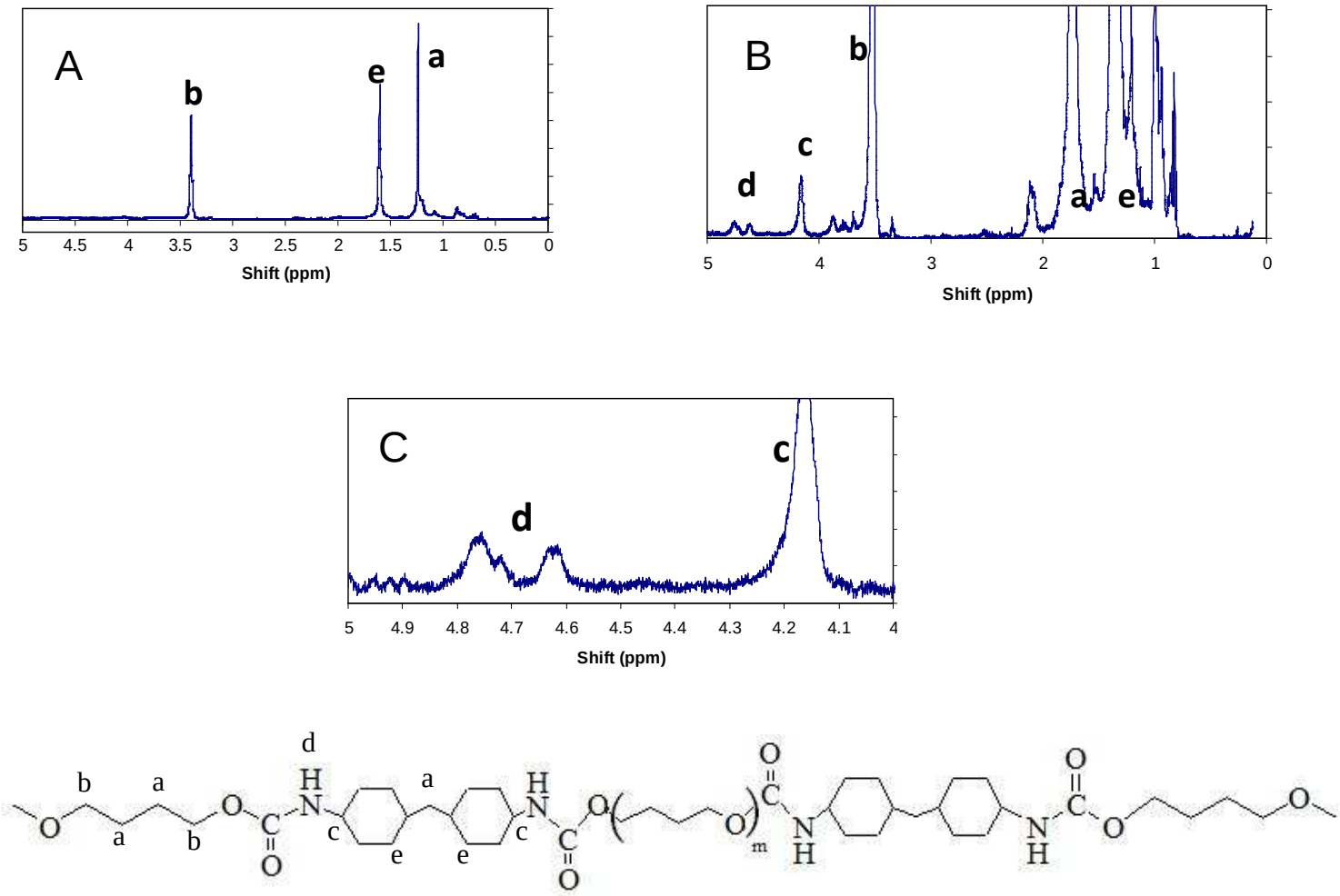

Figure 1.8. [1]H NMR Spectra PU-4 HMDI/BD (30) PTMO (2000) A) methylene and ether peaks. B) All peaks. C) urethane amide peaks.

Thermal Analysis. Modulated differential scanning calorimetry, MDSC, was used to determine thermal transitions of soft and hard segments. By using MDSC it is possible to resolve normal heat flow into reversing and non-reversing heat flow components. Using the reversing heat flow curves, more accurate T_gs are obtained by removing transitions associated with non-reversing heat flow, such as irreversible relaxations due to processing history, which can lead to misinterpretations.[29]

As seen in Figure 1.10A and Table 1.3, linear HMDI-BD (30wt%)-PTMO (2000) has a soft segment glass transitions at –77 ºC. This value is close to the reported T_g for PTMO.[30] Soft segment melting is indicated by an endotherm at 20 ºC. Hard block T_gs for this polyurethanes was 86-88 ºC, which is near that obtained for the HMDI/BD hard block alone that was previously synthesized (86 ºC).[19]

Thermograms for HMDI-(GL/BD-2.1) (30 wt%)-PTMO (2000), HMDI-(GL/BD-2.3) (30 wt%)-PTMO (2000) and HMDI-(GL/BD-2.5) (30 wt%)-PTMO (2000) crosslinked polyurethanes (Figure 1.9B-D) also showed soft segment T_gs at -77 ºC. HMDI-(GL/BD-2.1) (30 wt%)-PTMO (2000) showed an endotherm at 20 ºC. This indicates that soft segment still has some mobility and is capable of crystallizing. In comparing the two observed melting endotherms for HMDI-BD (30 wt%)-PTMO (2000) and HMDI-(GL/BD-2.1) (30 wt%)-PTMO (2000), the heat of fusion, ΔH_m, is 6.7×10^{-2} J and 7.8×10^{-3} J respectively. The higher ΔH_m of the linear PU is expected due to the fact the soft segment has more mobility above T_g than the soft segment of the HMDI-(GL/BD-2.1) (30wt%)-PTMO (2000) because of the lack of chemical crosslinks.

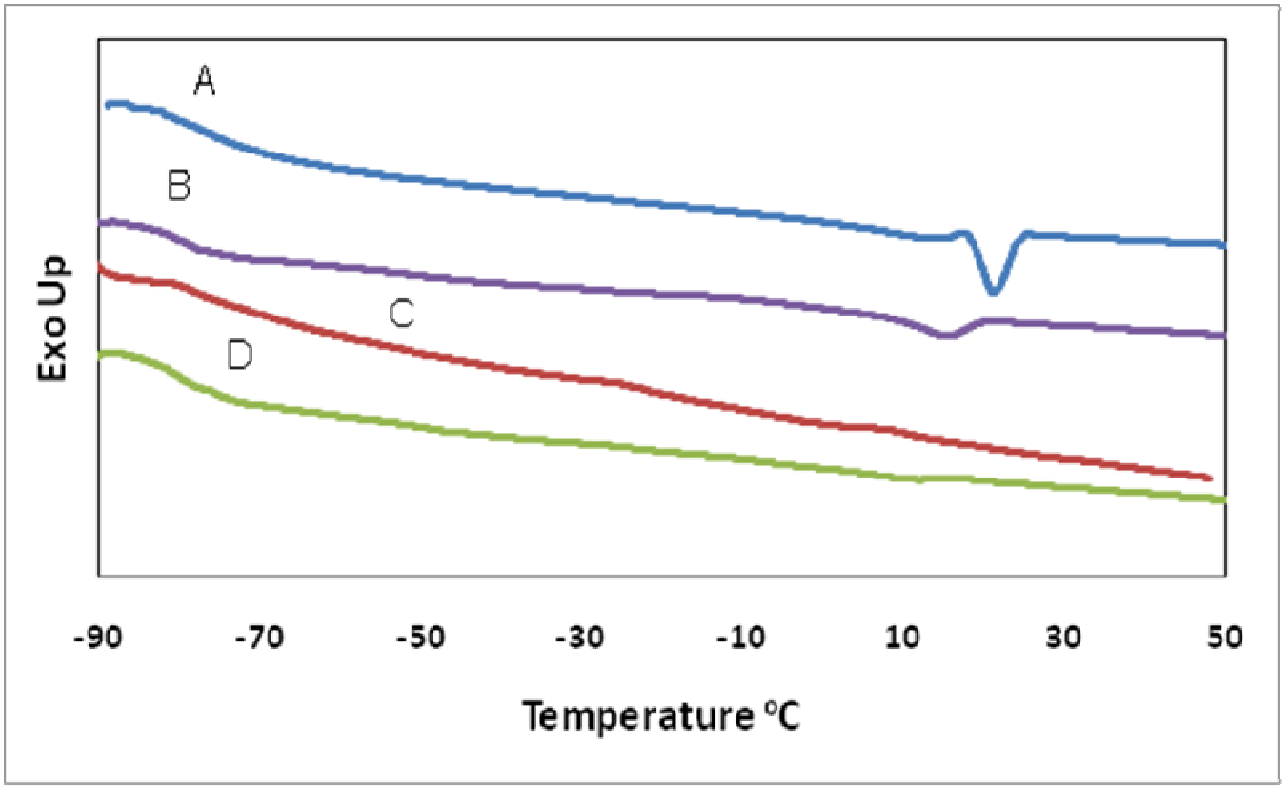

Figure 1.9. DSC thermogram HMDI-BD (30) PTMO (2000) Base polyurethane, A) Linear Polyurethane, B) HMDI-(BD/GL-2.1) (30wt%) after curing, C) HMDI-(BD/GL-2.3) (30wt%), after curing, D) HMDI-(BD/GL-2.5) (30wt%), after curing.

Table 1.2. Observed soft segment thermal transitions.

Sample	DSC Soft Segment T_g (^oC)	DSC Hard Segment T_g (^oC)	DSC Soft Segment T_m (^oC)	DMA Soft Segment T_g (^oC)	DMA Soft Segment T_g (^oC)
HMDI-BD (30) PTMO (2000)	-77	87	-20	-70	15
HMDI-(BD/GL-2.1) PTMO (2000)	-76	n/o	-17	-70	10
HMDI-(BD/GL-2.3) PTMO (2000)	-77	n/o	n/o	-70	n/o
HMDI-(BD/GL-2.5) PTMO (2000)	-78	n/o	n/o	-70	n/o

a. n/o, not observed

Uniaxial Tensile Testing. Tensile testing revealed that the degree of crosslinking affects the modulus. As seen in Table 1.3 and Figure 1.10, linear polyurethane has the lowest modulus of elasticity. Although the presence of the physical cross-links formed via hydrogen bonding between the hard segments gives significant strength to the linear polyurethane the low modulus relative to the crosslinked polyurethanes was expected due to the lack of chemical crosslinks.[23]

As evident from the stress strain curve, the degree of crosslinking for HMDI-(BD/GL-2.1) PTMO (2000) polyurethane was too low to affect modulus compared to the linear polyurethane. The increased crosslink density of HMDI-(BD/GL-2.3) PTMO (2000) and HMDI-(BD/GL-2.5) PTMO (2000) resulted in a significant increase in modulus and strength compared to the linear polyurethane and HMDI-(BD/GL-2.1) PTMO (2000). This strength and stability thereby make these polyurethanes attractive candidates as matrices for polymer surface modifiers.

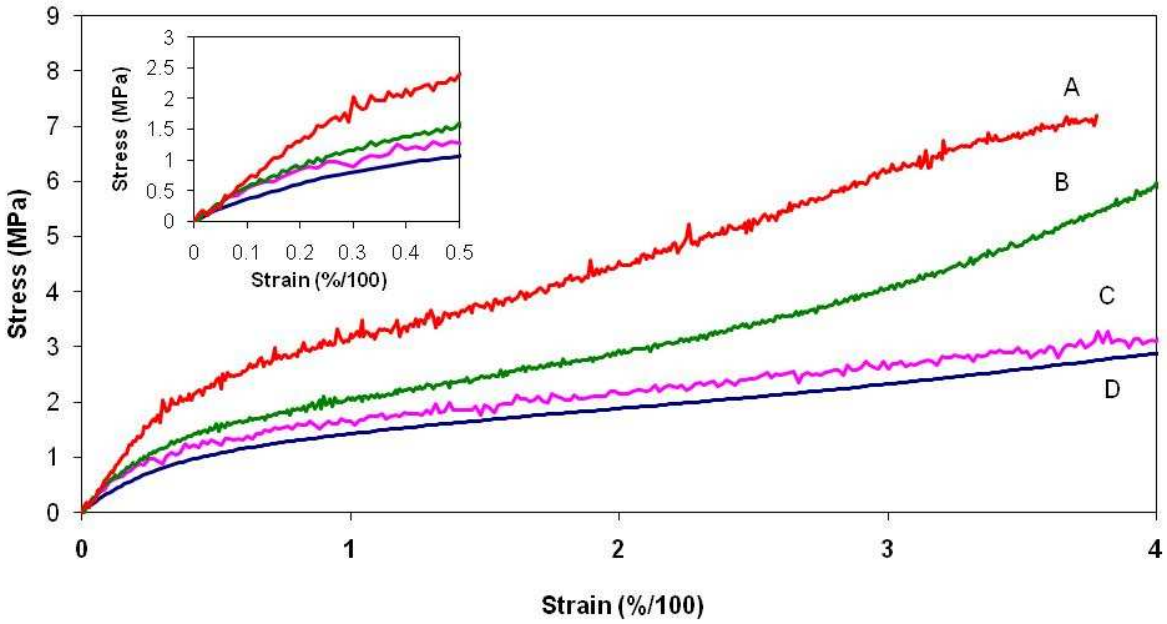

Figure 1.10. Stress vs. Strain Curve. A) HMDI-(BD/GL-2.5) PTMO (2000), B) HMDI-(BD/GL-2.3) PTMO (2000), C) HMDI-(BD/GL-2.1) PTMO (2000), D) HMDI-BD (30wt%) PTMO (2000).

Table 1.3. Modulus of elasticity for base polyurethanes.

Sample	Modulus (MPa)
HMDI-BD (30 wt%) PTMO-2000	3.7
HMDI-(BD/GL-2.1) PTMO-2000	4.5
HMDI-(BD/GL-2.3) PTMO-2000	5.9
HMDI-(BD/GL-2.5) PTMO-2000	6.4

Dynamic mechanical analysis (DMA). As seen in the storage modulus (E') vs. temperature curve, (Figure 1.11) the inflection in the curve between -80 and -60 ºC indicates that the soft segment glass transition was -70 ºC, is in good agreement with DSC (Table 1.3) The storage modulus curve for the linear polyurethane had an inflection at 10 ºC which indicates soft segment melting as observed in DSC (Figure 1.11A-a). This inflection was also observed in HMDI-(GL/BD-2.1)-PTMO (2000) (Figure 1.11A-b) which follows from HMDI-(GL/BD-2.1) (30wt%)-PTMO (2000) having a lower crosslink density and sufficient PTMO mobility to form crystalline regions. HMDI-(GL/BD-2.3)-PTMO (2000) and HMDI-(GL/BD-2.5)-PTMO (2000) (Figure 1.11B) did not display an inflection at 10 ^{o}C indicating that the soft segments are not as mobile due to higher crosslink densities.

The data point scattering seen after 60 ^{o}C in the loss modulus curves indicated that the linear polyurethane was losing mechanical strength. In comparison, all the crosslinked polyurethanes maintained mechanical strength up to 100 ºC. This improvement in the thermal stability of mechanical properties is accounted for by the chemically crosslinked matrix, which is not susceptible to weakening by heating. The contrasting mechanical behavior of the linear and crosslinked polyurethanes points out the value of DMA analysis concurred with DSC.

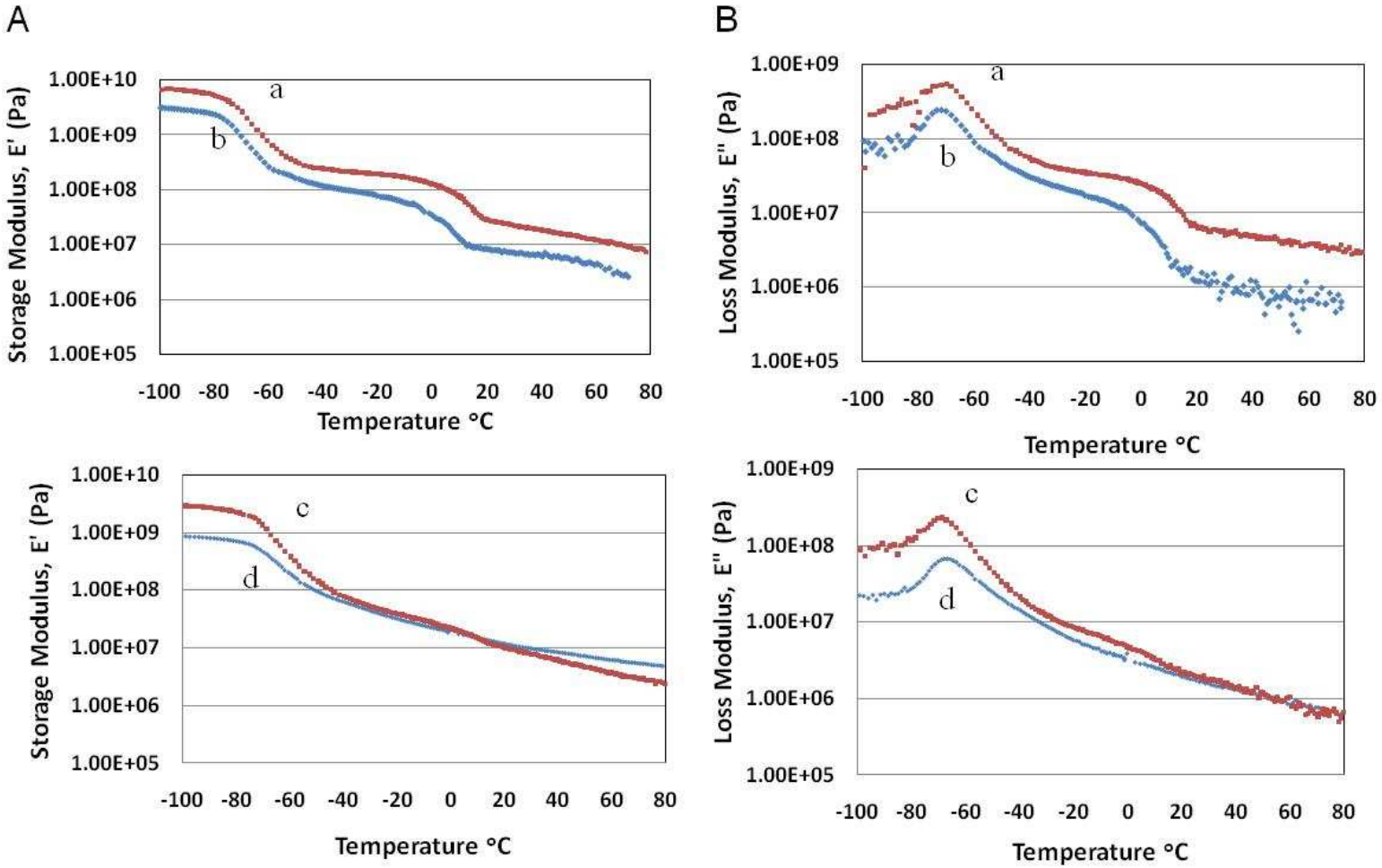

Figure 1.11. Storage and loss moduli vs. temperature: A) Storage Modulus, E' , a) HMDI-(BD/GL-2.1)-PTMO (2000). b) HMDI-BD (30wt%)-PTMO (2000), c) HMDI-(BD/GL-2.5)-PTMO (2000), d) HMDI-(BD/GL-2.3)-PTMO (2000). B) Loss Modulus, E", a) HMDI-(BD/GL-2.1)-PTMO (2000), b) HMDI-BD (30wt%)-PTMO (2000), c) HMDI-(BD/GL-2.5)-PTMO (2000), b) HMDI-(BD/GL-2.3)-PTMO (2000).

Tapping mode atomic force microscopy (TM-AFM). TM-AFM was utilized to provide information on surface morphology, that is, phase separation between the hard and soft segment of the polyurethane. In TM-AFM phase images, usually a light image portion (positive phase angle) indicates a more elastic interaction of the tip with the surface, while a darker image portion (negative phase angle) indicates interactions with a soft surface feature such as the soft domain in polyurethane.[4 26 31]

As seen in AFM phase images (Figure 1.12), the as cast and annealed linear HMDI-BD (30wt%)-PTMO (2000) showed phase separation typical of polyurethanes (Figure 1.12A1-A2). In a comparison of the two phase images, the ordered hard segment domains of the as cast film are smaller and more dispersed than those of the annealed sample. Growth of the ordered domains during sub T_g/T_m annealing is analogous to Ostwald ripening and related growth processes.[32-38]

Sequentially prepared HMDI-(BD/GL-2.1) (30wt%)-PTMO (2000) showed some phase separation although not to the extent seen in the linear polyurethane. Figure 1.13B1-B2 displays a pattern in phase separation similar to what is observed with the linear polyurethane but with a less intense contrast. This lower intensity indicates that the domains are less organized as a result of the chemical crosslinks hindering the association of hard segments.

As cast samples of the HMDI-(BD/GL-2.5) (30wt%)-PTMO (2000) made via simultaneous addition of reactants showed significant phase separation with some features ranging between 200-400 nm (Figure 1.13). These features are not due to hard block domains rather the features are attributed to gel formation during ambient curing. Gel domains are areas where crosslink density is higher than other regions. The higher

density crosslink of gel domains resulted in regions of higher modulus and thus resulted in the characteristic golden-yellow features.

Sequentially prepared HMDI-(BD/GL-2.3) PTMO (2000) and HMDI-(BD/GL-2.5) PTMO (2000) showed little near surface phase separation for the as-cast samples or for samples after complete cure (Figure 1.12 C-D). Also, coatings prepared by sequential additions of butanediol and glycerol showed little evidence of gel formation at the nano and microscales. This lack of phase separation is caused by the higher crosslink density of the polyurethane chains which greatly hinders chain motions and hampers association between hard segments via hydrogen bonding.

Further analysis of the linear and fully cured crosslinked polyurethane at varying amplitude setpoint ratios showed the observed phase separation in the crosslinked sample remained constant going from softer to harder tapping as evident from Figure 1.14. Since feature attributed to hard domains at $A_o/A_{sp} = 0.95$ are more prominent than the ones seen in the phase image of the linear polyurethane at the same set point ratio, the hard segment domains of the crosslinked polyurethane are likely closer to the surface than those of the linear polyurethane. This is attributed to polymer chains in the crosslinked polyurethane having limited near surface mobility. These results in the presence of hard segment at the surface thereby making its less soft segment dominate than the surface of linear polyurethanes.

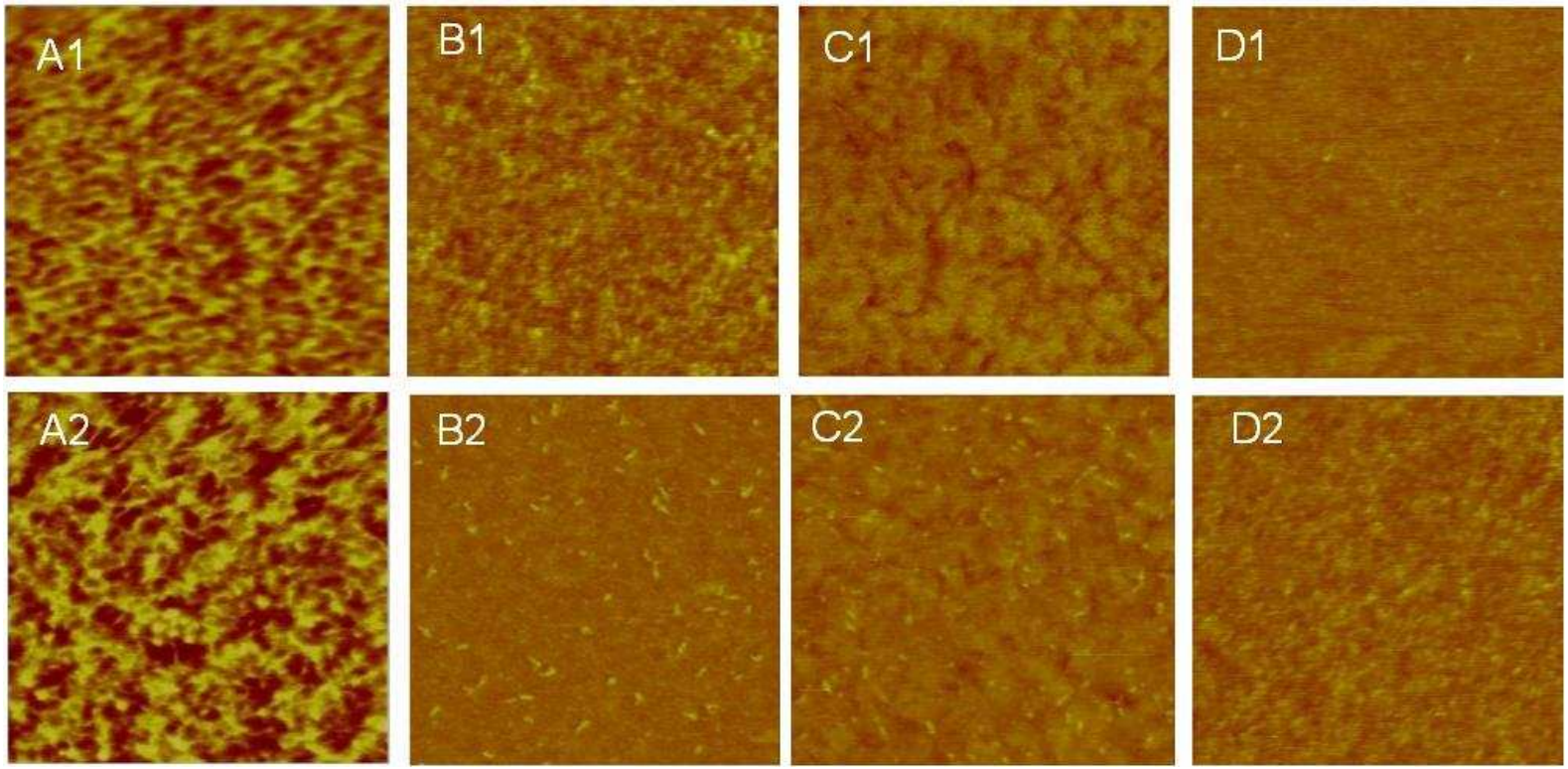

Figure 1.12. TM-AFM phase images of matrix polyurethane. Scan size 1 x 1 um, z = 30^{o} A_{sp}/A_{o} = 0.9 A1) As cast linear HMDI-BD (30 wt%) PTMO (2000), A2) Annealed (60 ^{o}C, 24 hrs) HMDI-BD (30) PTMO (2000) B1) As cast HMDI-(BD/GL-2.1) (30) PTMO (2000), B2) Cured (60 ^{o}C, 24 hrs) HMDI-(BD/GL-2.1) (30 wt%) PTMO (2000) C1) As cast HMDI-(BD/GL-2.3) (30 wt%) PTMO (2000), C2) Cured (60 ^{o}C, 24 hrs) HMDI-(BD/GL-2.3) (30 wt%) PTMO (2000) D1) As cast HMDI-(BD/GL-2.5) (30 wt%) PTMO (2000), D2) Cured (60 ^{o}C, 24 hrs) HMDI-(BD/GL-2.5) (30 wt%) PTMO (2000)

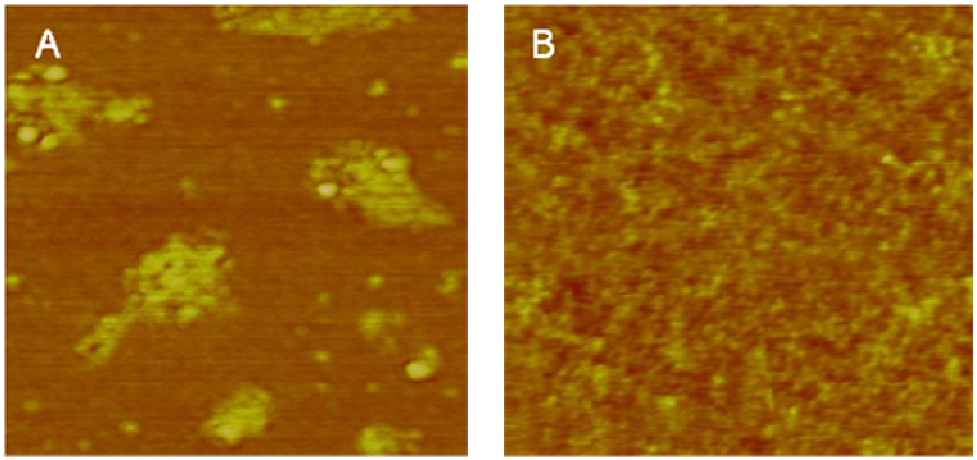

Figure 1.13. TM-AFM phase images of matrix polyurethane. Scan size 1 x 1 um, z = 30^{o} A_{sp}/A_{o} = 0.9 A) As cast HMDI-(BD/GL-2.5) (30wt%) PTMO (2000) film made by simultaneous addition of BD and GL, B) As cast HMDI-(BD/GL-2.5) (30wt%) PTMO (2000) film made by sequential addition of BD and GL respectively.

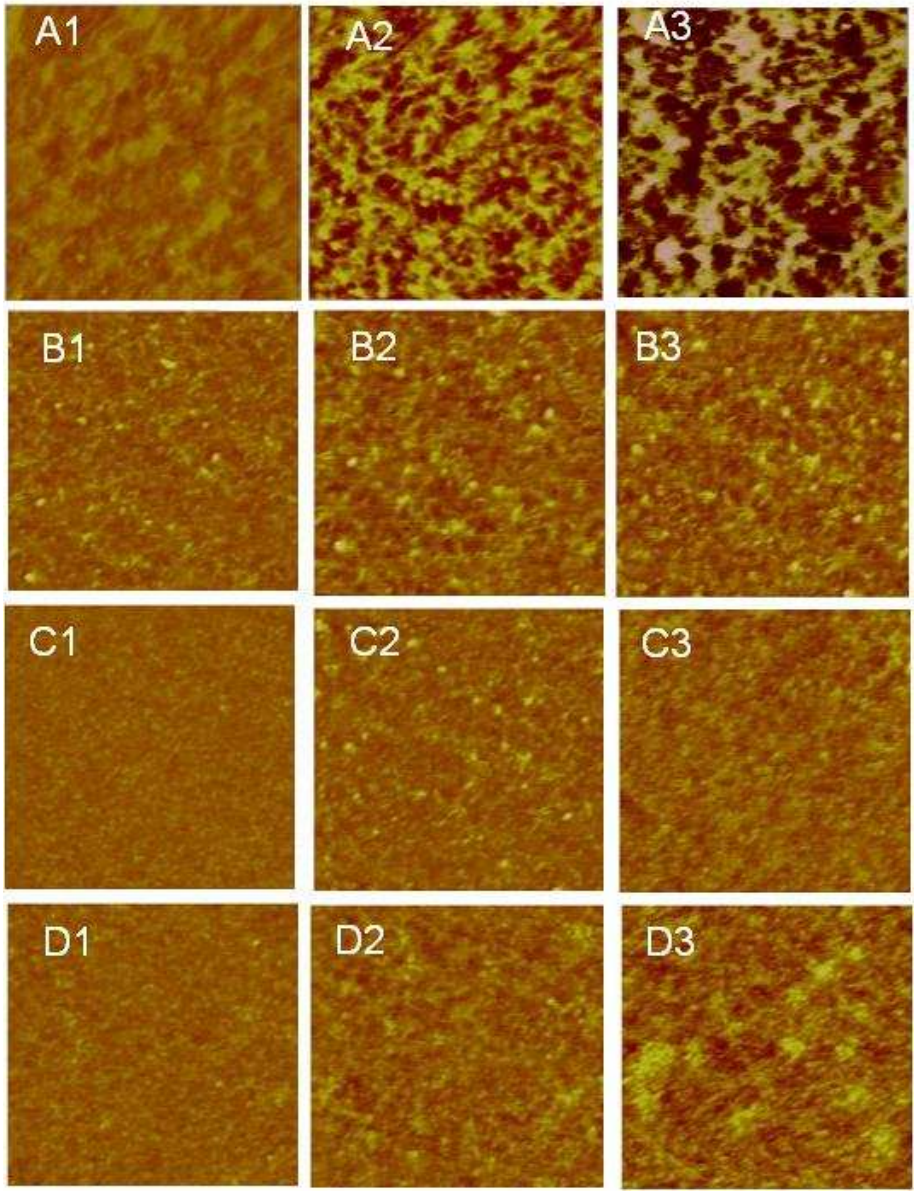

Figure 1.14. TM-AFM phase images of matrix polyurethane annealed and cured samples. Scan size 1 x 1 um, z = 30^{o} , left to right for scans 1-3 respectively, A) HMDI-BD (30wt%) PTMO (2000) A_{sp}/A_0 = 0.95, 0.9. 0.8, B) HMDI-(BD/GL-2.1) (30 wt%) PTMO (2000) A_{sp}/A_o= 0.95, 0.9, 0.8, C), HMDI-(BD/GL-2.3) (30 wt%) PTMO (2000) A_{sp}/A_o = 0.95, 0.9, 0.8 respectively, D), HMDI-(BD/GL-2.5) (30 wt%) PTMO (2000) A_{sp}/A_0 = 0.95, 0.9, 0.8

Dynamic contact angle analysis (DCA). DCA was utilized to examine the effects of crosslinking on the wetting behavior of the base polyurethanes. By understanding wetting behavior of the base polyurethanes the effects of surface modification can be better understood.

Linear HMDI-BD(30 wt%)-PTMO(2000). Figure 1.15 shows DCA for HMDI-BD (30)-PTMO (2000). The initial advancing contact angle, $\Delta\theta_{adv\text{-}1}$, for both the as cast and annealed linear polyurethanes was 94^o ($\pm 1^o$). After four immersion/emersion cycles the advancing contact angle, $\theta_{adv\text{-}5,}$ was 82^o. The receding contact angle increased from 44^o to 58^o for the same cycles. In summary, force distance curves (fdc's) for the linear base polyurethane (Figure 1.16) show that the surface gradually changes from slightly hydrophobic ($\Delta\theta_{adv} > 90^o$) to slightly hydrophilic ($\Delta\theta_{adv} < 90^o$).

The change in contact angles as a function of immersion cycle must reflect a combination of chemisorption of water and surface rearrangement. Driven by thermodynamically favorable hydrogen bonding with water, it is likely that some area fraction of near surface hard block (AFM) changes place with the soft block.

Crosslinked polyurethanes. The crosslinked PUs also showed changes in contact angle after repeated interrogation cycles. Advancing contact angles for the as cast and completely cured (60 ^{o}C) crosslinked polyurethanes ranged from 101^o-90^o while the receding contact angle range from 60^o-45^o. In general, contact angles were significantly higher (Figures 1.16-18) compared to the linear polyurethane.

From comparing the change in the advancing and receding contact angles after five immersion/emersion cycles (Figure 1.19 A and B) an interesting trend in contact angle hysteresis is observed. For samples cured at 60 ^{o}C, as the crosslink density

increases the change in the advancing contact angle hysteresis, $\Delta\theta_{adv}$ (θ_{adv} cycle 5-θ_{adv} cycle 1) decreased. This decrease in $\Delta\theta_{adv}$ is attributed to the difference in soft segment mobility between linear and crosslinked PUs. The linear PU lacks chemical crosslinks which allows the soft segment chains to have more mobility. Upon wetting, this mobility allows for the polar component of the soft segment, which may include near surface hard segment, to change conformation and interact with the water. This continued interaction over repeated interrogation cycles results in the adsorption of addition water molecules that results in increasing hydrophilicity. For crosslinked PUs, increased crosslink density decreases the soft segment mobility. This decrease in mobility hinders near surface conformational changes of the soft segments and thereby decreases the interaction of the polar components with water. This decreased interaction with water limits the adsorption of water molecules to the surface which results in lower $\Delta\theta_{adv.}$

While $\Delta\theta_{adv}$ decrease with successive immersion cycles, $\Delta\theta_{red}$ increases. Thus θ_{rec1}- θ_{rec-5} is negative. This counter-intuitive change is not understood but may be due to increasing meniscus slippage with increase water adsorption. That is, water adsorption may reduce the meniscus adhesion at the three phase contact line. This increase of $\Delta\theta_{rec}$ with increased immersion cycles will be the subject of future studies.

A)

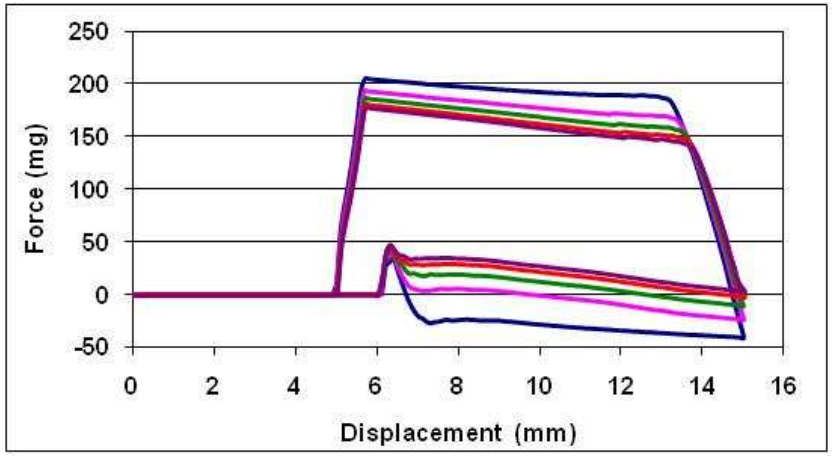

HMDI-BD (30wt%) PTMO (2000) as cast			
Cycle	θ_{adv}	θ_{rec}	Hysteresis
1	95	44	51
2	92	51	41
3	87	55	32
4	83	56	27
5	82	58	24

B)

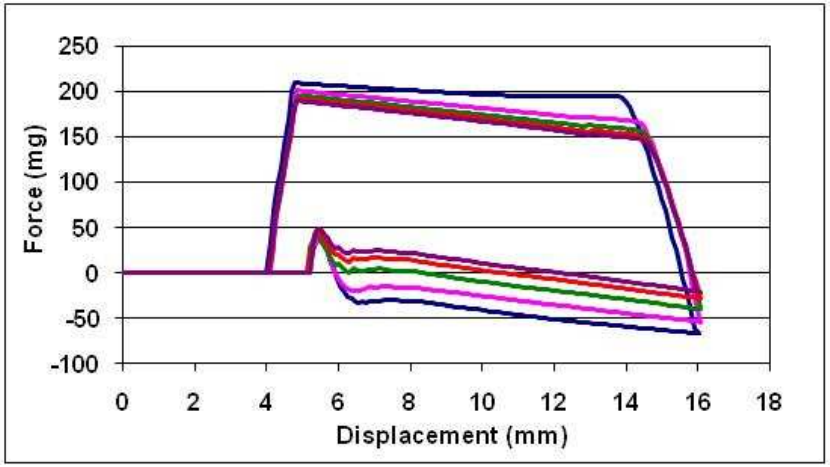

HMDI-BD (30wt%) PTMO (2000) annealed (60 °C)			
Cycle	θ_{adv}	θ_{rec}	Hysteresis
1	93	45	48
2	91	52	39
3	88	55	33
4	86	56	30
5	82	60	22

Figure 1.15. Force-Distance curve HMDI-BD (30)- PTMO (2000). A) as cast. B) Annealed (60^{o}C).

A)

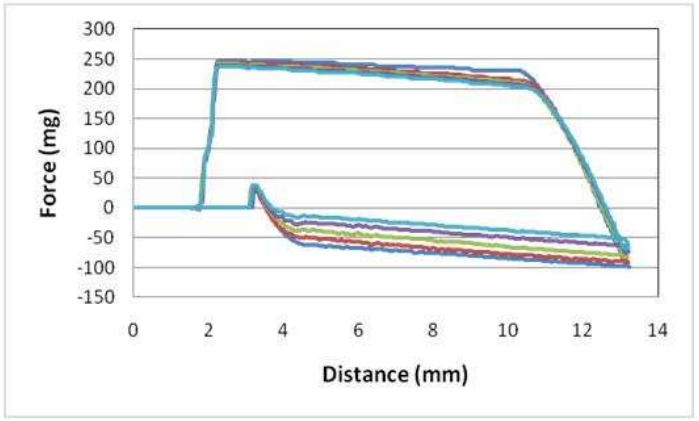

HMDI-BD (BD/GL-2.1) PTMO (2000) as cast			
Cycle	θ_{adv}	θ_{rec}	Hysteresis
1	100	41	59
2	98	41	57
3	95	42	53
4	93	43	50
5	91	43	48

B)

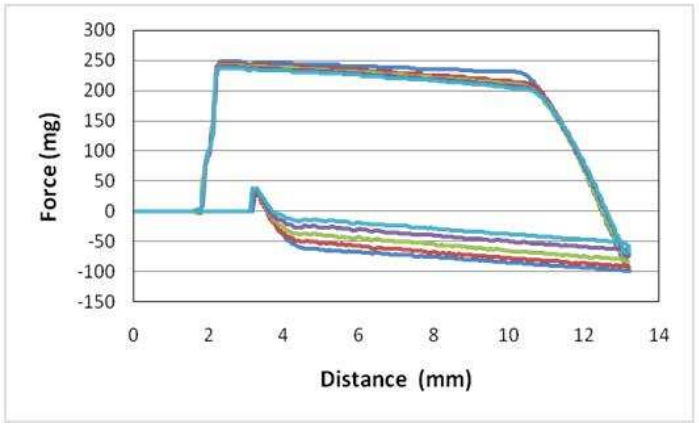

HMDI-BD (BD/GL-2.1) PTMO (2000) annealed (60 °C)			
Cycle	θ_{adv}	θ_{rec}	Hysteresis
1	97	51	46
2	89	55	34
3	85	57	28
4	84	57	27
5	84	57	27

Figure 1.15. Force-Distance curve HMDI-(BD/GL-2.1) PTMO (2000). A) as cast. B) Annealed (60^{o}C).

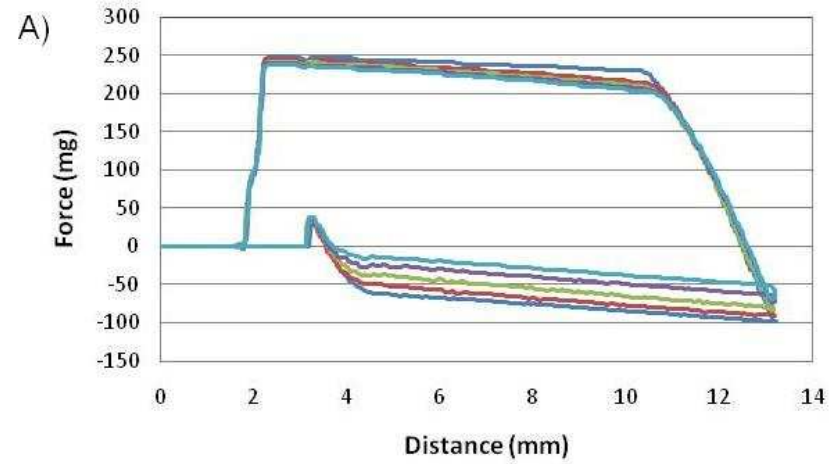

HMDI-BD (BD/GL-2.3) PTMO (2000) as cast			
Cycle	θ_{adv}	θ_{rec}	Hysteresis
1	101	42	59
2	97	41	56
3	94	41	53
4	93	43	50
5	90	44	46

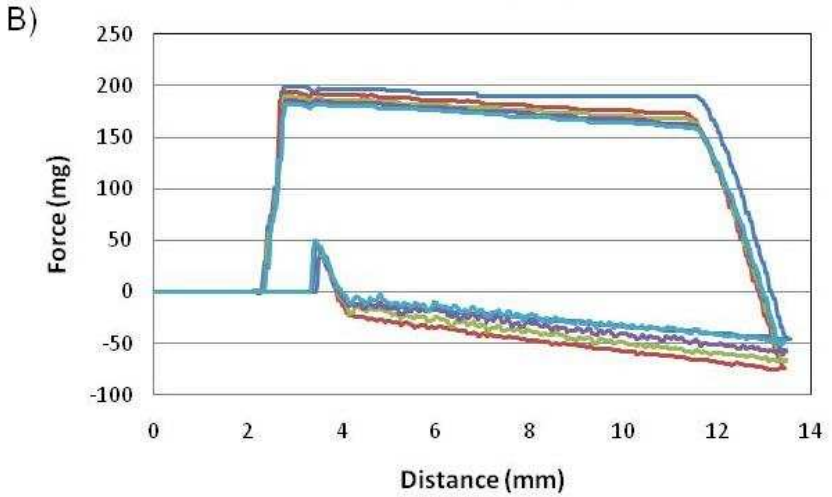

HMDI-BD (BD/GL-2.3) PTMO (2000) annealed (60 °C)			
Cycle	θ_{adv}	θ_{rec}	Hysteresis
1	95	52	43
2	93	56	37
3	91	57	34
4	91	58	33
5	90	58	32

Figure 1.17. Force-Distance curve HMDI-(BD/GL-2.3) PTMO (2000). A) as cast. B) Annealed (60^{o}C).

A)

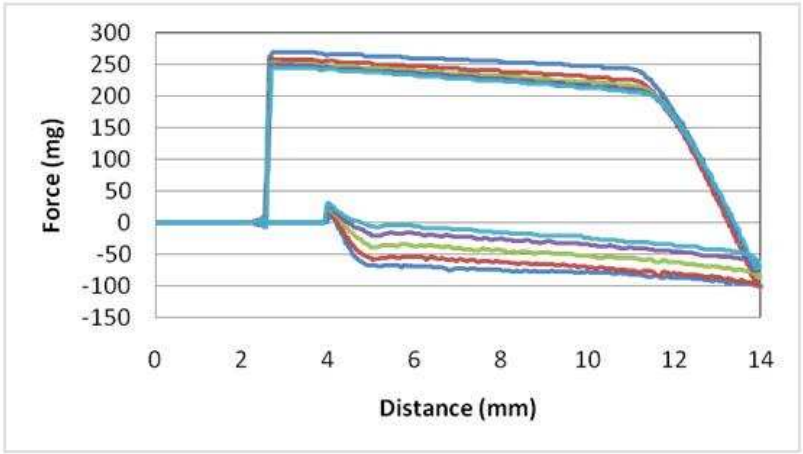

HMDI-BD (BD/GL-2.5) PTMO (2000) as cast			
Cycle	θ_{adv}	θ_{rec}	Hysteresis
1	101	35	66
2	98	38	60
3	94	40	54
4	92	41	51
5	90	42	48

B)

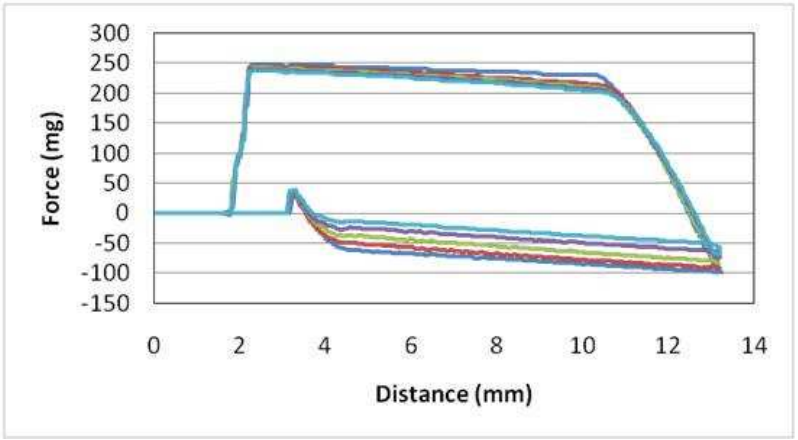

HMDI-BD (BD/GL-2.5) PTMO (2000) annealed (60 °C)			
Cycle	θ_{adv}	θ_{rec}	Hysteresis
1	92	53	39
2	94	54	40
3	92	55	37
4	91	55	36
5	91	56	35

Figure 1.18. Force-Distance curve HMDI-(BD/GL-2.5) PTMO (2000). A) as cast. B) Annealed (60^{o}C).

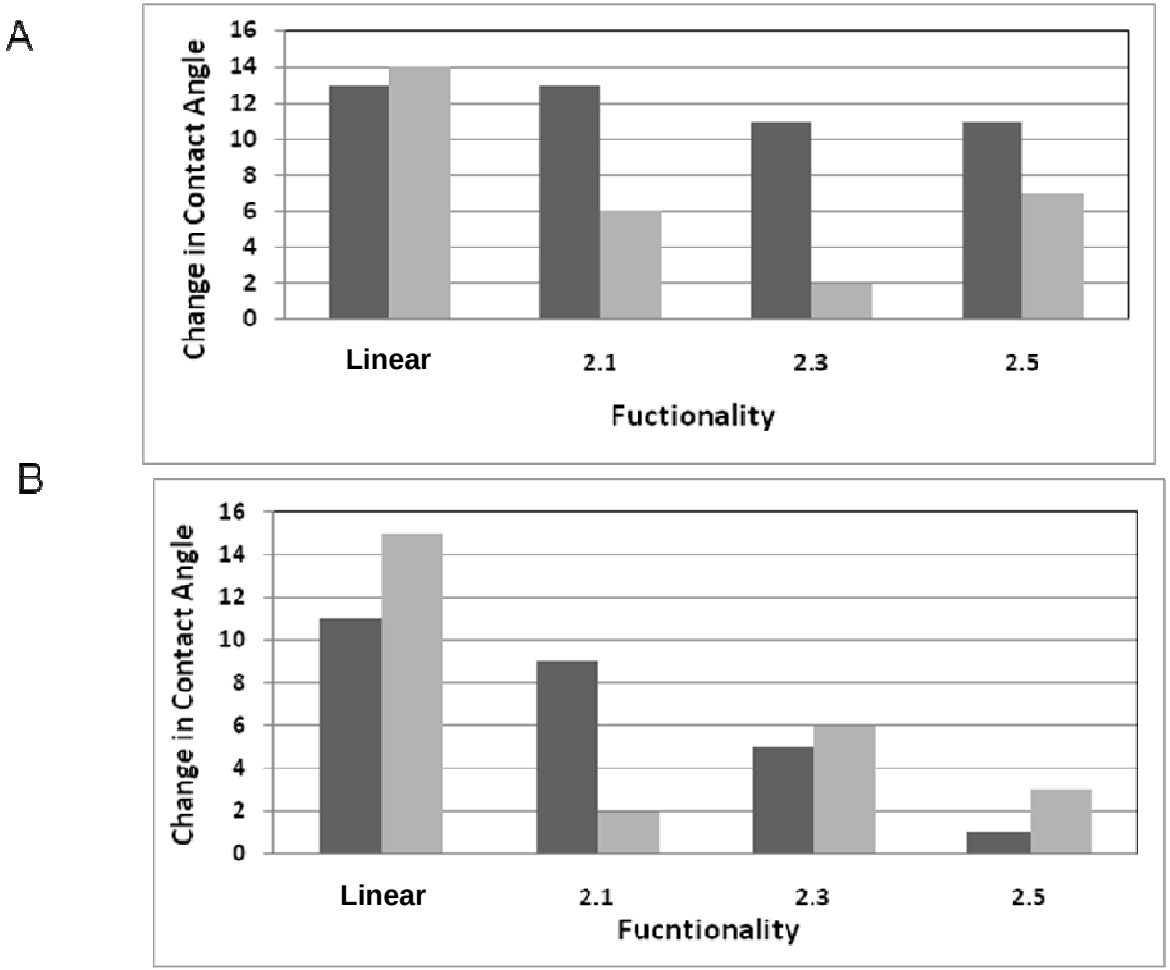

Figure 1.19. Change in advancing and receding contact angle as a function of functionality. ■ Change in advancing contact angle, □ Change in receding contact angle. A) as cast, B) annealed

Conclusion. Considering the results obtained during this study, it appears that a cross-linked polyurethane will be more suitable as a matrix for polymer surface modifiers. Uniaxial tensile testing demonstrated that the crosslinked PUs, particularly HMDI-(BD/GL-2.3) PTMO (2000) and HMDI-(BD/GL-2.5) PTMO (2000), have a significantly higher modulus of elasticity meaning that crosslinked PUs would be more mechanically durable than their linear counterparts.

As seen from DMA, the crosslinked polyurethane with 2.3 and 2.5 functionality possess better thermal stability and mechanical strength between 0-80 ºC. Unlike the linear and 2.1 functionality polyurethanes, the 2.3 and 2.5 functionality polyurethanes did not exhibit any melting or other transitions between 0-60 ºC. This type of stability in this temperature range could facilitate the stabilization of the desired surface morphology and surface chemistry.

TM-AFM data illustrated that the crosslinked PUs show little change in morphology with heating while DCA illustrated stable wetting behavior. This coupled with the DMA and tensile testing result illustrates that along with bulk stability the crosslinked base PUs possess improved surface stability compare to the linear PU. For biocidal and other surface modification applications, this may prevent surface morphological and chemistry changes, which jeopardize the surface biocidal activity.

Provided that the triol cross-linker is added last during preparation the crosslinked polyurethanes have little morphological complexity. The usual hard/soft block morphology of linear polyurethanes is suppressed due to chain immobilization. Thus crosslinked base polyurethane HMDI-(BD/GL-2.3) PTMO (2000) provides a “blank morphological canvas” that may facilitate changes in surface morphology brought about by polymer surface modifiers.

Chapter 2

Molecular weight control of random co-polyoxetane telechelics via monomer-initiator ratio.

Introduction

Functionalization of polymer surfaces focuses on creating a desired surface characteristic without altering bulk properties. Several approaches have been used to perform functionalization including grafting, coating and blending. In the work by Bernacca *et al.*, polyurethanes films utilized in artificial heart valves were functionalized via grafting (Figure 2.1A) with poly(ethylene oxide) (PEO), heparin, taurine, 3-aminopropyltriethoxysilane, or glucose or glucosamine in a study aimed at reducing thrombogenicity.[39] Results from this study showed that only a few modifiers are effective in reducing thrombogenicity overall. Surfaces modified with heparin, taurine, or the aminosilane, showed no difference in platelet activation compared to the control. High molecular weight (2000 D) polyethylene oxide reduced platelet activation slightly. Only glucose attachment to the surface produced a significant reduction in platelet activation. All the surface modifiers were effective in reducing the activation of complement C3 however the glucosamine and PEO 400 modifiers significantly increase the activation of factor XII. Overall, this study found that PEO modified surface performed well while the glucose modifier surface had the best performance.

The work of Wang *et al.* demonstrated that polyurethanes surface properties could be modified with polyurethanes consisting of PDMS soft segments and 4,4-methylene diphenyl diisocyanate-butanediol (MDI-BD) hard segments via blending (Figure 2.1B). This was done in an attempt to create polyurethane surfaces that have the heat resistant properties of silicone.[40] Thermogravimetric analysis (TGA) was utilized to

examine the thermal stability of PDMS modified polyurethane in comparison to an unmodified control. From TGA it was shown that only 15 wt% PDMS modifier was required to improve the heat resistance of the PU blend. PDMS modified samples only lost 50% of their stating weight at 500 ^{o}C while the control lost 75% of at 500 ^{o}C. This increased heat resistance hinted that surface concentration of the PDMS modifier has occurred. X-ray photoelectron spectroscopy (XPS) of the modified sample confirmed this with the appearance of a Si_{2p} peak at 102.1 eV which indicates Si-O-Si bonds.

Transmission electron microscopy (TEM) revealed that modified sample exhibited a complex surface morphology with the PDMS modifier forming distinct phase separated domains at the surface. This also is in agreement with XPS observations of surface concentration of the siloxane modifier.

McCloskey *et al.* showed that polyurethane surfaces can be functionalized with fluorous groups via blending of a "base" polyurethane-urea with a fluorinated surface modifier. [41] The latter consisted of a hexamethylene diisocyanate - polytetramethylene oxide (HDI-PTMO) polyurethane end capped with PTFE oligomers. Attenuated total reflectance-infrared (ATR-IR) spectroscopy revealed surface concentration of the modifier. In a comparison of the carbonyl region in ATR-IR spectrum for modified and unmodified samples, it was found that the addition of the surface modifier affected the nature of the hydrogen bonding in the surface layer. Spectrum from the surface modified polyurethane urea showed a noticeable increase in the in free non-hydrogen bonded urea. This indicated that there is substantial disruption of the polyurethane-urea hard segment domains within the surface layer.

This surface concentration of the modifier was also confirmed by scanning electron microscopy (SEM) study where surface features measuring 1-4 μm were

observed in modified samples while unmodified control samples were featureless. Wetting behavior of the modified samples also differed from the control samples. Advancing and receding contact angles for modified samples were around 120^o and 80^o while control samples had advancing and receding contact angles of control was 90^o and 50^o respectively. These higher contact angles for the modified samples coupled with the data from SEM and ATR-IR indicate that the low surface energy fluorous groups of the modifier has concentrated on the surface.

The work of Khayet showed that fluoropolymers similar to those developed by McCloskey containing an 4,4 methylene bis phenyl diisocyanate (MDI) could be used to modify polymer surfaces other than polyurethanes, in this case polyetherimide. From this work, it was found by X-ray photoelectron spectroscopy (XPS) that just 2 wt% of the modifier produced a surface having 15% fluorine at 90^o take-off angle (TOA) and 24 atom% at 15^o TOA.[42]

Table 2.1. Results of elemental analysis by X-ray photoelectron spectroscopy on the SMM modified and unmodified poly (etherimde) (PEI) membranes at two take-off angles. [42]

Membrane[a]	90° take-off angle				15° take-off angle			
	F (%)	N (%)	O (%)	C (%)	F (%)	N (%)	O (%)	C (%)
PEI	0	5.4	17.9	76.5	0	4.9	17.1	77.9
PEI/SMM(0)	10.4	9.4	14.1	66.0	24.7	6.3	12.0	56.8
PEI/SMM(3)	11.1	9.8	14.6	65.2	25.9	7.4	11.4	55.3
PEI/SMM(5)	14.3	10.3	12.9	62.4	29.6	7.9	9.3	53.1

[a] PEI: unmodified membrane; PEI/SMM: modified membrane; (0), (3), (5) refer to solvent evaporation time

The primary focus of this research is to modify polymer surface so that they possess biocidal capabilities. These modified materials will be utilized in the creation of contact kill biocidal polymers for use in biomedical devices such as catheters.

There are currently several methods in creating biocidal surfaces via surface modification. The work of Kilbanov focused on grafting quaternary ammonium polymers to glass surfaces.[43] The modified surfaces were created via two methods. In the first NH_2 grafted slides were acylated with acryloyl chloride. The glass bound acryloyl moieties were then copolymerized with 4-vinylpyridine to produce poly (vinylpyridine) (PVP). After polymerization the grafted PVP slide were quaternized with an alkyl bromide (propyl (C3)- hexadecyl (C16)). The second method involved the immersing NH_2 glass slide in a solution of 1,4 dibromobutane, nitromethane and triethylamine. After 2h of stirring, the slides were removed dried and place in a solution of PVP, nitromethane and hexylbromide and dried after completion of reaction.

Bacteria challenges were conducted with S. aureus culture (10^6 Colony forming units (CFU)/mL) via a spray method to simulate the airborne spread of bacteria (i.e coughing, sneezing, or breathing). After testing the biocidal activity, it was determined that quaternary ammonium modifiers with shorter alkyl chains (propyl, butyl, and hexyl) were more effective (94% kill) than modifiers with longer alkyl chains (decyl, dodecyl and hexadecyl) which proved to be ineffective. The ineffectiveness of the modifiers with long alkyl side chains is primarily due to increased incidence of chain entanglements among longer alkyl chains which from aggregated of the polymer on the surface. These aggregates prevent the modifier from interacting with the bacteria cell and thus resulting in lower activity.

In an attempt to create permanent non-leaching biocidal surfaces similar to those of Kilbanov, Lee *et. al* modified glass and paper surfaces via a grafting method which utilized atom transfer radical polymerization (ATRP) of 2-(dimethylaminoethyl methacrylate) (DMAEMA).[44] The polymer was subsequently quaternization with a bromoalkyl compound. After quaternization the surface were then subjected to bacteria challenges by placing samples in 5mL of *E. coli* or *B. subtilis* at a concentration of 10^6 CFU/mL. From the biocidal test the log reductions for *E. coli* were 3.5 for paper and 2.8 for glass while *B. subtilis* has a log reduction of 4 on both glass and paper.

Although these methods have shown to effectively create non-leaching biocidal surfaces, there are issues that make this method of modification impractical. Since the surface is modified by grafting, in order to create a device with a non-leaching contact kill surface, elaborate step must be taken to modify the surface of devices post fabrication. This can lead to issues such as incomplete surface modification due to certain intricacies in the design of the device (i.e crevices or corners). Also since an extra step is needed for grafting modifiers to existing devices, more processing equipment would be need which would increase production cost.

A better method of surface modification would be to add the modifier to the base material prior to or during the production of a device. This way, the modified device can be made in a manner similar to that of conventional unmodified device such as extrusion from the melt or solvent casting.

The work of Grapski attempted to use this method of surface modification by creating of polyurethane based polymer surface modifiers with quaternized hard segment.[21] The modifier was made via a two-step polyurethane synthesis similar to that described in Scheme 1.1. The MDI portion of the hard segment is then reacted with N,N-

bis (2-hydroxyethyl) isonicotinamide (BIN) where the pyridine ring acts as a site for quaternization. The hard segment are then quaternized with alkyl halides specifically 1-iodooctane (C8) or 1-iodooctadecane (C18).

Samples of the biocidal PU where challenged with *S. aureus* (10^7 CFU/mL) via spreading of the culture solution on the surface of coated slides. After 30 min contact time the slides were analyzed via fluorescence microscopy. Results from the bacteria challenge indicate that the biocidal surfaces killed 95% of adherent *S. aureus.* Although the modifiers exhibited good biocidal activity high water absorption was observed in many compositions (C18 absorption ~40%). Although the dry PUs exhibited good mechanical properties, wetted coating became soft and tacky. This indicates that the mechanical properties are severely compromised which would render these biocidal PUs impractically for use in a hydrated environment.

To address the impracticality of the Grapski biocidal PUs, a different approach was taken regarding the non-leaching biocidal surfaces discussed in this dissertation. This method relies on modified soft segments rather that modified hard segments. By modifying the soft segment rather than the hard segment, the likelihood of concentrating quaternary charge on the surface increases due to polyurethane soft segments preferentially segregating to the surface as mentioned in Chapter 1. This strategy therefore leaves the hard segment intake and thus allow for the hydrogen bond interaction that given polyurethanes there strength.

The functional polymer surface modifiers discussed here consist of polyurethanes with co-polyoxetane (1,3-propylene oxide) soft segments having a relatively low quaternized side chain component (Figure 2.1C). As in the research of Kurt *et al.*,[18] polyoxetane soft segments were generated via the cationic ring opening polymerization

(Scheme 2.1).[45] Initially, an intermediate copolyoxetane is generated from oxetane monomers containing a fluorous (trifluoroethoxymethyl, 3FOx) side chain and a reactive (bromobutoxymethyl, BBOx) side chain (Scheme 2.1A). Subsequently, the reactive side chain was modified by quaternization with *N, N* dimethyldodecylamine to produce a quaternary moiety on the polyoxetane soft segment (Scheme 2.1B). Prior research on these functionalized polyurethanes has shown that 2 wt% blends of polymer surface modifiers in a base polyurethane were effective at killing bacteria via contact.[18, 46] This behavior is facilitated by the 3FOx side a chain "chaperones" that surface concentrate quaternary alkyl ammonium moieties (Figure 2.1C). These quaternary ammonium moieties then interact with the negatively charged cell walls of bacteria resulting in cell death.

Prior research on these functionalized polyurethanes has shown that 2 wt% blends of polymer surface modifiers in a base polyurethane were effective at killing bacteria via contact.[18, 46] This behavior is facilitated by the 3FOx side a chain "chaperones" that surface concentrate quaternary alkyl ammonium moieties (Figure 2.1C). These quaternary ammonium moieties then interact with the negatively charged cell walls of bacteria resulting in cell death.

Although the P[AB] copolyoxetane soft block polyurethanes demonstrated effective contact biocidal activity at low weight percents, a strategy was sought to increase the efficiency of surface modification. As noted in Chapter 1, the polyurethane soft segment dominates the surface when polyurethanes are processed in air. Increasing the molecular weight of the soft segment increases the root mean square end to end distance of the soft segment and in theory increases the thickness of the soft segment domain. Therefore by having a longer co-polyoxetane soft segments in the PSM, the

thickness of PSM soft segment domain in a blend would be enhanced and thus increase near surface concentration of quaternary charge.

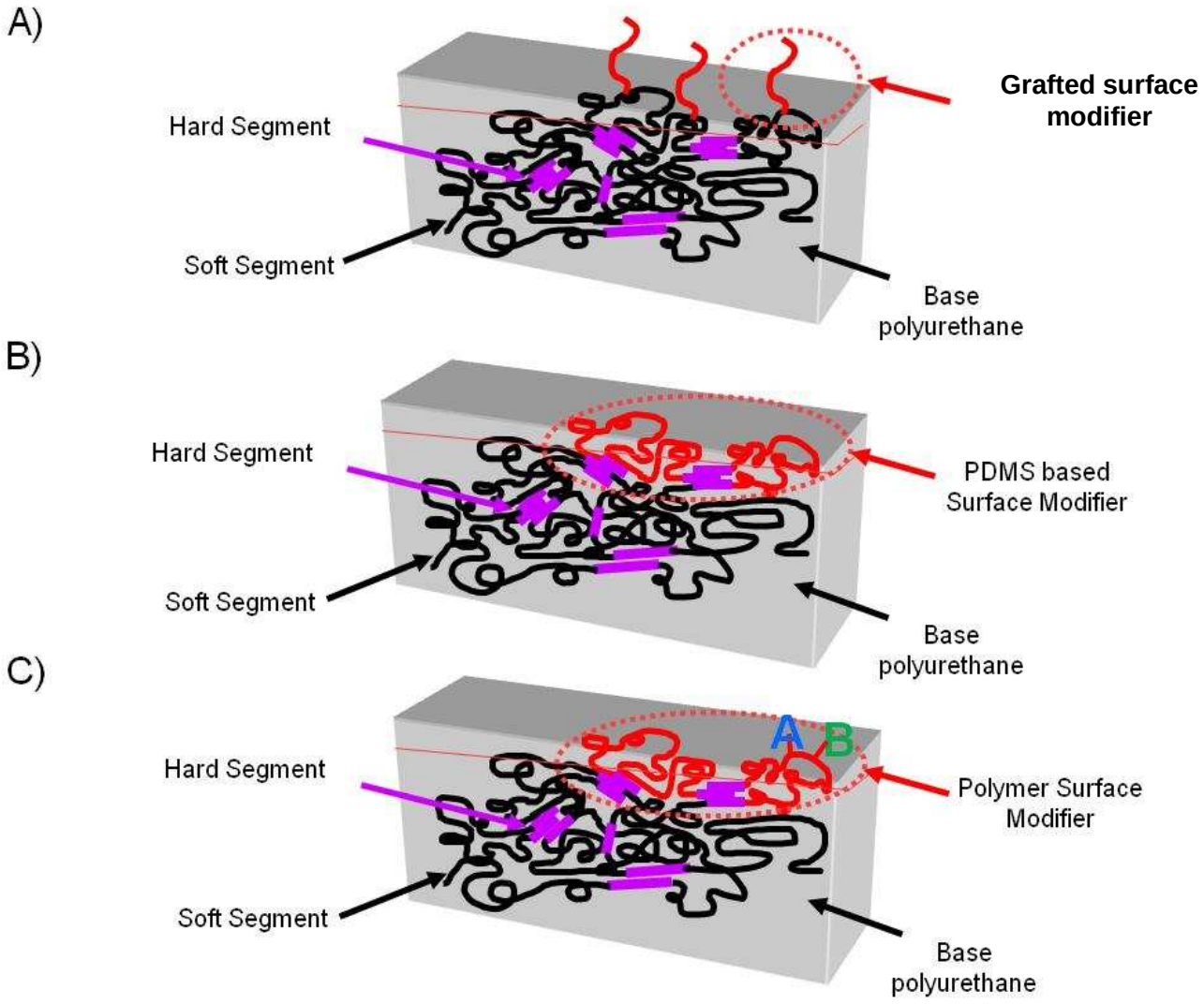

Figure 2.1. Surface modification methods. A) Grafting of modifier to surface of base material, B) Blending of PDMS-based surface modifier into base material, C) Blending of functionalized copolyoxetane PSM with base material.

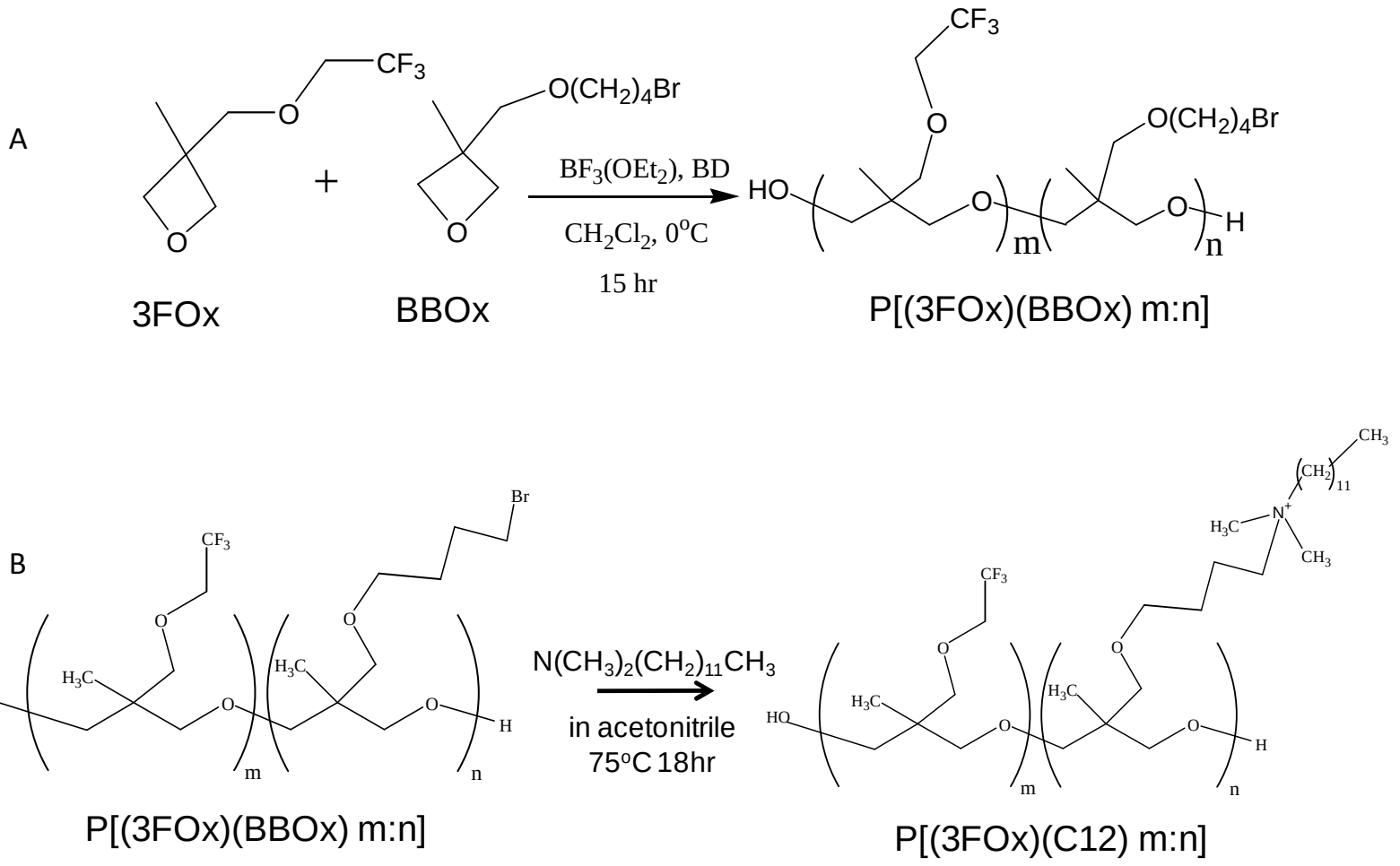

Scheme 2.1**.** Synthesis of co-polyoxetane telechelic. A) Ring opening polymerization. B) Alkyl ammonium functionalization

This chapter discusses the control of P[(3FOx)(BBOx) m:n] copolyoxetane molecular weight via manipulation of monomer to initiator ratios and the characterization these telechelics via proton NMR (^{1}H-NMR) and differential scanning calorimetry (DSC). The conversion of these telechelics to P[(3FOx)(C12) m:m] copolyoxetane according to Scheme 2.1B is also described. Finally, the incorporation of these P[(3FOx)(C12)-m:n] cotelechelics into polyurethanes is covered. These polyurethanes are the target polymer surface modifier (PSM). A subsequent chapter will further discuss the effect of telechelic molecular weight on PSM blend surface morphology.

Experimental Section

Materials. 3-(2,2,2-Trifluoroethoxymethyl)-3-methyloxetane (3FOx) was generous gift from OMNOVA Solutions (Akron, OH). *N*,*N*-Dimethyldodecylamine (C-12) was generous gift from Lonza (Allendale, NJ). Methylene chloride (CH_2Cl_2), *N*,*N* dimethylformamide (DMF), dimethylacetimide (DMAc) and tetrahydrofuran (THF) were obtained from Aldrich and dried by storing over 4 Å molecular sieves. Boron trifluoride dietherate (BF_3OEt_2), 4,4′-(methylene bis (*p*-cyclohexyl isocyanate)), HMDI dibutyltin dilaurate catalyst (T-12), tetrabutylammonium bromide (TBAB), 1,4-dibromobutane diethyl carbonate and 1,1,1 tris (hydroxymethyl) ethane were also obtained from Aldrich and used as received. 1,4-Butanediol (BD) and 2-(2-methoxyethoxy) ethanol were purchased from Acros Chemicals and used as received.

Monomers Synthesis. The BBOx precursor, 3-(hydroxymethyl)-3methyl oxetane (HOOx) was prepared via the pyrolysis of diethyl carbonate and 1,1,1 tris (hydroxymethyl) ethane as described by Pattinson.[47] BBOx was prepared from HOOx and dibromobutane via a phase transfer catalyst after Kawakami.[48]

Cationic ring-opening polymerization (Scheme 2.1A) was found to be sensitive to monomer impurities, therefore monomers were fractionally distilled under vacuum distillation with a Vigreaux column and a chilled water distillation head. Purity of monomers was determined by gas chromatography-mass spectroscopy (GC-MS) (Hewlett –Packard 6890 gas chromatograph with a 5973 mass selection detector). From GCMS, monomer purity after distillation was 99.5-99.9%.

Telechelic ^{1}H-NMR spectra were recorded using a Varian spectrometer (Inova 400 MHz). Transmission FT-IR spectra were obtained using a Nicolet 400 FT-IR spectrometer. Telechelics were sandwiched between KBr disks, while polyurethanes were solution cast on KBr disks.

Polymer Synthesis. As described previously,[18] the precursor co-telechelic was produced by copolymerization of 3FOx and BBOx via cationic ring opening polymerization to yield P[(3FOx)(BBOx)-m:n-(M_n)] (Scheme 1B). Here P indicates a telechelic polymer comprised of ring-opened 3FOx and BBOx monomers with the mole ratio m:n. The number average molecular weight is designated by M_n.

The mechanism of polymerizations is described in Scheme 2.2. After the protonation of the oxetane ring by BF_3OEt_2 (1-3), a Lewis acid catalyst, successive ring opening occurs via nucleophilic attack of the oxygen in the second monomer unit (4). From this point polymerization can proceed via two pathways. In the active chain end

(ACE) mechanism, the tertiary oxonium ion is successively attacked by the oxygen of the oxetane monomer. This results in the opening of the terminal protonated oxetane ring and the formation of another tertiary oxonium ion at the chain end. The oxonium chain end can then proceed to react with other oxetane monomer.

In the active monomer (AM) mechanism oxonium ions of monomer units are successive attacked by oxygen in the terminal hydroxyl groups. This results in the ring opening of the active monomer and the formation of another terminal hydroxyl site for continued propagation by an active monomer. Propagation is terminated by reaction with DI water to end cap the reactive sites with hydroxyl groups.

After purification and drying of the P[(3FOx)(BBOx)] telechelic, the BBOx moieties are then modified via quaternization with a tertiary dimethyl dodecylamine and subsequently used as a soft segment in the production of the polymer surface modifier.

Initiation

(1)

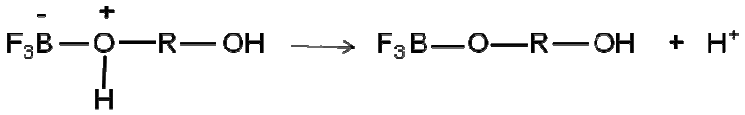

(2)

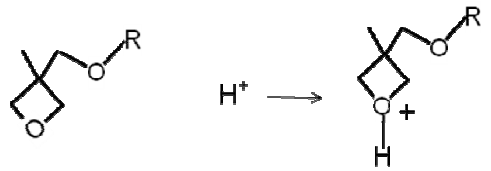

(3)

Propagation

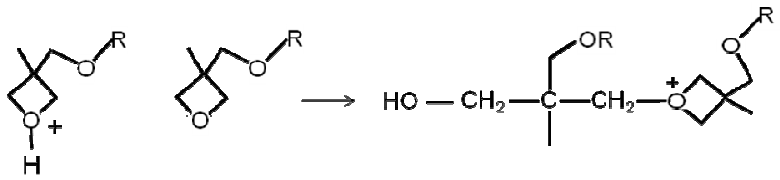

(4)

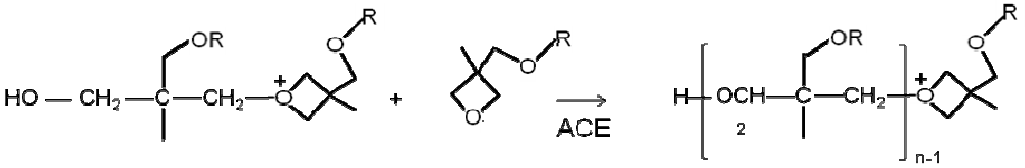

(5a)

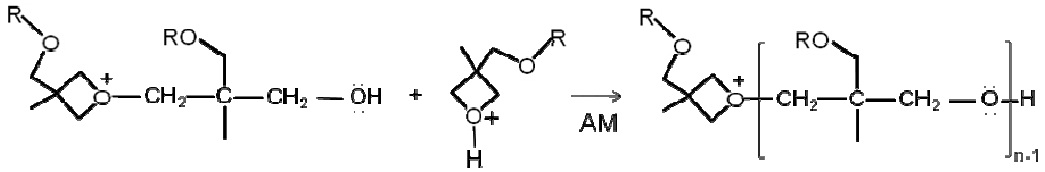

(5b)

Termination

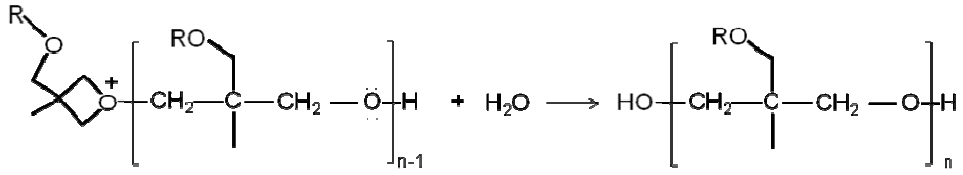

(6)

Scheme 2.2 Mechanism of cationic ring opening polymerization. R = $(CH_2)_4$-Br or CH_2CF_3.

Reaction Engineering. Previous as well as the current research discussed in this chapter involving fluorous homo and copolyoxetanes is based on synthesis techniques discovered by Malik *et al.* (U.S. patent 6,998,460).[49] In the method described by the patent, polymerization is conducted in the presence of an inert solvent, preferably a halogenated C1-C5 hydrocarbon (i.e CH_2Cl_2 or dichloroethane), a Lewis acid catalyst and initiator. As described by the patent, suitable Lewis acid catalyst are boron trifluoride complexes as well as complexes of phosphorus pentafluoride, zinc chloride, and aluminum bromide. However the preferred catalysts for fluorous oxetanes polymerization are the boron trifluoride complexes (i.e BF_3OEt_2). Suitable polymerization initiators are polyhydroxy aliphatic compounds with preference for 1,4 butanediol (BD) however, compounds such as ethylene glycol, propylene glycol trimethylolpropane and the like.

The catalyst to initiator mole ratio for effective polymerization can range from 1:1 to 5:1 however; the preferred catalyst to initiator ratio ranges between 1:1 and 2:1. The molecular weight of the copolyoxetane telechelic can be controlled by varying the monomer/initiator ratio. As described by Malik, monomer initiator ratios for producing polyoxetanes can range from 5:1 mol/mol to 300:1 mol/mol, however, the preferable range for fluorous polyoxetanes is 10:1 and 100:1. In general, lower monomer initiator ratios result in low molecular weight polyoxetanes.

Typically the catalyst, initiator and solvent are mixed for 5-10 min in the reaction vessel under nitrogen prior to monomer addition. However in the case of the telechelics discussed in this chapter the initiator was added to the monomer mixture in an initial attempt to increase copolyoxetane molecular weight. Since oxetane monomers possess high ring strain energy, the process of ring opening is very exothermic. Therefore in order

to control the reaction temperature the monomer addition is done slowly and the reaction temperature is typically kept between -10 ^{o}C and 5 ^{o}C. By adding monomer slowly and chilling the reactor the likelihood of run-away reactions and the production of monofunctional materials, typically terminated with semifluorinated chain ends for fluorous oxetanes, is observed. These monofunctional materials can act as chain terminators and thereby limit the molecular weight of the final polymer.

In previous work involving the synthesis of P[(3FOx)(BBOx)] telechelics there were problems concerning consistency in molecular weight. The prior method of copolyoxetane synthesis involved 3FOx and BBOx monomer addition to the reaction vessel via an addition funnel. The main problem with this method is that there is no control over the rate of monomer added to the reaction vessel nor was there a means of quantifying the rate of monomer addition. As mentioned above, having control of monomer addition rate is of importance because the rate of monomer addition can have an effect on the molecular weight of the copolyoxetane telechelic due to the formation of monofunctional materials.

In order to obtain scaled-up quantities of P[(3FOx)(BBOx)-87:13-(M_n)] with reproducible compositions and molecular weights a modification to the original reaction set-up was needed. This modification involved the addition of reagents by mechanical control via a programmable metering pump. Figure 2.2A and Figure 2.3 shows a process flow diagram (PFD) and picture respectively of the system utilized and identifies key components. Prior calibration of the metering pump was carried out as described in the pump manual. Upon setting the calibration flow rate (3 mL/min) the pump was set to dispense CH_2Cl_2 during a 60 s interval. After dispensing, the weight of the liquid was

measured and the volume was calculated from the density. Once the volume is determined the new value is set for the pump.

P[(3FOx)(BBOx)-87:13-(M_n)]. To produce a P[(3FOx)(BBOx)] telechelic with a mole ratio of 87:13, 3FOx (15 g, 81 mmol) and BBOx (2.85 g, 12 mmol) were added to 30 mL of anhydrous CH_2Cl_2 in a 50 mL round bottom flask (Figure 2.3). For each desired telechelic molecular weight, the initiator, butanediol was added to the monomer mixture according to the monomer/initiator mole ratios listed in Figure 2.4. This mixture was then delivered via a metering pump (0.138 mL/min) to a nitrogen purged reaction vessel which contained 30 mL of anhydrous CH_2Cl_2 and 2 mol of BF_3OEt_2 for each mole of butanediol delivered. The reaction vessel was kept at -5 ^oC during and polymerization was conducted for 15 hrs. After polymerization, the mixture was warmed to ambient temperature and quenched with 40 mL of H_2O. The organic layer was washed with 30 mL of 3 wt % HCl (aq), 30 mL of 3 wt % NaCl (aq) and 30 mL of deionized water respectively. The organic layer was placed in a rotary evaporator at 60 ^oC until CH_2Cl_2 was removed. The telechelic product was then placed in a vacuum oven at 60 ^oC for 24 hrs.

Use of the metering pump has shown to effectively deliver monomer consistently to the reaction vessel. As will be discussed later in the chapter repeat mole ratios and telechelic molecular weight were consistent with expected mole ratios and molecular weight. This consistency will increase the reproducibility of copolyoxetane telechelics synthesis and allow for better control of desired copolyoxetane composition.

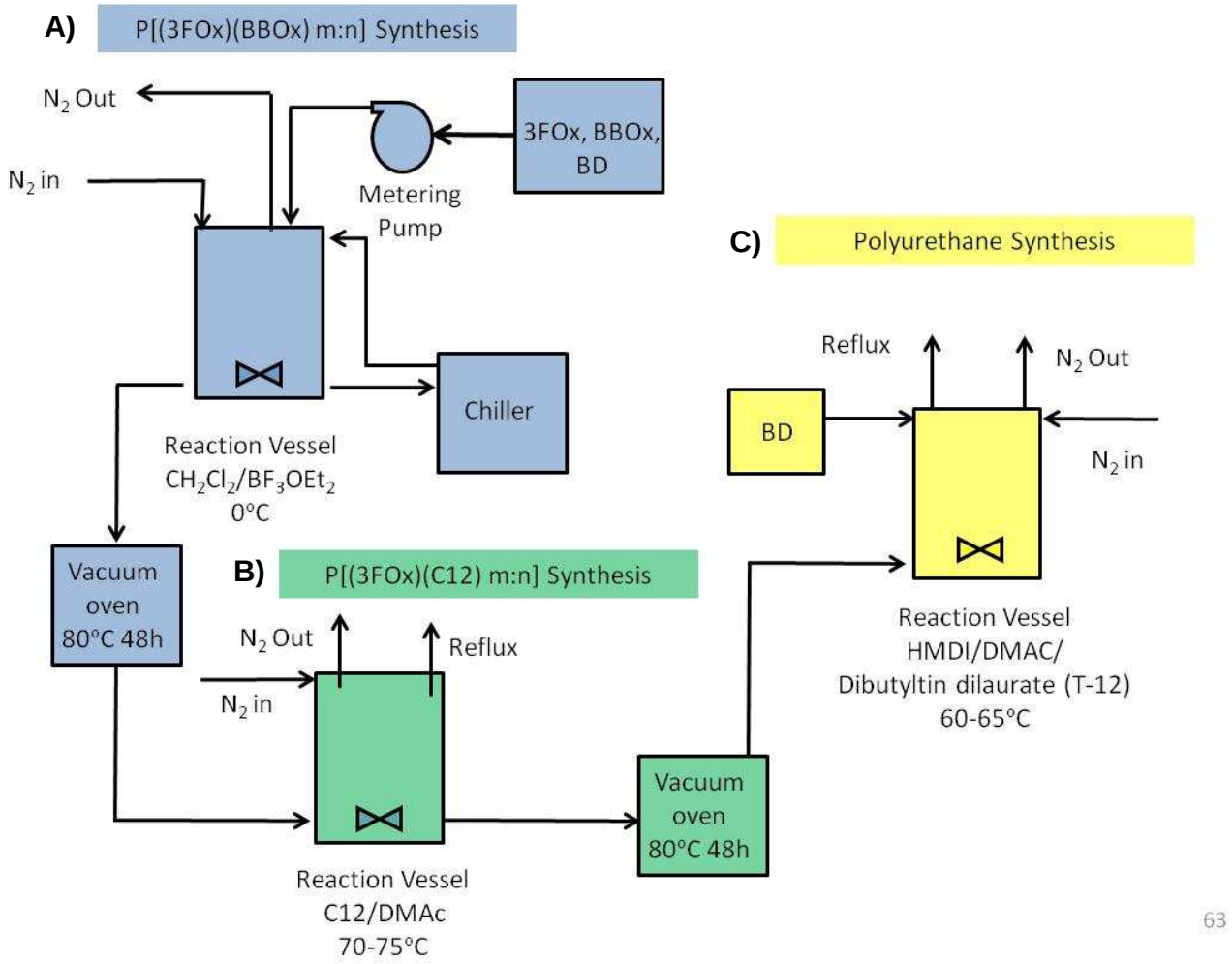

Figure 2.2. Process flow diagram of P[(3FOx)(C12)] synthesis A) P[(3FOx)(BBOx)] telechelic synthesis, B) P[(3FOx)(C12)] synthesis, C) HMDI-BD-P[(3FOx)(C12)] PSM synthesis.

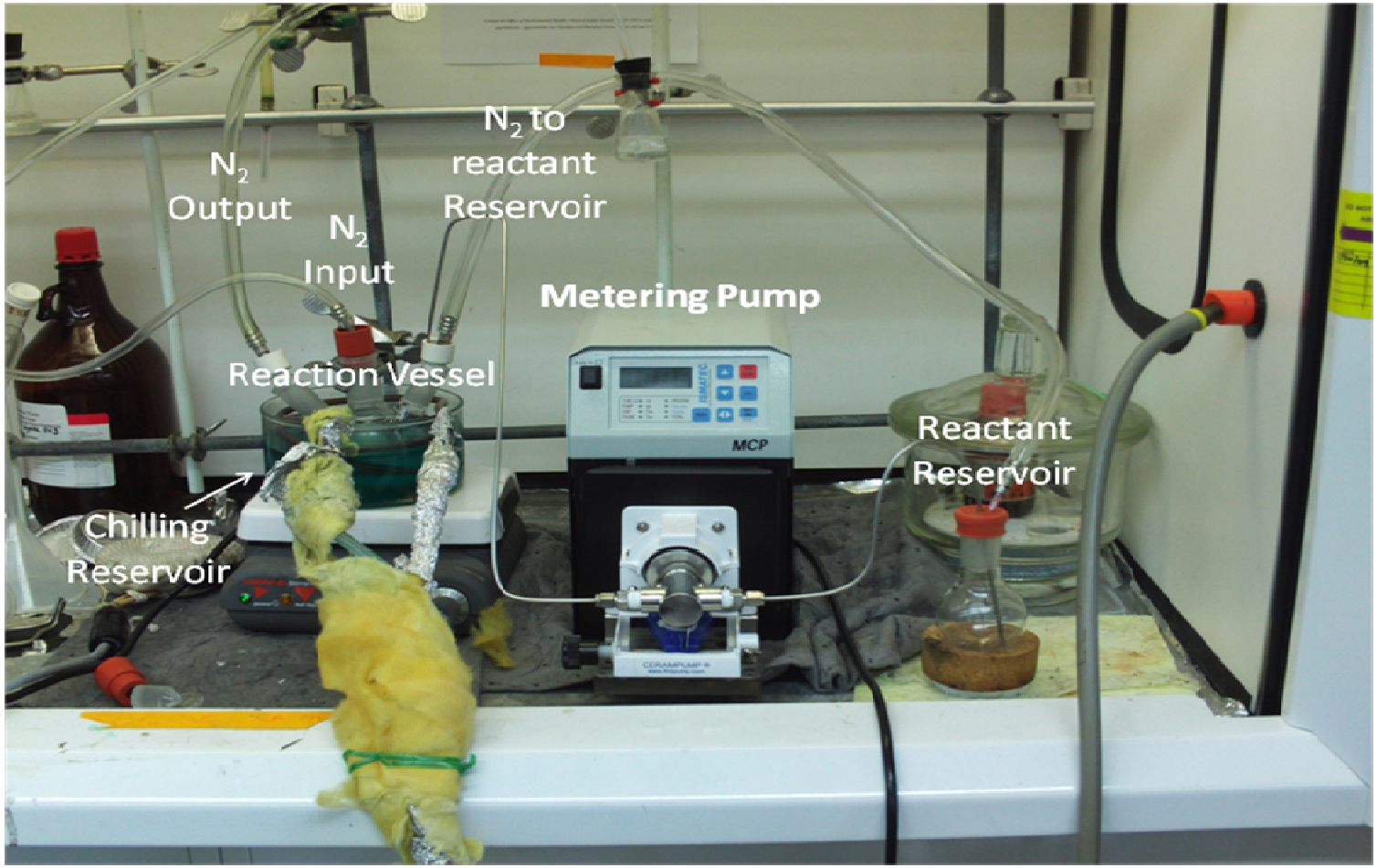

Figure 2.3. Reaction system for P[(3FOx)(C12)] synthesis.

Molecular Weight	Monomer per initiator
3500	11
5100	15
7900	20
11000	50
17900	100

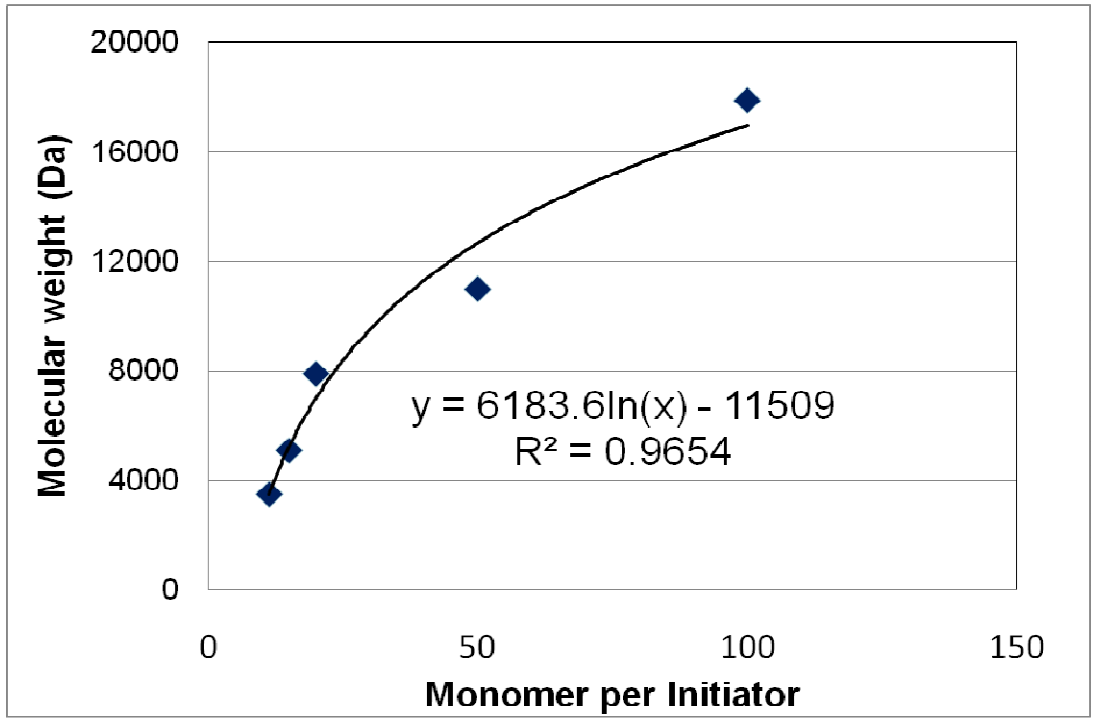

Figure 2.4. Monomer initiator ratio vs. P[(3FOx)(BBOx)] molecular weight.

P[(3FOx)(BBOx)] Mole Ratio Determination. The 3FOx:BBOx repeat unit ratio was determined using ^{1}H NMR spectroscopy. From the ^{1}H NMR spectrum, the area from the peaks corresponding to the methylene groups of the BBOx side chain (Figure 2.4, peaks A and B) as well as the total methyl area (peak C) were applied to the Eq. 1 to determine the mole faction of the BBOx methyl groups (A_{peakA} = the area of the BBOx peak A, A_{peakB} = the area of BBOx peak B, A_{peakC} = peak area of total methyl groups, $n_{BBOx_{CH_3}}$ = the mole fraction of the BBOx repeat unit).

$$\frac{3(A_{peakA} + A_{peakB})}{4(A_{peakC})} = n_{BBOx} \quad (1)$$

Since the telechelic is a binary random copolymer, the 3FOx mole faction can be determined. An example calculation is as follows.

$$\frac{3(2.23 + 2.15)}{4(24.98)} = 0.13$$

Therefore, n_{BBOx} = 0.13 and n_{3FOx} = 0.87

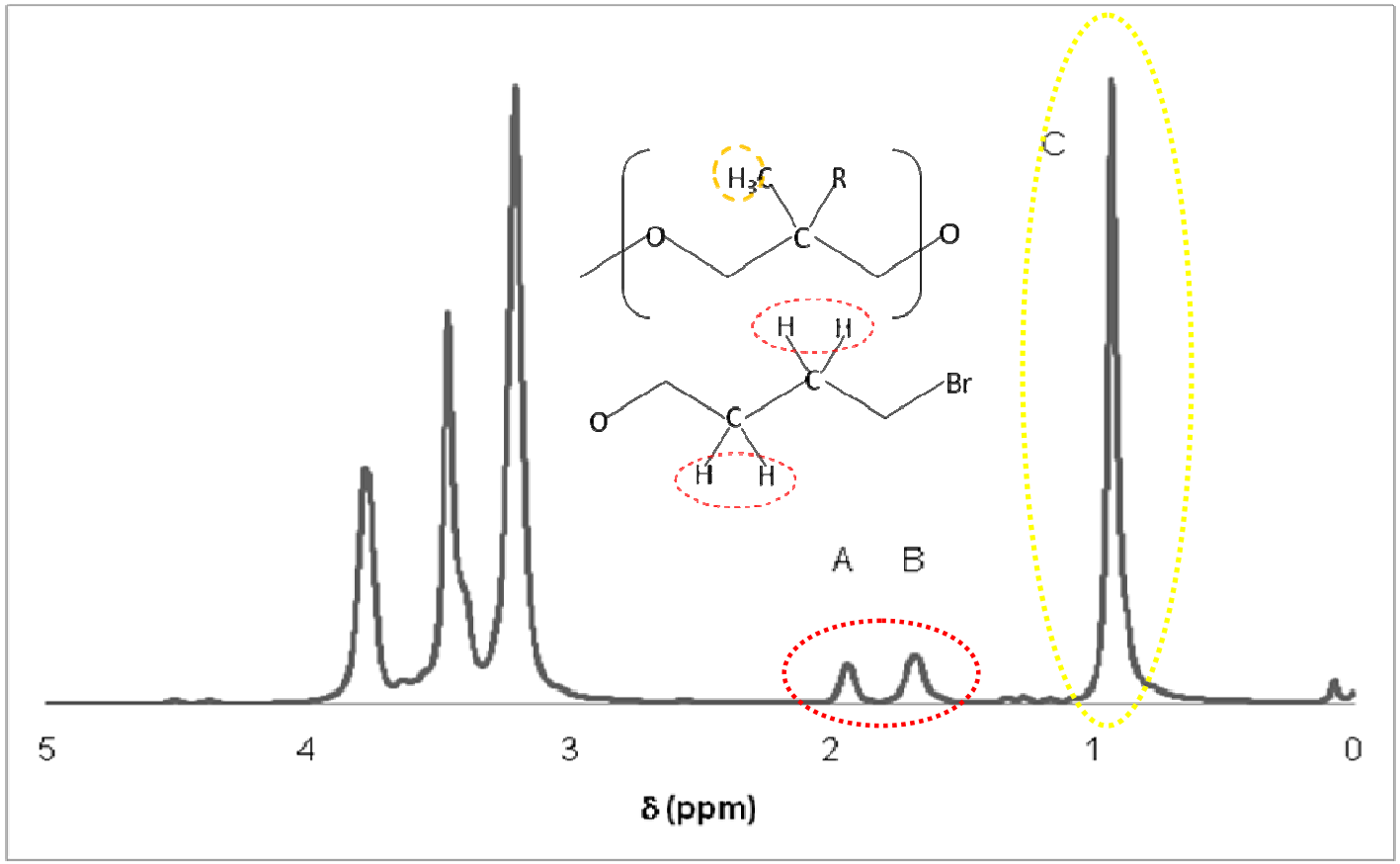

Figure 2.5. ^{1}H-NMR spectrum of P[(3FOx)(BBOx) 0.87:0.13]-5100 kDa. A and B represent the protons of the in the bromobutoxy side chain where C represents the protons of the methyl groups in the main chain.

Molecular Weight Determination. End Group Analysis. Co-telechelics (M_n) and the degree of polymerization (DP) and were determined by end group analysis, utilizing the reaction of trifluoroacetic anhydride (TFA) with co-telechelic hydroxyl end groups. An estimated 2-4 fold molar TFA excess was added to the co-telechelic solution in $CDCl_3$. The solution was then stirred at 40 °C for 1 h, and the ^{1}H NMR spectrum was obtained. Figure 2.5 shows a representative ^{1}H-NMR spectrum for end group analysis. The molecular weight of the co-telechelic was calculated with Eq. 2 where A_{TFAA} = the peak areas corresponding to methylene protons next to the fluoroacetyl group, A_{CH_3} = the 3-methyl group of the repeat unit, n_{BBOx} and n_{3FOx} = the mole faction of BBOx and 3FOx respectively, and MW_{BBOx} and MW_{3FOx} = molecular weight of the BBOx and 3FOx repeat unit respectively.

$$M_n = \left(\frac{4A_{CH_3}}{3A_{TFAA}} \right) \times \left(n_{BBOx} MW_{BBOx} + n_{3FOx} MW_{3FOx} \right) \quad (2)$$

An example calculation is as follows.

$$5100 g/mol = \left(\frac{4(25.26)}{3(1.26)} \right) \times \left(0.13(237 g/mol) + 0.87(185 g/mol) \right)$$

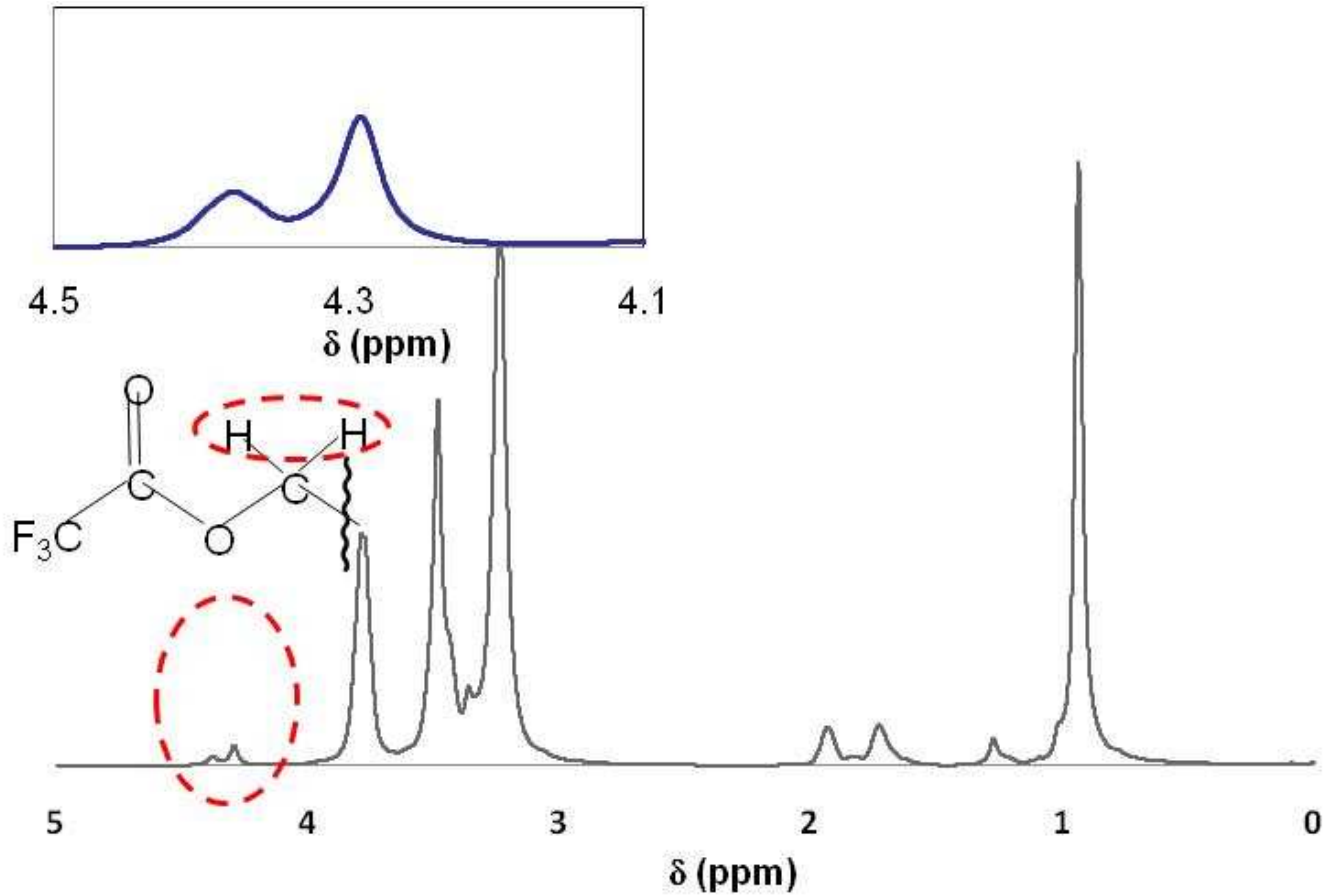

Figure 2.6. [1]H-NMR spectrum of P[(3FOx)(BBOx) 0.87:0.13]-5100 kDa after treatment with trifluoroacetyl anhydride.

Expected molecular weight were estimated using the desired monomer/initiator ratio and the expected 3FOx:BBOx mole ratio as described in Eq. 3

$$MW_{\exp} = M : I\left(n_{3FOx} MW_{3FOx} + n_{BBOx} MW_{BBOx}\right) \quad (3)$$

where MW_{exp} is the expected molecular weight, $M:I$ is the monomer/initiator ratio, n_{3FOx} is the mole fraction of 3FOx, MW_{3FOx} is the molecular weight of 3FOx monomer, n_{BBOx} is the mole fraction of BBOx monomer and MW_{BBOx} is the molecular weight of BBOx monomer. Calculated molecular weights are listed in Table 2.1. An example calculation is as follows:

$$9600 = 50/1\left(0.87(185) + 0.13(237)\right)$$

P[(3FOx)(C12)-87:13-(M_n). Quaternization of P[(3FOx)(BBOx)] telechelic is described in Scheme 2.1 B and Figure 2.2 B. Since the stoichiometric ratio of the bromide-ammonium exchange was 1:1, the moles of BBOx repeat units equaled the moles of C-12 needed to complete the substitution. To ensure complete substitution, a 1.5 x excess of dimethyldodecyl amine was used. Once each required quantity of (C-12) was determined it was reacted with 4 g of the corresponding molecular weight P[(3FOx)(BBOx)] at 70 ^{o}C for 24 hrs in acetonitrile. After completion of the reaction, the solution was slowly heated at 60 ^{o}C to remove solvent. The P[(3FOx)(C12)] co-telechelic was then dried in a vacuum oven at 60 ^{o}C for 24 hrs.

HMDI-BD (30wt%)-P[(3FOx)(C12)] (PSM). As seen on Scheme 2.3, HMDI-BD (30wt%)-P[(3FOx)(C12)] with a two-step polyurethane reaction similar to that described in chapter 1 (Scheme 1.2). 4 g of P[(3FOx)(C12)-87:13] telechelic was dissolved in 5 g of DMAc and added to a three neck round bottom flask containing ~1.35 g of HMDI. After addition of 5 drops of dibutyltin dilaurate (T-12) catalyst, the solution was heated to 60-65 ^{o}C under nitrogen purge. The progress of the prepolymer reaction was followed using FT-IR and observing the appearance of carbonyl peak (1716 cm^{-1}). When the carbonyl peak remained unchanged (3-4 hr) the prepolymer reaction is complete. After prepolymerization, 0.4 g of BD in 3 g of DMAc was added dropwise. The reaction temperature was maintained between 60-65 ^{o}C until complete disappearance of isocyanate (NCO) peak at 2267 cm^{-1} indicating completion of polymerization. The mixture was then added dropwise into 500 mL of DI water to precipitate the polyurethane. When emulsions were formed, NaBr was added until the emulsion was broken. The precipitated polyurethane was then washed in DI water to remove any residual NaBr.

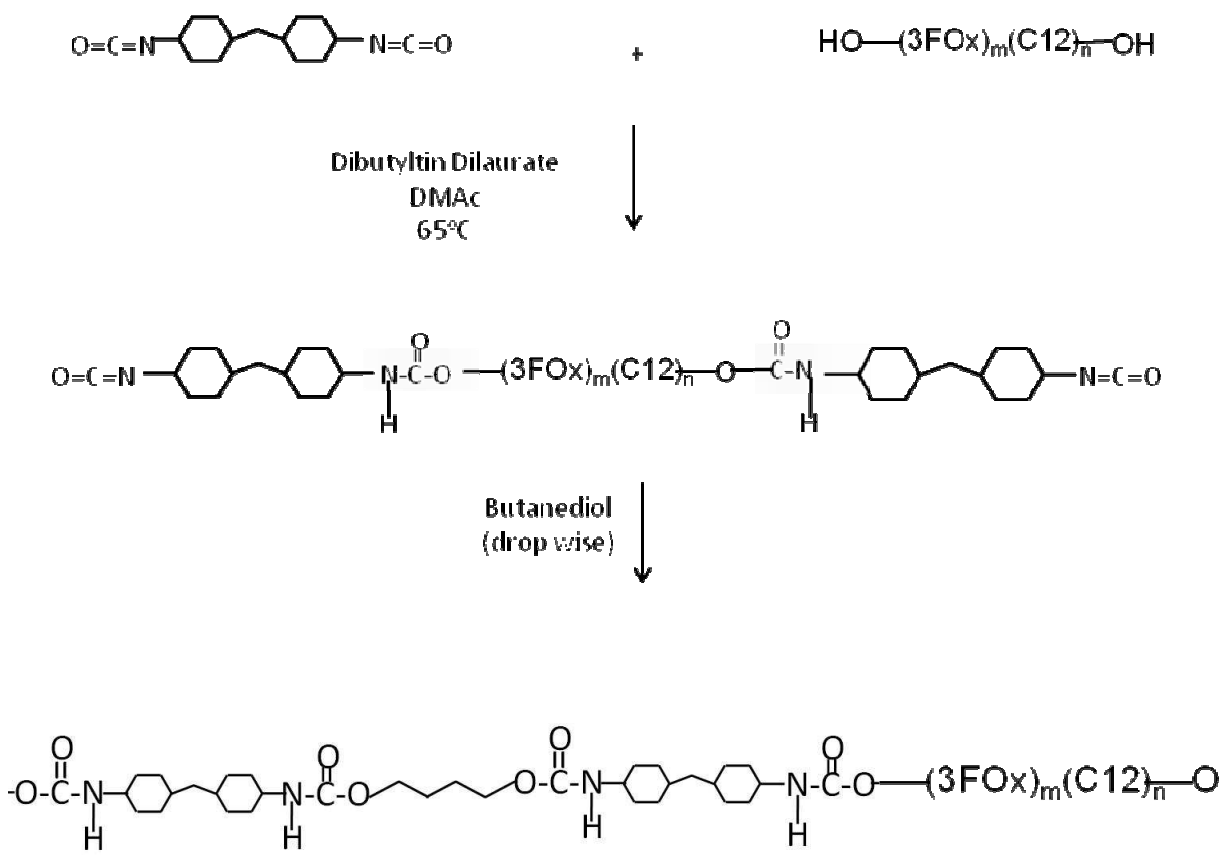

Scheme 2.3. Two polyurethane synthesis of polymer surface modifier.

Gel Permeation Chromatography. P[(3FOx)(BBOx)] as well as HMDI-BD (30wt%)-P[(3FOx)(C12)] molecular weights and polydispersities were estimated by GPC with a Viscotek TDA 302 triple detector array with polyethylene oxide standards. P[(3FOx)(BBOx)] test samples were dissolved in HPLC grade THF at concentrations between 5.8-6.4 mg/mL and passed through a 0.2 μm filter. PSM samples were prepared in a similar manner with molecular weight determined with polystyrene standards.

Thermal Properties. Temperature modulated differential scanning calorimetry (MDSC) was performed with a TA-Q 1000 Series instrument (TA Instruments) with a modulation amplitude of ± 0.5 °C, modulation period of 60 s, and heating rate of 3 °C/min from -70 to +20 °C for co-telechelics or to 100 °C for polyurethanes.

After determination of the polyurethane soft segment glass transition temperature, T_g, the Fox equation (Eq. 2) was applied to determine the extent of phase separation between hard and soft blocks.

$$\frac{1}{T_{g(cal)}} = \frac{w_{hb}}{T_{g,hb}} + \frac{w_{sb}}{T_{g,sb}} \qquad (2)$$

The weight fraction of hard and soft blocks are represented by w_{hb} and w_{sb} respectively while $T_{g,hb}$, $T_{g,sb}$, and $T_{g(cal)}$ represent the pure hard block, the pure soft block and the experimentally determined soft block glass transition temperatures.

Near Surface Morphology. The near surface morphology of HMDI-BD (30wt%) P[(3FOx)(C12)] PSMs were examined via tapping mode atomic force microscopy (TM-AFM) on a Digital Instruments Dimension 3100 TM-AFM with a Veeco Nanoscope V controller. Samples were prepared by drip coating 10 wt% PSM solutions on glass coverslips. The coatings were subsequently dried at ambient temperature for 24 hrs under vacuum. Upon complete drying, samples were scanned at an amplitude setpoint ratio (Asp/Ao) of 0.8 and a scan size of 1 x 1μm.

Results and Discussion

P[(3FOx)(BBOx)] Synthesis and Characterization. P[(3FOx)(BBOx)] telechelic was synthesized via cationic ring opening polymerization as described by Scheme 2.1. As seen in Table 2.2, the observed 3FOx:BBOx ratios for cotelechelics were close to the feed ratio of respective monomers (87:13).

The molecular weights determined by endgroup analysis were slightly higher than the theoretical molecular weights. Number average molecular weights determined by end group analysis were within ± 1.0-1.5 kDa of GPC determined values. Polydispersities (M_w/M_n) were between 1.3 and 1.7 which is similar to those observed by Kurt.[18] ^{1}H-NMR end group analysis and GPC analysis demonstrated that decreasing the monomer/initiator ratio decreased P[(3FOx)(BBOx)] molecular weight. Being able to control the telechelics molecular weight provides the opportunity to examine how polyurethanes containing soft segments with varying molecular weights used as surface modifiers affect surface morphology and biocidal activity.

Table 2.2. Effect of monomer/initiator ratio on molecular weight and experimentally determined 3FOx:BBOx mole ratio (see NMR section for discussion). The 3FOx:BBOx feed mole ratio was kept constant at 87:13. The monomer addition rate was 0.138 ml/min.

Designation [a]	Monomer/Initiator mole ratio	Calculated Molecular Weight (kDa)	NMR MW x 10^{-3} (kDa)	3FOx:BBOx Mole Ratio (^{1}H-NMR)	DP	GPC M_n x 10^{-3} (kDa)	GPC M_w x 10^{-3} (kDa)	M_w/M_n
P[(3FOx)(BBOx) 0.87:0.13-11 kDa]	50:1	9.6	11	87:13	57.4	10.1	17.2	1.7
P[(3FOx)(BBOx) 0.85:0.15-7.9 kDa]	20:1	5.2	7.9	85:15	41.2	7.05	9.17	1.3
P[(3FOx)(BBOx) 0.86:0.14-5.1 kDa]	15:1	3.1	5.1	86:14	26.6	6.49	8.86	1.4
P[(3FOx)(BBOx) 0.87:0.13-3.5 kDa]	11:1	2.1	3.5	87:13	18.3	4.46	6.74	1.5

a. M_n from ^{1}H-NMR used for MW

P[(3FOx)(C12) 87:13-M_n] Quaternization. Conversion of P[(3FOx)(BBOx) 87:13-M_n] to P[(3FOx)(C12) 87:13-M_n] was monitored by ^{1}H-NMR. From the ^{1}H-NMR spectrum full, conversion can be determined qualitatively or quantitatively. Qualitatively, the extent of substitution is assessed by peaks between 1.5 and 2.0 δ. The spectrum of P[(3FOx)(BBOx)] (Figure 2.6) has a characteristic pair of peaks (peaks A and B) which corresponds to the central methylene groups of the BBOx side chain. Upon conversion, these peaks disappear and are replaced by peaks that appear at 1.6-1.7 δ (Figure 2.7) which corresponds to the methylene groups at the β position on the alkyl ammonium chain.

Extent of functionalization can also be determined quantitatively by finding the sum of the peak areas corresponding to the γ and δ methylene groups and dividing it by the area of the β methylene peak (Figure 2.8). For telechelics with a 3FOx:C12 ratio of 87:13, $(\gamma + \delta)/\beta = 4.5$. Both qualitative and quantitative analysis revealed that the P[(3FOx)(BBOx) 87:13-M_n] was fully converted to P[(3FOx)(C12) 87:13-M_n].

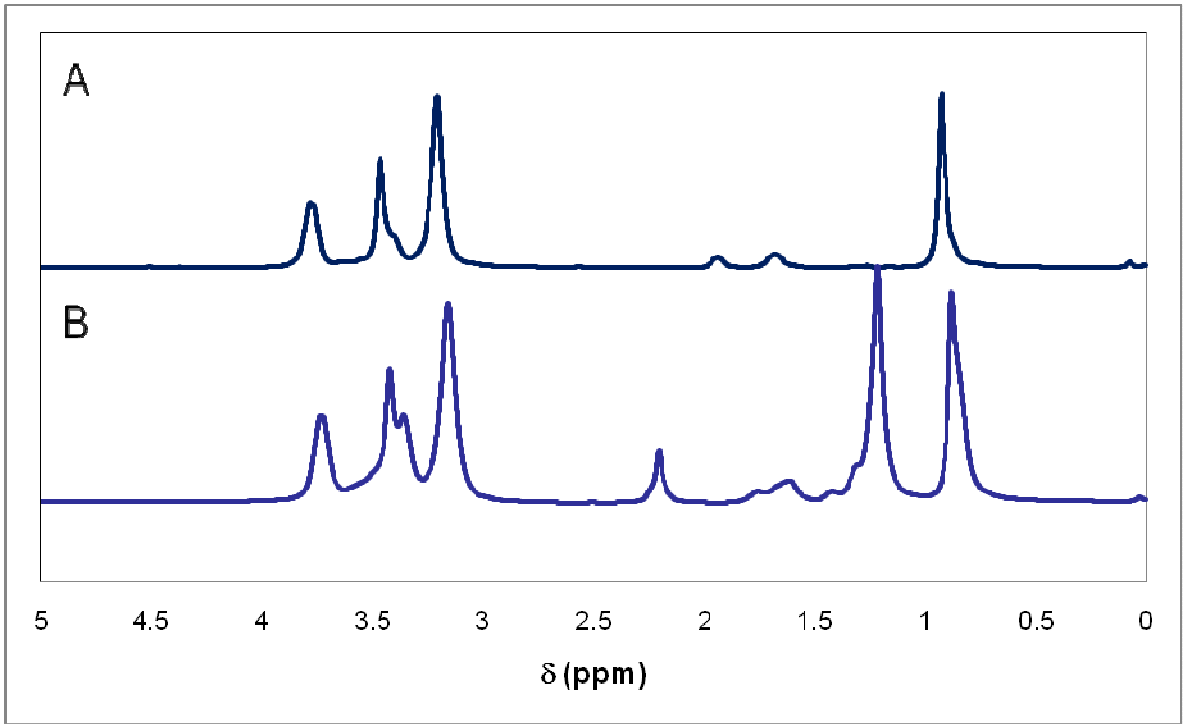

Figure 2.7 . ^{1}H NMR Spectra. A) P[(3FOx)(BBOx)-87:13-5100 Da] B) P[(3FOx)(C12)-87:13-5100 Da]

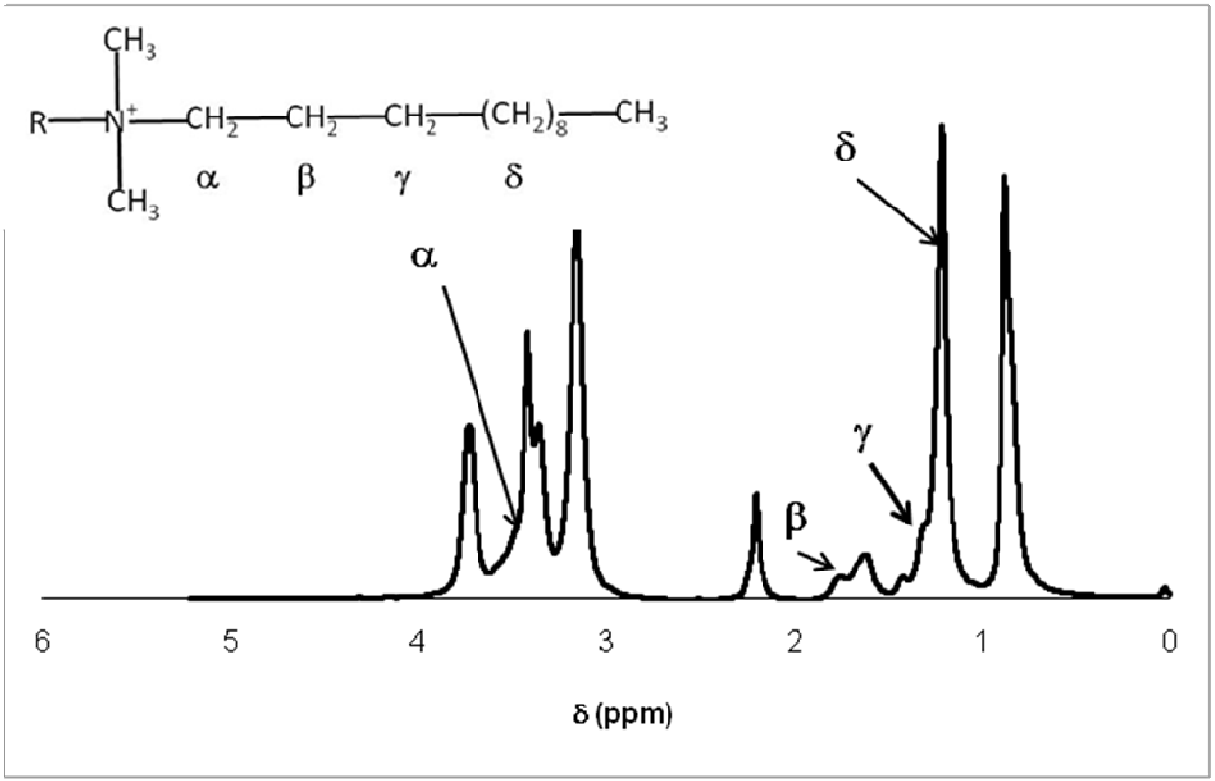

Figure 2.8. ^{1}H-NMR spectrum of P[(3FOx)(C12) 0.87:0.13]-5100 kDa .

Thermal analysis. The glass transition temperatures as determined by DSC for the 11 kDa, 7.9 kDa, 5.1 kDa and 3.5 kDa 3FOx:BBOx were -48 ^{o}C, -47 ^{o}C, -55 ^{o}C and -47 ^{o}C respectively (Figure 2.9-2.12). Upon alkyl ammonium substitution, the glass transition temperatures only showed a slight increase (-47 ^{o}C, -46 ^{o}C, -53 ^{o}C, and -46 ^{o}C respectively). This small increase, observed in prior work with similar polyoxetane telechelics, is likely associated with increased charge clustering due to quaternary cation/anion electrostatic interactions.[18]

P[(3FOx)(C12) 87:13-M_n]-PU. The PSM PU were synthesized via a soft block first, two step polymerization depicted in Scheme 2.3. PSM molecular weight (M_n = 50,000-60,000) were determined via GPC. As seen in Table 2.3, the polydispersity (M_w/M_n) is typical for polyurethanes prepared by a two step process.[19]

Table 2.3. Molecular weight of HMDI-BD (30wt%) P[(3FOx)(C12)-87:13-M_n]

M_n	M_n x 10^4 (Da)	M_w x 10^4 (Da)	M_w/M_n
3.5 kDa	4.8	8.2	1.7
5.1 kDa	5.1	7.1	1.4
7.9 kDa	6.2	8.1	1.3
11 kDa	5.5	9.9	1.8

Fox equation analysis showed good phase separation among the hard and soft segment of the PSM. As seen in Table 2.4, the 7.9 kDa and 5.1 kDa PSM the soft segment phases were composed of 98% and 99% soft block respectively while the 11

kDa and 3.5 kDa soft segment phases each contained 93% soft segment. This purity within each domain of the PSM suggest that upon processing in air, the surface would primarily consist of the P[(3FOx)(C12)] soft segment.

Table 2.4. Glass transition temperatures for BBOx and alkylammonium co-telechelics and polyurethane soft blocks.

Composition	BBOx, T_g ^oC	C12, T_g ^oC	PU Soft Block	wt fraction of pure soft block in soft segment
P[(3FOx)(C12)-3.5 kDa	-47	-46	-40	0.93
P[(3FOx)(C12)-5.1 kDa	-55	-53	-52	0.99
P[(3FOx)(C12)-7.9 kDa	-47	-46	-44	0.98
P[(3FOx)(C12)-11 kDa	-48	-47	-41	0.93

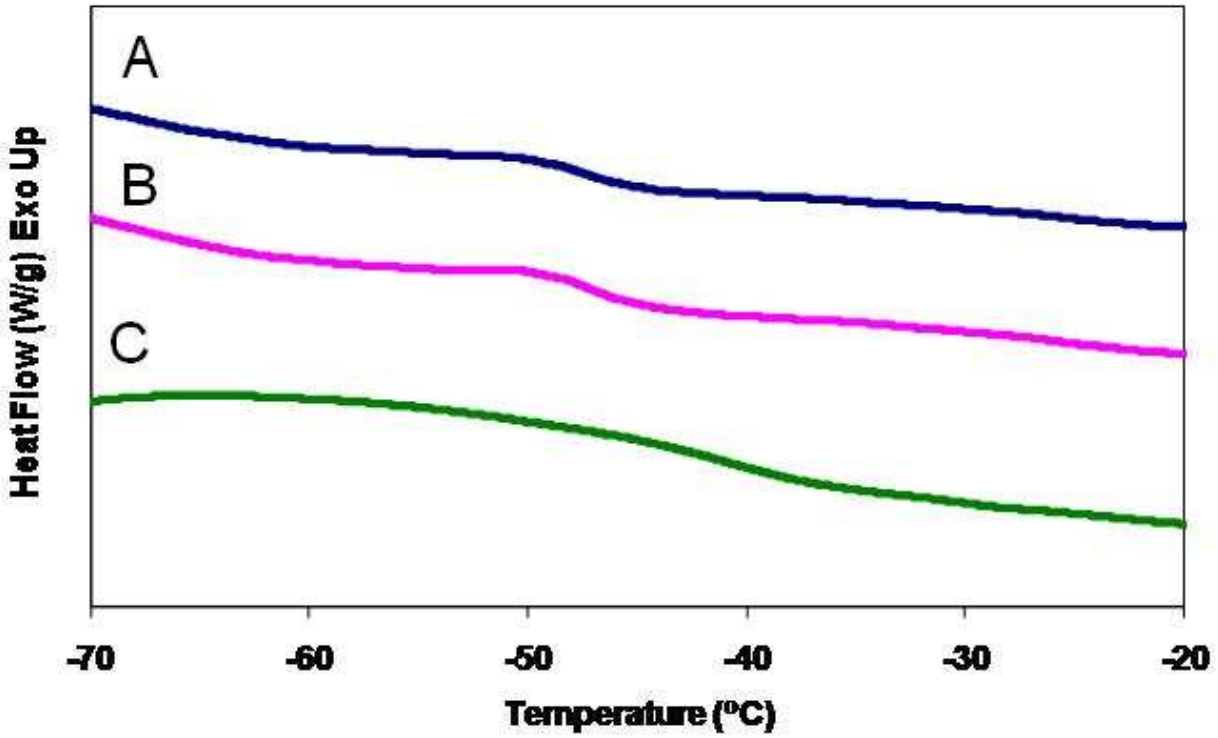

Figure 2.9. DSC thermograms. A) P[(3FOx)(BBOx)-3.5 kDa] precursor telechelic, B) P[(3FOx)(C12)-11 kDa] functionalized telechelics, C)P[(3FOx)(C12)-11 kDa] soft segment.

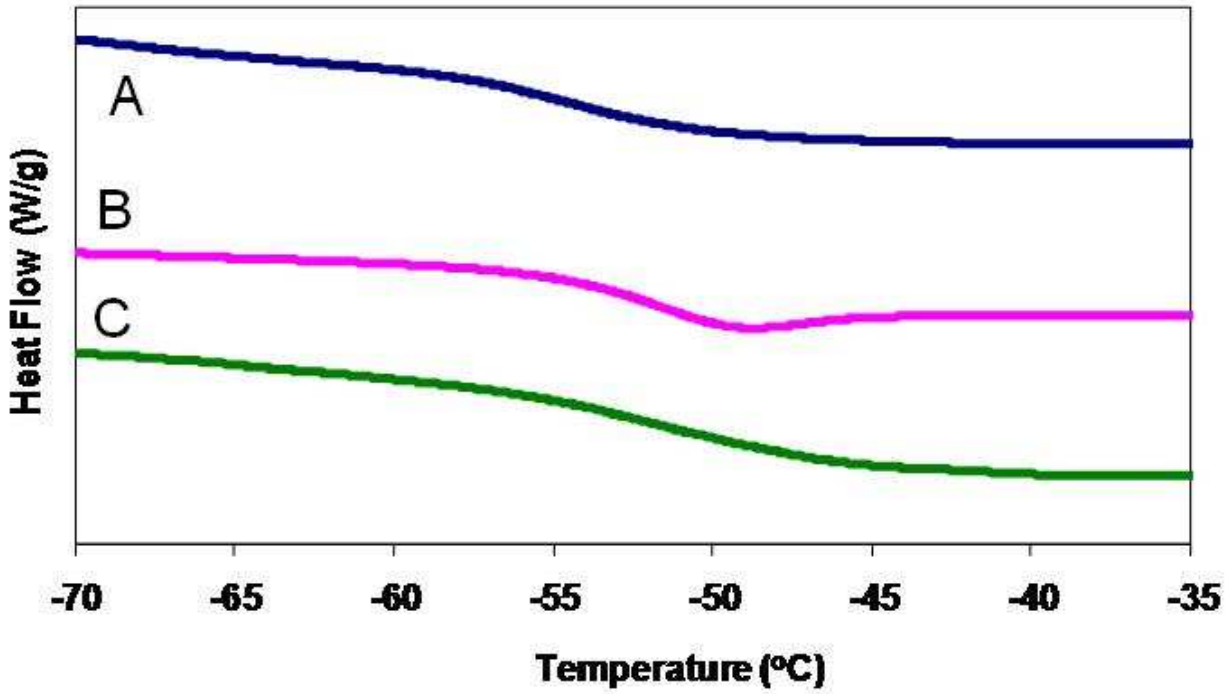

Figure 2.10. DSC thermograms. A) P[(3FOx)(BBOx)-5.1 kDa] precursor telechelic, B) P[(3FOx)(C12)-7.9 kDa] functionalized telechelics, C)P[(3FOx)(C12)-7.9 kDa] soft segment.

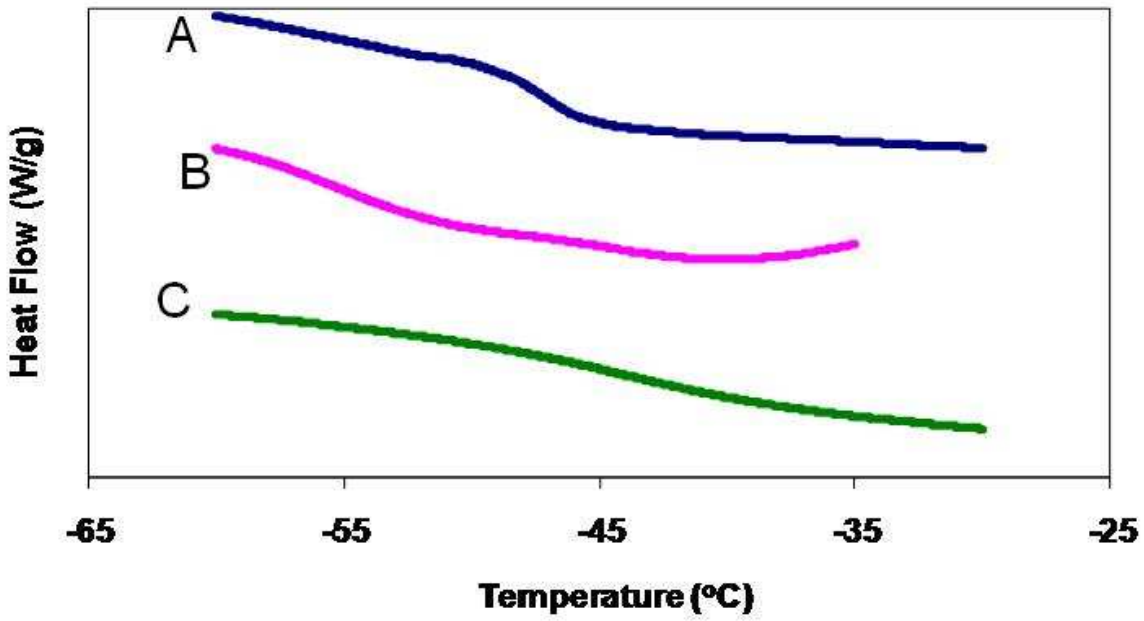

Figure 2.11. DSC thermograms. A) P[(3FOx)(BBOx)-7.9 kDa] precursor telechelic, B) P[(3FOx)(C12)-5.1 kDa] functionalized telechelics, C)P[(3FOx)(C12)-5.1 kDa] soft segment.

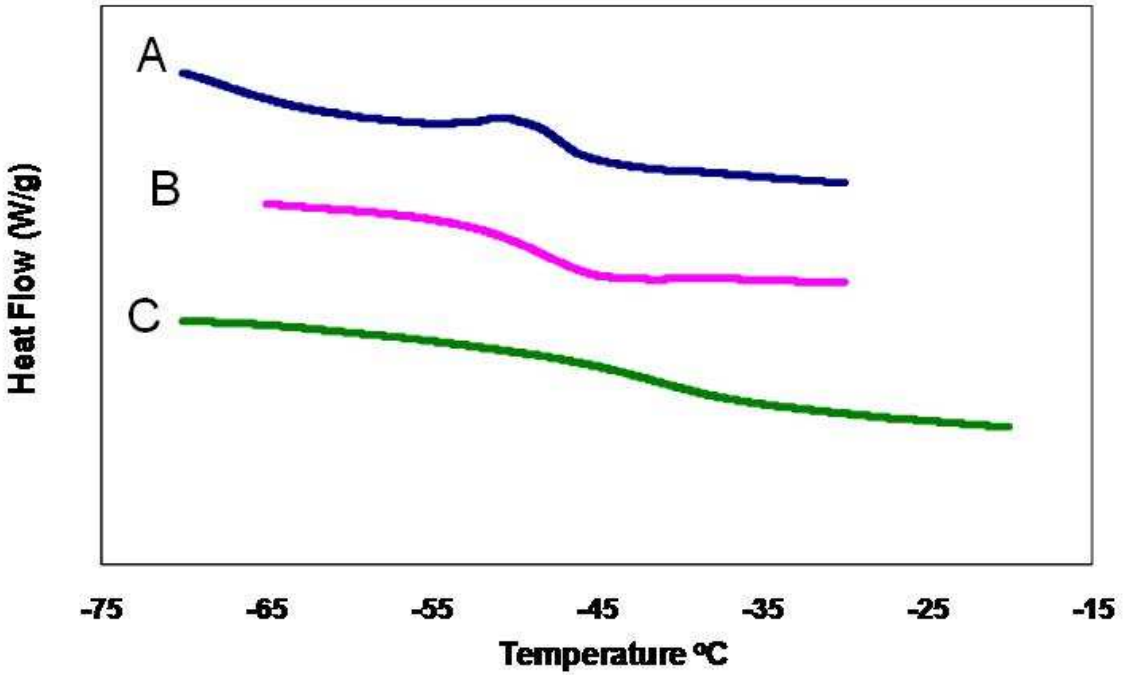

Figure 2.12. DSC thermograms. A) P[(3FOx)(BBOx)-11 kDa] precursor telechelics, B) P[(3FOx)(C12)-3.5 kDa] functionalized telechelics, C)P[(3FOx)(C12)-3.5 kDa] soft segment.

Near Surface Morphology. As seen in Figure 2.13, the near surface morphology of the HMDI-BD (30wt%) P[(3FOx)(BBOx)-0.87:0.13-M_n] PSMs displays the characteristic phase separation between hard and soft segment. In comparing the scans for each sample, it can be seen that the the definition and size of the hard segment domains increases with increased soft segment molecular weight. This increase in size and definition is due to the decreasing entropy of mixing, $\Delta S_{mix,}$ between the hard soft segment. As the soft segment molecular weight increases, it becomes less thermodynamically favorable for the soft segment chains to uncoil and blend with the hard segment. This unfavorability in uncoiling result the formation of separate hard and soft segment domains.

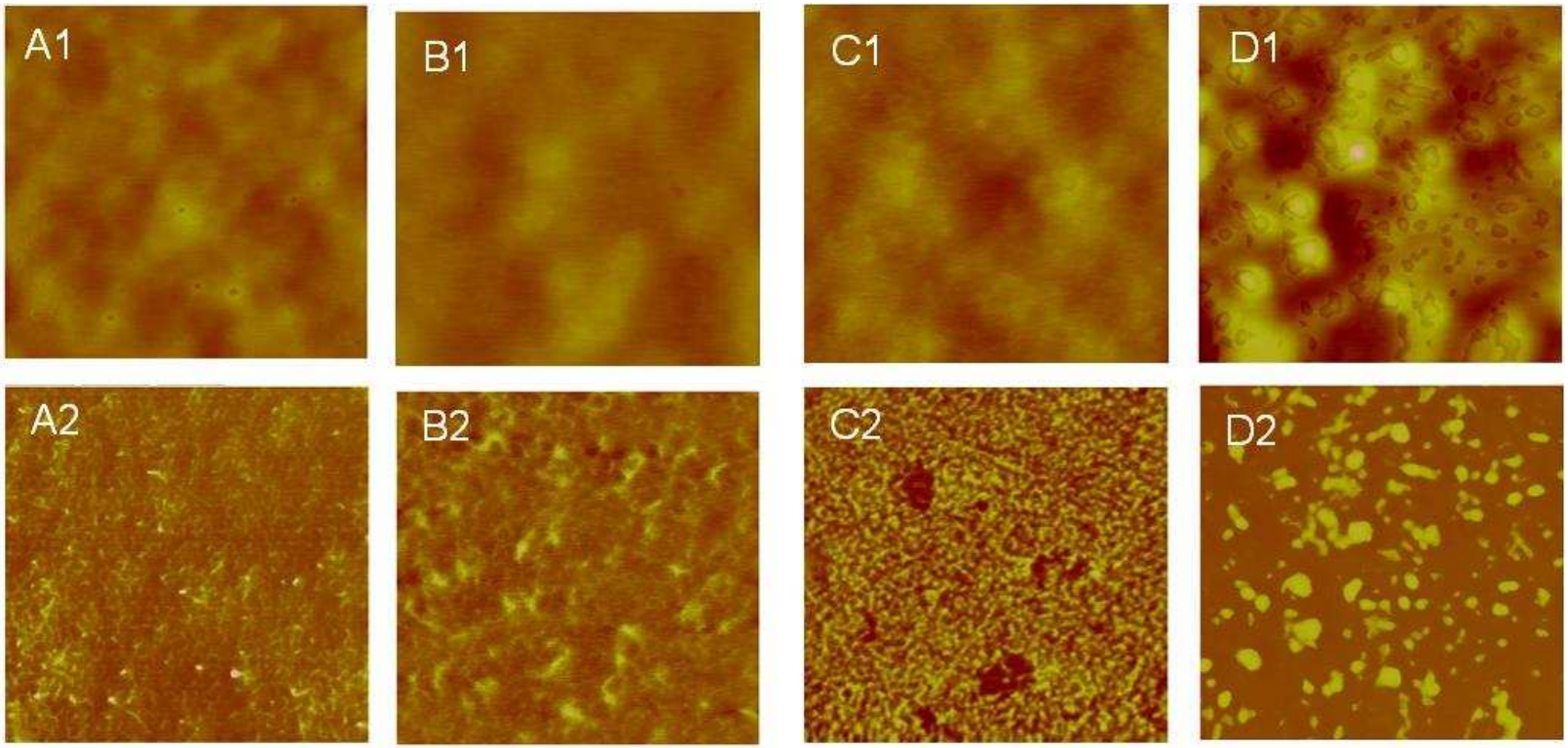

Figure 2.13. TM-AFM of HMDI-BD (30 wt%) P[(3FOx)(C12)-Mn-87:13] scan size 1 x 1 um, z = 30 nm, 30^{o} A_{sp}/A_{o} = 0.9 . A1) 3.5 kDa height image, B2) 3.5 kDa phase image, B1) 5.1 kDa height image, B2) 5.1 kDa phase image, C1) 7.9 kDa height image, C2) 7.9 kDa phase image, D1) 11 kDa height image, D2) 11 kDa phase image.

Conclusion. As demonstrated from NMR and GPC, the molecular weight of random P[(3FOx)(C12)] polyoxetanes can be controlled by varying the monomer/initiator ratio during cationic ring opening polymerization. Thermal analysis of these telechelics showed that although the molecular weight was changed significantly, the bulk thermal properties of the telechelics remained similar to those reported in previous studies of similar materials.[18] As seen with other P[(3FOx)(C12)] compositions[18] DSC indicated that addition of the alkyl ammonium side chain does not greatly affect the soft segment T_g and suggest that there is only a modest effect (Tg increases by an average of 2 ^{o}C) on segmental motion between the soft segment chains.

Fox equation analysis and TM-AFM showed that the PSMs soft and hard segment domains are well phase separated with HMDI-BD (30 wt%)-P[(3FOx)(C12) 87:13-11 kDa] displaying the most defined phase separation. This well defined phase separation suggests that the PSMs are capable of having a homogenous surface soft segment layer. Having a homogenous layer of P[(3FOx)(C12)] soft segment at the surface should, in principle, maximize the available quaternary charge thus allowing for a more effective biocidal surface.

Chapter 3

Influence of soft segment molecular weight on phase separation of fluorous-quaternary co-polyoxetane polyurethane polymer surface modifiers.

Introduction

This chapter addresses polyurethane surface phase separation involving a linear base polyurethane (PU) and a surface modifier. The base PU consists of a methylene bis cyclohexyl diisocyanate and butanediol (HMDI-BD) (hard segment) and poly (tetramethylene oxide) (PTMO) (soft segment) while the polymer surface modifier (PSM) has the same HMDI-BD hard segment and a random P[AB] copolyoxetane soft segment. A is a semifluorinated group (trifluoroexthoxy,-OCH_2CF_3, 3FOx) and B is an alkylammonium (dimethyldodecyl ammonium, C12) side chain.[46] A model of this two polymer system is shown in Figure 2.1B (Chapter 2). As discussed in Chapter 2, the objective of this research was to increase the concentration of near-surface quaternary ammonium charge by increasing the molecular weight of the PSM soft segment. Unexpectedly, in the course of examining near surface morphology by AFM and SEM, a time dependent near surface phase separation was discovered. The morphological consequences of this will be discussed.

Polymer phase separation is a phenomenon of central importance to the field and has been studied experimentally and through various modeling approaches.[50-54] Early studies of polymer phase separation relied on solid and liquid phase separation models developed by Holenberg and Halprin.[53] These proved inadequate however, because polymers have intrinsic viscoelastic properties with behavior intermediate between solids and fluids. For short deformation times, the response for polymers is typical of a solid

where stress is proportional to applied strain, while during long deformation times, polymers exhibit fluid-like behavior where stress is proportional to strain rate. Therefore polymers exhibit phase separation behavior similar to the fluid model at long time scales.[55]

Phase separation in polymers occurs via spinodal decomposition where in early stages the phase separation is governed by concentration fluctuations and decrease of bulk energy while in the latter stages, phase separation is controlled by material diffusion and the decrease surface energy.[56] Depending on the control parameters (e.g. annealing temperature and solvent evaporation rate), nano- to micro-scale morphologies vary from interconnected islands, separated dots, or line-like domains with ordered or disorder spatial orientation.[57, 58]

As described in Chapter 2, the functionalization of polymer surfaces via the use of polymer surface modifiers is a method of creating a desired surface characteristic without altering bulk properties.[39-42] Prior research on P[(3FOx)(C12)] PSMs has shown that 2 wt% blends of polymer surface modifiers in a base polyurethane were effective at killing bacteria via contact.[18, 46] Nanoscale phase separation (200 nm) was also observed. Prior research of Kurt focused on biotesting and surface science of modified coatings that were only a few days old. No connection was made between PSM phase separation and loss of contact antimicrobial effectiveness. The unexpected phase separation phenomenon that is the subject of this Chapter was discovered in studies of aging an biocidal durability over weeks.[18, 46]

Experimental

Terminology. All polymer blends analyzed in this chapter contained polymer surface modifiers (PSMs) with a random P[(3FOx)(C12)-87:13-M_n] soft segment (Chapter 1, Scheme 1.1). To examine the effects of P[(3FOx)(C12)] molecular weight on phase separation, P[(3FOx)(C12)] soft segments were synthesized at molecular weights of 11 kDa, 7.9 kDa, 5.1 kDa and 3.5 kDa (Chapter 2). To simplify the identification of blends mentioned in this paper they will be designated as q-MW-T where q is the weight percentage of the PSM and MW is the PSM soft segment molecular weight and T is the annealing temperature in degrees Celsius. The annealed temperature of as cast samples will be represented by the ambient temperature (25 ^{o}C). As an example, 0.5-3.5-25 is a base polyurethane (Scheme 1.1) with 0.5 wt% P[(3FOx)(C12) 87:13 (3500)] cast and de-volatilized at 25 ^{o}C. An important discovery was time dependent surface phase separation thus a time designation is added such as the following example: 0.5-5.1-25-2, where 0.5 = 0.5 wt% PSM, 5.1 = M_n, 25 = 25 ^{o}C casting/devolitization temperature and 2 = 2wks aging at 25 ^{o}C.

Sample preparation. PSM blend solutions were prepared by co-dissolving 0.5, 1, or 2 wt% PSM with base PU in THF in a fashion similar to Kurt et al.[46] Samples were stored at ambient temperature or annealed at 37 ^{o}C or 60 ^{o}C. Samples used for AFM were analyzed at 0, 2, 4, and 8 weeks after casting or annealing. SEM samples were cut from cast films and mounted on graphite sample stages via carbon tape.

Characterization

TM-AFM analysis. Morphological analyses were carried out using a Dimension 3100 (Digital Instruments, CA) atomic force microscope with a Nanoscope V controller. Imaging was performed in air using silicon cantilevers (40 N/m, Veeco Santa Barbara, CA). The tapping force was maintained at soft tapping by keeping the amplitude setpoint ratio (r_{sp} or A_{sp}/A_o) at 0.9 where A_{sp} is the experimental oscillation amplitude and A_o is the free oscillation amplitude. As mentioned in Chapter 1, an amplitude setpoint close to 1 allows for the measure of the true topography however there are insufficient tip-sample force interactions to produce a phase image with high contrast between regions of differing moduli. Therefore in order to distinguish between regions with different moduli (i.e. the soft and hard segment domains) r_{sp} was lowered to 0.9 in order to detect hard segment domains while not creating a height image with over exaggerated topographical features. Scans at 50 or 10 μm were analyzed using Nanoscope v710r1 software.

SEM analysis. Images of surface morphology were taken using a Hitachi SU-70 scanning electron microscope. Samples were mounted on graphite stages and analyzed without metal sputtering to insure that surface features were not concealed or altered. Since the samples were not sputter coated, analysis was done with low beam energy (1.0 kV) to prevent excessive charging. Sample working distance was set to 15 mm and no tilt was used during analysis.

Results

In the aging studies described below, samples were drip coated and devolatilized at 25 ^{o}C. These samples were either kept at ambient temperature (as cast) or annealed overnight at 60 ^{o}C (or in some cases at 37 ^{o}C). In all cases aging (0,2,4,8 weeks) was carried out at ambient temperature.

Characterization of 3.5 kDa blends

TM-AFM 0.5 and 1 wt% blend. 0.5 wt% and 1 wt% 3.5 kDa blends (t= 0) are virtually featureless (Figure 3.1 and 3.4) with the exceptions of a few 100-200 nm nanodots in the phase image of 0.5-3.5-25-0 (Table 3.1). At t = 2 wks nanodots are clearly observed in as cast and annealed films. Along with the increase development of nanodots, the formation nanopeaks and micropeaks (0.2-0.5 μm) are observed in the 3D height images (Figure 3.2 and 3.5). At t = 4wks, further coarsening of the surface morphology is observed with micropeaks of increased diameter (3-4 μm). At t = 8 wks (Figure 3.3 and 3.7) there is no apparent increase in micropeak diameter which may indicate that the morphology is beginning to stabilize. Overall, there is a trend to larger phase separated features/micropeaks with 60 ^{o}C annealed.

This stabilization of surface morphology was seen in binary polystyrene (PS)-poly (methyl methacrylate (PMMA) systems studied by Kumacheva et al. where it was observed via laser confocal fluorescent microscopy (LCFM) that PMMA rich surfaces domains grew and then froze into the final observed structures.[57]

SEM 0.5 and 1 wt% blend. SEM images for 0.5-3.5 and 1-3.5 blends confirmed morphological development seen in AFM. At t = 0 wks as cast (3.5-25) blends are featureless, but nanodots similar to those observed from AFM are seen for 3.5-60 which

indicate that phase separation has started (Figure 3.1D and H, Figure 3.4D and H). At t = 2 wks surface features began to coarsen in the same manner seen in the AFM images of 0.5 and 1 wt% blends. The phase separated features increase in size at t = 4 wks and display little further change at t = 8 wks (Figure 3.3D and H, Figure 7D and H).

TM-AFM-2wt% blend. At t = 0 wks, 2-3.5- 25 blends displayed a few nanodots similar to those observed in 0.5-3.5-25 blends (Figure 3.8). By t = 2 wks coarsening of the surface features is observed in a same manner as the 0.5 and 1 wt% blend with micropeaks 2-3 µm in diameter (Figure 3.9). At t = 4 wks and 8 wks (Figure 3.10-3.11) 2-3.5-25 showed an increase in the number of rounded features observed while the morphology observed for 2-3.5 -37 and 2-3.5-60 appeared as interconnected domains.

SEM-2 wt% blend. A similar trend in morphological features development is observed for 2-3.5 blends, but there are added complexities. At t = 0 wks (Figure 3.8D and H) SEM imaging show a complex morphology for the as cast (2-3.5-25) and annealed (2-3.5-60) blends. Nanodots observed in AFM for as cast films show that the PSM is beginning to phase separate while phase separation in the 2-3.5-37 and 2-3.5-60 progressed to the point that separate domains form. At t = 2 wks, the as cast films show larger phase separated domains similar to those observed by AFM while the annealed films developed more phase separated features with well defined boundaries between domains. At week 4, the morphology of 2-3.5-25, 2-3.5-37 and 2-3.5-60 (Figure 3.10D and H) coarsens further with the as cast film displaying interconnected domains and micropeaks of similar dimensions observed in AFM. At 8 wks (Figure 3.11D and H), the morphology of the 2-3.5-25, 2-3.5-37 and 2-3.5-60 films do not show any further

development. This parallels what was observed via AFM and indicated that the morphology was stabilizing.

Table 3.1. Observed surface morphological features for HMDI-BD (50wt%) PTMO (1000): HMDI-BD (30wt%) P[(3FOx)(C12) 87:13-3.5 kDa blends.

PSM Blends Designation	Temperature (°C)	Time (wks)	Nanodots Size (nm), Density (#/10 μm²)	Micropeaks Size (μm), Density (#/10 μm²)	Microcircles Size (μm), Density (#/10 μm²)	Interconnected
0.5-3.5	25 °C (ambient)	0	100-200, (100)	0.2-0.5, (10)	n.o.[a]	n.o.[a]
		2	100-200, (200)	0.2-0.5, (10)	n.o.[a]	n.o.[a]
		4	100-200, (200)	0.5-1, (10)	n.o.[a]	n.o.[a]
		8	100-200, (200)	0.5-1, (10)	n.o.[a]	n.o.[a]
	37 °C	0	100-200, (100)	0.2-0.5, (10)	n.o.[a]	n.o.[a]
		2	100-200, (200)	0.2-0.5, (10)	n.o.[a]	n.o.[a]
		4	100-200, (200)	1-2, (10)	n.o.[a]	n.o.[a]
		8	100-200, (100)	2-3, (10)	n.o.[a]	n.o.[a]
	60 °C	0	100-200, (100)	0.5-1, (10)	n.o.[a]	n.o.[a]
		2	100-200, (200)	0.5-1, (10)	n.o.[a]	n.o.[a]
		4	100-200, (200)	2-3, (10)	n.o.[a]	n.o.[a]
		8	100-200, (200)	2-3, (10)	n.o.[a]	n.o.[a]
1-3.5	25 °C (ambient)	0	100-200, (200)	0.2-0.5, (10)	n.o.[a]	n.o.[a]
		2	100-200, (300)	0.2-0.5, (10)	n.o.[a]	n.o.[a]
		4	100-200, (300)	2-3,(10)	n.o.[a]	n.o.[a]
		8	100-200, (300)	2-3,(10)	n.o.[a]	n.o.[a]
	37 °C	0	100-200, (200)	0.2-0.5, (10)	1-2, (5)	n.o.[a]
		2	100-200, (300)	2-3, (10)	n.o.[a]	n.o.[a]
		4	100-200, (300)	3-4, (10)	n.o.[a]	n.o.[a]
		8	100-200, (300)	3-4, (10)	n.o.[a]	n.o.[a]
	60 °C	0	100-200, (200)	0.2-0.5, (10)	2-3, (5)	n.o.[a]
		2	100-200, (300)	2-3, (10)	n.o.[a]	n.o.[a]
		4	100-200, (300)	3-4, (10)	n.o.[a]	n.o.[a]
		8	100-200, (300)	3-4, (10)	n.o.[a]	n.o.[a]
2-3.5	25 °C (ambient)	0	100-200, (100)	n.o.[a]	n.o.[a]	n.o.[a]
		2	100-200, (100)	n.o.[a]	2-3, (15)	n.o.[a]
		4	100-200, (100)	0.5-2, (50)	2-3, (30)	20-40
		8	100-200, (100)	0.5-2, (50)	2-3, (30)	20-40
	37 °C	0	100-200, (150)	n.o.[a]	10-20	n.o.[a]
		2	100-200, (200)	n.o.[a]	10-15	n.o.[a]
		4	100-200, (250)	0.5-1, (50)	15-20	20-40
		8	100-200, (250)	0.5-1, (50)	n.o.[a]	20-40
	60 °C	0	100-200, (200)	n.o.[a]	5-10, (5)	n.o.[a]
		2	100-200, (250)	n.o.[a]	5-10, (15)	n.o.[a]
		4	100-200, (300)	0.5-1, (50)	n.o.[a]	20-40
		8	100-200, (300)	0.5-1, (50)	n.o.[a]	20-40

a. n.o., not observed.

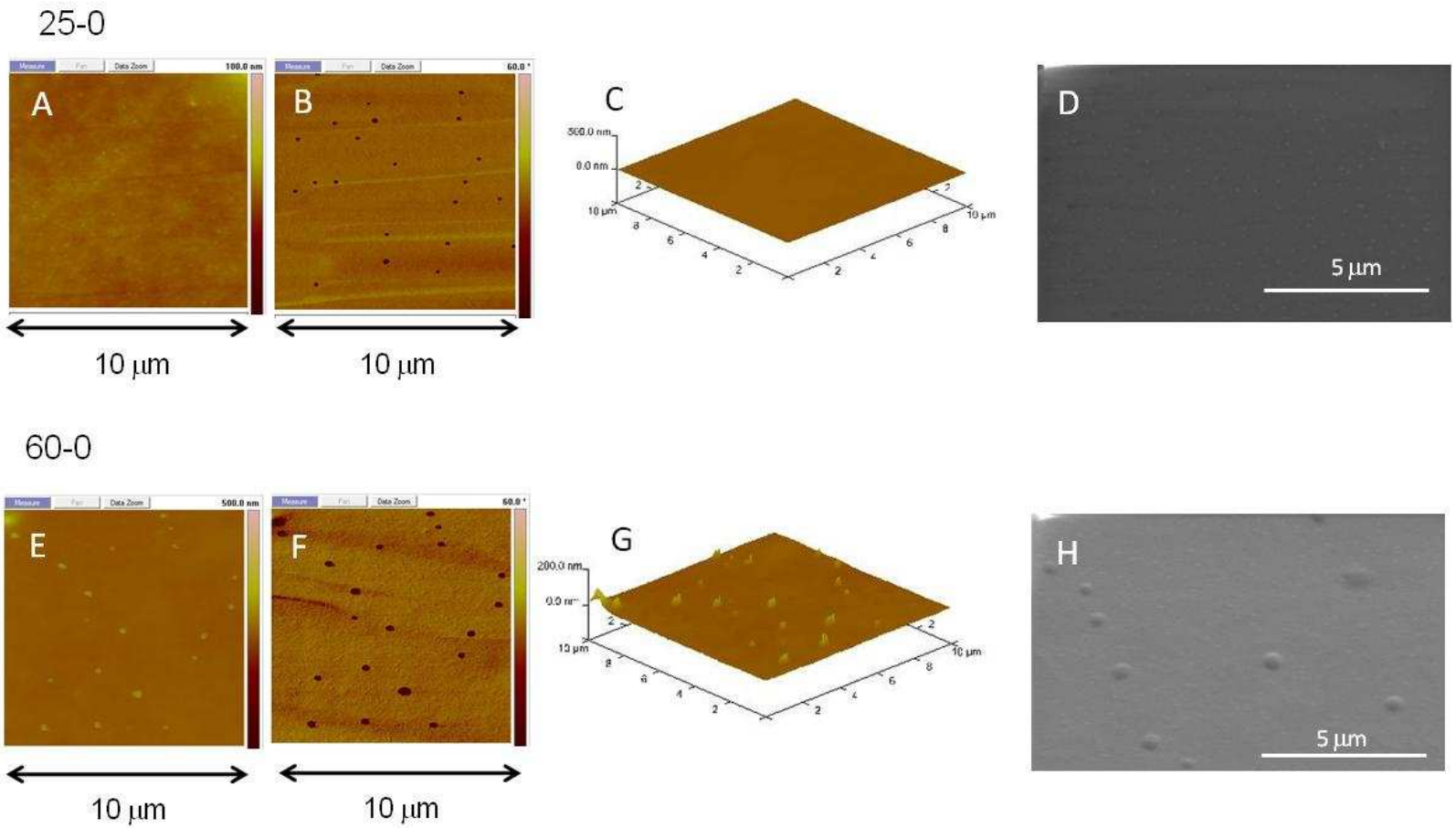

Figure 3.1. Surface Morphology of 0.5-3.5 blends (0 wks). Upper set (A-D). Cast, devolatilized at 25 ^{o}C; lower set (E-F) same process as upper set with annealing at 60 ^{o}C (24 h). Left to right 10 x 10 µm TM-AFM height image, phase image, and 3D height images. Right, 11k magnification SEM image.

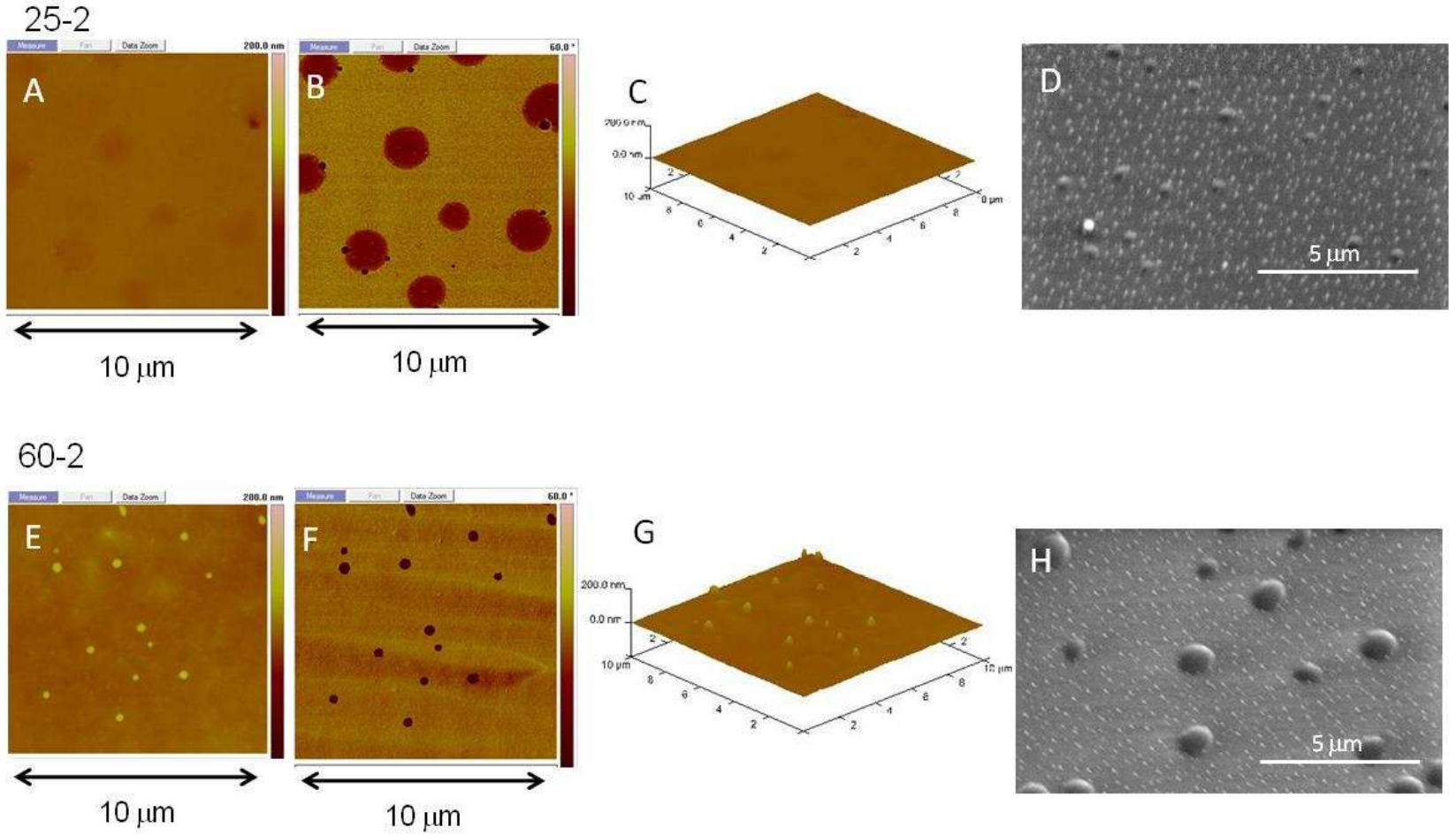

Figure 3.2 Surface Morphology of 0.5-3.5 blends (2 wks). Upper set (A-D). Cast, devolatilized at 25 ^{o}C; lower set (E-F) same process as upper set with annealing at 60 ^{o}C (24 h). Left to right 10 x 10 μm TM-AFM height image, phase image, and 3D height images. Right,11k magnification SEM image.

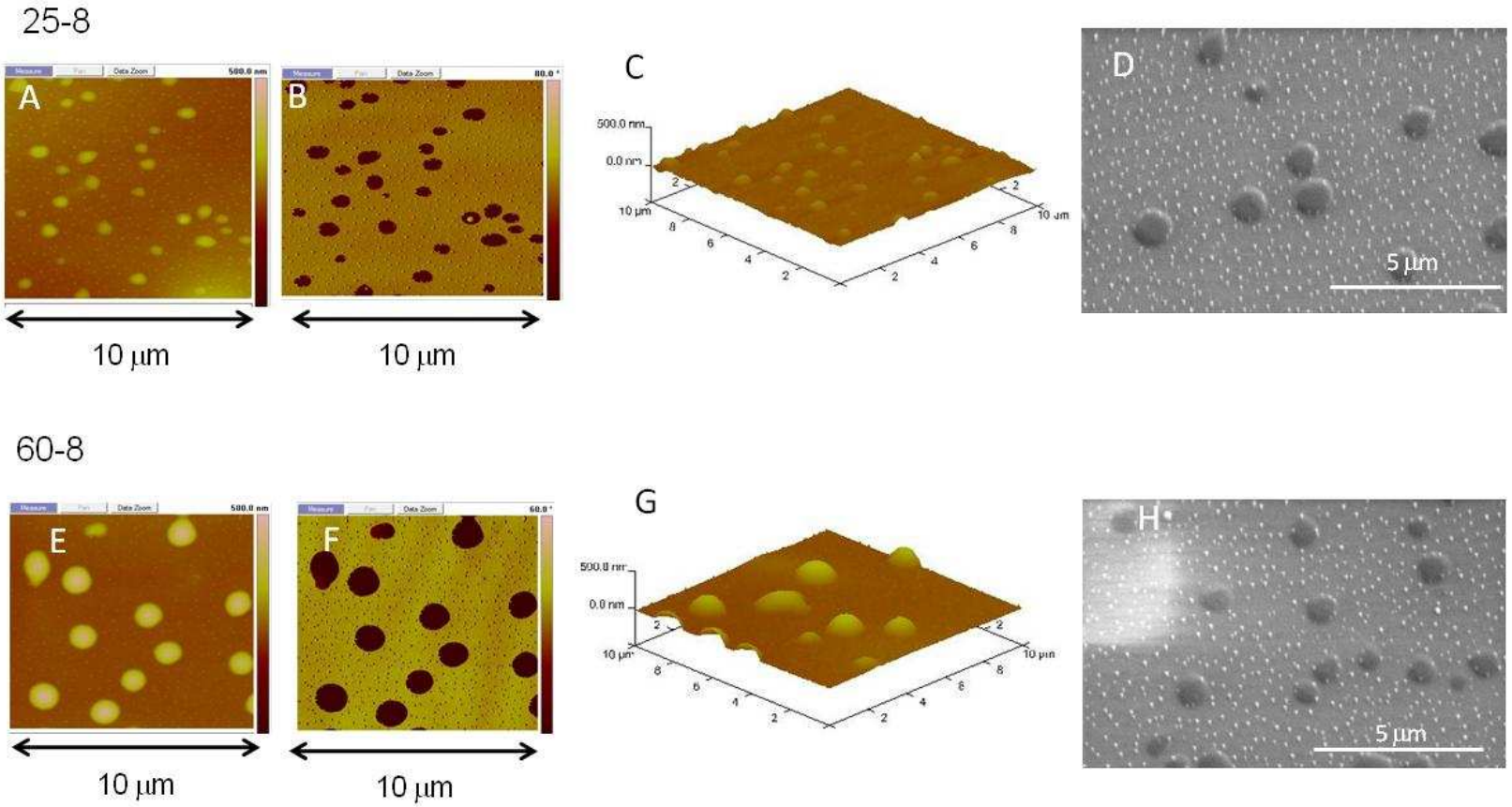

Figure 3.3. Surface Morphology of 0.5-3.5 blends (8 wks). Upper set (A-D). Cast, devolatilized at 25 ^{o}C; lower set (E-F) same process as upper set with annealing at 60 ^{o}C (24 h). Left to right 10 x 10 μm TM-AFM height image, phase image, and 3D height images. Right, 11k magnification SEM image.

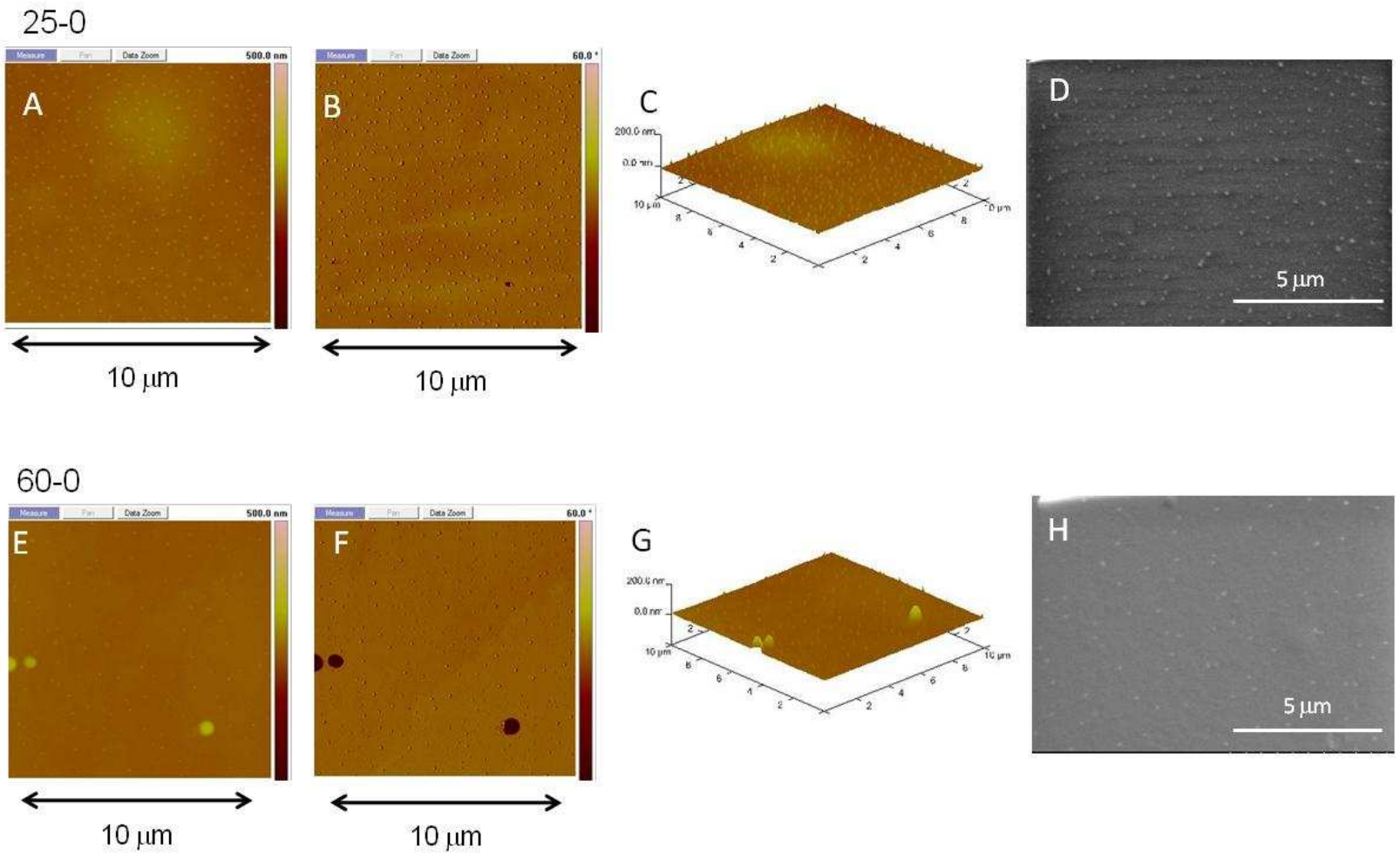

Figure 3.4. Surface Morphology of 1-3.5 blends (0 wks). Upper set (A-D). Cast, devolatilized at 25 ^{o}C; lower set (E-F) same process as upper set with annealing at 60 ^{o}C (24 h). Left to right 10 x 10 μm TM-AFM height image, phase image, and 3D height images. Right, 11k magnification SEM image.

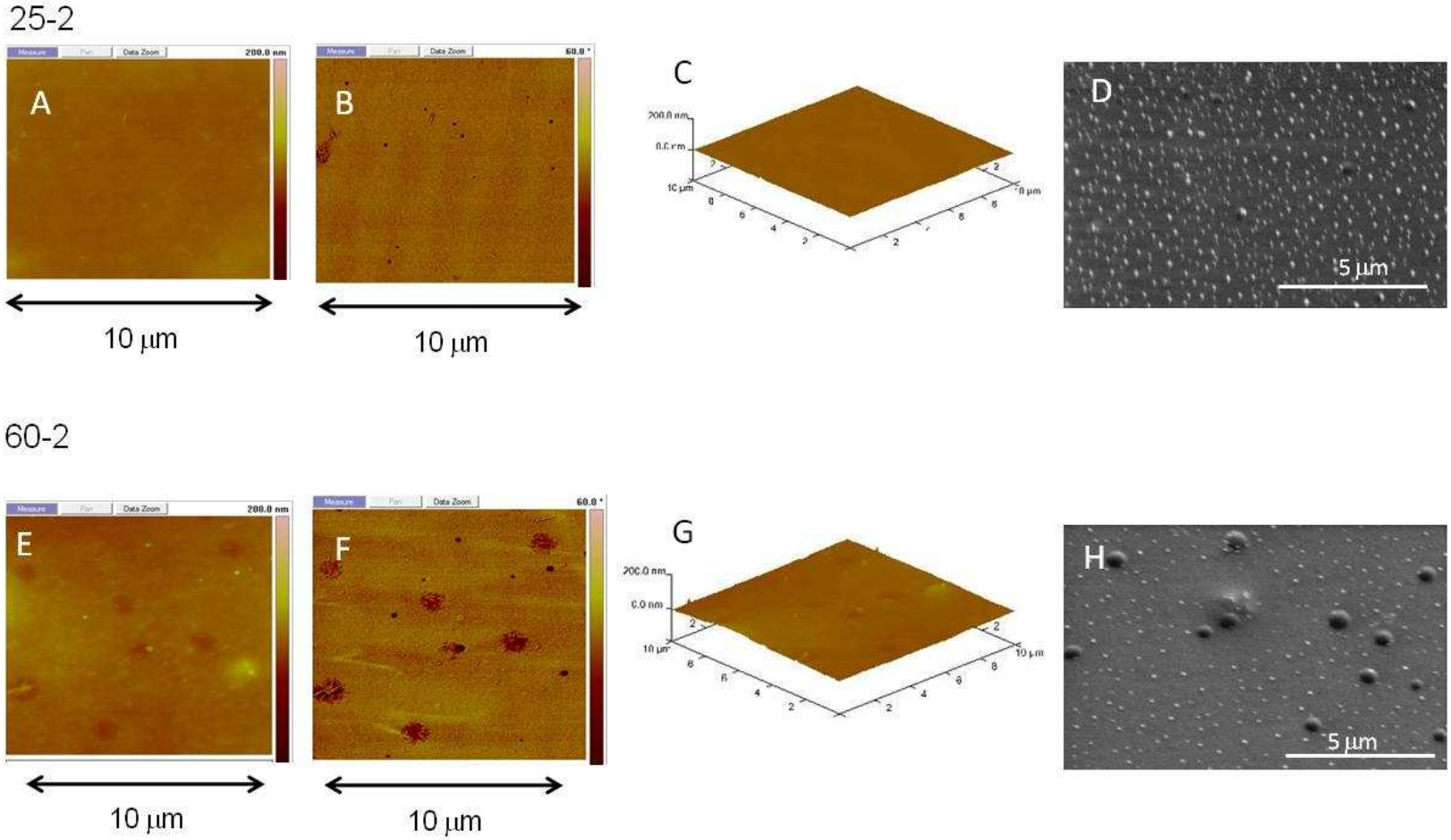

Figure 3.5. Surface Morphology of 1-3.5 blends (2 wks). Upper set (A-D). Cast, devolatilized at 25 ^{o}C; lower set (E-F) same process as upper set with annealing at 60 ^{o}C (24 h). Left to right 10 x 10 μm TM-AFM height image, phase image, and 3D height images. Right, 11k magnification SEM image.

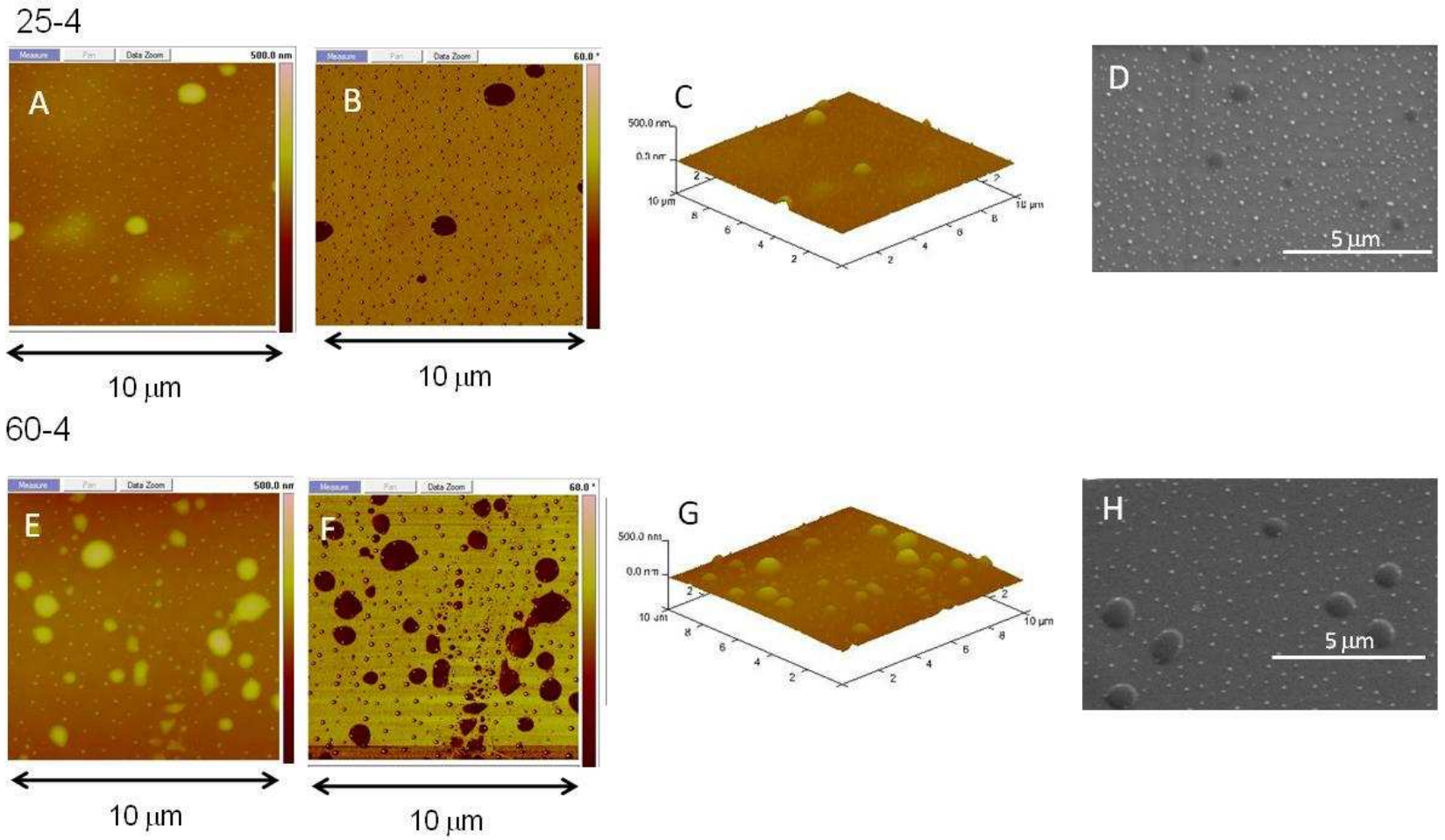

Figure 3.6. Surface Morphology of 1-3.5 blends (4 wks). Upper set (A-D). Cast, devolatilized at 25 ^{o}C; lower set (E-F) same process as upper set with annealing at 60 ^{o}C (24 h). Left to right 10 x 10 µm TM-AFM height image, phase image, and 3D height images. Right, 11k magnification SEM image.

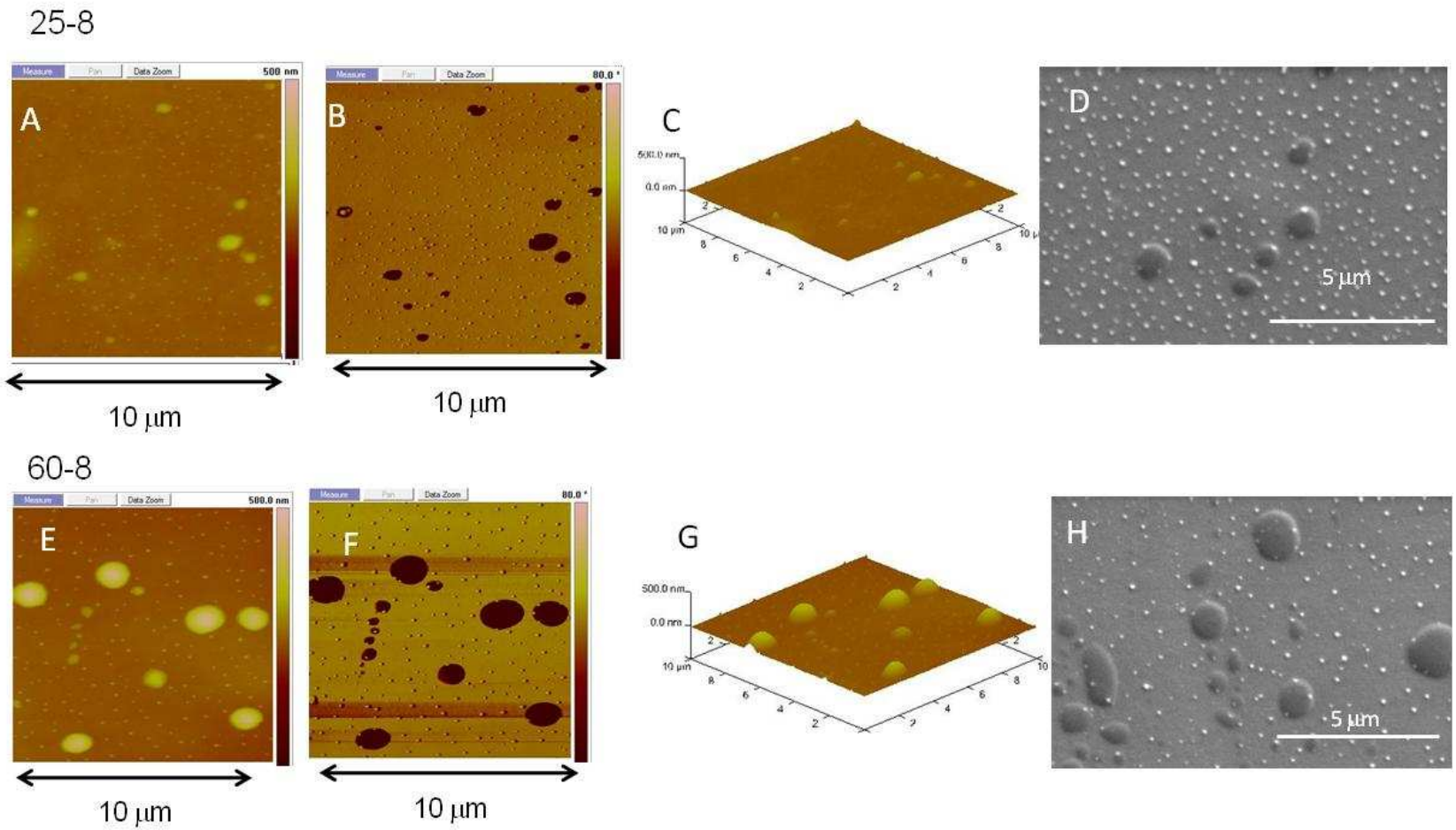

Figure 3.7. Surface Morphology of 1-3.5 blends (8 wks). Upper set (A-D). Cast, devolatilized at 25 ^{o}C; lower set (E-F) same process as upper set with annealing at 60 ^{o}C (24 h). Left to right 10 x 10 µm TM-AFM height image, phase image, and 3D height images. Right, 11k magnification SEM image

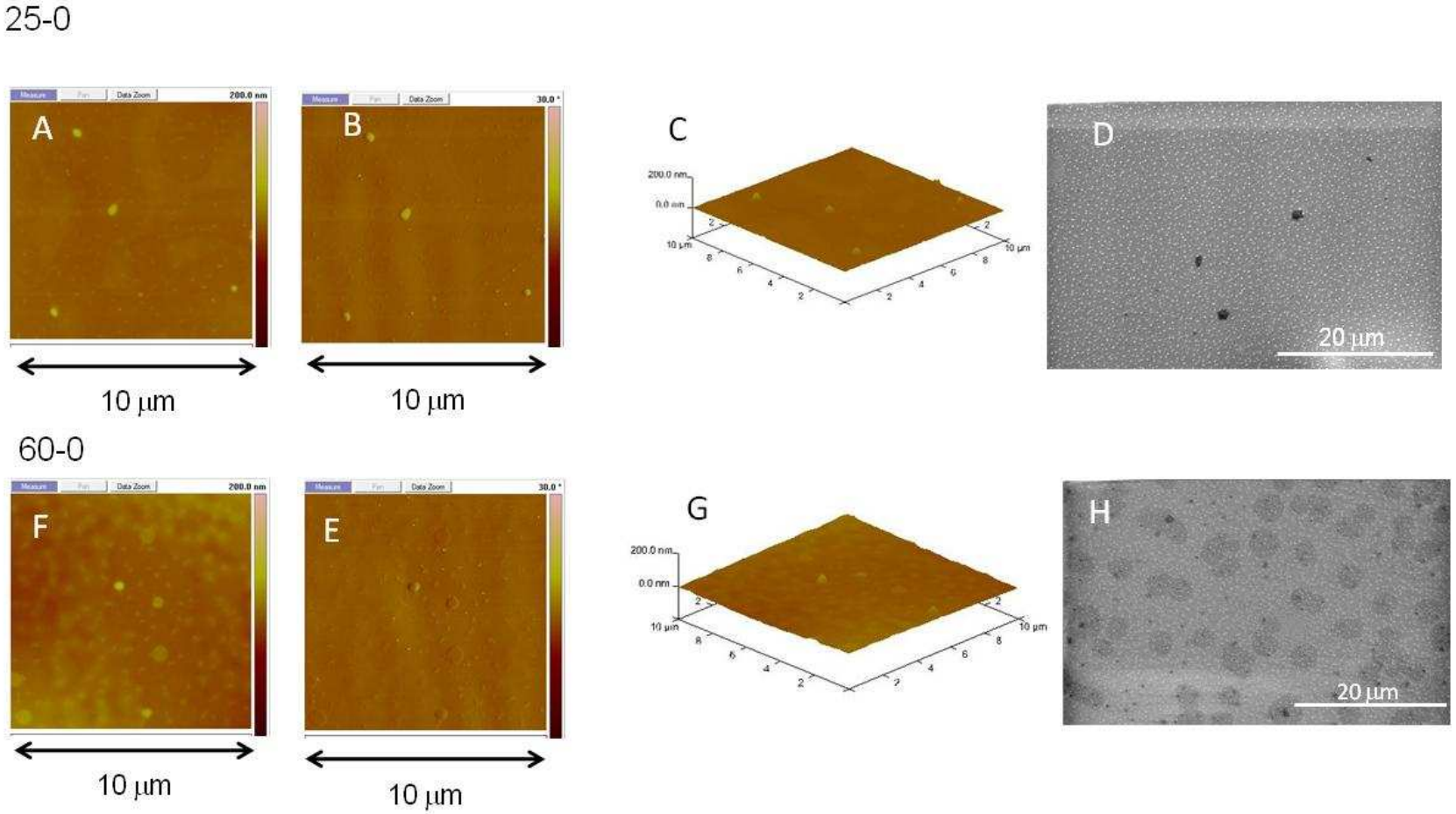

Figure 3.8. Surface Morphology of 2-3.5 blends (0 wks). Upper set (A-D). Cast, devolatilized at 25 ^{o}C; lower set (E-F) same process as upper set with annealing at 60 ^{o}C (24 h). Left to right 10 x 10 μm TM-AFM height image, phase image, and 3D height images. Right, 2.5k magnification SEM image.

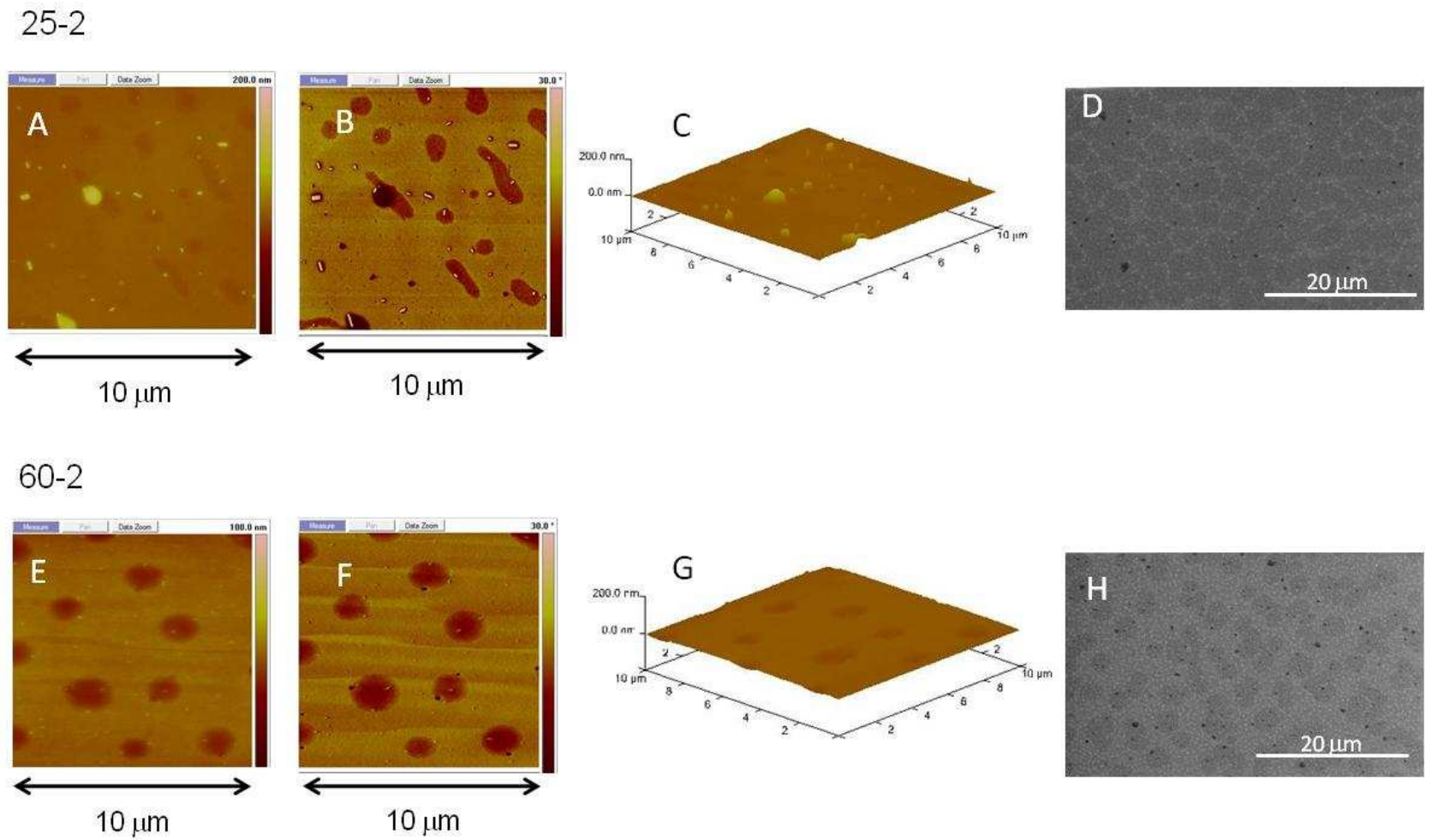

Figure 3.9. Surface Morphology of 2- 3.5 blends (2 wks). Upper set (A-D). Cast, devolatilized at 25 ^{o}C; lower set (E-F) same process as upper set with annealing at 60 ^{o}C (24 h). Left to right 10 x 10 μm TM-AFM height image, phase image, and 3D height images. Right, 2.5k magnification SEM image.

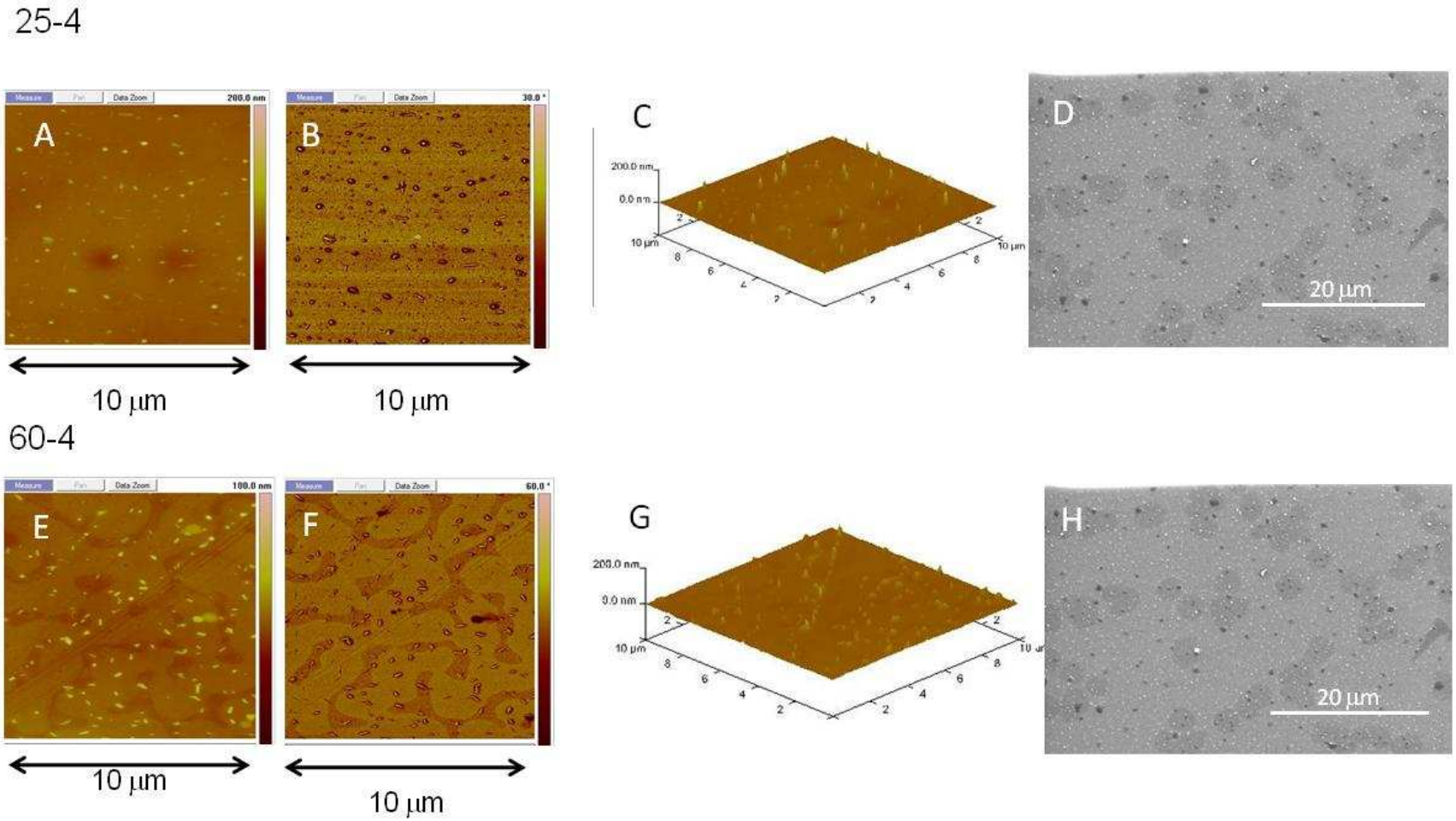

Figure 3.10. Surface Morphology of 2- 3.5 blends (4 wks). Upper set (A-D). Cast, devolatilized at 25 ^{o}C; lower set (E-F) same process as upper set with annealing at 60 ^{o}C (24 h). Left to right 10 x 10 μm TM-AFM height image, phase image, and 3D height images. Right, 2.5k magnification SEM image.

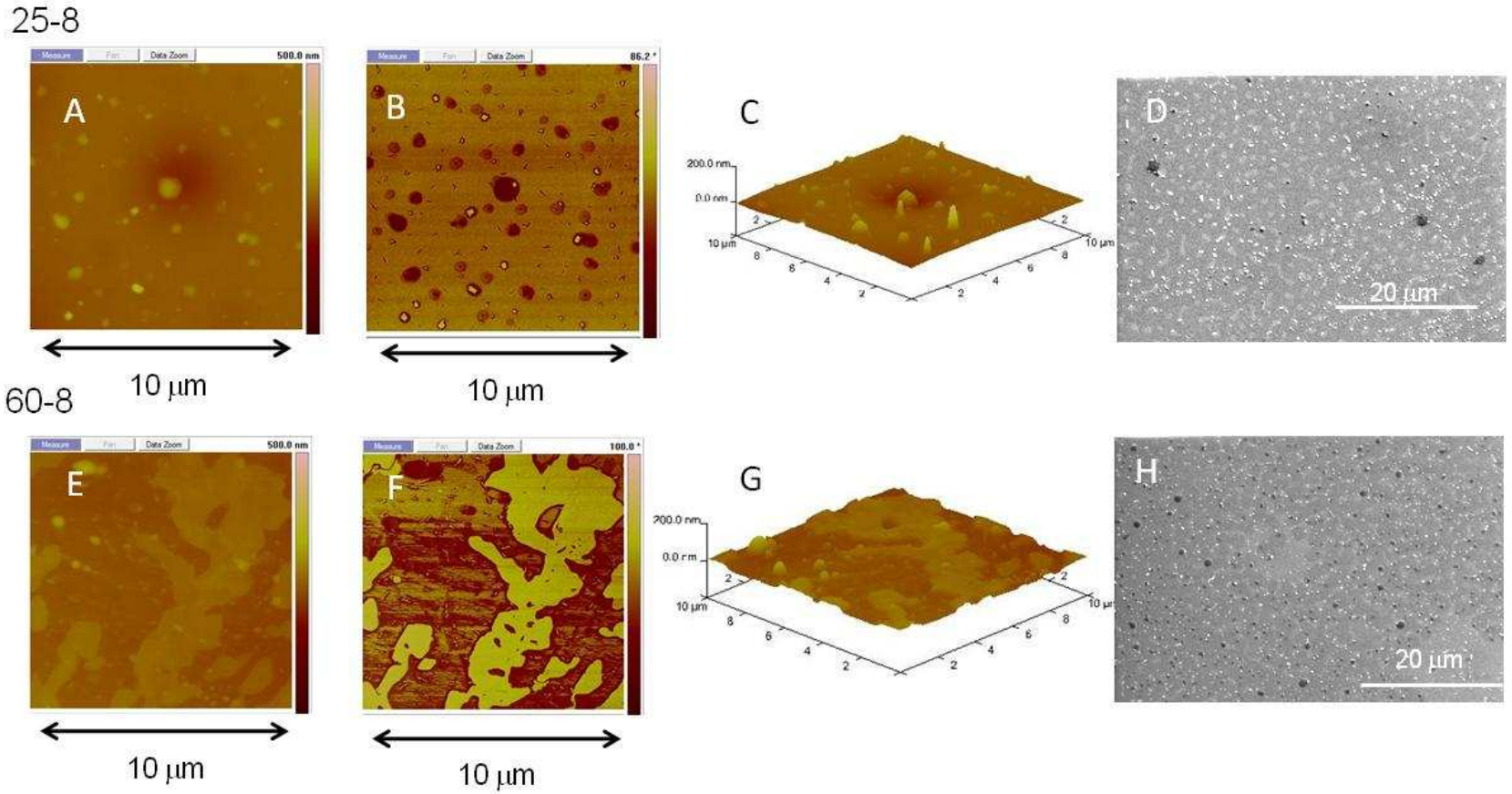

Figure 3.11. Surface Morphology of 0.5- 3.5 blends (0 wks). Upper set (A-D). Cast, devolatilized at 25 ^{o}C; lower set (E-F) same process as upper set with annealing at 60 ^{o}C (24 h). Left to right 10 x 10 μm TM-AFM height image, phase image, and 3D height images. Right, 2.5k magnification SEM image.

Characterization of 5.1 kDa blends

TM-AFM- 0.5 wt% blends. At t = 0 wks as cast AFM images appeared featureless much like those of the 0.5-5.1 kDa blends, however annealing generated 1-3 μm microcircles (Figure 3.12F). At t = 2 wks, these circular features become more distinct with increased prominence as initial annealing temperature increased (Figure 3.13). At t = 4-8 wks this circular phase separated morphology remained unchanged (Figure 3.14).

SEM-0.5wt% blend. SEM images for as cast and annealed 0.5-5.1 films were featureless at t = 0 wks (Figure 3.12D and H). At t = 2 wks the as cast (0.5-5.1-25) and annealed at 37 ^{o}C (0.5-5.1-37) film still showed no significant phase separation however the annealed at 60 ^{o}C (0.5-5.1-60) films (Figure 3.13H) began to show the formation of the micropeaks measuring between 300 nm-1 μm and well as the nanodots features observed in the 3.5 kDa blends. At t = 4 wks the micropeaks seen in the 0.5-5.1-60 film appeared in the 0.5-5.1-25 and 0.5-5.1-37 films with peak diameter similar to those seen in 0.5-5.1-60 at t = 2 wks. The micropeaks that were previously seen 0.5-5.1-60 films appeared to have slightly increased in size (1-1.5 μm) and number. At t = 8 wks (Figure 3.14H) many of micropeaks seen at 4 wks remained unchanged while the nanodots increased in number and size as a function of annealing temperature.

TM-AFM- 1 wt% blends. AFM for 1 wt% blends exhibited no significant phase separation for as cast films t = 0. As with the annealed 1wt%-3.5 kDa films at t = 0 wks (1-3.5-37-0 and 1-3.5-60-0), annealed 1-5.1 films developed phase separated micropeaks. At 2 wks (Figure 3.16 and Table 2) these micropeaks begin to appear in the as cast films while proliferating further in the annealed films. At t = 4 and 8 wks (Figure 3.17) micropeaks larger (5-10 μm) than those observed in 3.5 kDa blends.

SEM-1 wt% blend. SEM images for 1-5.1 blends did not display any significant features at t = 0 wks (Figure 3.15D and H). This was in agreement with the TM-AFM height image of 1-5.1 blends, but signs of phase separation are observed in the phase image. At t = 2 wks (Figure 3.16D and H) micropeaks similar to those observed in the 0.5 wt% sample were visible in the as cast and annealed films with the number of peaks present increasing with annealing temperature. As seen with previous samples the peak-like features seen in the 1 wt%-5.1 kDa blends increase in size and prominence as a function of time with the samples at t = 8 wks have the most prominent features (Figures 3.17D and H).

TM-AFM 2 wt% blends. 2-5.1 blends showed no significant phase separation at t = 0 wks for the as cast films while the annealed films began to develop micropeak features seen in the 0.5 and 1 wt% blends (Figure 3.18). At t = 2 wks the presence of microscale features for 2-5.1-25 become pronounce however while both the 2-5.1-37 and the 2-5.1-60 (Figure 3.19D-H) films had a significant number of micropeaks measuring 5-10 μm in diameter and 200 nm in height (Table 3.2) . At t = 4wks (Figure 3.19), the micropeaks were observed in the 2-5.1-25 film while the 2-5.1-37 and the 2-5.1-60 films showed an increase in the number of peaks present on the surface. These features exhibit further increase in size and number at t = 8wks (Figure 3.20) with features measuring diameter (10-15 μm).

SEM-2 wt% blend. Similar to the TM-AFM images, the SEM images of the 2-5.1 blends (Figure 3.18D and H) did not exhibit any significant phase separation at t = 0 wks for as cast and annealed films. At 2 wks the phase separated features were immediately apparent and similar to the structures observed via TM-AFM (Figure 3.19D and H). Upon annealing, these micropeaks showed an increase in prominence with the 2-5.1-60 film having the most distinct features. Also noticeable with the 2-5.1-60 film is that the micropeaks have a larger diameter (2-4 μm) than

those seen in the 2-5.1-25 or the 2-5.1-37 films. This increase in peak diameter is likely due to the increased mobility of the polymer at the annealing temperature. Since the annealing temperature of 60 ^{o}C is well above the glass transition temperature of the PSM soft segment and is also the softening temperature of the base polyurethane (See DMA, Figure 1.10) the PSM can migrate to the surface more readily and grow into larger domains.

At t = 4 wks (Figure 3.19D and H) the micropeaks were similar to those at 2 wks but had an overall increased diameter (1-3 μm at 2 wks to 2-4 μm at 4wks). At t = 8 wks (Figure 3.20D and H) the morphological features in all films had increased in size and had also become irregularly shaped. The shape irregularity is likely due to coalescence of surface features as the film ages. Many of the irregular features are oblong or appear to have narrower features from merging two domains.

Table 3.2. Observed surface morphological features for HMDI-BD (50wt%) PTMO (1000): HMDI-BD (30wt%) P[(3FOx)(C12) 87:13-5.1 kDa blends.

PSM Blends Composition	Temperature (°C)	Time (wks)	Nanodots Size (nm), Density (#/10 μm^2)	Micropeaks Size (μm), Density (#/10 μm^2)	Microcircles Size (μm), Density (#/10 μm^2)
0.5-5.1	25 °C (ambient)	0	n.o.[a]	n.o.[a]	1-3, (10)
		2	n.o.[a]	n.o.[a]	1-3, (10)
		4	100-200, (50)	1-2, (10)	1-3, (10)
		8	100-200, (200)	1-2, (10)	1-3, (10)
	37 °C	0	n.o.[a]	n.o.[a]	1-3, (10)
		2	n.o.[a]	n.o.[a]	1-3, (10)
		4	100-200, (50)	1-2, (10)	1-3, (10)
		8	100-200, (50)	1-2, (10)	1-3, (10)
	60 °C	0	n.o.[a]	n.o.[a]	1-3, (10)
		2	100-200, (150)	1-2, (15)	1-4, (10)
		4	100-200, (150)	2-3, (15)	1-4, (10)
		8	100-200, (200)	2-3, (30)	1-4, (10)
1-5.1	25 °C (ambient)	0	n.o.[a]	n.o.[a]	n.o.[a]
		2	100-200, (50)	n.o.[a]	n.o.[a]
		4	100-200, (50)	0.5-1, (20)	n.o.[a]
		8	100-200, (50)	0.5-1, (20)	n.o.[a]
	37 °C	0	n.o.[a]	n.o.[a]	n.o.[a]
		2	100-200, (100)	n.o.[a]	n.o.[a]
		4	100-200, (100)	1-2, (30)	n.o.[a]
		8	100-200, (100)	1-2, (30)	n.o.[a]
	60 °C	0	n.o.[a]	n.o.[a]	n.o.[a]
		2	100-200, (200)	0.5-1, (10)	n.o.[a]
		4	100-200, (200)	1-2, (30)	n.o.[a]
		8	100-200, (200)	1-2, (30)	n.o.[a]
2-5.1	25 °C (ambient)	0	n.o.[a]	n.o.[a]	n.o.[a]
		2	100-200, (115)	1-3, (5)	n.o.[a]
		4	100-200, (200)	2-4, (5)	n.o.[a]
		8	100-200, (200)	5-10, (5)	n.o.[a]
	37 °C	0	n.o.[a]	n.o.[a]	n.o.[a]
		2	100-200, (120)	1-3, (5)	n.o.[a]
		4	100-200, (200)	2-4, (5)	n.o.[a]
		8	100-200, (200)	5-10, (5)	n.o.[a]
	60 °C	0	n.o.[a]	n.o.[a]	n.o.[a]
		2	100-200, (120)	2-5, (5)	n.o.[a]
		4	100-200, (200)	4-5. (5)	n.o.[a]
		8	100-200, (200)	5-10, (5)	n.o.[a]

a. n.o, not observed

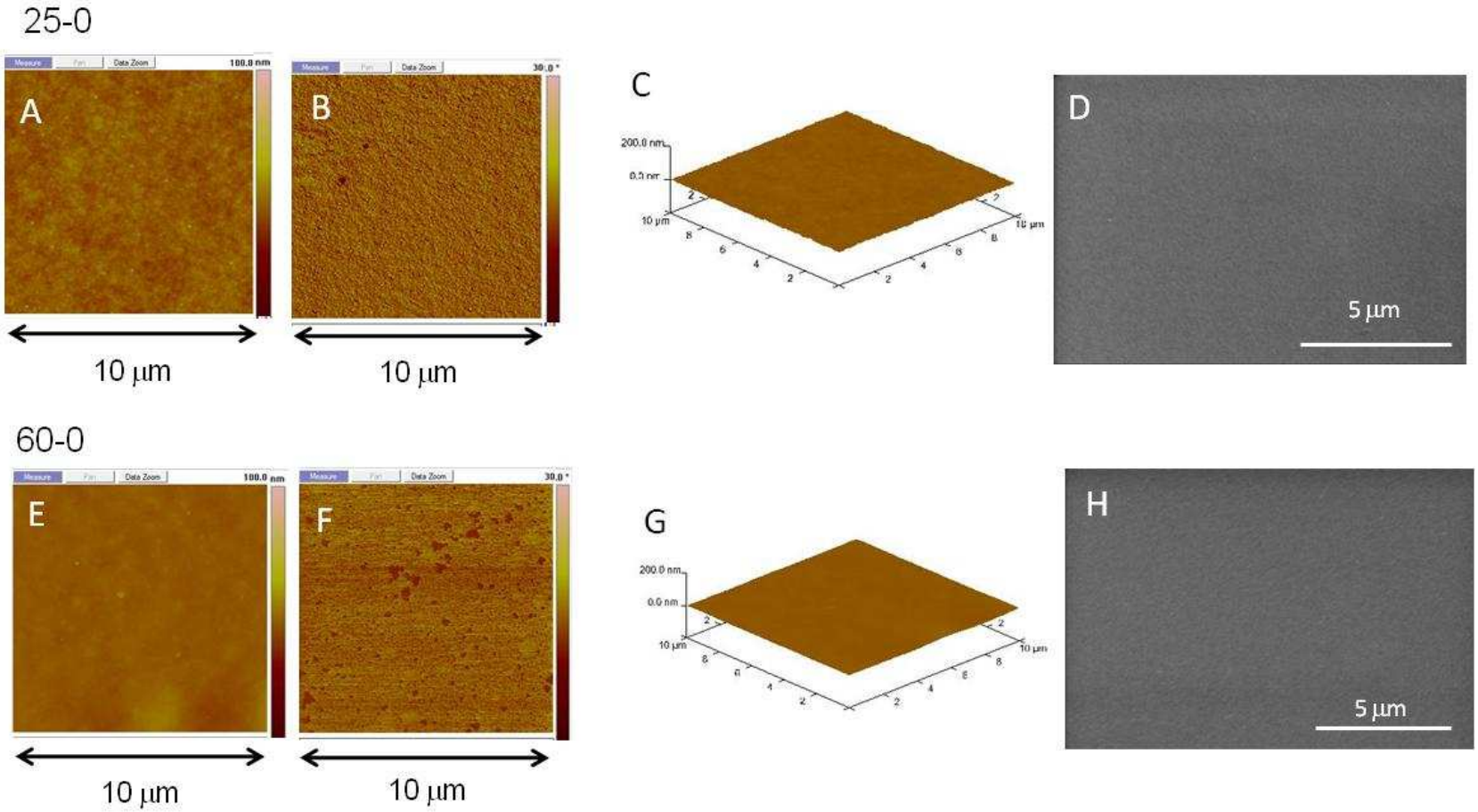

Figure 3.12. Surface Morphology of 0.5-5.1 blends (0 wks). Upper set (A-D). Cast, devolatilized at 25 ^{o}C; lower set (E-F) same process as upper set with annealing at 60 ^{o}C (24 h). Left to right 10 x 10 μm TM-AFM height image, phase image, and 3D height images. Right, 11k magnification SEM image.

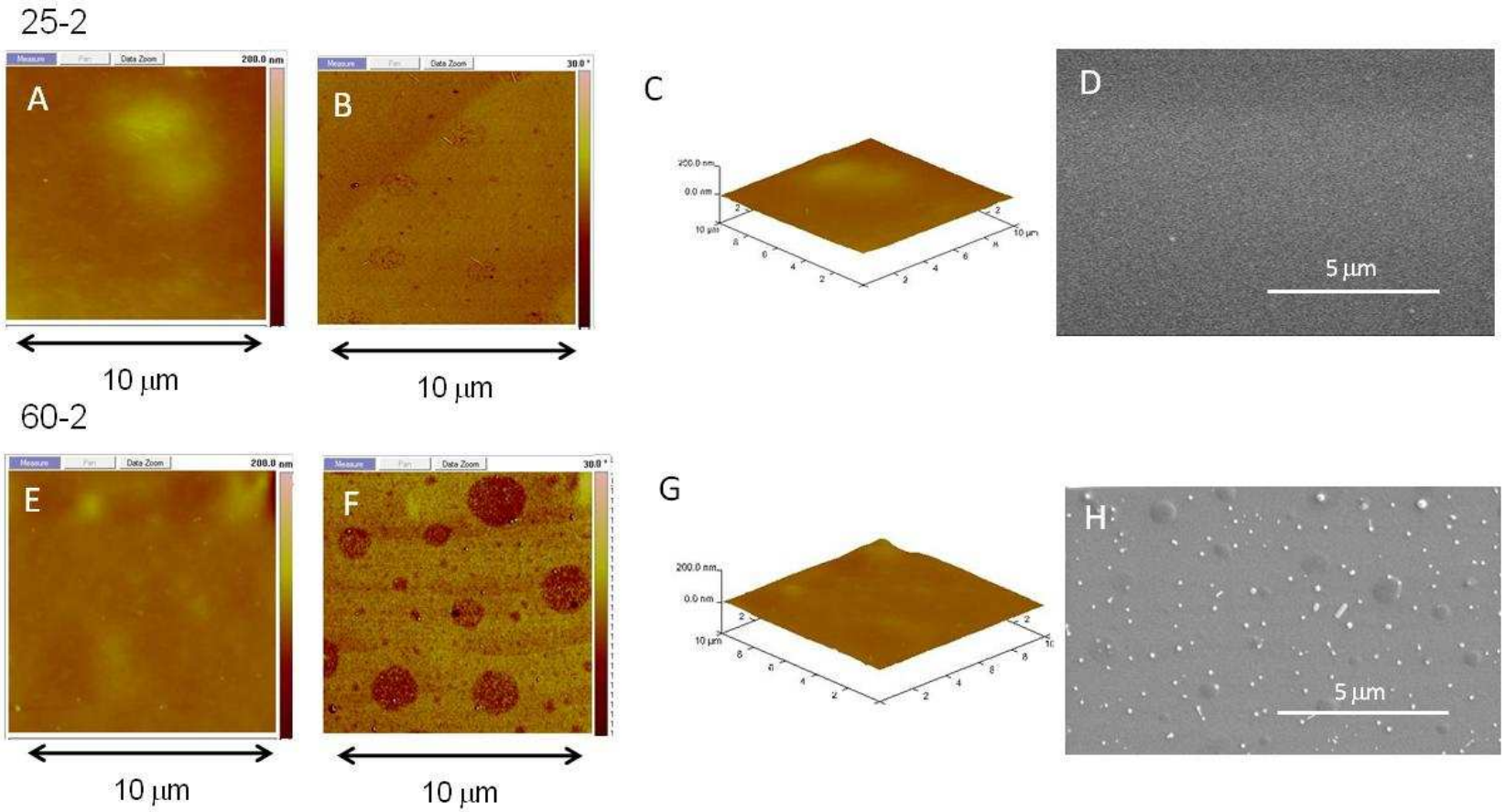

Figure 3.13. Surface Morphology of 0.5- 5.1 blends (2 wks). Upper set (A-D). Cast, devolatilized at 25 ^{o}C; lower set (E-F) same process as upper set with annealing at 60 ^{o}C (24 h). Left to right 10 x 10 μm TM-AFM height image, phase image, and 3D height images. Right, 11k magnification SEM image.

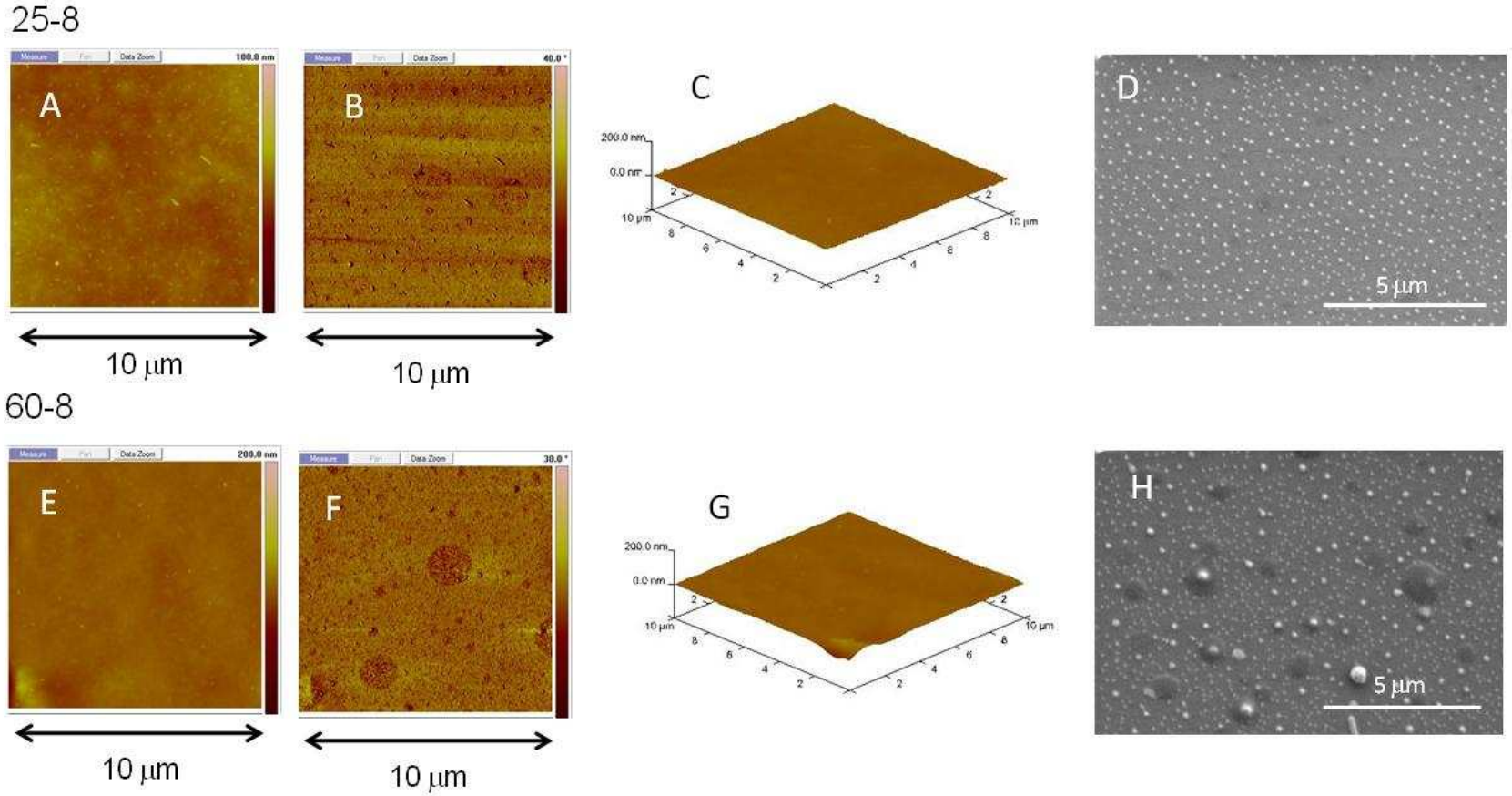

Figure 3.14. Surface Morphology of 0.5- 5.1 blends (8 wks). Upper set (A-D). Cast, devolatilized at 25 ^{o}C; lower set (E-F) same process as upper set with annealing at 60 ^{o}C (24 h). Left to right 10 x 10 μm TM-AFM height image, phase image, and 3D height images. Right, 11k magnification SEM image.

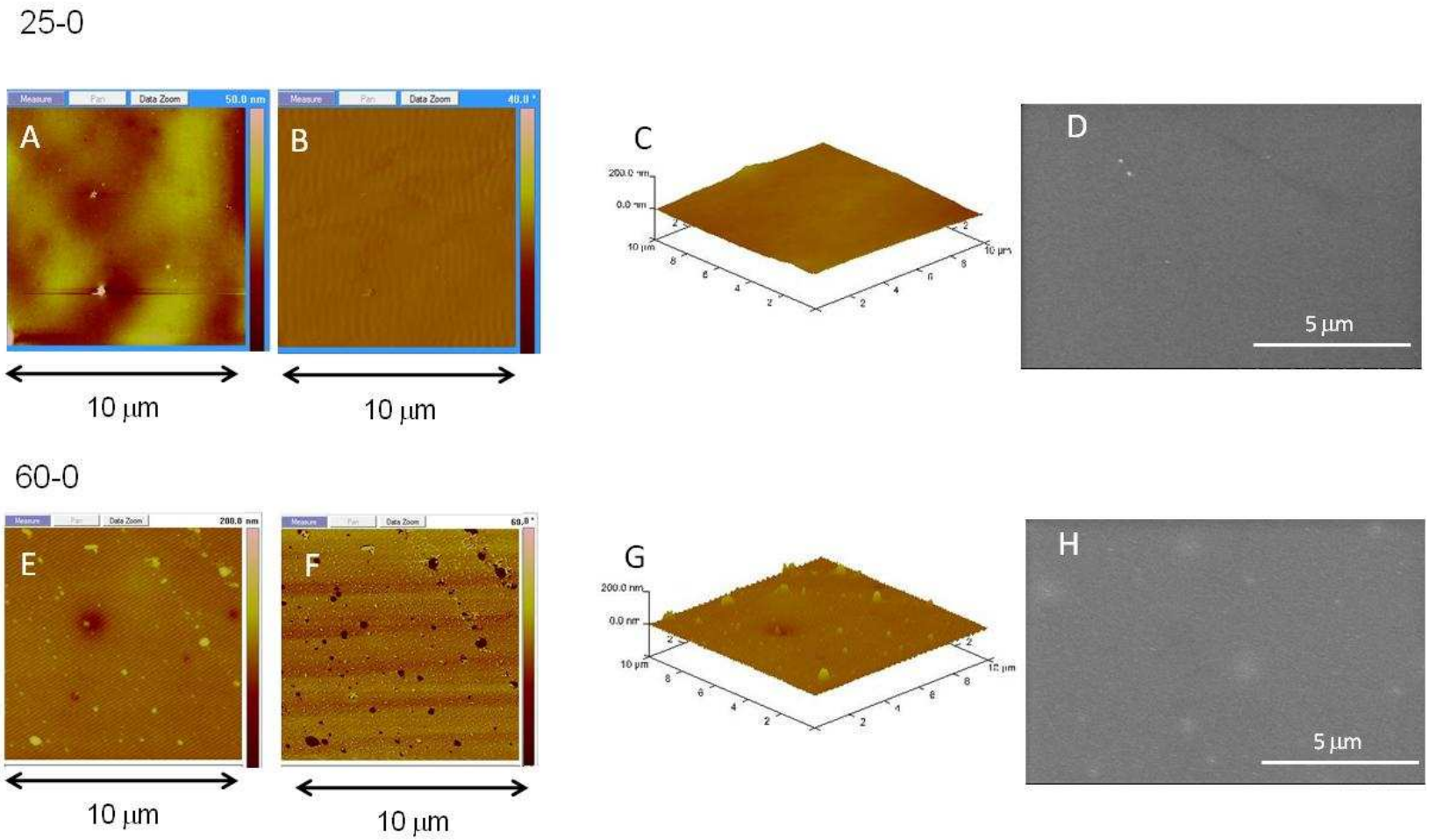

Figure 3.15. Surface Morphology of 1-5.1 blends (0 wks). Upper set (A-D). Cast, devolatilized at 25 ^{o}C; lower set (E-F) same process as upper set with annealing at 60 ^{o}C (24 h). Left to right 10 x 10 μm TM-AFM height image, phase image, and 3D height images. Right, 11k magnification SEM image.

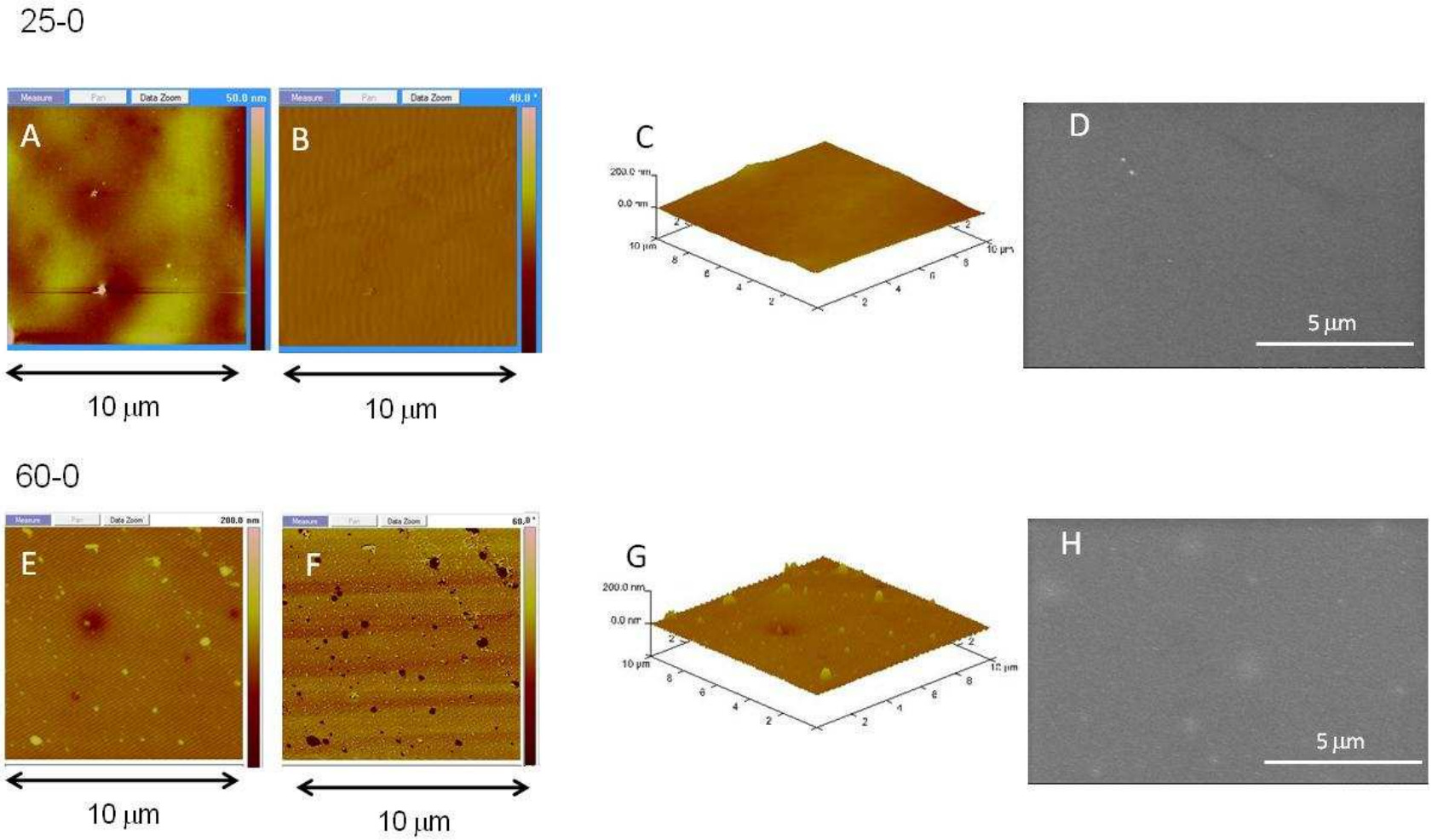

Figure 3.16. Surface Morphology of 1- 5.1 blends (2 wks). Upper set (A-D). Cast, devolatilized at 25 ^{o}C; lower set (E-F) same process as upper set with annealing at 60 ^{o}C (24 h). Left to right 10 x 10 μm TM-AFM height image, phase image, and 3D height images. Right, 11k magnification SEM image.

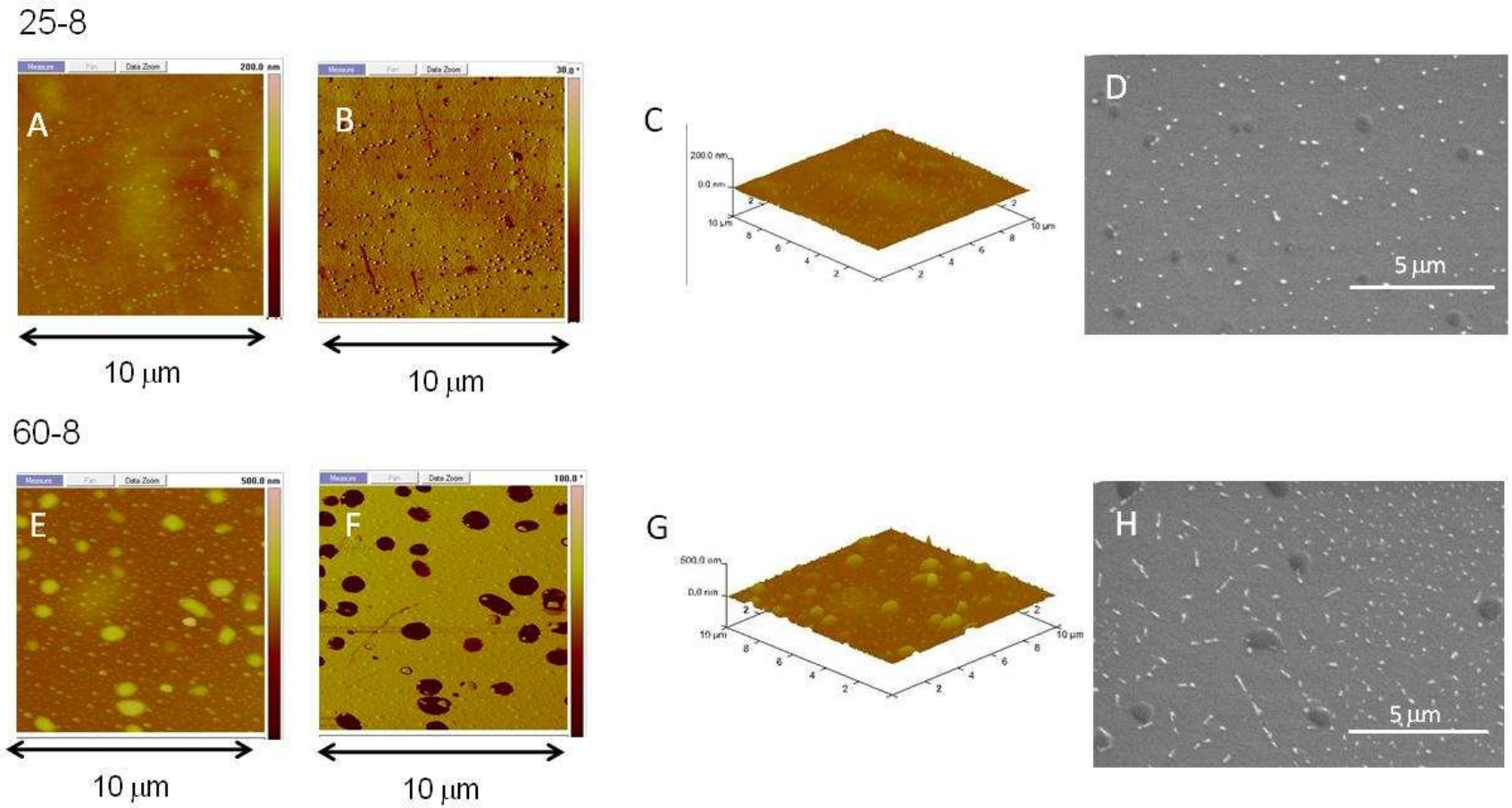

Figure 3.17. Surface Morphology of 1- 5.1 blends (8 wks). Upper set (A-D). Cast, devolatilized at 25 ^{o}C; lower set (E-F) same process as upper set with annealing at 60 ^{o}C (24 h). Left to right 10 x 10 μm TM-AFM height image, phase image, and 3D height images. Right, 11k magnification SEM image.

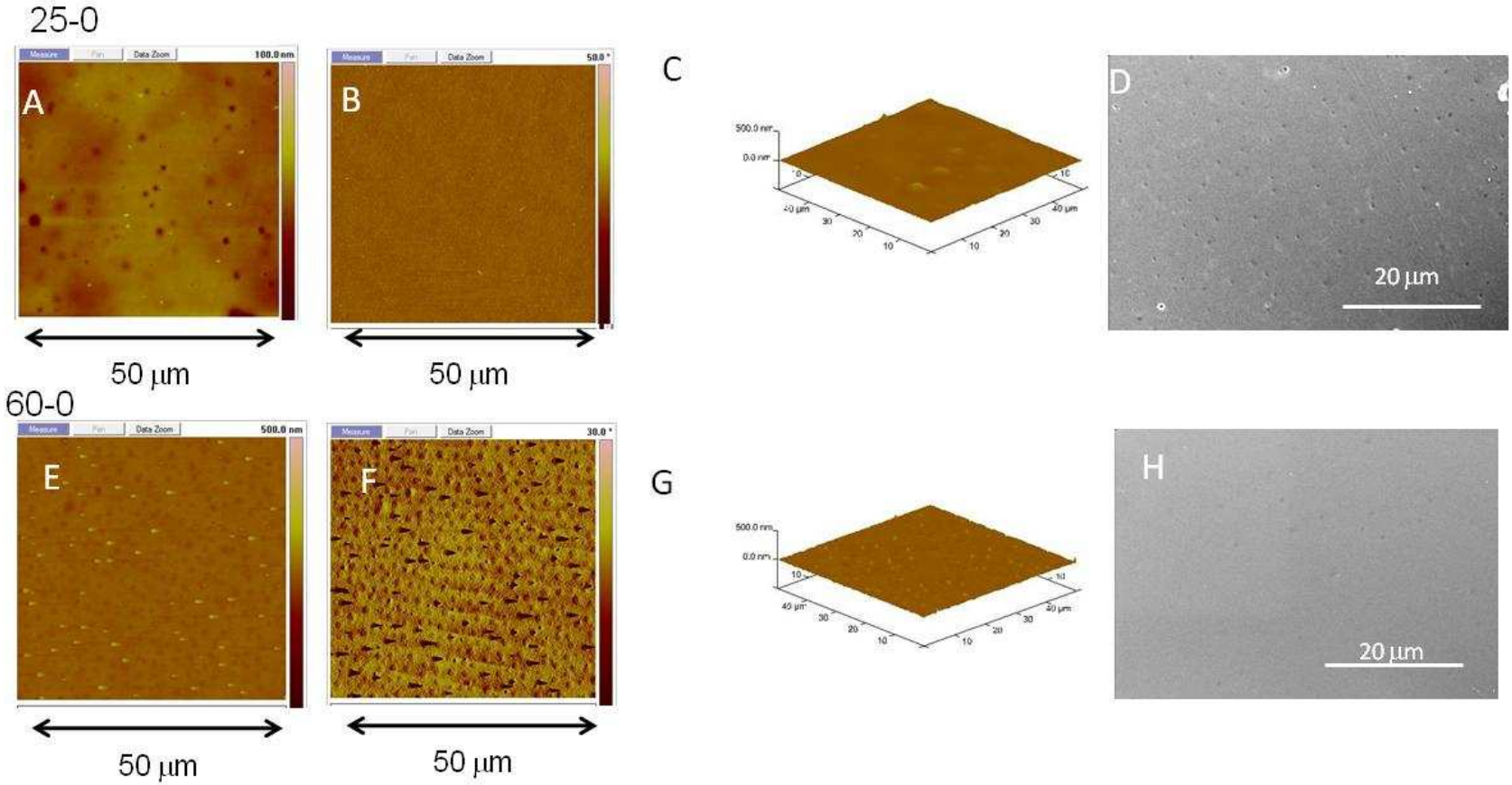

Figure 3.18. Surface Morphology of 2- 5.1 blends (0 wks). Upper set (A-D). Cast, devolatilized at 25 ^{o}C; lower set (E-F) same process as upper set with annealing at 60 ^{o}C (24 h). Left to right 50 x 50 μm TM-AFM height image, phase image, and 3D height images. Right, 2.5k magnification SEM image.

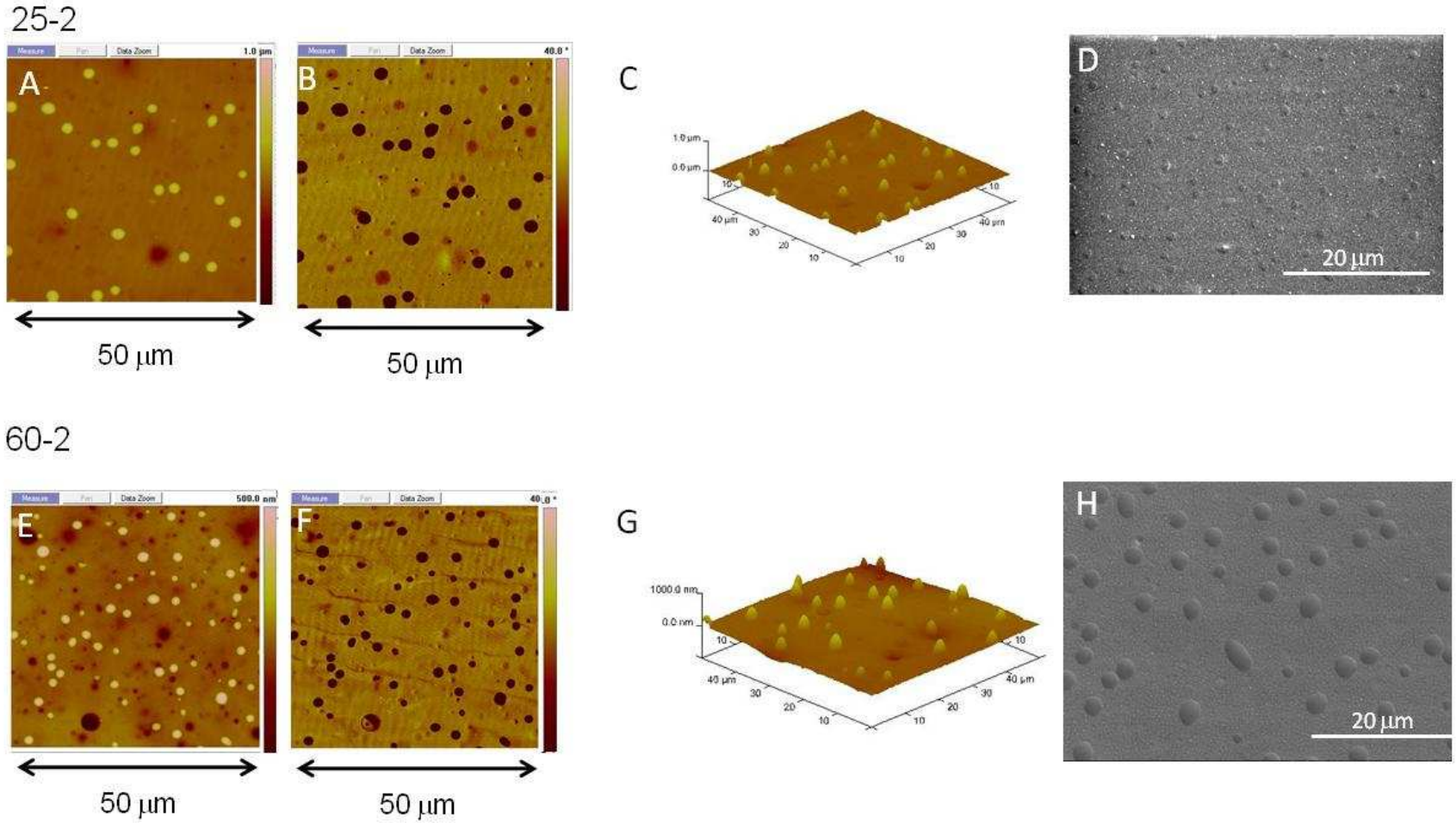

Figure 3.19. Surface Morphology of 2- 5.1 blends (2 wks). Upper set (A-D). Cast, devolatilized at 25 ^{o}C; lower set (E-F) same process as upper set with annealing at 60 ^{o}C (24 h). Left to right 50 x 50 μm TM-AFM height image, phase image, and 3D height images. Right, 2.5k magnification SEM image.

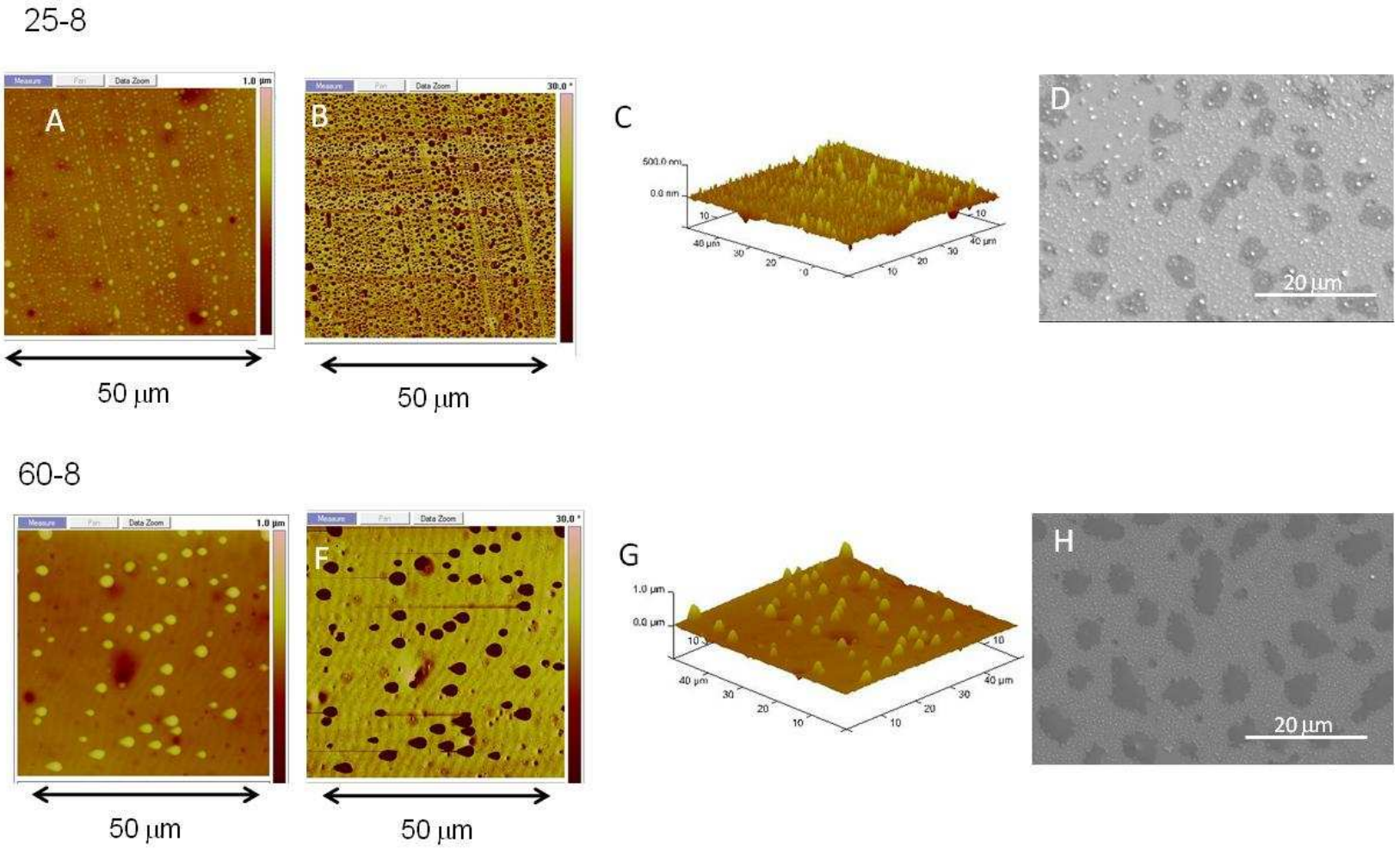

Figure 3.20. Surface Morphology of 2- 5.1 blends (8 wks). Upper set (A-D). Cast, devolatilized at 25 ^{o}C; lower set (E-F) same process as upper set with annealing at 60 ^{o}C (24 h). Left to right 50 x 50 μm TM-AFM height image, phase image, and 3D height images. Right, 2.5k magnification SEM image.

Characterization of 7.9 kDa blends

TM-AFM-0.5 wt% and 1wt% blends. 0.5-7.9 blends did not have any significant morphological features at t = 0 wks to 4wks. At 8 wks, as cast and annealed films began to develop nanodots similar to those in the 3.5 and 5.1 kDa blends (Figure 3.22). The morphology of the 1wt% blends appeared featureless in height images however phase images show irregular microcircles (0.3 μm- 1 μm) (Figure 3.23). At 2 wks these irregular microcircles become more distinct but there is no significant change in height features. As seen in Figures 3.24-25, 0.5-7.9 and 1-7.9 blends at 4 and 8 wks are similar to those at 2 wks. Features in the phase image associated with those in 2D and 3D images are more distinct.

SEM-0.5 wt% and 1wt% blend. At t = 0 wks, the morphology of the 0.5 wt% blends displayed prominent nanodots similar to those previously observed in the 3.5 and 5.1 kDa blends. At t = 2 wks there were no new types of morphological features formed however the number of nanodots increased with the 0.5-7.9-60 film showing the most distinct features at t = 2 wks. At t = 4 and 8 wks there was no significant change in morphology from that observed at 2 wks for all 0.5 wt% films indicating the morphology had reached stability (Figure 3.22D and H). SEM images of the 1wt% blends where in agreement with what was observed via AFM. At t = 0 wks (Figure 3.23) no significant height features could be detected at 2.5k x or 11k x magnification however microlines (1-3 μm) were apparent. SEM micrographs of 2 week old 1-7.9 films showed an increase in the appearance of the microlines as well as nanodots. This morphology remained relatively unchanged to samples at t = 4 wks and 8 wks (Figure 3.24-25).

TM-AFM-2 wt% blends. Unlike the 2-3.5-25 and 2-5.1-25 films, the 2-7.9-25 films showed immediate phase separation at t = 0 wks in the form of micropeaks measuring 0.5-1 μm in diameter. At t = 0 wks, the 2-7.9-37 and 2-7.9-60 did begin to show signs of micropit formations (0.2-1 μm) as well as the micropeaks seen in the as cast films. At t = 2 wks there is no significant change in morphology for 2-7.9-25, however, films that were annealed at 37 ^{o}C and 60 ^{o}C did have increased pitting after 2 wks . At 4 wks, micropits became detectable on the 2-7.9-25 films while the micropeak features observed in the 2-7.9-37 and 2-7.9-60 films became more prominent, similarly to those observed in the 3.5 and 5.1 kDa samples but of a smaller diameter (1-2 μm). Also seen in the 2-7.9- 60 were morphological features that appeared to be aggregations of nanodots (Figure 3.27F). At 8 wks, increases in micropits and micropeaks are seen for all 2 wt% films as well as microcircles measuring from 600 nm to as large as 3 μm. 2-7.9-60 ^{o}C films also displayed microlines measuring 1-4 μm in length (Figure 3.28).

SEM-2 wt% blends. As with the AFM images of the 2-7.9 blends, phase separated features were observed in SEM at t = 0 wks (Figure 3.26D and H). The microline and nanodot features observed in the 2-7.9 films appeared similar to those seen in SEM micrographs of the 0.5 and 1wt% blends, however the present of small micropeaks (0.5-1 μm) can be detected. At t = 2 wks (Figure 3.27D and H) the micropeaks increase in number and size (1-2 μm) in all 2-7.9 films. There is also the development of interconnected features that could be PSM rich domains. At t = 4 wks and 8 wks many of the features present at 2 wks become more distinct. The peaks like features also showed size increase with annealing temperature similar to what was observed in the 5.1 kDa blends (Figure 3.28).

Table 3.3. Observed surface morphological features for HMDI-BD (50 wt%) PTMO (1000): HMDI-BD (30 wt%) P[(3FOx)(C12) 87:13-7.9 kDa blends.

PSM Blends Composition	Temperature (°C)	Time (wks)	Observed Morphological Features					
			Micropits Size (μm), (Density (#/10 μm^2))	Nanodots Size (nm), Density (#/10 μm^2)	Micropeaks Size (μm), Density (#/10 μm^2)	Microcircles Size (μm), Density (#/10 μm^2)	Microlines Size (μm), Density (#/10 μm^2)	Interconneced (μm), (Density, (#/10 μm^2))
0.5-7.9	25 °C (ambient)	0	n.o.[a]	100-200, (50)	n.o.[a]	n.o.[a]	n.o.[a]	n.o.[a]
		2	n.o.[a]	100-200, (100)	n.o.[a]	n.o.[a]	n.o.[a]	n.o.[a]
		4	n.o.[a]	100-200, (100)	n.o.[a]	n.o.[a]	n.o.[a]	n.o.[a]
		8	n.o.[a]	100-200, (100)	n.o.[a]	n.o.[a]	n.o.[a]	n.o.[a]
	37 °C	0	n.o.[a]	100-200, (50)	n.o.[a]	n.o.[a]	n.o.[a]	n.o.[a]
		2	n.o.[a]	100-200, (100)	n.o.[a]	n.o.[a]	n.o.[a]	n.o.[a]
		4	n.o.[a]	100-200, (100)	n.o.[a]	0.3-1, (5)	n.o.[a]	n.o.[a]
		8	n.o.[a]	100-200, (100)	n.o.[a]	0.3-1, (5)	n.o.[a]	n.o.[a]
	60 °C	0	n.o.[a]	100-200, (50)	n.o.[a]	n.o.[a]	n.o.[a]	n.o.[a]
		2	n.o.[a]	100-200, (100)	n.o.[a]	n.o.[a]	n.o.[a]	n.o.[a]
		4	n.o.[a]	100-200, (100)	n.o.[a]	0.3-1, (5)	n.o.[a]	n.o.[a]
		8	n.o.[a]	100-200, (100)	n.o.[a]	0.3-1, (5)	n.o.[a]	n.o.[a]
1-7.9	25 °C (ambient)	0	n.o.[a]	100-200, (100)	n.o.[a]	0.3-1, (12)	1-2, (10)	n.o.[a]
		2	n.o.[a]	100-200, (100)	n.o.[a]	0.3-1, (25)	1-2 (10)	n.o.[a]
		4	n.o.[a]	100-200, (100)	n.o.[a]	0.3-1, (20)	1-2, (10)	n.o.[a]
		8	n.o.[a]	100-200, (100)	n.o.[a]	0.3-1, (20)	1-2, (10)	n.o.[a]
	37 °C	0	n.o.[a]	100-200, (100)	n.o.[a]	0.3-1, (15)	1-2, (10)	n.o.[a]
		2	n.o.[a]	100-200, (100)	n.o.[a]	0.3-1, (25)	1-2, (10)	n.o.[a]
		4	n.o.[a]	100-200, (100)	n.o.[a]	0.3-1, (25)	1-2, (10)	n.o.[a]
		8	n.o.[a]	100-200, (100)	n.o.[a]	0.3-1, (25)	1-2, (10)	n.o.[a]
	60 °C	0	n.o.[a]	100-200, (100)	n.o.[a]	0.3-1, (15)	1-2, (10)	n.o.[a]
		2	n.o.[a]	100-200, (100)	n.o.[a]	0.3-1, (25)	1-2, (10)	n.o.[a]
		4	n.o.[a]	100-200, (100)	n.o.[a]	0.3-1, (25)	1-2, (10)	n.o.[a]
		8	n.o.[a]	100-200, (100)	n.o.[a]	0.3-1, (25)	1-2, (10)	n.o.[a]
2-7.9	25 °C (ambient)	0	n.o.[a]	100-200, (50)	0.5-1, (1)	n.o.[a]	1-4, (5)	n.o.[a]
		2	n.o.[a]	100-200, (50)	0.5-1, (1)	n.o.[a]	1-4, (10)	30, (3)
		4	1-2, (10)	100-200, ()	1-2, (5)	n.o.[a]	1-4, (10)	30, (8)
		8	1-2, (10)	100-200, ()	1-2, (5)	2-3, (5)	1-4, (10)	30, (8)
	37 °C	0	1-2, (15)	100-200, (50)	0.5-1, (5)	n.o.[a]	1-4, (5)	n.o.
		2	1-2, (15)	100-200, (50)	0.5-1, (5)	n.o.[a]	1-4, (10)	30, (5)
		4	1-2, (15)	100-200, (50)	1-2, (5)	n.o.[a]	1-4, (10)	30, (10)
		8	1-2, (15)	100-200, (50)	1-2, (5)	2-3, (20)	1-4, (10)	30, (10)
	60 °C	0	1-2, (20)	100-200, (50)	0.5-1, (5)	n.o.[a]	1-4, (5)	n.o.[a]
		2	1-2, (20)	100-200, (50)	0.5-1, (5)	n.o.[a]	1-4, (10)	30, (5)
		4	1-2, (20)	100-200, (50)	2-3, (5)	n.o.[a]	1-4, (10)	30, (10)
		8	1-2, (20)	100-200, (50)	1-2, (5)	2-3,(15)	1-4, (10)	30, (10)

a. n.o., not observed

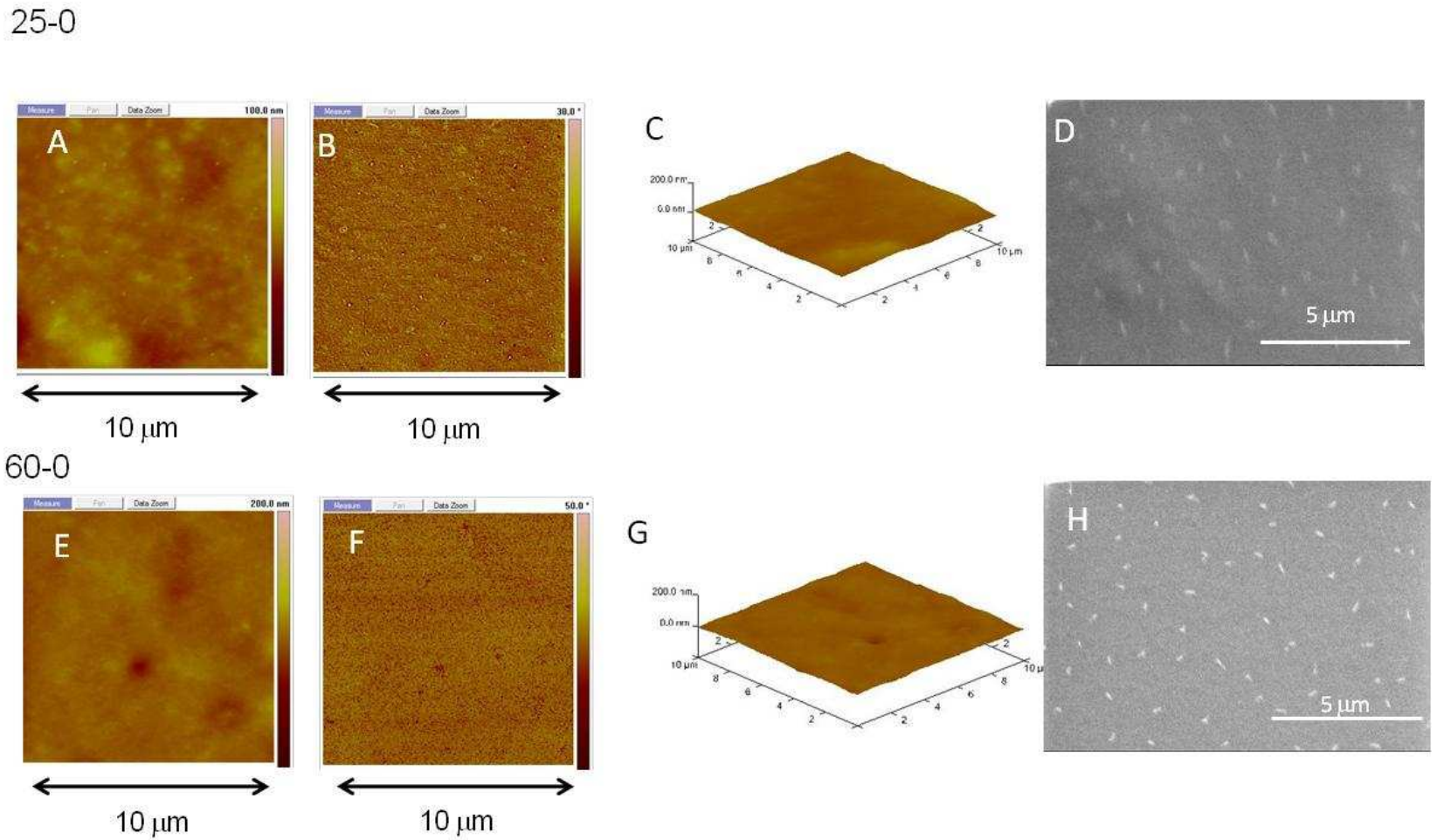

Figure 3.21. Surface Morphology of 0.5- 7.9 blends (0 wks). Upper set (A-D). Cast, devolatilized at 25 ^{o}C; lower set (E-F) same process as upper set with annealing at 60 ^{o}C (24 h) Left to right 10 x 10 µm TM-AFM height image, phase image, and 3D height images. Right, 11k magnification SEM image.

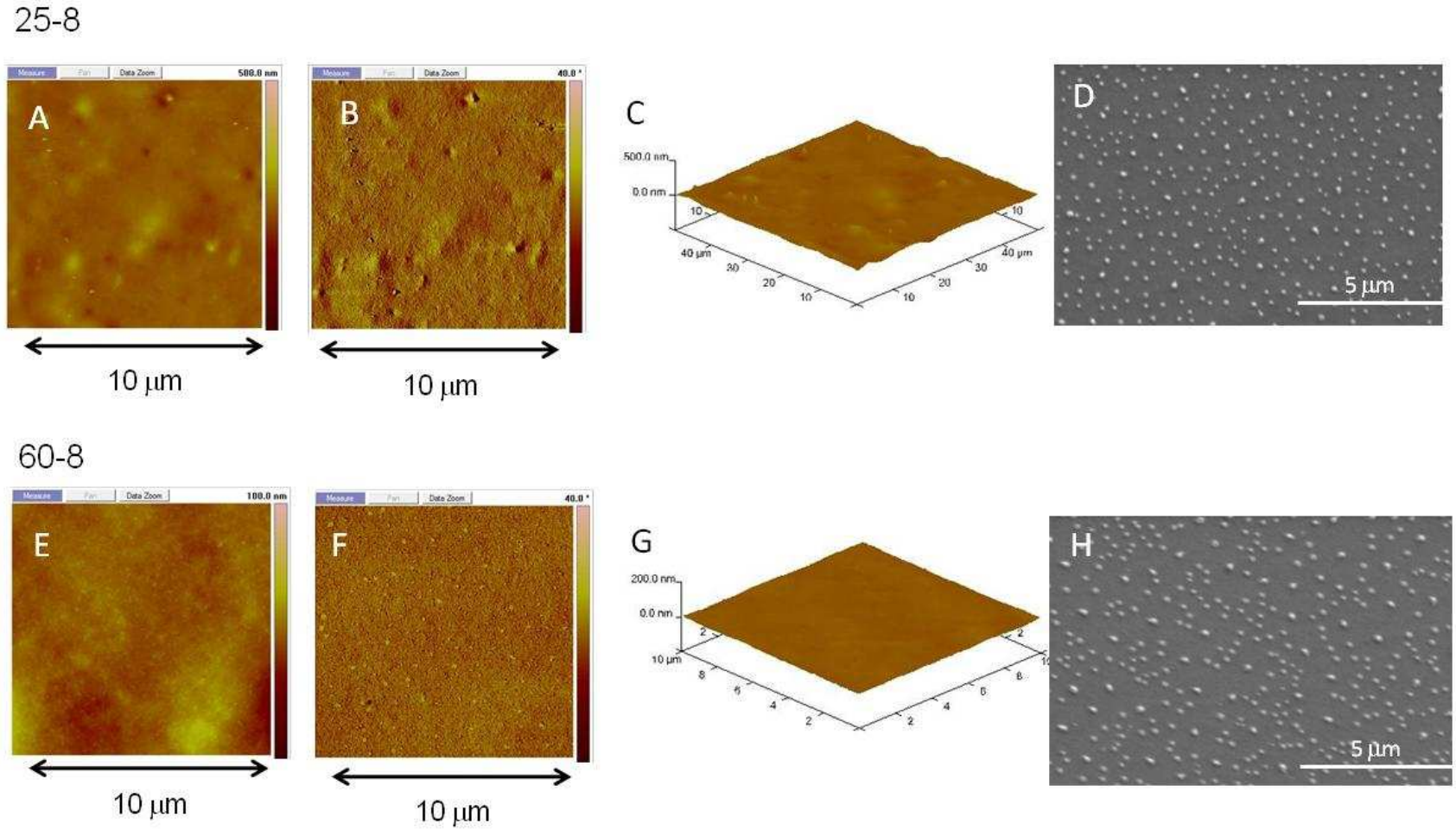

Figure 3.22. Surface Morphology of 0.5- 7.9 blends (8 wks). Upper set (A-D). Cast, devolatilized at 25 ^{o}C; lower set (E-F) same process as upper set with annealing at 60 ^{o}C (24 h). Left to right 10 x 10 μm TM-AFM height image, phase image, and 3D height images. Right, 11k magnification SEM image.

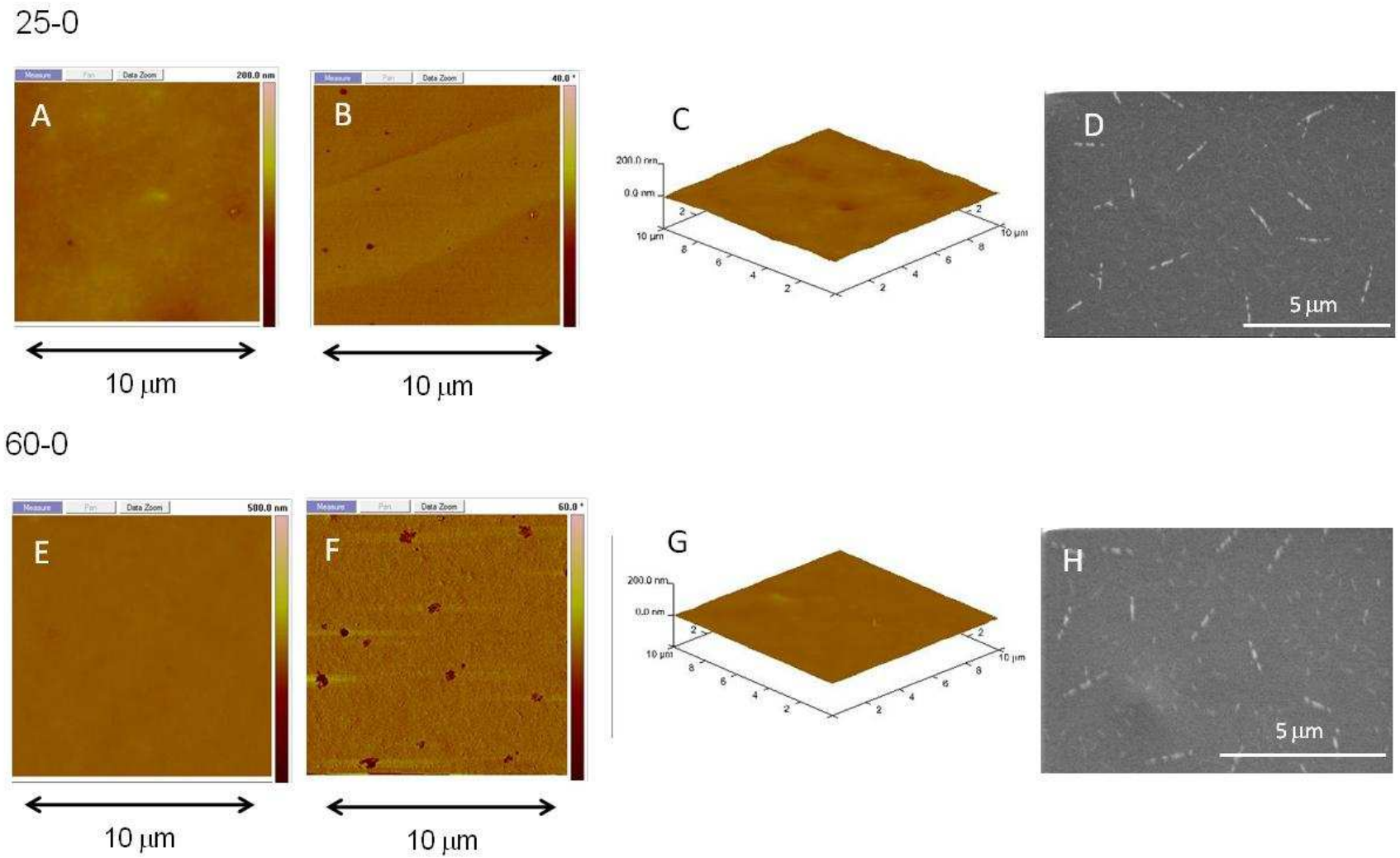

Figure 3.23. Surface Morphology of 1- 7.9 blends (0 wks). Upper set (A-D). Cast, devolatilized at 25 ^{o}C; lower set (E-F) same process as upper set with annealing at 60 ^{o}C (24 h). Left to right 10 x 10 μm TM-AFM height image, phase image, and 3D height images. Right, 11k magnification SEM image.

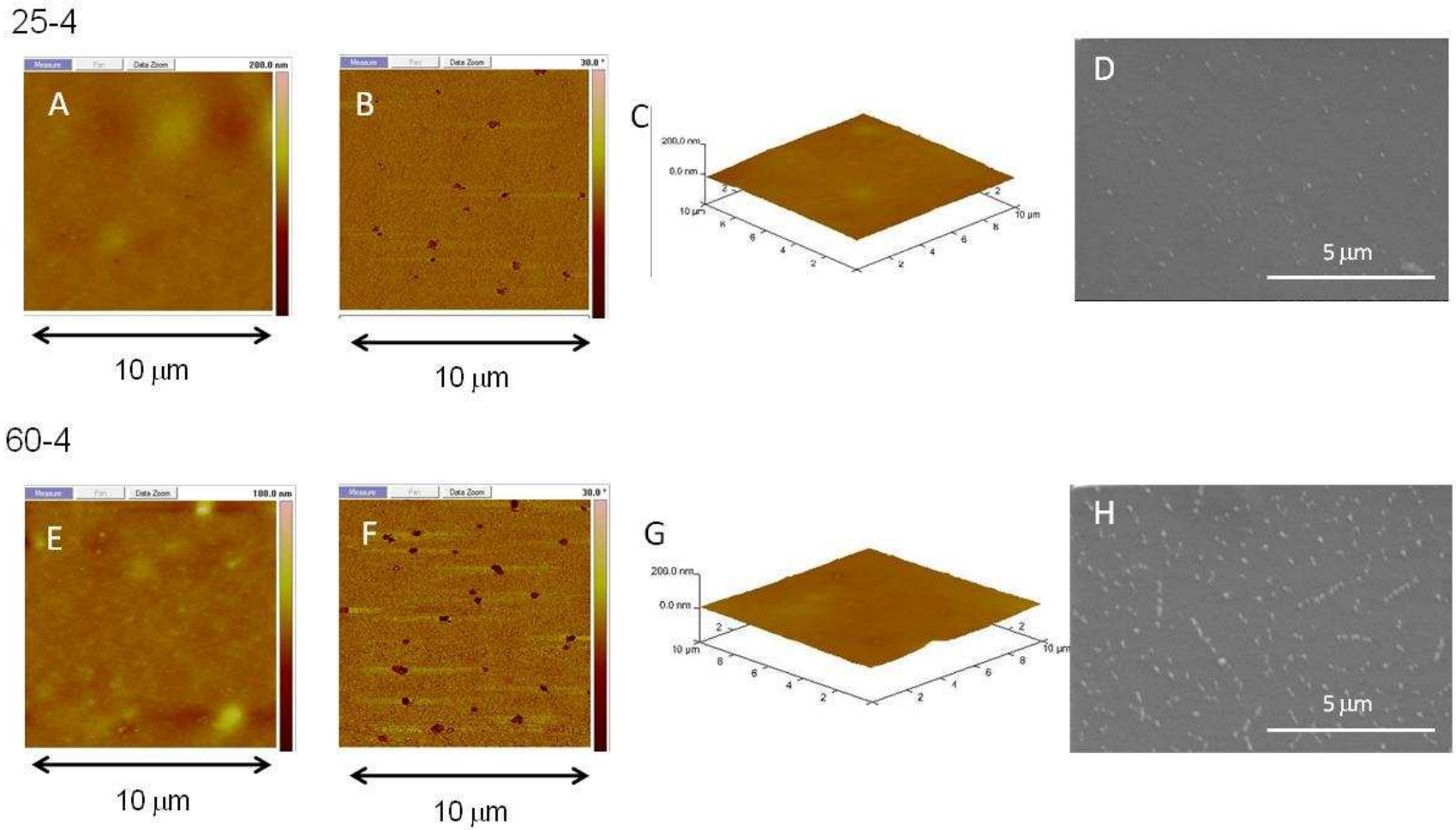

Figure 3.24. Surface Morphology of 1- 7.9 blends (4 wks). Upper set (A-D). Cast, devolatilized at 25 ^{o}C; lower set (E-F) same process as upper set with annealing at 60 ^{o}C (24 h). Left to right 10 x 10 μm TM-AFM height image, phase image, and 3D height images. Right, 11k magnification SEM image.

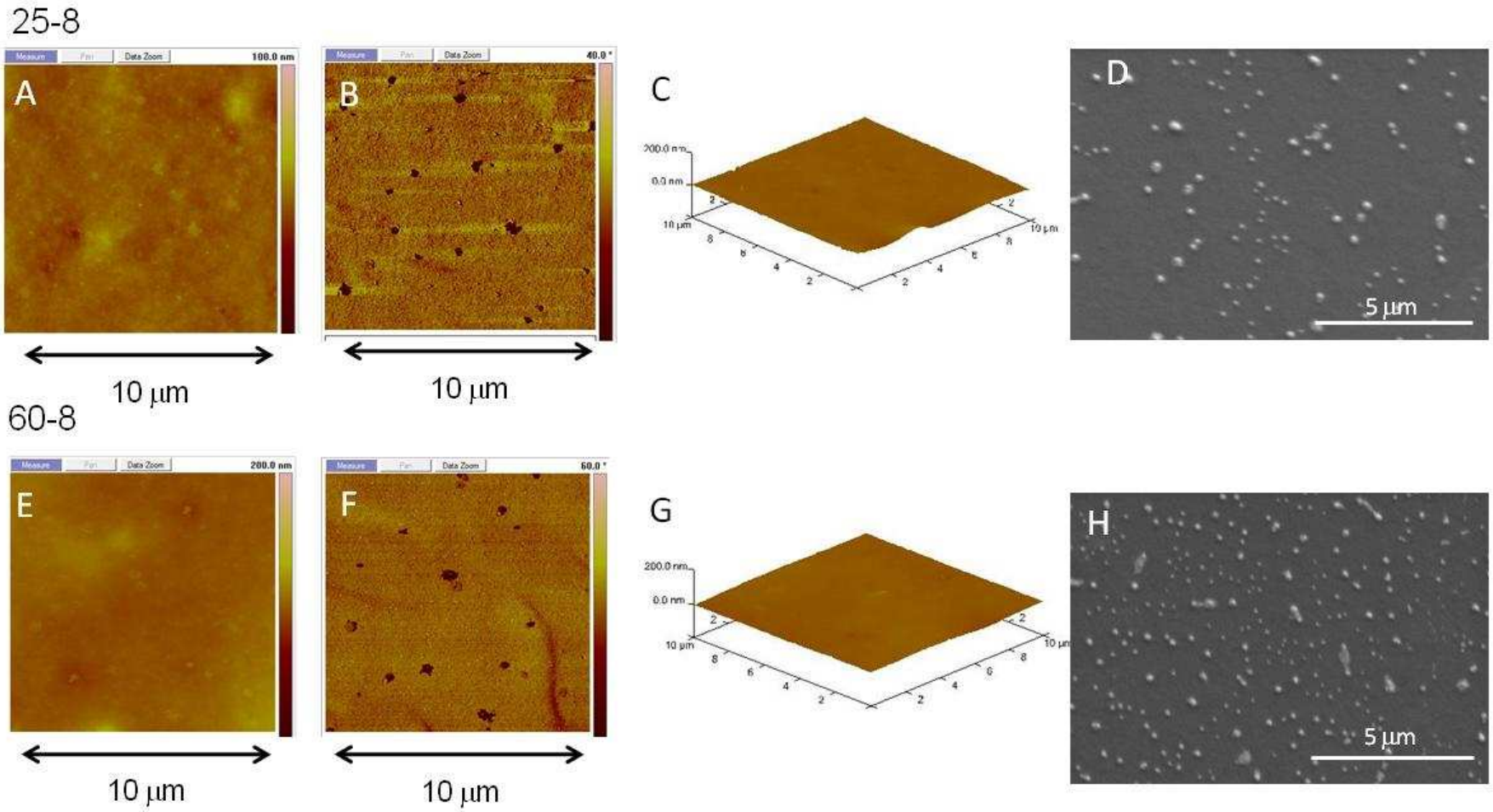

Figure 3.25. Surface Morphology of 1- 7.9 blends (8 wks). Upper set (A-D). Cast, devolatilized at 25 ^{o}C; lower set (E-F) same process as upper set with annealing at 60 ^{o}C (24 h). Left to right 10 x 10 μm TM-AFM height image, phase image, and 3D height images. Right, 11k magnification SEM image.

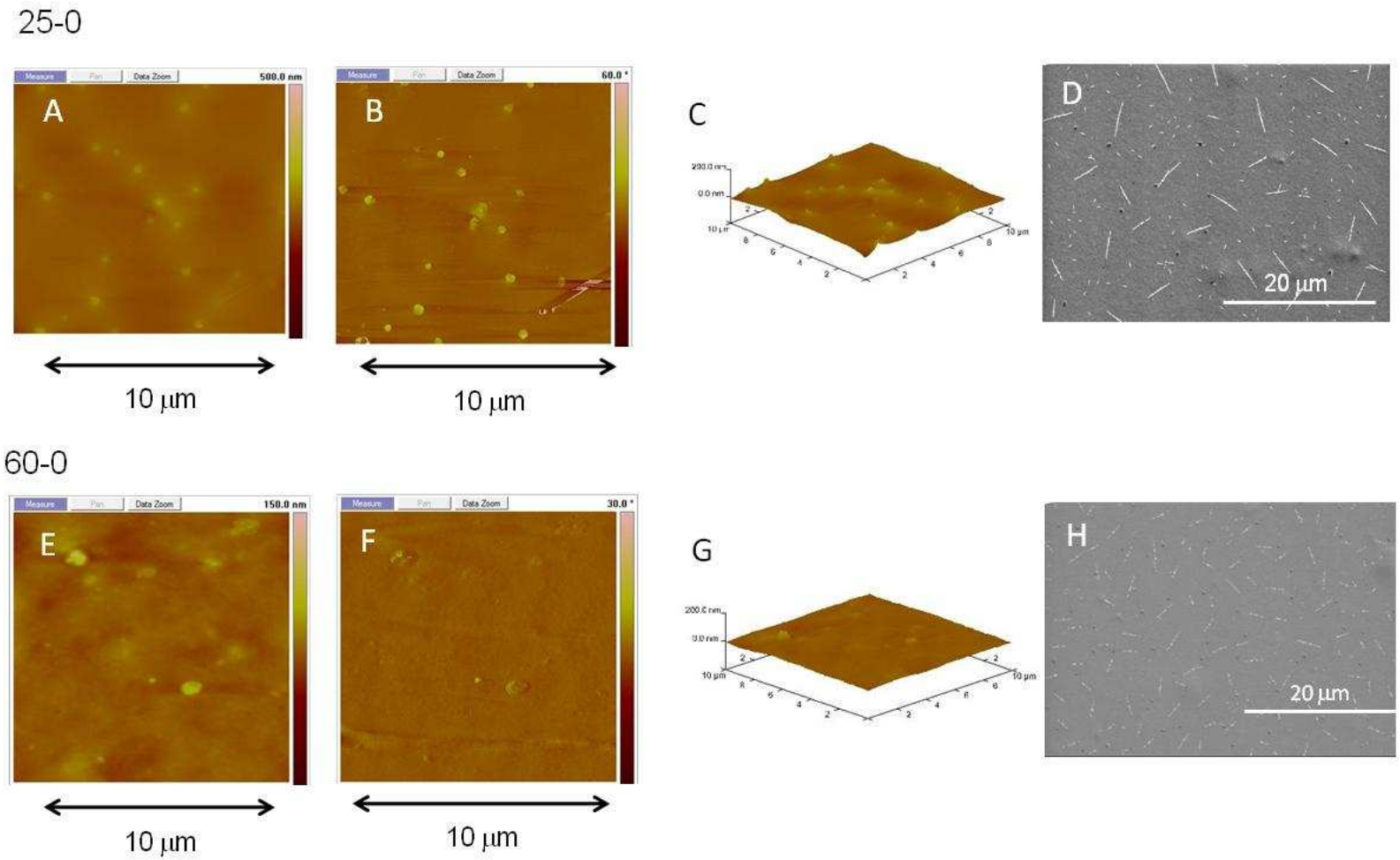

Figure 3.26. Surface Morphology of 2- 7.9 blends (0 wks). Upper set (A-D). Cast, devolatilized at 25 ^{o}C; lower set (E-F) same process as upper set with annealing at 60 ^{o}C (24 h). Left to right 10 x 10 μm TM-AFM height image, phase image, and 3D height images. Right, 2.5k magnification SEM image.

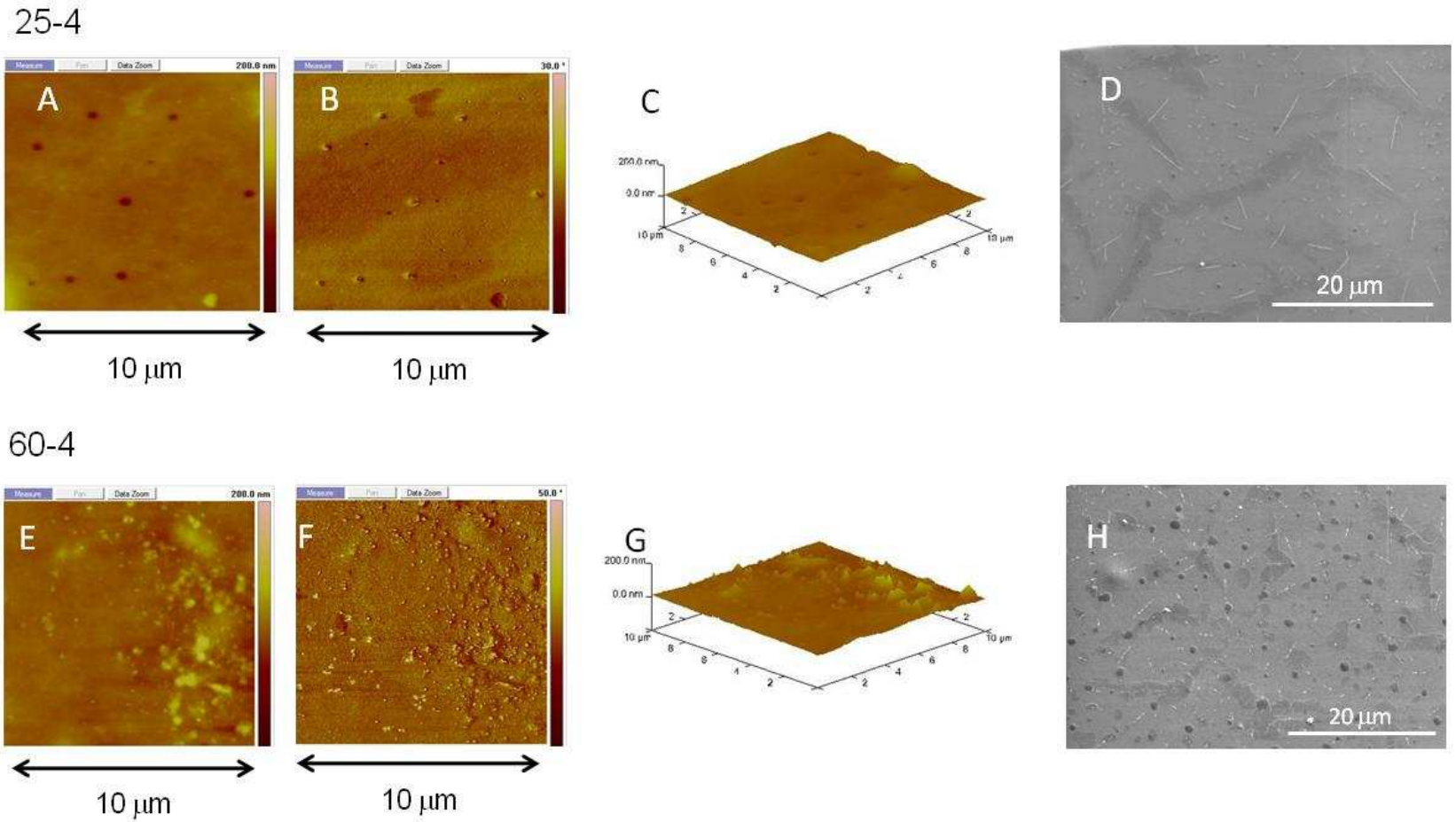

Figure 3.27. Surface Morphology of 2- 7.9 blends (4 wks). Upper set (A-D). Cast, devolatilized at 25 ^{o}C; lower set (E-F) same process as upper set with annealing at 60 ^{o}C (24 h). Left to right 10 x 10 μm TM-AFM height image, phase image, and 3D height images. Right, 11k magnification SEM image.

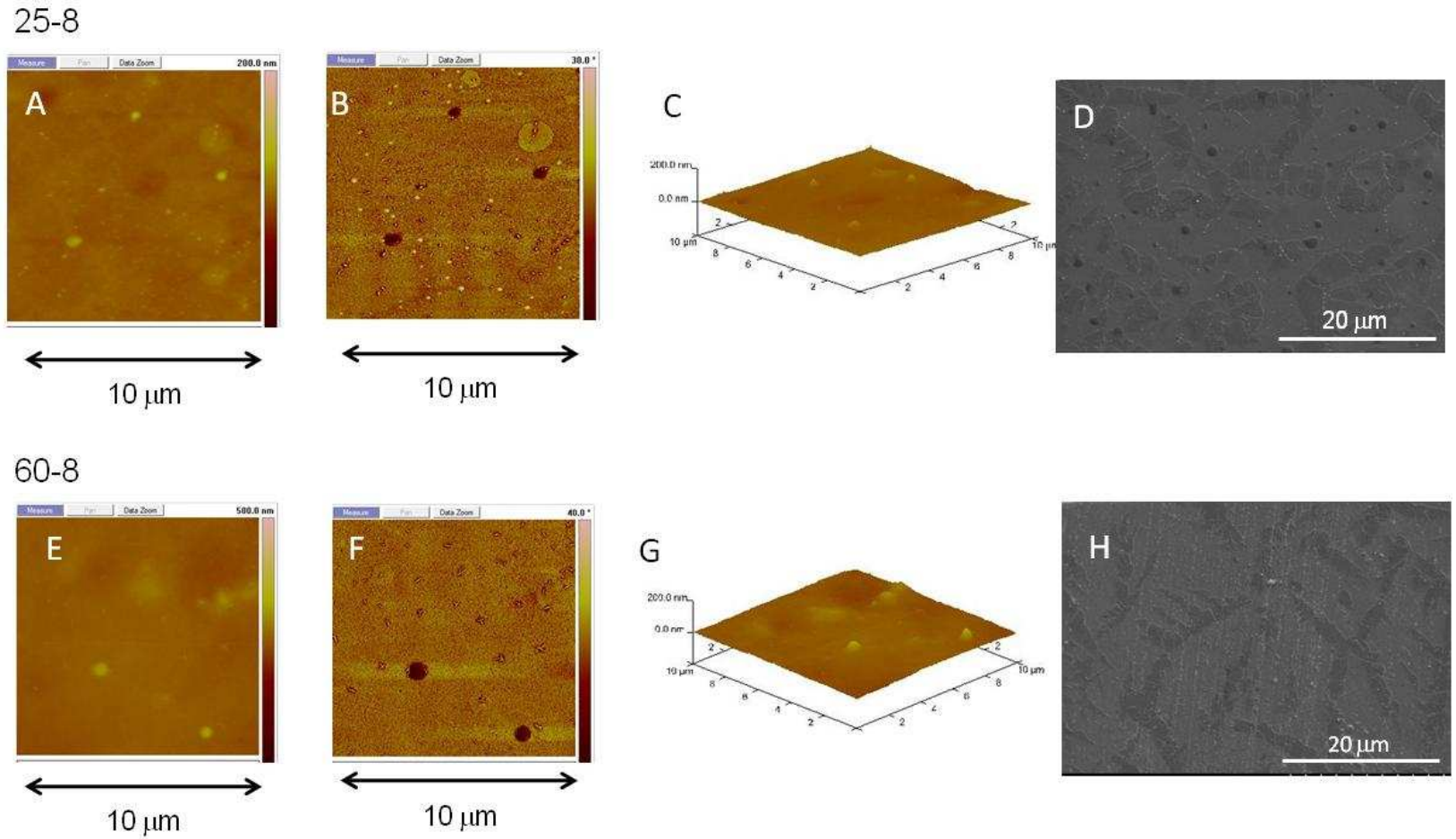

Figure 3.28. Surface Morphology of 2- 7.9 blends (8 wks). Upper set (A-D). Cast, devolatilized at 25 ^{o}C; lower set (E-F) same process as upper set with annealing at 60 ^{o}C (24 h). Left to right 10 x 10 µm TM-AFM height image, phase image, and 3D height images. Right, 11k magnification SEM image.

Characterization of 11 kDa PSM

TM-AFM-0.5 wt% and 1wt% blend. The 0.5-11 films exhibited similar micropeak features as observed in the 3.5, 5.1 and 7.9 kDa blends difference being the size (300 nm-1 μm) and number. At t = 0wks, phase features were observed for 0.5-11-25, 0.5-11-37 and 0.5-11-60 (Figure 3.29). At t = 2 wks (Figure 3.30), further growth of phase separated features was limited. The morphology stabilized at t = 4 and 8 wks (Figure 3.31).

AFM 50 x 50 μm or 10 x 10 μm images for the 1-11-25 blend at t = 0 wks were largely featureless. However, phase separation was observed in scans of 1-11-37 and 1-11-60 (Figure 3.32). These samples displayed similar phase features as the 0.5-11-37 and 0.5-11 60 blends but the features were larger (3-4 μm). At t = 2 wks, (Figure 3.33) micropeaks in the as cast film began to appear while these features are more distinct for 1-11-37 and 1-11-60. At t = 4wks, the micropeaks become larger and more distinct (1-2 μm in diameter) with 20-50 nm heights. At t = 8 wks (Figure 3.34) the morphology was similar to that at 4wks.

SEM- 0.5wt% and 1 wt% blend. 0.5wt% and 1 wt% samples showed similar morphological development, however due to lower concentrations of PSM in the 0.5wt% blends, the features are smaller. SEM images of the 1-11 kDa samples exhibited a morphology similar to that in AFM. Analogous to the AFM images, the 1-11-25 film did not display any significant morphological features at t = 0 wks at 2.5 k magnification however, at 11k magnification nanodots are noticeable (Figure 32). 1-11-37 and 1-11-60 films did not have any discernable features at 2.5k magnification but did show nanocircles like those seen in the as cast film at 11k magnification. At t = 2 wks, the microcircles observed in these samples at 0 wks become more prominent. What also becomes noticeable in SEM images is the formation of the micropeaks observed via AFM and SEM in other blends (Figure 33). These micropeaks become more

distinct with at higher annealing temperatures and larger with age. The micropeak diameters increased from 0.5-1 μm to 2-3 μm at t = 8 wks (Figure 3.34).

TM-AFM-2 wt% blend. Phase separation between the PSM and the base was apparent for the 2-11-25, 2-11-37 and 2-11-60 films at t = 0 wks. Although phase separation was not discerned in 50 x 50 μm images, the 10 x10 μm images revealed the presence of 1-2 μm micropits (Figure 3.35 and Table 3.4). In addition to micropits, nanodots (100-200 nm) were present as they were in blends previously discussed. At t = 2 wks all the 2wt% blends showed a proliferation of micropits and nanodots with further increases in the number of surface features at t= 4 wks and 8 wks (Figure 3.37-38). Although over time the quantity of features increased, the size of the larger features remained between 1-2 μm while the separated dots remained between 100-200 nm.

SEM-2 wt% blend. Phase separation in the 2-11 films was also apparent at t = 0 wks in SEM images. Many of the morphological features seen in the SEM images were similar those in AFM, however SEM imaging revealed 2-3 μm microcircles similar to those in the 1wt% blends (Figure 3.35). With aging, these microcircles become more distinct. Microlines also appear with dimensions similar to those for 7.9 kDa blends (Figures 3.36-37). At t = 8 wks micropeaks similar to those observed in the 7.9 kDa blends were observed in as cast and annealed coatings (1-2 μm) (Figure 3.38).

Table 3.4. Observed surface morphological features for HMDI-BD (50wt%) PTMO (1000): HMDI-BD (30wt%) P[(3FOx)(C12) 87:13- 11 kDa blends.

PSM Blends Composition	Temperature (°C)	Time (wks)	Observed Morphological Features				
			Micropits Size (μm), (Density (#/10 μm^2))	Nanodots Size (nm), Density (#/10 μm^2)	Micropeaks Size (μm), Density (#/10 μm^2)	Microcircles Size (μm), Density (#/10 μm^2)	Microlines Size (μm), Density (#/10 μm^2)
0.5-11	25 °C (ambient)	0	n.o.[a]	n.o.[a]	n.o.[a]	n.o.[a]	n.o.[a]
		2	n.o.[a]	100-200, (100)	n.o.[a]	n.o.[a]	1-2, (10)
		4	n.o.[a]	100-200, (320)	0.200-1, (8)	n.o.[a]	n.o.[a]
		8	n.o.[a]	100-200,	0.200-1, (8)	n.o.[a]	n.o.[a]
	37 °C	0	n.o.[a]	n.o.[a]	n.o.[a]	n.o.[a]	n.o.[a]
		2	n.o.[a]	100-200, (200)	n.o.[a]	n.o.[a]	1-2, (10)
		4	n.o.[a]	100-200, (350)	0.200-1, (10)	n.o.[a]	1-2, (10)
		8	n.o.[a]	100-200,	0.200-1, (12)	n.o.[a]	1-2, (10)
	60 °C	0	n.o.[a]	n.o.[a]	n.o.[a]	n.o.[a]	n.o.[a]
		2	n.o.[a]	100-200, (200)	n.o.[a]	n.o.[a]	1-2, (15)
		4	n.o.[a]	100-200, (350)	0.200-1, (36)	n.o.[a]	1-2, (15)
		8	n.o.[a]	100-200,	0.200-1, (40)	n.o.[a]	1-2, (15)
1-11	25 °C (ambient)	0	n.o.[a]	100-200, (82)	n.o.	n.o.[a]	n.o.[a]
		2	n.o.[a]	100-200, (250)	.5-1 (15)	n.o.[a]	n.o.[a]
		4	n.o.[a]	100-200, (300)	0.5-1, (10)	n.o.[a]	n.o.[a]
		8	n.o.[a]	100-200	0.2-2, (10)	n.o.[a]	n.o.[a]
	37 °C	0	2-3, (6)	100-200, (60)	n.o.[a]	n.o.[a]	n.o.[a]
		2	2-3, (10)	100-200, (266)	.5-1 (8)	n.o.[a]	n.o.[a]
		4	2-3, (6)	100-200, (300)	0.2-1, (5)	n.o.[a]	n.o.[a]
		8	2-3, (7)	100-200, (300)	0.2-2, (15)	n.o.[a]	n.o.[a]
	60 °C	0	2-3, (30)	100-200, (50)	0.2-2, (12)	n.o.[a]	n.o.[a]
		2	2-3, (6)	100-200, (200)	0.500-2, (7)	n.o.[a]	n.o.[a]
		4	2-3, (5)	100-200, (300)	0.5-5, (8)	n.o.[a]	n.o.[a]
		8	2-3, (5)	100-200, (300)	0.5-2, (10)	n.o.[a]	n.o.[a]
2-11	25 °C (ambient)	0	1-2, (3)	100-200, (100)	n.o.[a]	2-3	1-2, (10)
		2	1-2, (5)	100-200, (80)	n.o.[a]	2-3	1-2, (10)
		4	1-2, (15)	100-200, (105)	n.o.[a]	2-3	1-2, (5)
		8	1-2, (25)	100-200, (101)	1-2, (6)	2-3	n.o.
	37 °C	0	1-2, (15)	100-200, (100)	n.o.[a]	2-3	1-2, (10)
		2	1-2, (30)	100-200, (83)	n.o.[a]	2-3	1-2 (10)
		4	1-2 (30)	100-200, (141)	n.o.[a]	2-3	1-2, (10)
		8	1-2, (30)	100-200, (80)	1-2, (5)	2-3	n.o.
	60 °C	0	1-2, (20)	100-200, (100)	n.o.[a]	2-3	1-2,(10)
		2	1-3, (27)	100-200, (90)	n.o.[a]	2-3	1-2 (10)
		4	1-2, (33)	100-200, (150)	1-2	2-3	1-2, (10)
		8	1-2, (37)	100-200, (250)	1-2	2-3	1-2, (10)

a. n.o., not observed

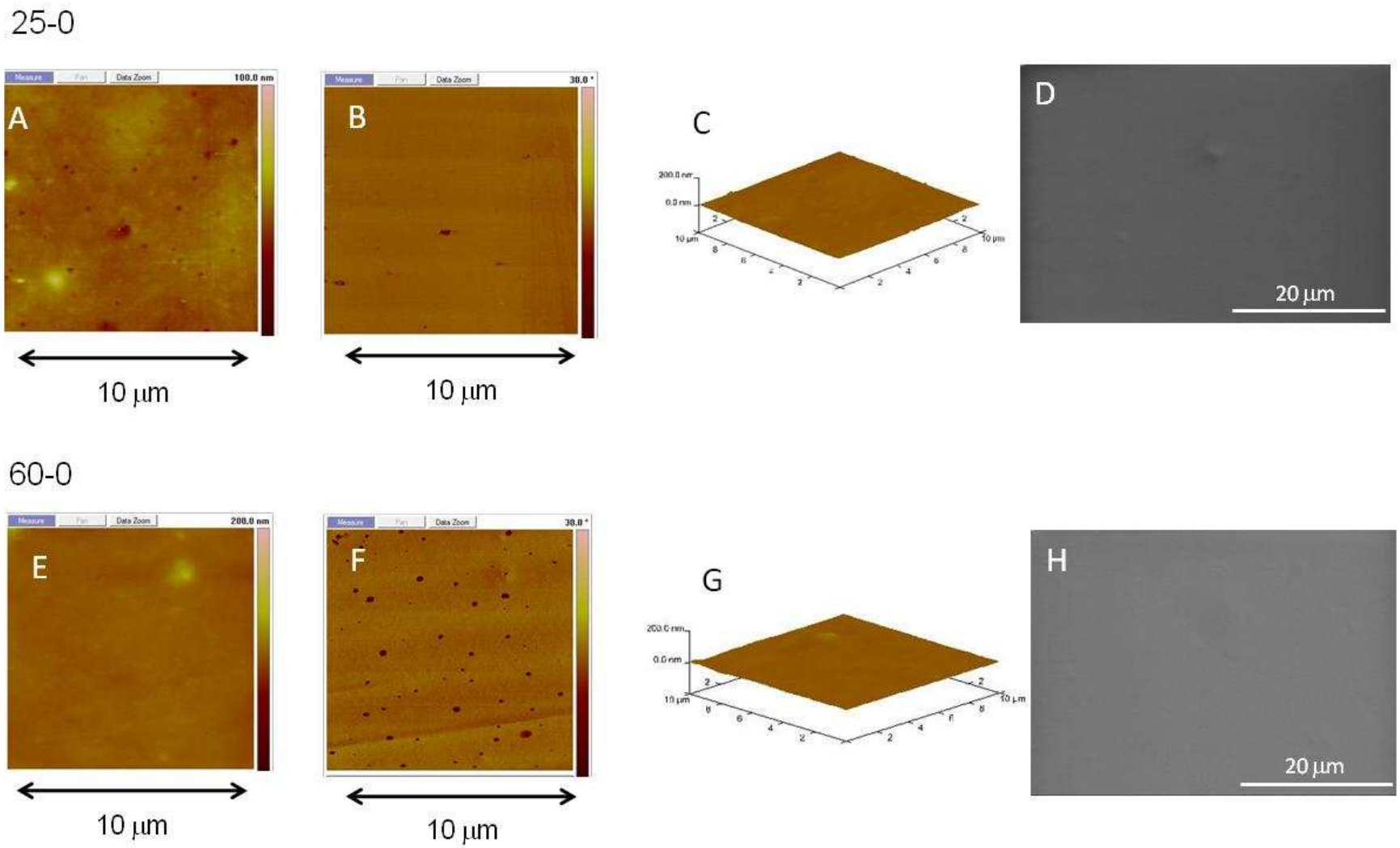

Figure 3.29. Surface Morphology of 0.5- 11 blends (0 wks). Upper set (A-D). Cast, devolatilized at 25 ^{o}C; lower set (E-F) same process as upper set with annealing at 60 ^{o}C (24 h). Left to right 10 x 10 μm TM-AFM height image, phase image, and 3D height images. Right, 2.5k magnification SEM image.

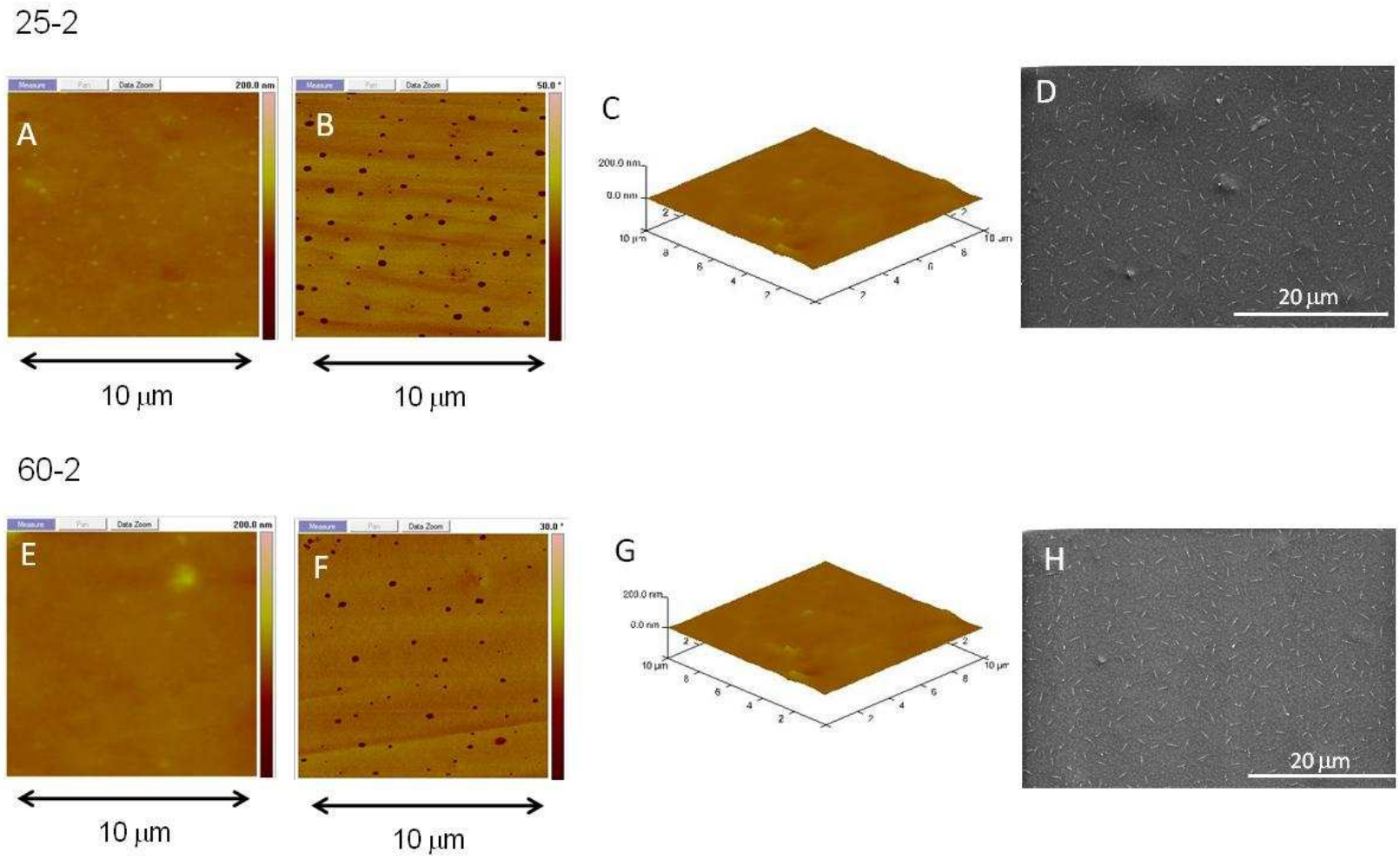

Figure 3.30. Surface Morphology of 0.5- 11 blends (2 wks). Upper set (A-D). Cast, devolatilized at 25 ^{o}C; lower set (E-F) same process as upper set with annealing at 60 ^{o}C (24 h). Left to right 10 x 10 μm TM-AFM height image, phase image, and 3D height images. Right, 2.5k magnification SEM image.

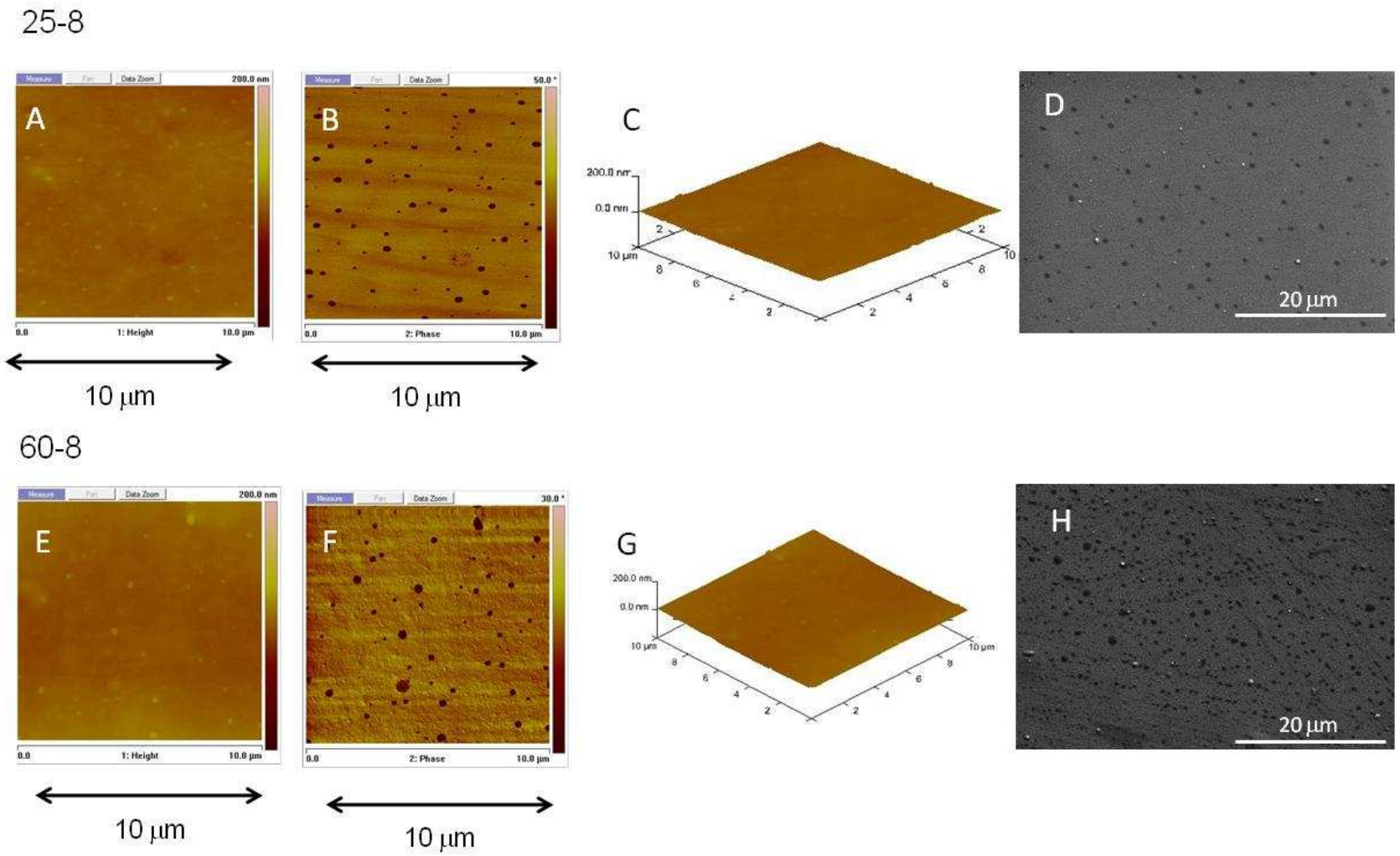

Figure 3.31. Surface Morphology of 0.5- 11 blends (8 wks). Upper set (A-D). Cast, devolatilized at 25 ^{o}C; lower set (E-F) same process as upper set with annealing at 60 ^{o}C (24 h). Left to right 10 x 10 μm TM-AFM height image, phase image, and 3D height images. Right, 2.5k magnification SEM image.

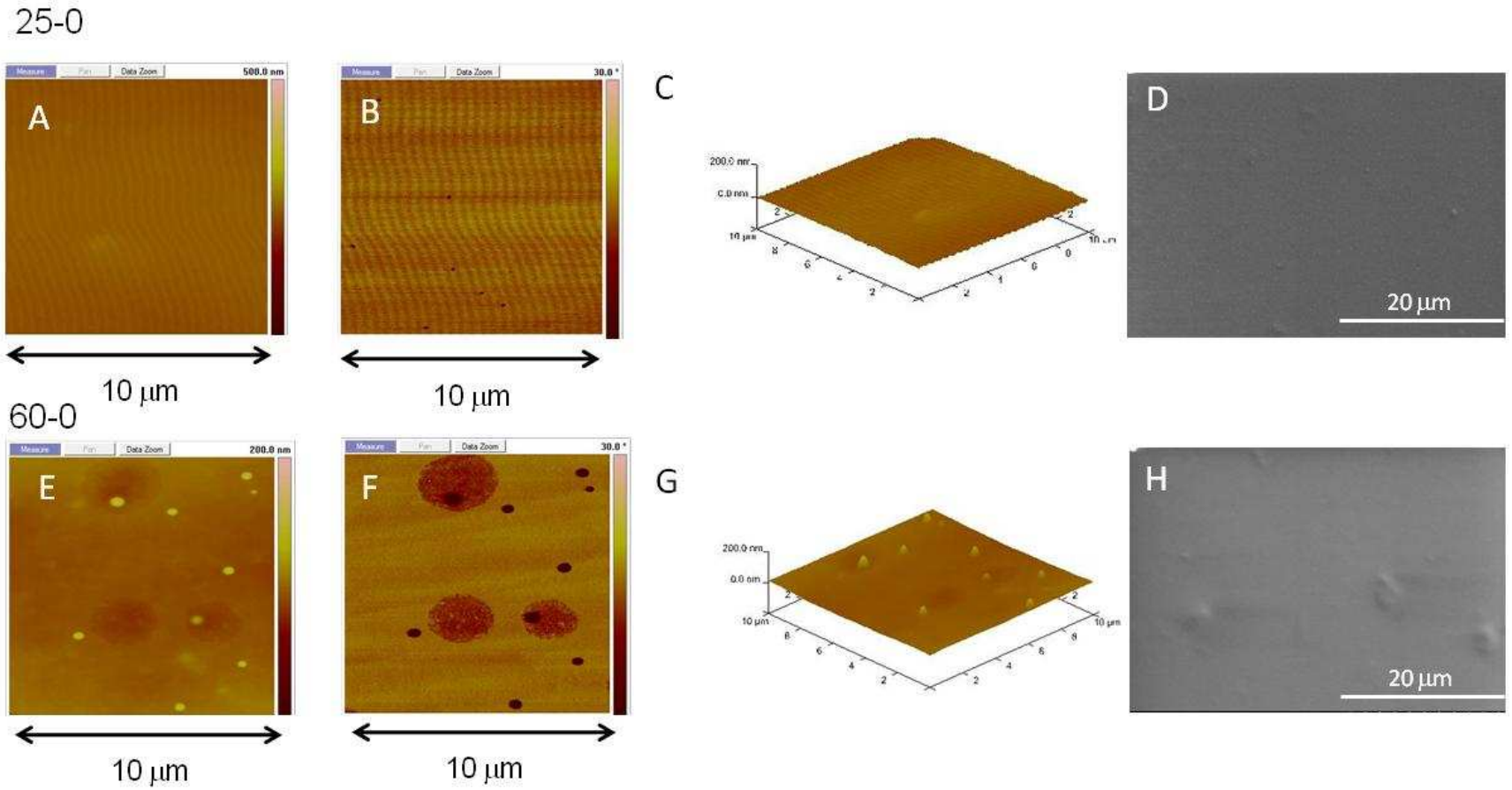

Figure 3.32. Surface Morphology of 1- 11 blends (0 wks). Upper set (A-D). Cast, devolatilized at 25 ^{o}C; lower set (E-F) same process as upper set with annealing at 60 ^{o}C (24 h). Left to right 10 x 10 μm TM-AFM height image, phase image, and 3D height images. Right, 2.5k magnification SEM image.

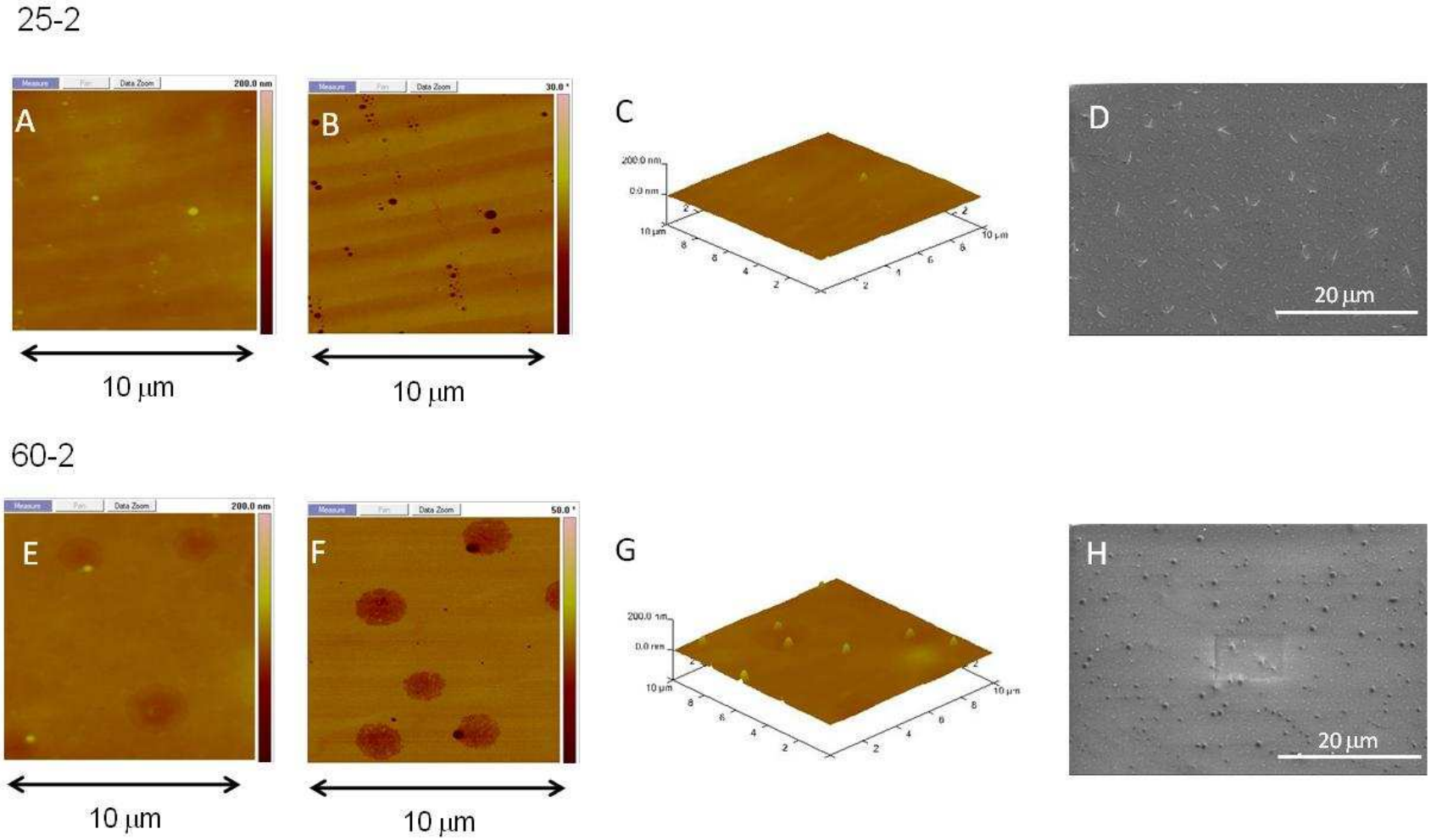

Figure 3.33. Surface Morphology of 1- 11 blends (2 wks). Upper set (A-D). Cast, devolatilized at 25 ^{o}C; lower set (E-F) same process as upper set with annealing at 60 ^{o}C (24 h). Left to right 10 x 10 μm TM-AFM height image, phase image, and 3D height images. Right, 2.5k magnification SEM image.

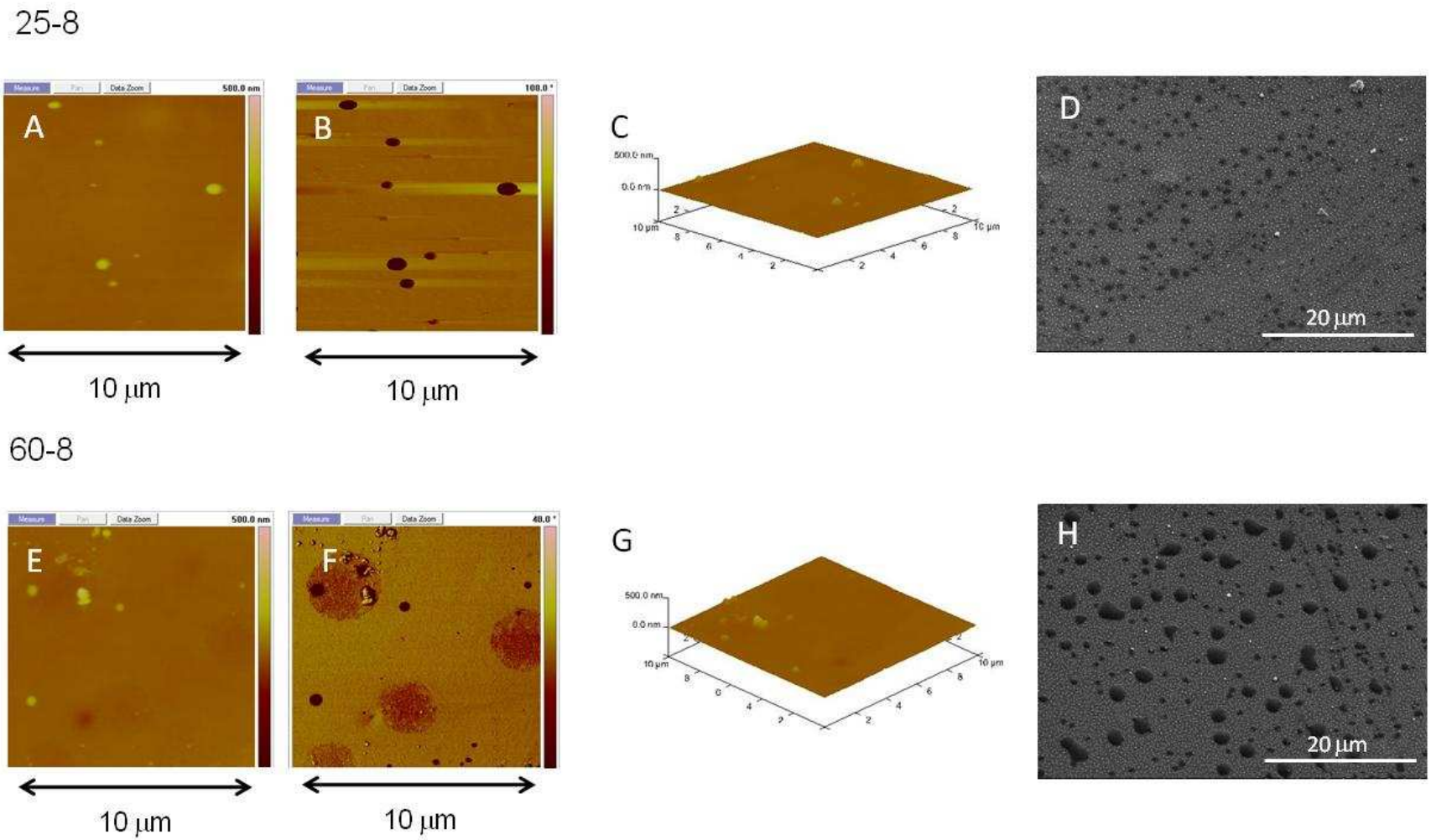

Figure 3.34. Surface Morphology of 1- 11blends (8 wks). Upper set (A-D). Cast, devolatilized at 25 ^{o}C; lower set (E-F) same process as upper set with annealing at 60 ^{o}C (24 h). Left to right 10 x 10 µm TM-AFM height image, phase image, and 3D height images. Right, 2.5k magnification SEM image.

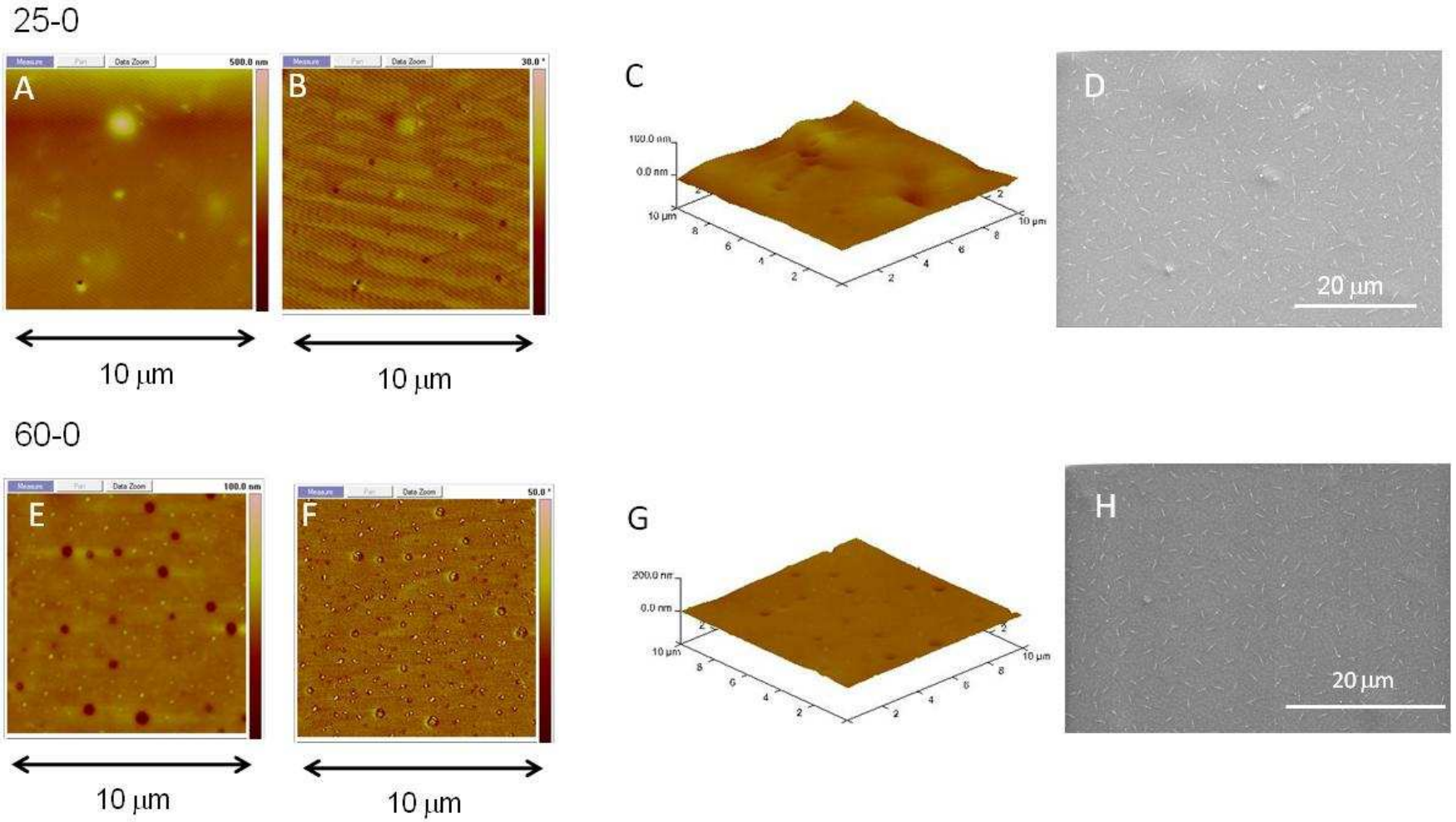

Figure 3.35. Surface Morphology of 2- 11 blends (0 wks). Upper set (A-D). Cast, devolatilized at 25 ^{o}C; lower set (E-F) same process as upper set with annealing at 60 ^{o}C (24 h). Left to right 10 x 10 μm TM-AFM height image, phase image, and 3D height images. Right, 2.5k magnification SEM image.

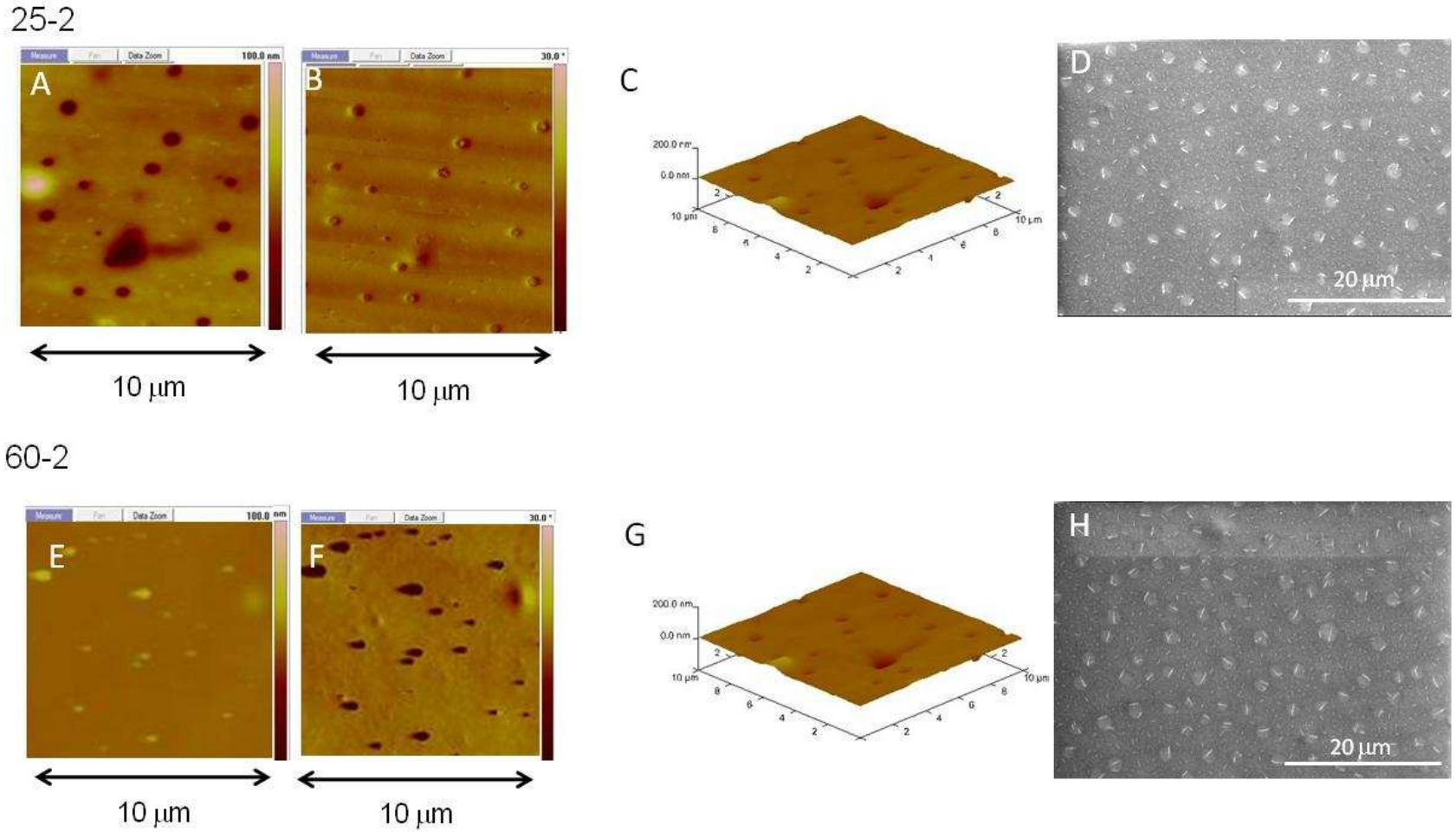

Figure 3.36. Surface Morphology of 2- 11 blends (2 wks). Upper set (A-D). Cast, devolatilized at 25 ^{o}C; lower set (E-F) same process as upper set with annealing at 60 ^{o}C (24 h). Left to right 10 x 10 μm TM-AFM height image, phase image, and 3D height images. Right, 2.5k magnification SEM image.

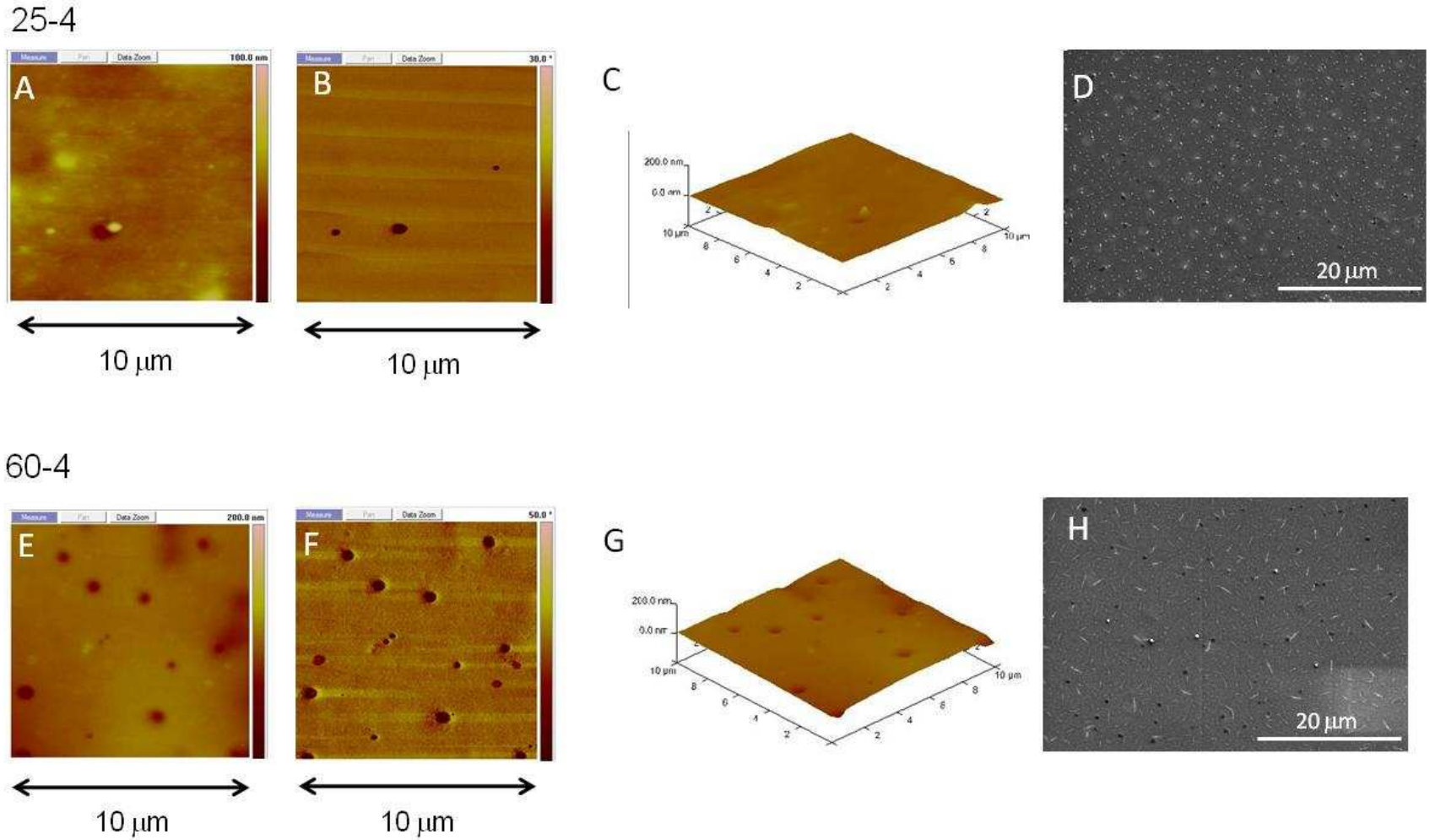

Figure 3.37. Surface Morphology of 2- 11 blends (4 wks). Upper set (A-D). Cast, devolatilized at 25 ^{o}C; lower set (E-F) same process as upper set with annealing at 60 ^{o}C (24 h). Left to right 10 x 10 μm TM-AFM height image, phase image, and 3D height images. Right, 2.5k magnification SEM image.

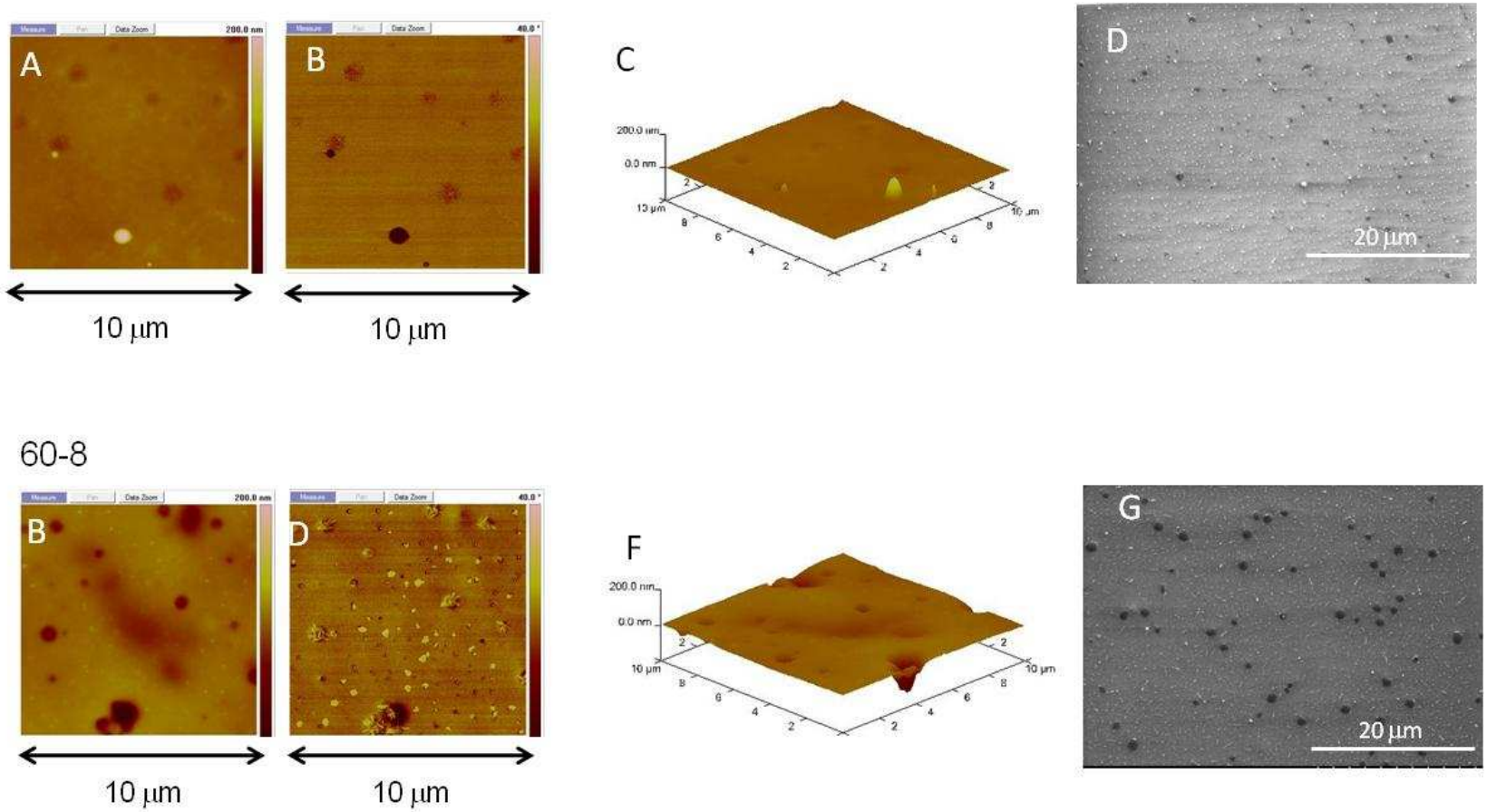

Figure 3.38. Surface Morphology of 2- 11 blends (8 wks). Upper set (A-D). Cast, devolatilized at 25 ^{o}C; lower set (E-F) same process as upper set with annealing at 60 ^{o}C (24 h). Left to right 10 x 10 μm TM-AFM height image, phase image, and 3D height images. Right, 2.5k magnification SEM image.

Discussion of Observed Morphology

The occurrence of domain growth in polymer blends has been modeled by others. [59] It is shown with similar patterns to those observed with the HMDI-BD (30 wt%) P[(3FOx)(C12) 87:13-M_n] blends and other polymer blend. The work of Kontis *et al.* explains that growth of a domain occurs via the transport of like chains from one location to another. [59]This transport was described by two mechanisms. In the first, type 1 polymer chains diffuse out of a type 2 rich domain across the interface into the type 1 rich phase. This results in the formation of type 1 domain. The second mechanism occurs via interfacial dynamics were the polymer chains diffuse parallel to the interface and the morphology undergoes constant reorganization of interfaces to reduces overall interfacial energy. In both cases the interface can be sharp enough to cause a substantial loss of conformational entropy of polymer chains. This causes an entropic barrier for chain transport across the interface that is proportional to the polymer chain length. This chain length and thus molecular weight dependency of the entropic barrier at the domain interface provide further explanation of the large growth in domain size seen in the 3.5 kDa and 5.1 kDa blends. Since the chain length of the 3.5 and 5.1 kDa PSM are rather short compared to the 7.9 and 11 kDa PSM, ΔS for the polymer chains changing conformation at the interface to add new molecules is lower for the 3.5 and 5.1 kDa PSMs. This translates into a lower entropic barrier at the domain interface, thus causing larger phase separated domains and in the case of the 3.5 kDa blend interconnected domains.

Another observation is that many of the blends exhibited more a complex surface morphology with higher weight percentage of PSM. A similar phenomenon was also

observed in the work of Li *et al*. where increasing the weight fraction of PMMA in PS-PMMA blends produced surface morphologies that increased in the prevalence of PMMA.[60] This occurred because the solvent (THF) dissolved PS better than PMMA thus PMMA rich-regions are able to form early. This is what likely occurs with the PSM. Since this PSM is not as soluble in THF as the base polyurethane during casting, it is likely to form PSM rich domains. Therefore the more PSM which is present the larger the PSM domains will become.

Conclusion. This study has demonstrated that the molecular weight of the 3FOx-C12-copolyoxetanes soft block in the HMDI-BD surface modifier has a profound influence on base polyurethane-PSM surface morphology. As the molecular weight of the P[(3FOx)(C12)]-copolyoxetane soft block-PU modifiers with low MW soft blocks (3.5, 5.1 kDa) are initially miscible with the base polyurethane. As reported by Kurt and confirmed in this work, surface concentration is high as well as alkyl ammonium functionality. This accounts for the high contact antimicrobial activity discussed in the next chapter. In contrast to hypothesized increase in near surface functionality, the complex morphologies arising from surface phase separation of the PSM has a negative effect on contact antimicrobial function as described in the next Chapter.

Chapter 4

Effect of PSM soft segment molecular weight on biocidal activity and available surface quaternary charge.

Introduction

In the U.S., hospital acquired infections (HAIs) have been a major problem in healthcare facilities for many years. Based on the 35 million patients admitted to 7,000 acute-care institutions in the United States, the incidence of HAIs is more than 2 million cases per year.[61] HAIs result in an additional 26,250 deaths and added expenditures in excess of $4.5 billion. Principally, these are urinary tract infections (UTIs), bloodstream infections, surgical site infections, and respiratory infections. Many of these infections are caused by *E. coli, Pseudomonas aeruginosa,* and *Staphylococcus aureus*.[62]

Many devices that are currently available rely on the release of a antimicrobial agent such as ions or particles of copper or silver.[63-65] Copper has been used to disinfect fluids and solids for many years dating back as far as ancient Greece. Copper is well known as being safe for humans while microorganisms are extremely susceptible to copper.[63] The bacteriostatic effects of copper surfaces were studied by Kuhn in 1983.[63, 66] In this study, strips of stainless steel, aluminum, and copper were inoculated with cultures (10^7 CFU/mL) of *E. coli, S. aureus Streptococcus D,* and *Pseudomonas* species. The strips were then air dried for 24 hrs at room temperature, inoculated onto blood agar plates and incubated for 24 hrs at 37 ^{o}C. The results from these experiment showed that there was little to no growth for the copper strip while heavy growth was seen for

aluminum and stainless steel for all bacteria types. This demonstrated that copper is an effective biocide and could have applications developing biocidal device.

Although modifying hard surfaces with copper could produce antimicrobial surfaces, layering metallic copper on the surface of soft materials (i.e polymers) may be impractical. In the case of creating biocidal soft materials copper compound are usually incorporated as a dopant for release kill strategies.

Like copper compounds, silver has been utilized in release kill biomedical devices to prevent infection from traumatic wounds, burns, diabetic ulcers and implants.[67] Silver containing bandages such as Silverlon (Argentum Medical) and Actosorb Silver (Johnson and Johnson) have shown to be effective in preventing sepsis of wounds while silver treated catheters (Algid Ag IV, Deroyal) have shown to prevent bacteria colonization associated with urinary tract infections.

Both copper and silver ions are thought to kill bacteria by interfering with bacterial membrane respiratory electron transport chains as well as components of DNA replication.[67] Although this has been shown to be effective; the major drawback to these devices is that they are subject to depletion. This limits release kill devices(i.e. bandages) to short term use. Therefore an alternative to the release kill mechanisms must be utilized in order to create devices for long term use (i.e chronic catheter use). This alternative involves the implementation of non-leaching contact kill surfaces.

As discussed in Chapter 2, prior research has shown that non-leaching contact biocidal surfaces are a viable means of creating hospital equipment with antimicrobial surfaces. [43, 68, 69]

This can be accomplished by polymer surface modification which, as discussed previously, is a well known method to introduce desired functionality to polymer surfaces. Because of their low surface free energy, the affinity of fluorous groups for polymer surfaces after processing in air lead to the idea of combining fluorous groups with a biocidal agent so that the former might act as "chaperones" for surface concentrating biocidal agents during processes such as coating. The biocidal agent of choice in this case contains quaternary ammonium charge which has shown to be effective in killing bacteria.[70 71 72]

Employing a biocidal polymer blend with mechanically robust base polyurethanes is envisioned for infection resistant medical devices such as catheters. Such material engineering could minimize or eliminate infections cause by medical devices. The polymer surface modifiers (PSM) employed in this study are HMDI-BD based polyurethanes containing random P[AB] copolyoxetane soft segments, where A contains a trifluoroethoxy (3FOx) side chain and B contains a 12 carbon quaternary (C12) side chain (Scheme 2.1, Chapter 2). The base polyurethane also consists of HMDI-BD hard segments which favors miscibility, while the semifluorinated groups of the PSM soft segment are immiscible with the base polyurethane. This strategy is aimed at producing a surface consisting of the semifluorinated and quaternary ammonium moieties that would be physically stabilized by the mixing of hard segments between the PSM and the bulk polyurethane (Figure 2.1B, Chapter 2).

Prior research has shown that polymer surfaces modified with surface active polyurethanes containing P[(3FOx)(C12)m:n] polyoxetane soft segments have the capability to kill bacteria via a non-leaching contact kill strategy.[18] As shown in Chapter

3, the surface morphology of blends containing P[(3FOx)(C12)m:n] PSMs is influenced by molecular weight. This chapter will investigate the effect of P[(3FOx)(C12)] molecular weight on the biocidal activity of PSM blends.

Experimental

Bacterial Aerosol Challenge. Having an effective method of testing the biocidal efficacy of non-leaching biocidal material is of great importance. Being that the biocidal agent in immobilized the challenge method must insure that good contact of the bacteria with the biocidal surface in order or effectively determine biocidal activity. The current ATSM standard method for determining biocidal activity for immobilized biocidal agent (ASTM E2149-01) consists of shaking the samples of surface bound materials in a concentrated bacterial suspension (10^6 CFU/mL). Although this method of testing has shown to be effective in determining biocidal activity,[73] it does not represent a real world depositing of bacterial. There are two major means depositing bacteria on surface. The first involves skin contact on surfaces which primarily occurs when the surface of object are physically handled. The second is via an aerosol which can occur during talking, sneezing, coughing or breathing.[74]

Prior research by Tiller *et al.* utilized a method where bacteria were sprayed on surface modified glass slides and place sprayed-side down in a Petri dish after 2 min drying time. This method has shown to be affective for the semi-quantitative determination of the biocidal activity of release and non-release biocidal materials,[74, 75] however there are major differences between this method and the one used in this study which be explained later in the chapter.

Bacteria Culture Preparation. Agar plated were streaked with *P. aeruginosa* from a stock culture kept frozen at -70 ^{o}C and incubated at 37 ^{o}C for 18-24 hrs. From this plate a single colony was collected and used to inoculate 6 mL of Luria broth. This culture solution was incubated for 18-24 hrs at 37 ^{o}C. After incubation, a 1:50 dilution of the culture was prepared and incubated at 37 ^{o}C until an optical density of 0.2-0.3 was observed for 1 mL of culture. Once the desired optical density has been achieved, the culture solution is used in bacteria challenges.

Sample Preparation and Bacteria Challenge. Slides coated with P[(3FOx)(C12)] PSM blends were prepared as previously described in the Chapter 3, p.74. A biocidal test was devised to deposit *P. aeruginosa* via an aerosol spray as depicted in Figure 4.2.

Although the use of bacterial aerosols has shown to be an effective strategy in testing surface biocidal activity, there are some problems associated with it. Prior experiments utilized a pump spray bottle filled with bacteria culture. This method was able to deliver a bacterial aerosol; however, there were inconsistencies in spray volume and drop size. These inconsistencies in the application of bacteria to sample slide produced inconsistent results from bacteria challenge experiments. To solve this problem, a better method of delivering bacteria to the surface of the samples needed to be developed.

There were several issues to consider when developing the spray system. It was desired that the pumping system would run with constant air flow instead of the pumping action required with the use of a spray bottle. This required the use of a pressure pump to deliver air to a chromatography sprayer. When this was initially done it was discovered

that the pump delivered air in an inconsistent pulsing manner which created a pulse like spray pattern. To solve the issue with pulsation, a more elaborate setup was needed. This setup involved using the pressure pump to create a pressurized system.

Figure 4.1 shows the system used to deliver the challenge bacteria aerosol. It consists of a single head pressure pump connected to a pressure regulator valve via a series of tubing connections. Within the connection between the pump and the main valve was an empty vessel with a volume of 20 mL. This dead volume serves as a reservoir for the pump to fill with air prior to it going to the spray apparatus. Filling this reservoir pressurized the system and removes the pulsation that would have occurred if the sprayer had been directly connected to the pump. Following the pressure regulator, an adjustable flow meter set to displace 10 mL of water/min controls the flow of air to the sprayer.

The use of the pressurized pumping system has shown to be more effective at delivering bacteria aerosol compared to the pump type spray apparatus. Both drop size and spray volume were more consistent with 1s sprays producing 5-7 μL of spray volume. This improved consistency has resulted in an experiment with better reproducibility and reliability.

Letter keys in Figure 4.2 correspond to the following steps of the biocidal challenge: (A) Using a stock bacteria concentration of 10^6 colony forming units (CFU)/mL, slides (B) coated with 2wt% and 1wt% PSM blends were sprayed (C) for 1 s and weighed to determine the amount of bacteria solution deposited. (D) Sprayed slides were then placed in a constant humidity (85-95%) environment. Keeping samples at constant humidity is important because control experiments in ambient air showed irreproducible fractions of dead bacteria as a function of time. These irreproducible

results are the result of uncontrolled bacterial desiccation in air or possibly to bacteria experiencing osmotic shock. (E) After 30 min, the slides were placed in saline solution and vortex stirred for 2 min with a Fisher Scientific G-560 Vortexer. (F) One hundred microliter aliquots and (x 10) dilutions were removed and spread onto agar plates that were incubated at 37 °C for 18 h. (G) After incubation for 24 h, bacteria colonies were counted to obtain the percent kill and log reduction. Example calculations are shown below:

Percent Kill Calculation

$$\%kill = 1 - \frac{CFU_{sample}}{CFU_{control}} \times 100 \qquad (1)$$

$$100\% = 1 - \frac{0}{189} \times 100$$

Log Reduction Calculation

$$\text{Log Reduction} = \log\left(\frac{CFU_{control}}{CFU_{sample} + 1}\right) \qquad (2)$$

$$2.28 = \log\left(\frac{189}{0 + 1}\right)$$

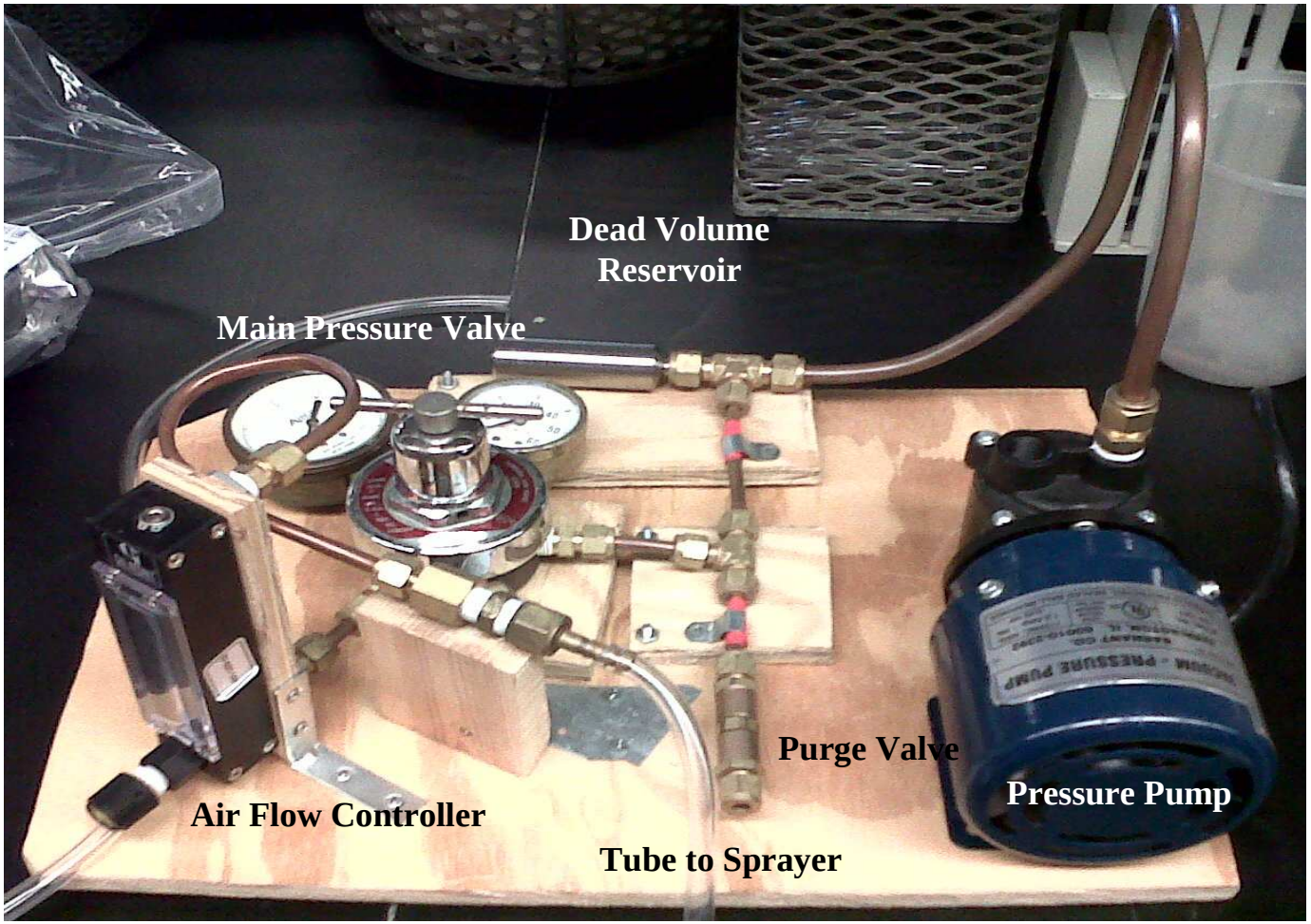

Figure 4.1 Bacteria challenge pumping system

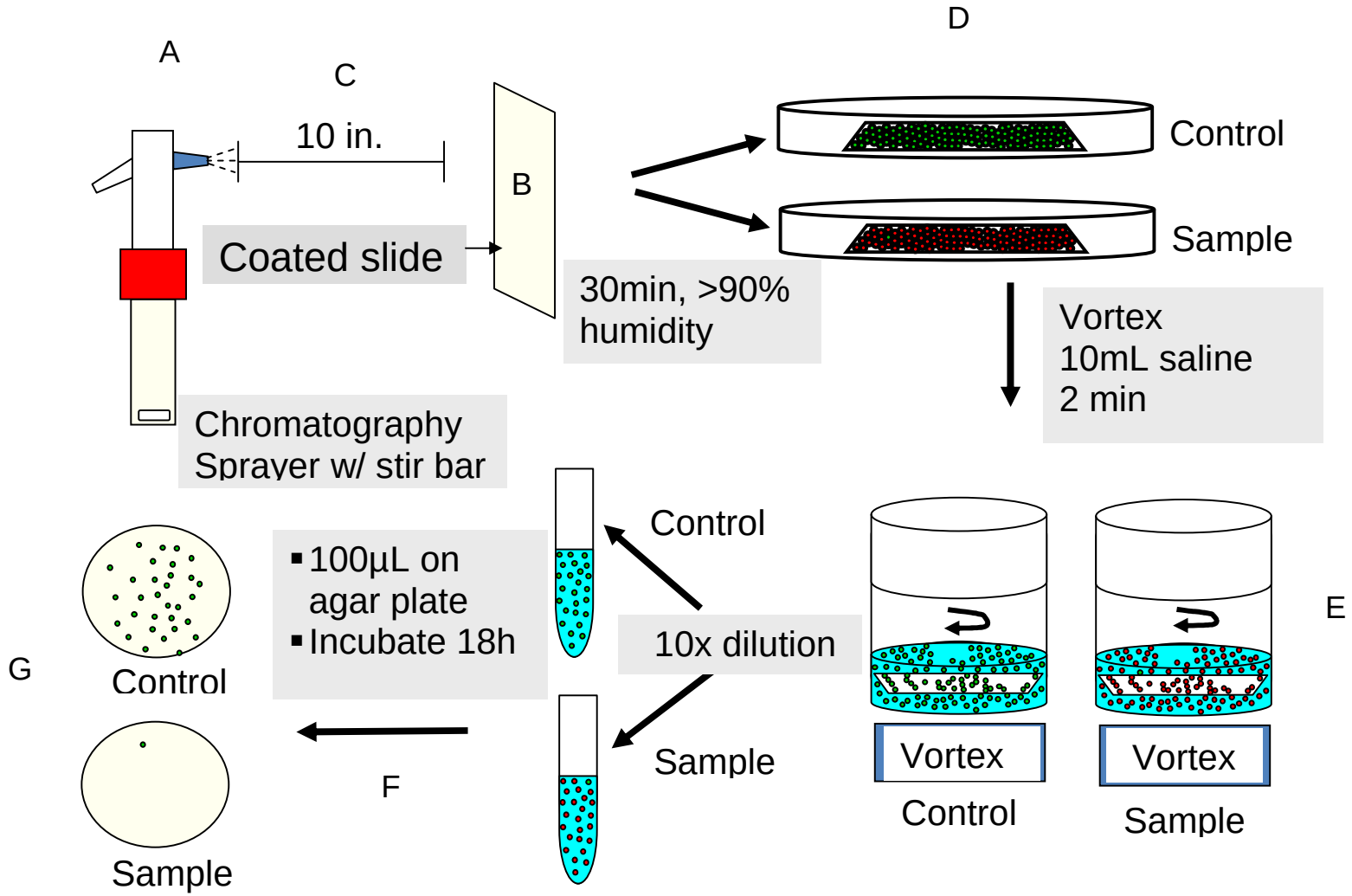

Figure 4.2. Schematic of biocidal spray test with *P. aeruginosa*

Results and Discussion.

Bacteria Challenges. Biocidal challenges revealed that as cast 3.5 kDa blends at t = 0 wks exhibited good biocidal activity as seen in Figure 4.3. 0.5, 1, 2 wt% blends had 100 % kills resulting in log reductions of 2.4. Coatings that were annealed had lower kill percentages (Table 4.1). Biocidal activity for the as cast films that have been devolatilized and stored at ambient temperature is not stable over time as indicated in Figure 4.4 and Table 4.1. At t = 2 wks, 0.5, 1, and 2 wt% films all showed a considerable loss of activity.

Challenges of the 5.1 kDa blend revealed similar results as those for the 3.5 kDa blend where the 0.5, 1 and 2 wt% films at t = 0 wks had 100% kills and log reductions of 2.3 (Figure 4.5 and Table 4.1). However as with the 3.5 kDa blends, reduced activity occurs with annealing and aging (Figure 4.6). This decrease in activity is likely due to PSM phase separation discussed in the Chapter 3. As seen in Figures 3.1, 3.4 and 3.8 in Chapter 3, the as cast films exhibited no significant phase separation. However, since the soft segment is above its T_g at ambient temperature, the available thermal energy is sufficient for slow PSM phase separation with time (Figures 3.2, 3.5 and 3.9, Chapter 3). These aggregates sequester quaternary ammonium charge from the surface thereby resulting in a surface that gradually becomes inactive (Figure 4.9). This time dependent phase separation is not desirable as such coatings would have a short “shelf life” and temperature sensitivity.

PSM blends with 7.9 and 11 kDa soft blocks exhibited low biocidal activity at t = 0 wks (Figure 4.7 and 4.8). As seen in Table 1, 0.5 and 1 wt% blends exhibited kill percentages less that 40% while in comparison the as cast and annealed films with 2wt%

7.9 kDa and 11 kDa had kill percentages of 50-60%. Again, this correlates with phase separation of the PSM as shown in Chapter 3. This immediate phase separation after coating formation is shown in Figures 3.28 and 3.35, Chapter 3. This phase separation much like the time dependent phase separation seen in the 3.5 and 5.1 kDa blends sequesters quaternary charge from the surface which results in reduced activity.

Given the morphological studies in Chapter 3, quaternary charge sequestration can be explained by reference to the phase diagram schematic in Figure 4.9. In the case of as cast 3.5 and 5.1 kDa blends at t = 0 wks one phase is observed via AFM and SEM. This corresponds to the metastable state M in the phase diagram. This explains the excellent biocidal activity (Table 4.1), as this state corresponds to the model at the lower right where B, the biocidal group is concentrated at the surface. With time, or with annealing, the metastable state undergoes spinodal decomposition to a stable PSM rich and poor phases labeled S.

When the soft block molecular weight was increase to 7.9 and 11 kDa, even coatings at t = 0 wks display surface phase separation indicating the formation of two phases. This phase separated S state results in decreased biocidal activity.

Table 4.1. Results from aerosol spray testing of HMDI-BD (50wt%)-PTMO (1000):HMDI-BD (30wt%)-P[(3FOx)(C12)-0.87:0.13-11 kDa] coatings.

P[(3FOx)(C12)0.87:0.13-M_n]	PSM Weight Percentage					
	0.5 wt%		1wt%		2 wt%	
	% killed	log reduction	% killed	log reduction	% killed	log reduction
11 kDa t = 0 wks as cast	6.4	0.03	19.7	0.03	56.1	0.35
11 kDa t = 0 wks annealed 60 °C	15.5	0.07	20.6	0.1	67.5	0.48
7.9 kDa t= 0 wks as cast	10.3	0.05	23	0.11	44.6	0.25
7.9 kDa t= 0 wks annealed 60 °C	20.8	0.1	37.2	0.2	48	0.28
5.1 kDa t = 0 wks as cast	100	2.43	100	2.43	100	2.43
5.1 kDa t = 0 wks annealed 60 °C	2.6	0.01	47.6	0.28	62.5	0.44
5.1 kDa t = 2 wks as cast	15.5	0.02	6.9	0.03	24.2	0.12
5.1 kDa t = 2 wks annealed 60 °C	0.5	0	1.8	0.01	10.4	0.05
3.5 kDa t = 0 wk as cast	100	2.37	100	2.37	100	2.37
3.5 kDa t = 0 wks annealed 60 °C	8.2	0.03	16.8	0.08	18.2	0.08
3.5 kDa t = 2 wks as cast	1.3	0	6.3	0.03	12.5	0.06
3.5 kDa t = 2 wks annealed 60 °C	5	0.07	6.2	0.03	9.9	0.04

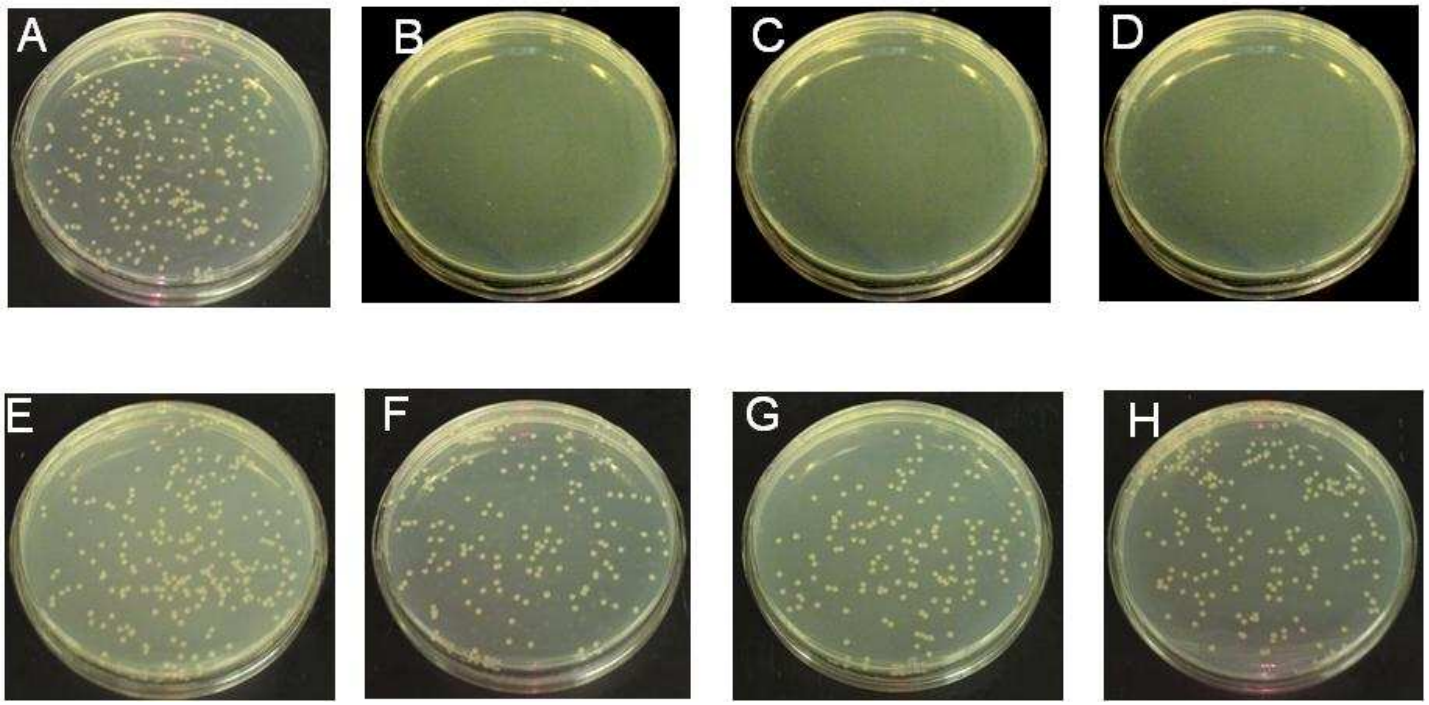

Figure 4.3. Agar plates of P. aeruginosa challenges on HMDI-BD (50wt%)-PTMO (1000):HMDI-BD (30wt%)-P[(3FOx)(C12)-0.87:0.13-3.5 kDa] blends , t = 0wks. Challenge concentration = 2.3 x 10^6 CFU/mL A) As cast base PU (control), B) 0.5 wt% as cast, C) 1wt% as cast, D) 2 wt% as cast, E) Base PU annealed at 60 ^oC, F) 0.5 wt% annealed at 60 ^oC, G) 1wt% annealed at 60 ^oC, H) 2 wt% annealed at 60 ^oC

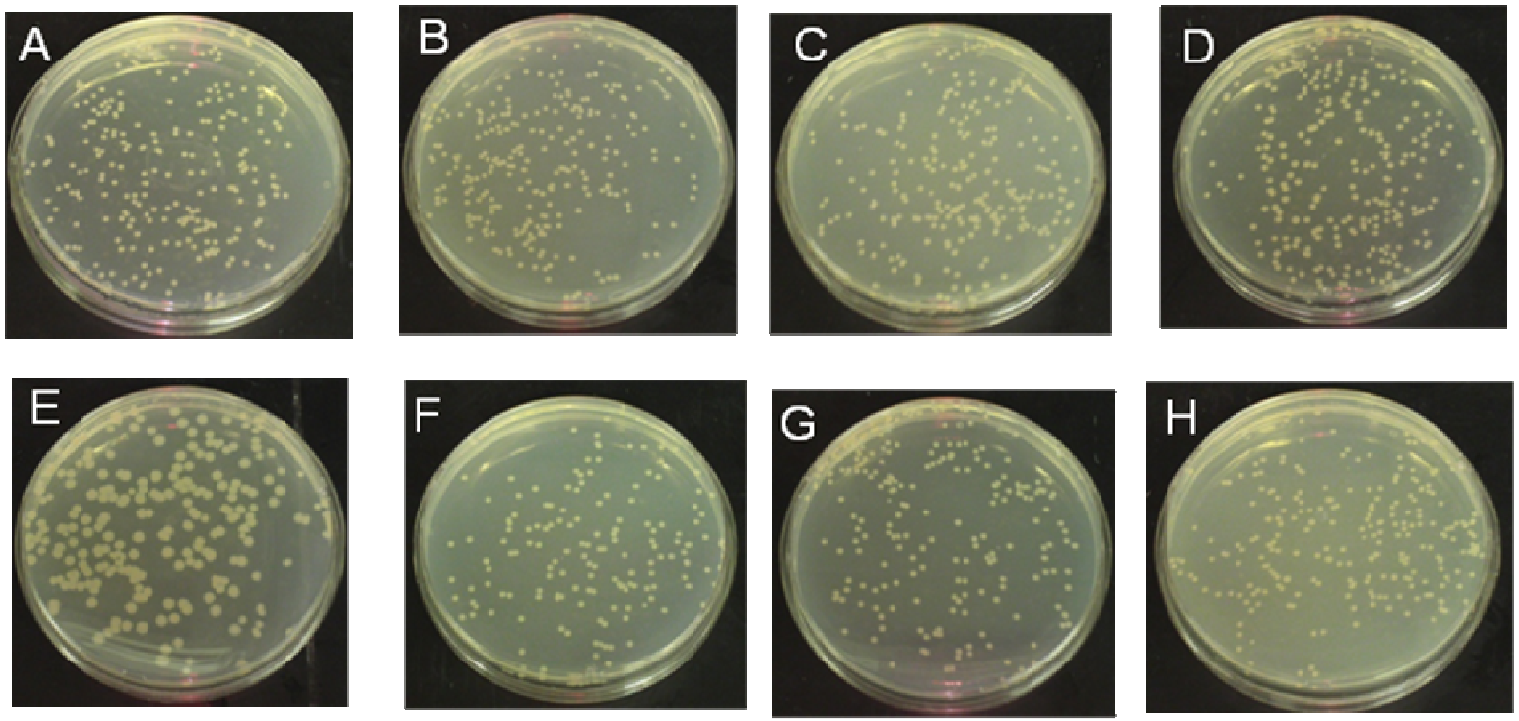

Figure 4.4. Agar plates of P. aeruginosa challenges on HMDI-BD (50wt%)-PTMO (1000):HMDI-BD (30wt%)-P[(3FOx)(C12)-0.87:0.13-3.5 kDa] blends , t = 2 wks. Challenge concentration = 2.3 x 10^6 CFU/mL A) As cast base PU (control), B) 0.5 wt% as cast, C) 1wt% as cast, D) 2 wt% as cast, E) Base PU annealed at 60 ^oC, F) 0.5 wt% annealed at 60 ^oC, G) 1wt% annealed at 60 ^oC, H) 2 wt% annealed at 60 ^oC

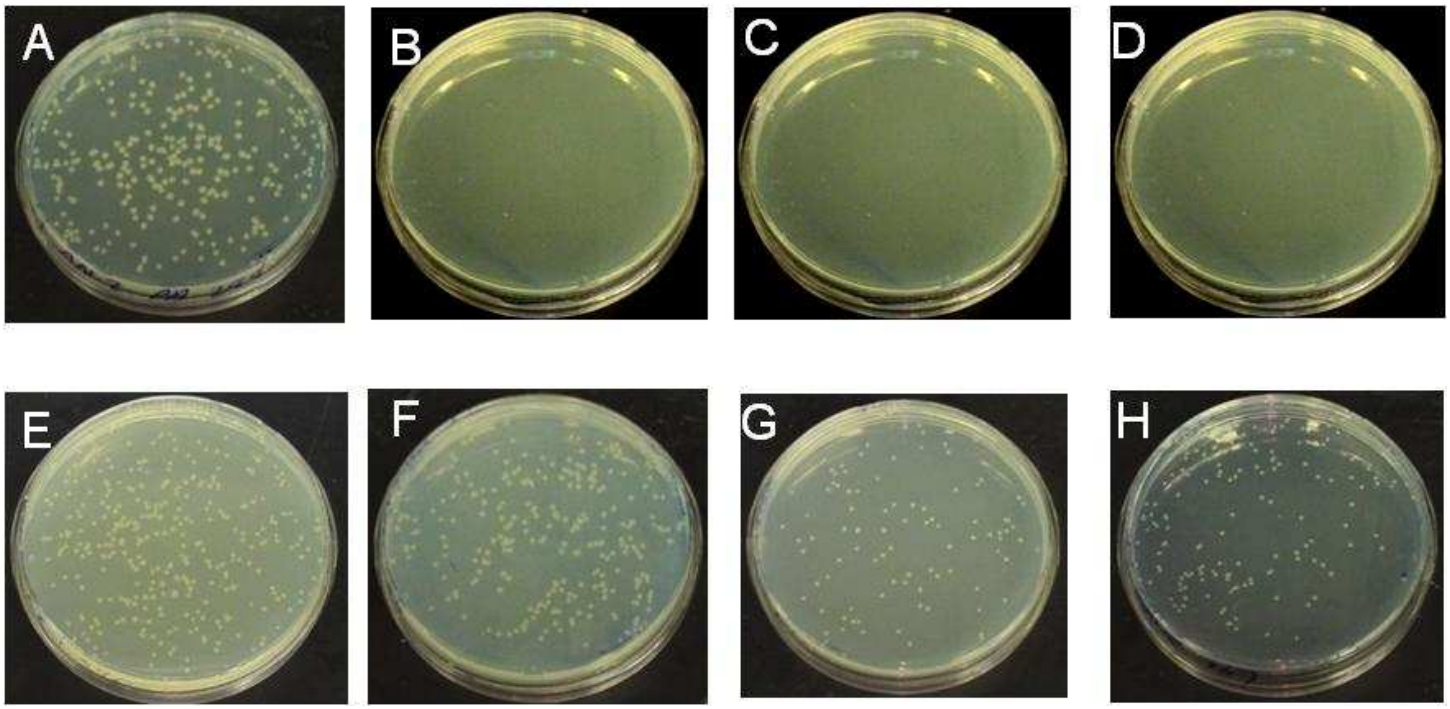

Figure 4.5. Agar plates of P. aeruginosa challenges on HMDI-BD (50wt%)-PTMO (1000):HMDI-BD (30wt%)-P[(3FOx)(C12)-0.87:0.13-5.1 kDa] blends , t = 0 wks. Challenge concentration = 2.11 x 10^6 CFU/mL A) As cast base PU (control), B) 0.5 wt% as cast, C) 1 wt% as cast, D) 2 wt% as cast, E) Base PU annealed at 60 ^oC, F) 0.5 wt% annealed at 60 ^oC, G) 1 wt% annealed at 60 ^oC, H) 2 wt% annealed at 60 ^oC

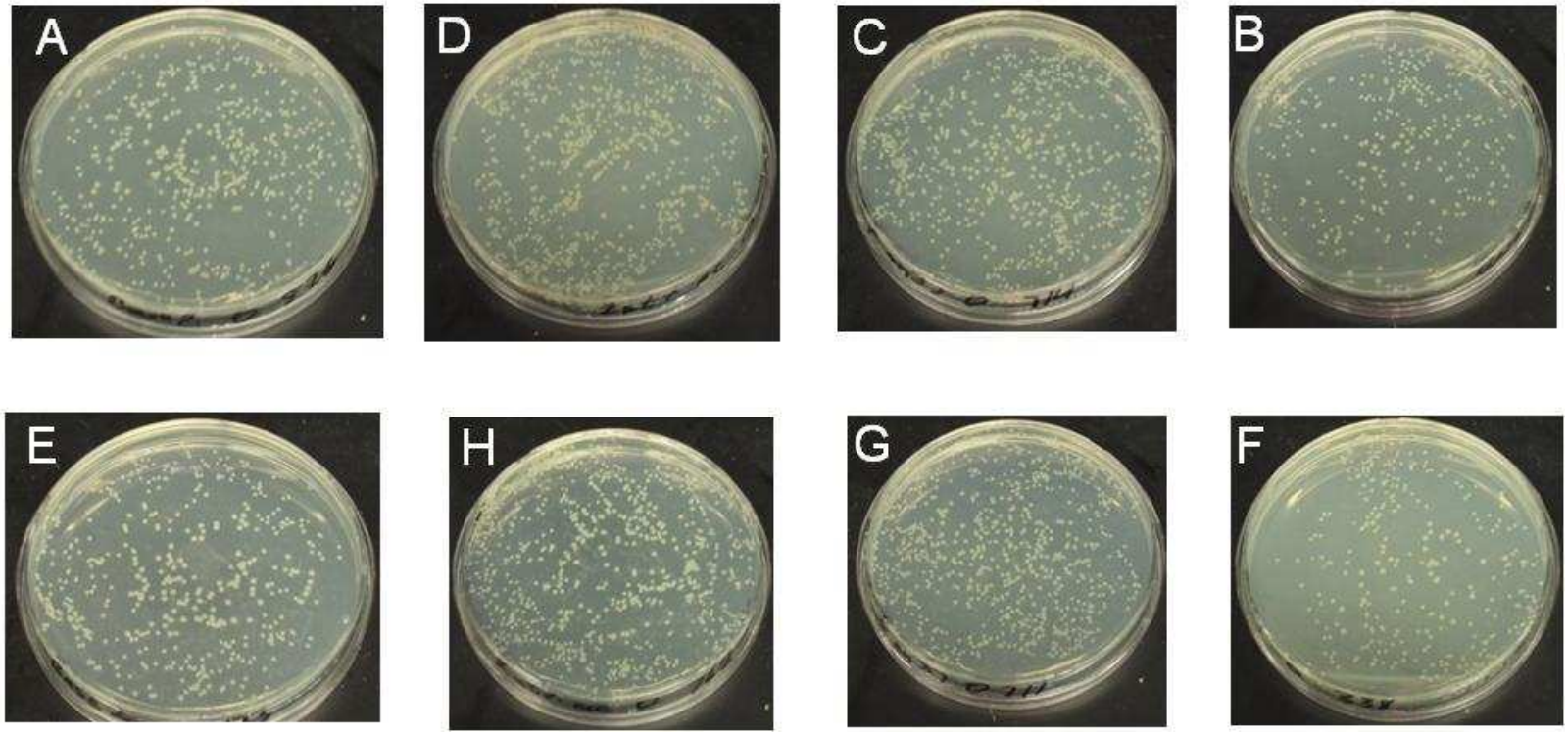

Figure 4.6. Agar plates of P. aeruginosa challenges on HMDI-BD (50wt%)-PTMO (1000):HMDI-BD (30wt%)-P[(3FOx)(C12)-0.87:0.13-5.1 kDa] blends , t = 2 wks. Challenge concentration = 2.2 x 10^6 CFU/mL A) As cast base PU (control), B) 0.5 wt% as cast, C) 1wt% as cast, D) 2 wt% as cast, E) Base PU annealed at 60 ^oC, F) 0.5 wt% annealed at 60 ^oC, G) 1wt% annealed at 60 ^oC, H) 2 wt% annealed at 60 ^oC.

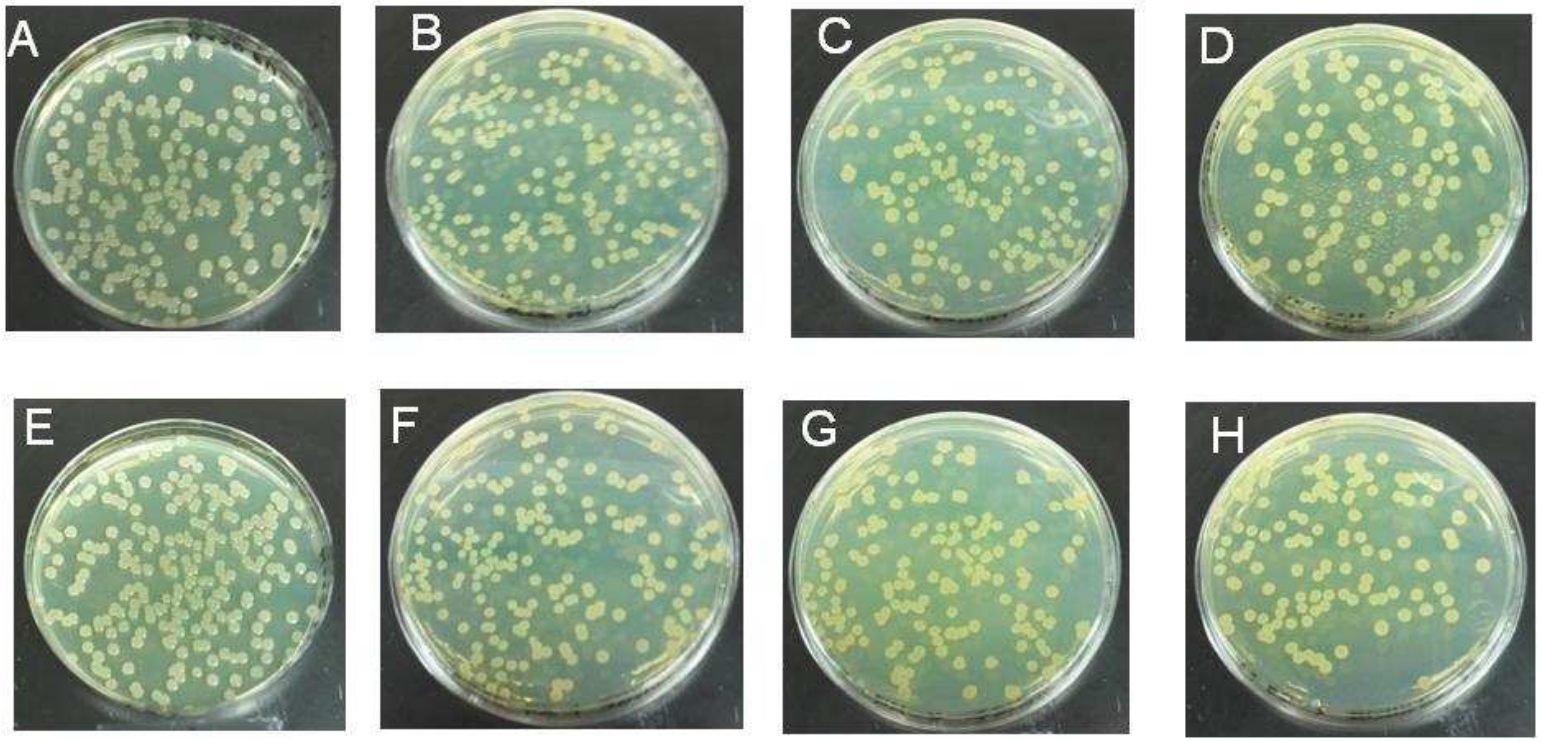

Figure 4.7. Agar plates of P. aeruginosa challenges on HMDI-BD (50wt%)-PTMO (1000): HMDI-BD (30wt%)-P[(3FOx)(C12)-0.87:0.13-7.9 kDa] blends , t = 0 wks. Challenge concentration = 2.3 x 10^6 CFU/mL A) As cast base PU (control), B) 0.5 wt% as cast, C) 1wt% as cast, D) 2 wt% as cast, E) Base PU annealed at 60 ^oC, F) 0.5 wt% annealed at 60 ^oC, G) 1wt% annealed at 60 ^oC, H) 2 wt% annealed at 60 ^oC

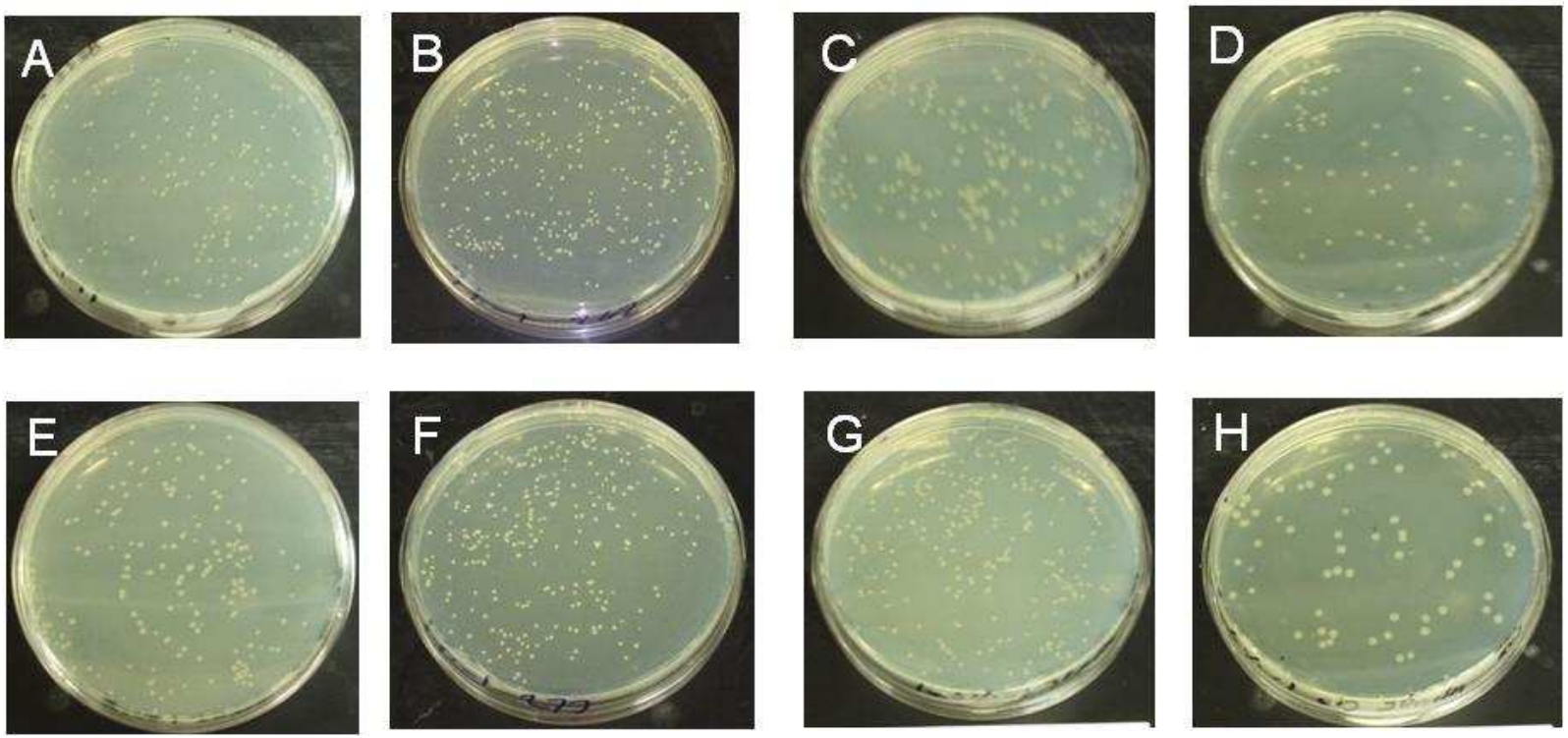

Figure 4.8. Agar plates of P. aeruginosa challenges on HMDI-BD (50wt%)-PTMO (1000):HMDI-BD (30wt%)-P[(3FOx)(C12)-0.87:0.13-11 kDa] blends , t = 0wks. Challenge concentration = 2.1 x 10^6 CFU/mL A) As cast base PU (control), B) 0.5 wt% as cast, C) 1 wt% as cast, D) 2 wt% as cast, E) Base PU annealed at 60 ^oC, F) 0.5 wt% annealed at 60 ^oC, G) 1wt% annealed at 60 ^oC, H) 2 wt% annealed at 60 ^oC

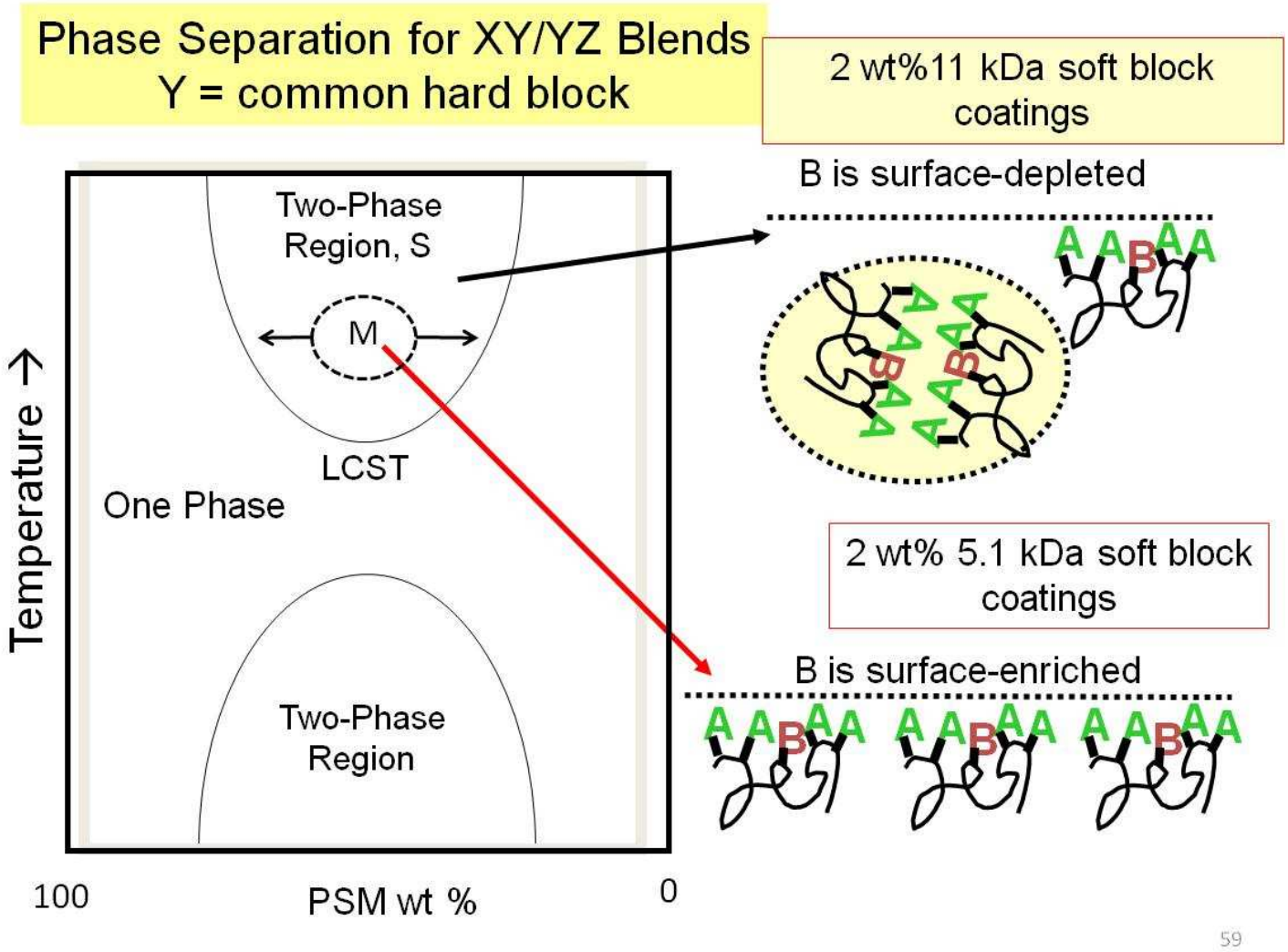

Figure 4.9. Phase separation and sequestering of quaternary ammonium charge, M is the metastable region, S is the two phase stable region.

Conclusion. The biocidal study demonstrated that microscale surface phase separation of PSM-base polyurethane blends negatively affects biocidal activity. As revealed by the morphological study, PSM soft segment molecular weight has a profound influence on the phase separation of the modifier with the lower molecular weight PSMs showing an initially stable morphology that slowly phase separated with time. In parallel, contact antimicrobial effectiveness also attenuates with time. Both the as cast 3.5 and 5.1 kDa PSMs showed considerable biocidal activity at t = 0 wks. This activity however showed considerable diminution with annealing and aging. This loss of activity presents several problems such as thermal stability and shelf life which would render any device containing these modifiers ineffective after extended storage or significant temperature increases during storage or use. In an attempt to solve the issue of morphological instability two approaches are currently under investigation and are discussed in the following chapter.

Chapter 5

Conclusion and Future Research: Stabilizing Surface Morphology of Modified Polyurethane Blends

In this study of P[(3FOx)(C12)] copolyoxetane based polymer surface modifiers, several discoveries are important for synthesis and processing of surface modifiers and materials with biocidal surfaces. First, the molecular weight of the telechelics plays a significant role in surface modification and it can be manipulated by controlling the monomer to initiator ratio. This provides an ability to tune copolyoxetane molecular weight to desired specification. This discovery was used to create telechelics of varying molecular weight in an attempt to find the optimum copolyoxetane telechelic molecular weight for incorporation into polymer surface modifiers. Upon making polymer surface modifiers from telechelics of varying molecular weight two other discoveries were made. The first of these is that telechelic molecular weight has an influence on the initial (t = 0 wks) surface morphology where PSMs with lower molecular weight telechelics (3.5 and 5.1 kDa) exhibited no apparent surface phase separation while PSMs with higher molecular weight telechelics (7.9 and 11 kDa) showed phase separation at t = 0 wks. The second of these is that the apparent single phase surface morphology observed in the blend containing the 3.5 and 5.1 kDa PSM began to develop microscale surface phase separated feature with time (t = 2 wks) and annealing (37 and 60 ^{o}C). As discussed in Chapter 4, this destabilization of the surface morphology results in the loss of biocidal efficacy and indicated that the surfaces of the modified polyurethanes are not robust for practical applications.

In order for P[(3FOx)(C12)-0.87:0.13] polymer surface modifiers to be more practical for use, a method for controlling the extent of phase separation must be devised. One method woudl be to utilize a crosslinked base matrix. By blending the PSM with a matrix polymer and then crosslinking that matrix, this should in principle slow the aggregation of the PSM polymer chains due to it being blended among the less mobile crosslinked chains. Crosslinking was used by Waschinski to incorporate a biocide into an acrylic coating. By crosslinking the material, enough surface concentration was effected to generate long term contact antimicrobial effectiveness (activity maintained after 45 days).[76] By incorporating the polyurethane PSMs discussed here into a crosslinking matrix, PSM aggregation may be slowed or eliminated.

Crosslinked matrix polyurethanes (those which were mentioned in Chapter 1) are currently being investigates with P[3FOx] base PSM and have shown some promise in controlling microscale phase separation.[20] As seen in AFM images of PSM- crosslinke base PU blends (Figure 5.1), when the PSM is blended with a linear HMDI-BD (50 wt%) PTMO-1000 matrix, large microscale phase separated feature are observed. When the same PSM is incorporated into a crosslinked matrix the microscale phase separated features are smaller and more dispersed. In the case of P[(3FOx)(C12)] PSMs, this more dispersed morphology could mean more even distribution of quaternary ammonium charge and consistent contact biocidal activity.

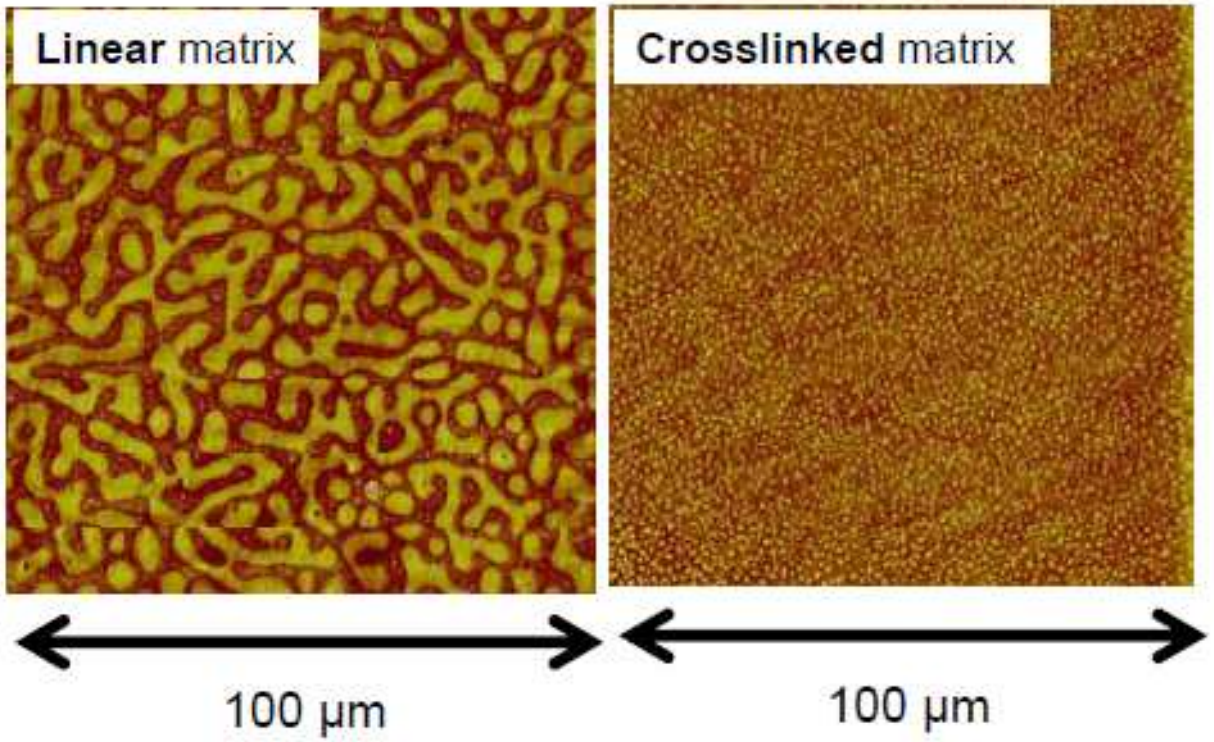

Figure 5.1. Polyurethane coatings with 5 wt% 3FOx semifluorinated surface modifiers. Left: linear base polyurethane as the matrix. Right: crosslinked polyurethane as the matrix.

Another method that could help control PSM phase separation is to utilize polyoxetane soft blocks that are more miscible with the base polyurethane (whether linear or crosslinked) than P[(3FOx)(C12)]. In work of Kurt *et al.* PSMs that contained PEG-like side chains (-CH2-$(OCH_2CH_2)_2OCH_3$) or "ME2Ox" rather than 3FOx resulted in a very good contact biocidal PSM, which was attributed to the "self-surface-concentrating" effect of C12 side chains. Whether the hydrophilic nature of ME2Ox will facilitate antimicrobial action or present other difficulties is not known. However, several opportunities for "tuning" copolyoxetanes surface modifiers are underway so as to ultimately create economical, effective, and durable contact antimicrobial coatings.

References

1. Makal, U. W., L; Ohman,D; Wynne, K J, Polyurethane biocidal polymeric surface modifiers. *Biomaterials* **2006,** 27, 1316-1326.

2. Kurt, P.; Wood, L.; Ohman, D. E.; Wynne, K. J., Highly Effective Contact Antimicrobial Surfaces via Polymer Surface Modifiers. *Langmuir* **2007,** 23, (9), 4719-4723.

3. Lamba, N. M. K., Woodhouse, Kimberly A. , Cooper, Stuart L., Structure and Physical Characterization of Polyurethane. In *Polyurethanes in BIomedical Applications*, CRC Press LLC: Boca Raton, Fl, 1998; pp 68-72.

4. Garrett, J. T. Phase separation and morphology of poly(urethane urea) block copolymers. 2001.

5. Gunatillake, P. A.; Meijs, G. F.; McCarthy, S. J.; Adhikari, R., Poly(dimethylsiloxane)/poly(hexamethylene oxide) mixed macrodiol based polyurethane elastomers. I. Synthesis and properties. *J. Appl. Polym. Sci.* **2000,** 76, (14), 2026-2040.

6. Gunatillake, P. A.; Meijs, G. F.; McCarthy, S. J.; Adhikari, R.; Sherriff, N., Synthesis and characterization of a series of poly(alkylene carbonate) macrodiols and the effect of their structure on the properties of polyurethanes. *J. Appl. Polym. Sci.* **1998,** 69, (8), 1621-1633.

7. Huang, S.-L., Lai, Juin-Yih, Structure-Tensile Properties of Polyurethane. *European Polymer Journal* **1997,** 33, (10-12), 1563-1567.

8. Hwang, K. K. S., Hemker, David J., Cooper Stuart L., Phase Diagram and Morphology of a Urethane Model Hard Segment and Polyether Macroglycols. *Macromolecules* **1984,** 17, 307-315.

9. Kang, W.; Stoffer, J. O. In *Effect of hard segments on morphology of polyurethanes*, 2000; American Chemical Society: 2000; pp POLY-070.

10. Cooper, S. L.; Tobolsky, A. V., Viscoelastic behavior of segmented elastomers. *Text. Res. J.* **1966,** 36, (9), 800-3.

11. Krause, S., Phase separation in block copolymers. *Journal of Polymer Science Part A* **1969,** 7, 249.

12. Garrett, J. T., Siedlecki, Christorpher A., Runt, James, Microdomain Morphology of Poly(urethane urea) Multiblock Copolymers. *Macromolecules* **2001,** 34, (20), 7066-7070.

13. Tsen, W. C.; Chuang, F. S., Phase transition and domain morphology of siloxane-containing hard-segmented polyurethane copolymers. *J. Appl. Polym. Sci.* **2006,** 101, (6), 4242-4252.

14. Lee, D.-K.; Tsai, H.-B.; Tsai, R.-S.; Chen, P. H., Preparation and properties of transparent thermoplastic segmented polyurethanes derived from different polyols. *Polym. Eng. Sci.* **2007,** 47, (5), 695-701.

15. Miller, J. A., Lin, Shaow B., Hwang, Kirk K.S., Wu, K.S., Gibson P.E, Cooper, Stuart L., Properties of Polyether-Polyurethane Block Copolymers: Effects of Hard Segment Length. *Macromolecules* **1985,** 18, (1), 32-44.

16. Seymour, R. W., Cooper, S.L., Thermal analysis of Polyurethane Block Polymers. *Macromolecules* **1972,** 6, (1), 48-53.

17. Seymour, R. W., Allegrezza, Jr., A.E. Cooper, S.L., Segmental Orientation Studies of Block Polymers. I. Hydrogenbonded Polyurethanes. *Macromolecules* **1973,** 6, (6), 896-902.

18. Kurt, P., Wynne, Kenneth J, Co-Polyoxetane with Alkylammonium and Fluorous or PEG-Like Side Chains: Soft Blocks for Surface Modifying Polyurethanes. *Macromolecules* **2007,** 40, 9537-9543.

19. Brunson, K. Synthesis and Characterization of 4,4 Methylene bis cyclohexyl diisocyanate based polyurethanes. Virginia Commonwealth University, Richmond, VA, 2006.

20. Zhang, W., Wang, Chenyu, Wynne, Kenneth J. In *Network Constrained Surface Phase separation,* ACS Fall meeting 240, Boston, Massachusettes, 2010; American Chemical Society: Boston, Massachusettes, 2010.

21. Grapski, J. A. C., S. L, Synthesis and characterization of non-leaching biocidal polyurethanes. *Biomaterials* **2001,** 22, 2239-2246.

22. de Lima, V.; Pelissoli, N. d. S.; Dullius, J.; Ligabue, R.; Einloft, S., Kinetic study of polyurethane synthesis using different catalytic systems of Fe, Cu, Sn, and Cr. *J. Appl. Polym. Sci.* 115, (3), 1797-1802.

23. Oprea, S., Structure and properties of cross-linked polyurethane copolymers. *Adv. Polym. Technol.* **2009,** 28, (3), 165-172.

24. Yuecedag, F.; Atalay-Oral, C.; Erkal, S.; Sirkecioglu, A.; Karasartova, D.; Sahin, F.; Tantekin-Ersolmaz, S. B.; Guener, F. S., Antibacterial oil-based polyurethane films for wound dressing applications. *J. Appl. Polym. Sci.* 115, (3), 1347-1357.

25. Malik, A. A., Archibald; Thomas G. Solvent-free process for the preparation of mono-substituted fluorinated oxetane monomers March 14, 2000, 2000.

26. Magonov, S. N., Atomic Force Microscopy in Analysis of Ploymers. In *Encyclopedia of Analytical Chemistry*, Meyers, R. A., Ed. John Wiley & Sons: Chichester, 2000; pp 7432-7491.

27. Uilk, J. J., E; Bullock,S; Wynne, K J, Surface Characterization, Microstucture and Wetting of Network from α,ω-Dihydroxy(poldimethylsiloxane) and 1,1,2,2-tetrahydrotrideca. *Macromolecular Chemistry and Physics* **2002,** 203, 1506-15-11.

28. Silverstein, R. M., Bassler, G.C., Morrill, T.C., Proton Magnetic Resonance Spectrophotometry. In *Spectrophotmetric Identification of Organic Compound*, 5th ed.; John Wiley & Sons: 1991; pp 165-226.

29. TA-Instruments Modulated DSC (MDSC). http://www.tainstruments.com/main.aspx?siteid=11&id=86&n=1 (5-12-2010),

30. Brandrup, J., Immergut, E.H, *Polymer Handbook.* 2nd ed.; John Wiley & Sons: New York, NY, 1975.

31. Garrett, J. T.; Xu, R.; Cho, J.; Runt, J., Phase separation of diamine chain-extended poly(urethane) copolymers: FTIR spectroscopy and phase transitions. *Polymer* **2003,** 44, (9), 2711-2719.

32. Cavanaugh, T. J.; Nauman, E. B., Particulate growth in phase-separated polymer blends. *J. Polym. Sci., Part B: Polym. Phys.* **1998,** 36, (12), 2191-2196.

33. Crist, B.; Nesarikar, A. R., Coarsening in Polyethylene-Copolymer Blends. *Macromolecules* **1995,** 28, (4), 890-6.

34. Fortelny, I.; Zivny, A.; Juza, J., Coarsening of the phase structure in immiscible polymer blends. Coalescence or Ostwald ripening? *J. Polym. Sci., Part B: Polym. Phys.* **1999,** 37, (3), 181-187.

35. Hill, M. J.; Barham, P. J., Ostwald ripening in polyethylene blends. *Polymer* **1995,** 36, (17), 3369-75.

36. Kim, W. K.; Char, K.; Kim, C. K., Control of droplet size of polymer-diluent blends through thermally induced phase separation. *J. Polym. Sci., Part B: Polym. Phys.* **2000,** 38, (23), 3042-3052.

37. Mirabella, F. M., Jr.; Barley, J. S., Ostwald ripening in immiscible polyolefin blends. *J. Polym. Sci., Part B: Polym. Phys.* **1995,** 33, (16), 2281-7.

38. Plate, N. A.; Litmanovich, A. D.; Kudryavtsev, Y. V.; Govorun, E. N., Interplay of chemical and physical factors in reacting polymer blends. Theoretical considerations. *Macromol. Symp.* **2003,** 191, (Molecular Order and Mobility in Polymer Systems), 11-20.

39. Bernacca, G. M., Gulbrasen, M. J. , Wilkenson, R., Wheatley, D. J., In vitro blood compatibilty of surface-modified polyurethanes. *Biomaterials* **1998,** 19, 1151-1165.

40. Wang, L. F., Ji, Q., Glass, T.E., Ward, T.C., McGrath, J.E.,Muggli, M., Burns, G.,Sorathia, U., Synthesis and characterization of organosiloxane modified segmented polyether polyurethanes. *Polymer* **2000,** 41, 5083-5093.

41. McCloskey, C. B., Yip, C. M., Santerre, J. P., Effect of Fluorinated Surface-Modifying Macromolecules on the Molecular Surface Structure of a Polyether Poly (urethane urea). *Macromolecules* **2002,** 35, 924-933.

42. Khayet, M., Membrane surface modification and characterization by X-ray photoelectron spectroscopy, atomic force microscopy and contact angle measurements. *Applied Surface Science* **2004,** 238, 269-272.

43. Klibanov, A. M., Permanently microbicidal materials coatings. *Journal of Materials Chemistry* **2007,** 17, (24), 2479-2482.

44. Lee, S. B.; Koepsel, R. R.; Morley, S. W.; Matyjaszewski, K.; Sun, Y. J.; Russell, A. J., Permanent, nonleaching antibacterial surfaces. 1. Synthesis by atom transfer radical polymerization. *Biomacromolecules* **2004,** 5, (3), 877-882.

45. Makal, U. W., Uilk, J., Kurt, P., Cooke R.S., Wynne, K.J, Ring opening polymerization of 3-semifluoro and 3-bromomethyloxetanes to poly(2,2-substituted-1,3-propylene oxide) telechelics for soft blocks in polyurethanes *Polymer* **2005,** 46, 2522-2530.

46. Kurt, P., Gamble, Lara,J., Wynne Kenneth J., Surface Characterization of Biocidal Polyurethane Modifiers Having Poly(3,3-substituted)oxetane Soft Blocks with Alkylammonium Side Chains. *Langmuir* **2008,** 24, 5816.

47. Pattison, Cyclic Ethers Made by pyrolysis of Carbonate Esters. *Journal of the American Chemical Society* **1957,** 79.

48. Kawakami, Y., Takahashi, K, Hibino, H, Synthesis of liquid crystalline polymers with a polyoxetane main chain. *Macromolecules* **1991,** 24, 4531-4537.

49. Malik, A. A., Archibald; Thomas G., Carlson, Roland P., Wynne, Kenneth J., Kresge, Edward N. Amorphous polyether glycols based in bis-substituted oxetane amd tetrahydrofuran monomers. 2006.

50. Bray, A. J., Theory of phase-ordering kinetics. *Advances in Physics* **1994,** 43, (3), 357.

51. Furukawa, H., A dynamic scaling assumption for phase separation. *Advances in Physics* **1985,** 34, (6), 703.

52. Lifshitz, I. M.; Slyozov, V. V., The kinetics of precipitation from supersaturated solid solutions. *Journal of Physics and Chemistry of Solids* **1961,** 19, (1-2), 35-50.

53. Hohenberg, P. C., Halperin, B. I., Theory of dynamic critical phenomena. *Reviews of Modern Physics* **1977,** 49, (3).

54. Tanaka, H., Unusual Phase Separation in a Polymer Solution Caused by Asymmetric Molecular Dynamics. *Physical Review Letters* **1993,** 71, (19).

55. Luo, K., Gronski, W., Friedrich, C., Viscoelastic phase separation in polymer blends. *European Physical Journal E* **2004,** 15, 177-187.

56. Zhou, D., Pingwen, Zhang, Weinan E, Modified model of polymer phase separation. *Physical Review E* **2006,** 73.

57. Kumacheva, E.; Li, L.; Mitchell, W.; Mitchell, A.; Shinozaki, D. M.; Cheng, P. C., Direct Imaging of Surface and Bulk Structures in Solvent Cast Polymer Blends. . *Langmuir* **1997,** 13, 2483-2489.

58. Li, X.; Xing, R.; Zhang, Y.; Han, Y.; An, L., Molecular weight effects on the phase morphology of PS/P4VP blend films on homogeneous SAM and heterogeneous SAM/Au substrates. *Polymer* **2004,** 45, (5), 1637-1646.

59. Kontis, M. A., Muthukumar, M., Entropy-incuded frozen morphology in unstable polymer blends. *Macromolecules* **1992,** 25, 1716-1724.

60. Li, H. M., Wang, Z., Chen, X. C., Xie, Z. D., Shu, D. J., Wang, M., Peng, R. W., Ming, N. B., Influence of weight ratio in polymer blend film on the phase separation structure and it optical properties. *The European Physical Journal: Applied Physics* **2009,** 45.

61. Wenzel, E. M., The impact of Hospital Acquired Blood Stream Infections. *Emerg Inf Dis* **2001,** 7, (174).

62. Richards MJ, E. J., Culver DH, Gaynes RP, Nosocomial infections in pediatric intensive care units in the United States. *Pediatrics* **1999,** 103, (4).

63. Borkow, G., Gabbay, Jeffery, Cooper as a biocidal tool. *Current Medical Chemistry* **2005,** 12, 2163-2175.

64. Kumar, R., Munstedt, Helmut, Silver ion release from antimicrobial polyamide/silver composites. *Biomaterials* **2004,** 26, 2081-2088.

65. Asavavisithchai, S.; Oonpraderm, A.; Ruktanonchai, U. R., The antimicrobial effect of open-cell silver foams. *J. Mater. Sci.: Mater. Med.* **2010,** 21, (4), 1329-1334.

66. Kuhn, P. www.cooper.org/enviroment/doorknob.html

67. Silver, S., Phung, Le T., Silver Gregg, Silver as biocides in burns abd wound dressings and biocidal bacteria resistance to silver compunds. *J Ind Microbiol Biotech* **2006,** 33.

68. Kuroda, K.; DeGrado, W. F., Amphiphilic polymethacrylate derivatives as antimicrobial agents. *Journal of the American Chemical Society* **2005,** 127, (12), 4128-4129.

69. Lawrence, C. A., *Surface-Active Quaternary Ammonium Germicides*. 1949; p 240 pp.

70. Witton, C. J., Detergents. *The American Journal of Nursing* **1950,** 50, (7), 410-412.

71. Landa, A. S.; Van, d. M. H. C.; Busscher, H. J. In *Detergents in oral health care products and microbial detachment*, 1998; Harwood: 1998; pp 311-322.

72. Bechinger, B.; Lohner, K., Detergent-like actions of linear amphipathic cationic antimicrobial peptides. *Biochim. Biophys. Acta, Biomembr.* **2006,** 1758, (9), 1529-1539.

73. Waschinski, C. J., Tiller, J. C., Poly(oxazoline)s with telechelic antimicrobial functions. *Biomacromolecules* **2005,** 6, (1).

74. Tiller, J. C.; Liao, C. J.; Lewis, K.; Klibanov, A. M., Designing surfaces that kill bacteria on contact. *Proceedings of the National Academy of Sciences of the United States of America* **2001,** 98, (11), 5981-5985.

75. Tiller, J. C.; Lee, S. B.; Lewis, K.; Klibanov, A. M., Polymer surfaces derivatized with poly(vinyl-N-hexylpyridinium) kill airborne and waterborne bacteria. *Biotechnology and Bioengineering* **2002,** 79, (4), 465-471.

76. Waschinski, C. J., Zimmerman, J, Salz, Hutzler, R, Sadowski, G, Tiller, J, Design od Contact-Active Antimicrobial Acrylate-Based Material Using Biocidal Macromers. *Advanced Materials* **2008,** 20, 104-108.

VITA

Kennard Marcellus Brunson, Jr. was born on November 20, 1980 in Richmond, VA. He graduated Salutatorian from John Marshall High School in 1998 followed by his enrollment at Virginia Commonwealth University. In May 2002 he received his B.S. degree in Chemical Engineering and on Aug 2006 received his M.S. in Engineering under the direction of Dr. Kenneth J Wynne. He is to receive his Ph.D. in Engineering from the Department of Chemical and Life Science Engineering at Virginia Commonwealth University in Aug 2010.